Synthesis of BODIPY-tagged transition-metal complexes

Development of novel fluorescent transition-metal complexes and their application for the study of catalytic transformations

TECHNISCHE UNIVERSITÄT DARMSTADT

Dem Fachbereich Chemie

der Technischen Universität Darmstadt

zur Erlangung des akademischen Grades eines

Doctor rerum naturalium (Dr. rer. nat.)

genehmigte

Dissertation

vorgelegt von

Roman Vasiuta, „Magister“

aus Iwano-Frankiwsk, Ukraine

Referent: Prof. Dr. Herbert Plenio
Korreferent: Prof. Dr. Felix Hausch

Tag der Einreichung: 16 November 2017
Tag der mündlichen Prüfung: 15 Januar 2018

Darmstadt 2018
D17

Acknowledgements

Firstly, I would like to express my sincere gratitude to my supervisor, Prof. Dr. Herbert Plenio, for the opportunity to carry out my doctoral study in his research group, and for his constant support, guidance, and encouragement throughout the course of this research work. I appreciate his understanding, patience, and motivation. I am very grateful for his assistance in writing this thesis.

I would like to give special thanks Ms. Eleonore Pfeifer for her support and kindness.

I wish to thank my lab-mates and colleagues M. Sc. Meike Egert, Dr.rer.nat. Jetmire Mersini, Dipl.-Ing. Natalie Peschek, Dipl.-Chem. Andreas Hegelein, M. Sc. Marvin Bergmann, Götz Hoffmann, M. Sc. Oliver Halter, Dr.rer.nat. Roman Savka, Dr.rer.nat Pavlo Kos and M. Sc. Yuki Kanai for the support, positive atmosphere during long working hours, and for all the fun we have had in the last four years.

Last but not least, I would like to thank my family and friends for their constant support throughout my Ph.D. and my life in general.

Die vorliegende Arbeit wurde am Eduard-Zintl-Institut für Anorganische und Physikalische Chemie der Technischen Universität Darmstadt unter der Leitung von Prof. Dr. H. Plenio in der Zeit von Dezember 2013 bis März 2017 angefertigt.

Teile dieser Arbeit sind bereits veröffentlicht oder zur Veröffentlichung eingereicht:

Papers

[1] **R. Vasiuta**, H. Plenio, *"Observing Initial Steps in Gold-Catalyzed Alkyne Transformations by Utilizing Bodipy-Tagged Phosphine-Gold Complexes"*, *Chem. Eur. J.* **2016**, *22*, 6353–6360.

[2] O. Halter, **R. Vasiuta (shared first author)**, I. Fernandez, H. Plenio, *"Systematic Modulation of the Fluorescence Brightness in Boron-Dipyrromethene (BODIPY)-Tagged N-Heterocyclic Carbene (NHC)–Gold–Thiolates"*, *Chem. Eur. J.* **2016**, *22*, 18066–18072.

Table of contents

1. Introduction

Due to the high sensitivity of detection and the non-invasive nature, luminescence techniques, and in particular fluorescence spectroscopy, have found a wide variety of applications in physical, chemical, biological, material and medical sciences.[1] Over the last decade, fluorescence methodologies were shown to be very promising tools for studying chemical processes and revealing mechanistic insights of molecular transformations.[2] In this respect, the high sensitivity of fluorescence detection perfectly suits the monitoring of catalytic species of transition-metal complexes, which (almost by definition) are present in very small concentrations during catalytic reactions. Pioneering work, which includes both ensemble[3] and single-molecule[4] experiments, has revealed the huge potential of fluorescence spectroscopy for the investigation of catalytic processes. One of the main requirements in such research is the labeling of transition-metal complexes with suitable fluorophores. Design and synthesis of novel fluorophore-tagged complexes would therefore greatly facilitate the development of this field of science. Except for mechanistic investigations, such complexes can be used as chemosensors,[5] triplet sensitizers,[6] biological sensing probes,[7] and even as therapeutic agents.[8]

The current chapter covers briefly the phenomenon of luminescence and related processes, with a special focus on fluorescence emission, its characteristics, and quenching pathways. The full information on fluorescence techniques with numerous examples of application in biology can be found in the excellent book of Joseph Lakowicz “Principles of Fluorescence Spectroscopy” (Springer-Verlag, 2010).[9] More advanced description of the physical principles of fluorescence methods is given in “Molecular Fluorescence: Principles and Applications” by Bernard Valeur (Wiley-VCH, 2001).[10] The next section is dedicated to the synthesis of BODIPY (4,4-difluoro-4-bora-3a,4a-diaza-*s*-indacene), which was chosen as the most suitable fluorophore for labeling metal complexes. Finally, different examples of the application of BODIPY-tagged transition-metal complexes will be shown.

1.1. Luminescence

Emission of light by any substance, which is not caused by heating, is called luminescence. More general, luminescence is the emission of electromagnetic energy, which results from electronically excited states. Depending on the excitation mode different types of luminescence are known: mechanoluminescence, electroluminescence, chemiluminescence, bioluminescence, etc. If the excitation is caused by absorption of a photon, the subsequent emission is defined as photoluminescence. Depending on the spin state of the excited system photoluminescence is further divided into fluorescence and phosphorescence. Fluorescence is characterized by a singlet excited state. Return of the system to the ground state is spin allowed and, therefore, emission occurs very fast. Typical fluorescence lifetimes are in the range of 10 nanoseconds. Phosphorescence, in contrast, occurs from triplet excited state. Such a process is spin forbidden and displays much longer lifetimes (milliseconds to minutes). In case, when the excited state cannot be strictly determined as singlet or triplet, delayed fluorescence occurs. It is characterized by intermediate lifetimes.

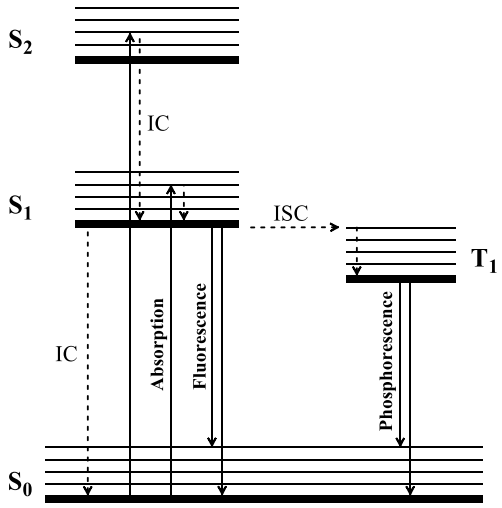

Figure 1.1. Jablonski diagram; S_0 – ground state, S_1, S_2 – singlet excited states, T_1 – triplet excited state, IC – internal conversion, ISC – intersystem crossing.

Photoluminescence and related processes can be illustrated by a Jablonski diagram (figure 1.1). The singlet electronic states are depicted as S_0 (ground state), S_1, S_2; triplet state – T_1. With each electronic state many vibrational levels are associated. Absorption of a photon leads to the excitation of the system from the ground state S_0 to the higher vibrational level of S_1 or S_2 states. Such transition, depicted with a vertical line, occurs very fast (10^{-15} s), so no changes in nuclei arrangement are possible (Franck-Condon principle). The system in the excited state is normally rapidly relaxed (10^{-12} s) to the lowest vibrational level of S_1 by a process called internal conversion. Finally, returning to the ground state can occur either by radiative process – fluorescence, which results in the emission of a photon, or by non-radiative internal conversion, which transforms excitation energy into the heat. Another possibility for the system in excited state S_1 is spin conversion to the excited triplet state T_1. This process is called intersystem crossing (ISC). The transition from T_1 to S_0 results in phosphorescence, which is characterized by longer wavelength (lower energy) than fluorescence emission. The presence of heavy atoms in the molecule normally facilitates ISC and subsequent phosphorescence.

1.1.1. Characteristics of fluorescence emission

The phenomenon of fluorescence emission is characterized by a number of different parameters, most of which can be quantitatively measured and analyzed.

The amount of emitted photons by a given fluorophore defines the fluorescence intensity *F*, whose value strongly depends on the experimental conditions. The dependence of fluorescence intensity on wavelength gives an emission spectrum. The emission spectrum is generally independent of the excitation wavelength. The reason for this is that irrespective of the energy of absorbed light, the excited molecule is quickly relaxed to the lowest vibrational level of S_1, from which fluorescence occurs.

The wavelength, which corresponds to the maximum intensity of fluorescence emission (emission maximum, λ_{em}), is generally longer than the absorbance maximum (λ_{abs}) for a given fluorophore. This phenomenon is known as Stokes Rule (named after Sir G. G. Stokes) and is characterized by the Stokes shift – the difference between λ_{em} and λ_{abs}. The Stokes Rule reflects the fact that part of excitation energy is lost due to vibrational relaxation or by other

non-radiative processes. Therefore, fluorescence emission always has lower energy (longer wavelength) than excitation light.

The efficiency of fluorescence emission is defined by the fluorescence quantum yield Φ. It is determined as the ratio between the number of emitted photons and the number of absorbed photons. A given fluorophore has a bright fluorescence emission if it is characterized by intense light absorbance and its quantum yield is larger than 0.9. In contrast, Φ values close to 0 mean no fluorescence occurs. The closely related parameter to quantum yield is fluorescence lifetime τ. It is defined as an average time the molecule spends in the excited state before return to the ground state, both by radiative and non-radiative processes.

In some experiments, polarized light is used for excitation. In this case, only those molecules are excited, whose transition dipole is parallel to the electric vector of the excitation light. Subsequent fluorescent emission can be also polarized. The extent of its polarization is characterized by two interchangeable parameters: fluorescence anisotropy I and fluorescence polarization P. Small molecules in fluid solutions typically rotate very fast, so the orientation of polarized emission is quickly randomized, which led to the disappearance of anisotropy. However, in the case of macromolecules (or viscous solutions), fluorescence polarization can be observed, and its measurements can provide useful information about the rate of rotational diffusion.

1.1.2. Mechanisms of fluorescence quenching

Application of fluorescence techniques critically relies on the detection of parameters, described above. Detectable changes of fluorescence intensity (the most basic parameter) can provide useful information about the molecular processes, which cause such changes. In this section, the main processes, leading to the fluorescence quenching (decreasing of fluorescence intensity), are briefly discussed.

Non-radiative deactivation of the excited-state fluorophore, which occurs upon collisional encounter with some other molecule (quencher), is known as collisional quenching. It requires molecular contact between fluorophore and quencher at the moment of excitation. Interacting molecules are not chemically modified in this type of process. A variety of compounds can act as collisional quenchers: oxygen, halogens, amines, amides, etc.

Intersystem crossing (ISC) is a non-radiative transition from the singlet excited state to a triplet excited. Generally, such transition is forbidden but can be facilitated by the presence of heavy atoms (as parts of the fluorophore or as external molecules), which increases spin-orbit coupling. Subsequent deactivation of the triplet state normally occurs by non-radiative pathways, although radiative de-excitation – phosphorescence – is also possible.

Quenching of fluorescence is often caused by photoinduced electron transfer (PET). Basically, it occurs due to the changes of redox properties of the fluorophore upon excitation. In the presence of another molecule, which can act as an electron donor (D) or acceptor (A) relative to the excited-state fluorophore, the charge transfer complex D^+A^- is formed, which subsequently returns to the ground state without emission. Depending on the direction of electron transfer reductive (acceptor-excited) or oxidative (donor-excited) types of PET are distinguished. As shown in figure 1.2, in case of reductive PET the fluorophore acts as an electron acceptor, whereas in oxidative PET it donates electrons. It should be also noted, that

both D and A are not necessarily different compounds, they can be also linked parts of the same molecule.

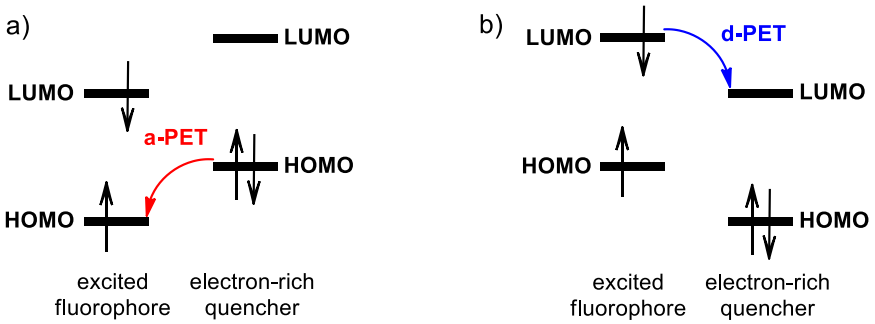

Figure 1.2. Different types of PET: a) reductive (acceptor-excited) PET; b) oxidative (donor-excited) PET.

The possibility of PET can be predicted based on the redox potentials of fluorophore and quencher. The energy change of PET is described by the Rehm-Weller equation:

$$\Delta G_{PET} = E_{1/2}(D^+/D) - E_{1/2}(A/A^-) - \Delta E_{00} - C$$

where $E_{1/2}(D^+/D)$ and $E_{1/2}(A/A^-)$ are reductive potentials for the respective processes; ΔE_{00} is the excitation energy of fluorophore corresponding to the $S_0 \rightarrow S_1$ transition; C – the coulombic attraction energy within formed ion pair D^+A^-.

Another quenching process, which requires contact between the orbitals of donor and acceptor, is electron exchange or Dexter quenching. An electron from the LUMO of the excited-state donor (fluorophore) is transferred to the LUMO of the acceptor (quencher). Either in a stepwise or concerted manner, an electron from the HOMO of the acceptor is transferred to the HOMO of the donor. Such electron exchange results in the energy transfer to acceptor and quenching of donor. Dexter interaction occurs at high concentrations of fluorophore and quencher when the average distance between molecules is relatively short.

Transfer of energy from an excited-state donor to an acceptor, which doesn't involve direct interaction of electron orbitals, is known as fluorescence resonance energy transfer (FRET). It can be described as a long-range dipole-dipole interaction, which occurs without the appearance of the photon. It requires an overlap between the emission spectrum of the donor and the absorbance spectrum of the acceptor. The efficiency E of FRET is determined as the fraction of energy absorbed by the donor which is transferred to the acceptor. It can be calculated from the experimental data using the following expression:

$$E = 1 - \frac{F_{DA}}{F_D}$$

where F_{DA} and F_D are fluorescence intensities of the donor in the presence and in the absence of acceptor respectively. FRET efficiency depends on the fluorescence properties of the donor, the degree of spectral overlap, mutual orientation of fluorophores, solvent properties and a distance between donor and acceptor. Dependence of FRET on the distance is defined by a given formula:

$$E = \frac{R_0^6}{r^6 + R_0^6}$$

where r is the distance between donor and acceptor; R_0 – Förster radius – corresponds to the distance of the transfer efficiency of 50%. This equation shows that FRET efficiency is very sensitive to the distance between donor and acceptor when r is comparable to R_0. In general, FRET can be used as a very sensitive molecular tool for the distance measurements. Common fluorophore pairs have values of Förster radius typically in the range from 2 to 9 nm, which is comparable to the size of biomolecules. Because of this FRET is widely used in the biological research, for example, for determination of protein folding or for the investigation of membrane fusion/aggregation.[9]

1.2. BODIPY fluorophores

In recent decades, the interest towards BODIPY-based dyes has grown dramatically.[11] The most important areas of their applications include biolabeling and bioimaging,[12] chemosensing,[13] photodynamic therapy,[14] fluorescent switches,[15] laser dyes[16] and solar cell sensitizers.[17] Such a widespread usage of BODIPY is due to its exceptional photophysical properties, the most essential of which are: strong absorbance, sharp emission band, high fluorescence quantum yield, chemical and photostability, relative inertness of photophysical properties to the environment conditions (temperature, solvent polarity, and pH). Another key feature of BODIPY is the huge potential of its structure towards chemical modification.[18] The photophysical properties, which strongly rely on the chemical structure, can be thus easily tuned by introducing a variety of substituents in the different positions of the BODIPY core.

1.2.1. BODIPY structure

The structure of the simplest unsubstituted difluoro*bo*ron *dipy*rromethene (BODIPY) is represented in figure 1.3 (left). Nomenclature name of BODIPY is 4,4-difluoro-4-bora-3*a*,4*a*-diaza-*s*-indacene, and the IUPAC numbering for this class of compounds is set similarly to the all-carbon tricyclic analog – indacene. The most chemically relevant positions are often specified as *meso*, α and β. The π-electron system is delocalized over the whole backbone as shown in figure 1.3 (right).

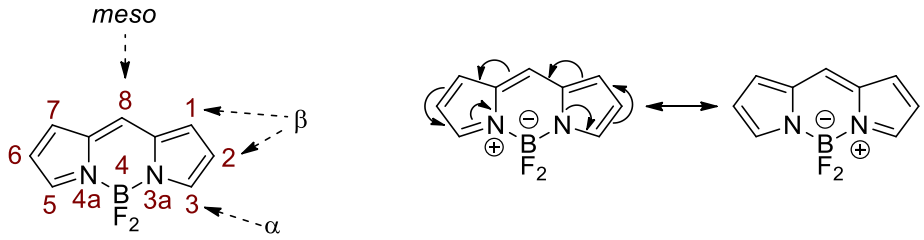

Figure 1.3. Left: structure of BODIPY and its atom numbering scheme. Right: selected delocalized structures of BODIPY.

BODIPY can be considered as a conformationally rigid monomethine cyanine dye, where both ends of the chain are held together with BF_2 unit[19] (figure 1.4). Restriction of the flexibility in dipyrromethene scaffold leads to the high quantum yield and sharp fluorescence band of the BODIPY fluorophore.

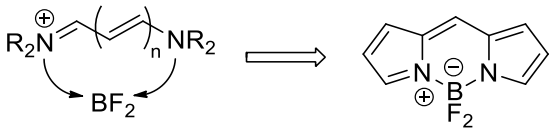

Figure 1.4. The relationship between structures of cyanines and BODIPY dyes.

1.2.2. Synthesis of BODIPYs

Synthesis of the first BODIPY derivative was reported by Treibs and Kreuzer in 1968.[20] After almost 50 years of vast synthetic efforts towards preparation, modification, and optimization of the structure, an enormous amount of various BODIPY-based fluorophores has been reported.[19, 21] Nonetheless, the synthesis of the simplest member of BODIPY family (figure 1.3) has remained a challenging task for a long time and was successfully accomplished only in the last decade.[22] Most probably, the high sensitivity of "naked" BODIPY skeleton towards electrophilic attack causes the low stability of this compound and limits its accessibility.

The general approach towards BODIPY synthesis typically includes condensation of α-free pyrrole with highly electrophilic carbonyl compounds (either aldehydes or acylium equivalents), followed by BF_2 complexation, as shown in figure 1.5.

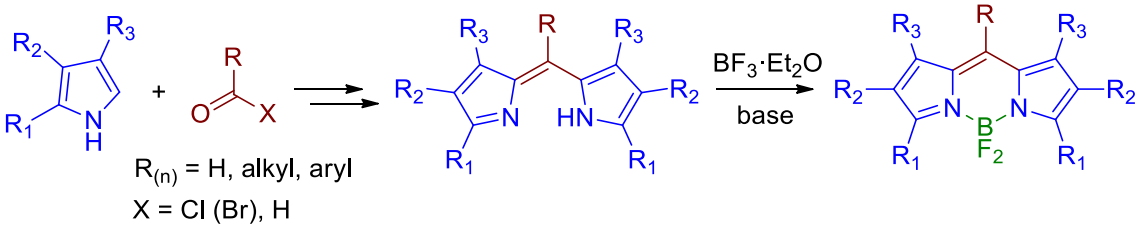

Figure 1.5. The general scheme of the synthesis of BODIPY core.

In case X = Cl, the condensation of pyrrole with an acid chloride leads to the formation of unstable dipyrromethene hydrochloride salt, which is normally not isolated and used directly for the next stage without purification.[16b] Subsequent treatment with $BF_3{\cdot}OEt_2$ in basic media yields BODIPY (figure 1.6).[23] With this approach, both alkyl and aryl groups can be introduced into *meso*-position. Instead of acid chlorides, acid anhydride[24] or orthoester[25] can be also used as acylium equivalent.

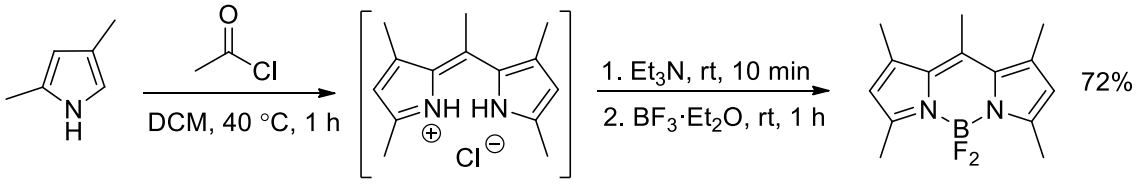

Figure 1.6. Synthesis of pentamethyl substituted BODIPY.[23]

Burgess and coworkers have used this approach to synthesize 3,5-diaryl BODIPYs (figure 1.7).[26] The reaction of different 2-arylpyrroles with 4-iodobenzoyl chloride proceeds through ketopyrrole intermediates and ends up with diarylpyrromethenes, which are subsequently converted to BODIPYs. The presence of halogen atom in *meso*-phenyl ring opens the way for further modification of the molecule via Pd-catalyzed cross-coupling reactions.[27]

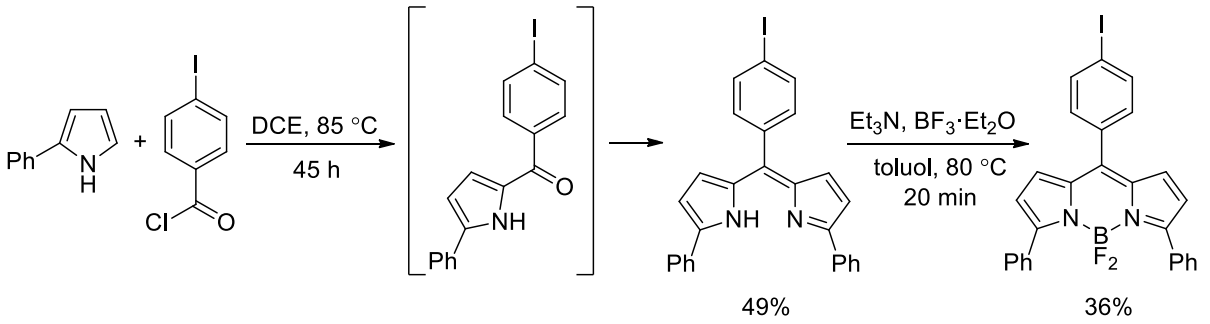

Figure 1.7. Synthesis 3,5-diphenyl BODIPY by Burgess and coworkers.[26]

In the case X = H (figure 1.5), an aldehyde (typically aromatic) reacts with pyrrole in the presence of a catalytic amount of Lewis acid to produce dipyrromethane. Subsequent oxidation with DDQ or *p*-chloranil leads to the formation of dipyrromethene, which is converted to BODIPY in the same way as described above. This methodology of BODIPY preparation is also known as Lindsey's approach (figure 1.8).[27a] It allows obtaining BODIPYs lacking any α- or β- substituents, although an excess of pyrrole is needed to suppress polymerization and/or porphyrin formation.[28]

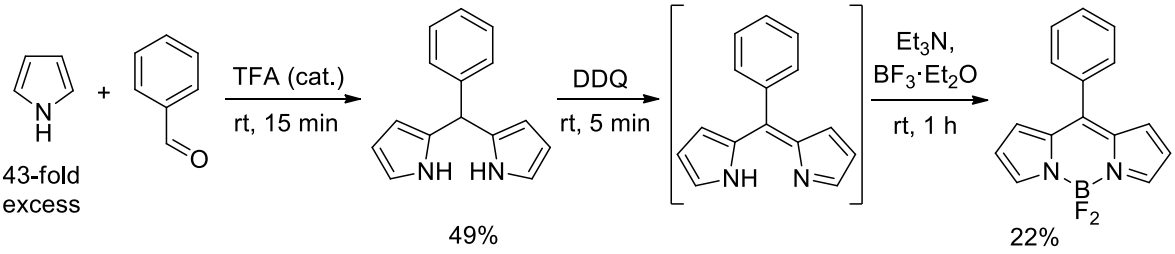

Figure 1.8. Synthesis of *meso*-phenyl BODIPY by Wagner and Lindsey.[27a]

If 2-substituted pyrroles (one of the α-positions is blocked) are used for the synthesis, the condensation reaction with aldehyde stops on the stage of dipyrromethane formation.[27a] Baruah et al. used[29] only two equivalents of 2-methylpyrrole (compare to aldehyde) in order to obtain *meso*-phenolic BODIPY (figure 1.9). Phenolic benzaldehyde was chosen as carbonyl component in this case since the application of acid chlorides would have introduced chemoselectivity problems.

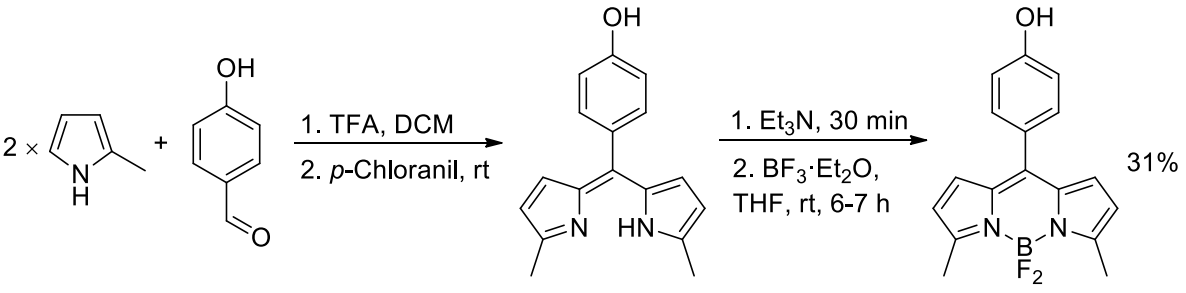

Figure 1.9. Synthesis of *meso*-phenolic BODIPY by Boens and coworkers.[29]

The disadvantage of this approach is additional synthetic step – oxidation, which also raises the amount of undesired by-products. Nonetheless, a variety of functionalized aromatic substituents can be introduced into *meso*-position using this methodology.[30] Application of aldehydes other than aromatic is rather rare and proceeds only with low yield,[31] since the oxidation stage tends to fail in these cases.

Asymmetric BODIPYs can be prepared by condensation of ketopyrrole (obtained on a separate stage) with another pyrrole fragment in the presence of Lewis acid. Lee et al. have used this approach[32] to synthesize asymmetrical BODIPY shown in figure 1.10.

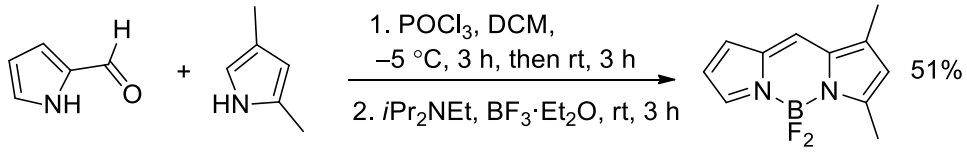

Figure 1.10. Synthesis of asymmetrical BODIPY.[32]

Similarly to the acid chloride approach, dipyrromethene hydrochloride salt is formed on the first stage. Again, the addition of base and $BF_3{\cdot}OEt_2$ yields BODIPY. Boens and coworkers have utilized this procedure[33] to prepare conformationally restricted asymmetric BODIPY with fused carbocycle (figure 1.11).

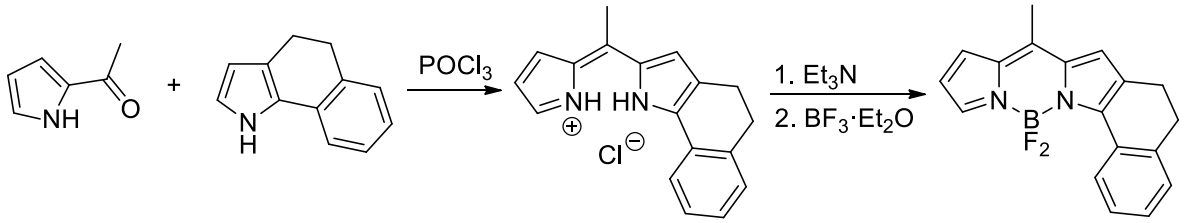

Figure 1.11. Synthesis of conformationally restricted asymmetric BODIPY.[33]

In the described above synthetic pathways, preparation of the desired target BODIPYs was achieved by careful choice of starting pyrrole and carbonyl components. The precursors already possess all the substituents to be introduced into the BODIPY core. In other words, the starting materials have been prefunctionalized, and the general synthetic strategy can be considered as prefunctionalization of BODIPY. Nonetheless, because of the chemical robustness of BODIPY core, its structure can be also modified after creation of the boradiazaindacene framework. The postfunctionalization strategy[18, 21] dramatically extends the diversity of the BODIPY family and opens access towards new dyes, which could not be synthesized by another approach. Both methodologies have its advantages and drawbacks and should be considered as complementary rather than competitive synthetic pathways.

Postmodification at *meso*-position is readily available by using 8-thiomethyl BODIPY, which was first prepared by Goud et al. (figure 1.12).[31] To synthesize this very important synthon, thiophosgene has been used instead of carbonyl compounds in the condensation reaction with pyrrole. The obtained thioketone was further reacted with methyl iodide to produce dipyrromethene hydroiodide (alkylation occurred at sulphur), following the common procedure to yield BODIPY.

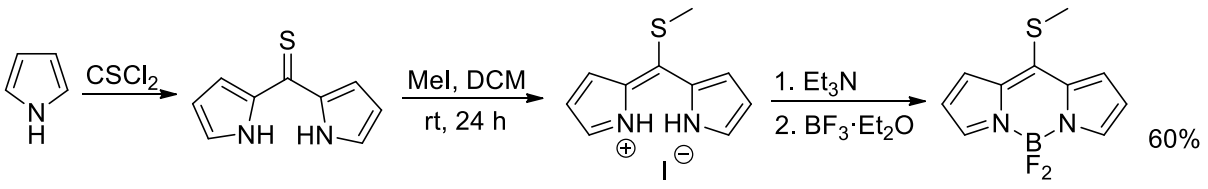

Figure 1.12. Synthesis of Bielmann's BODIPY.[31]

A variety of different groups can be introduced into *meso*-position of such BODIPY by using the Liebeskind–Srögl cross-coupling reaction (figure 1.13)[34] or via S_NAr processes.[35]

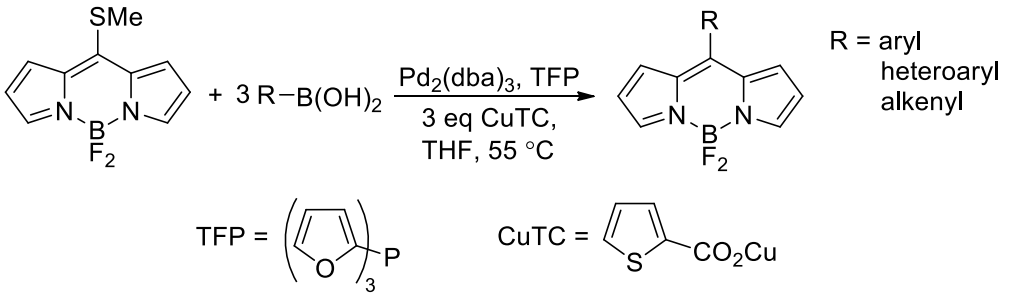

Figure 1.13. Cross-coupling of 8-thiomethyl BODIPY described by Peña-Cabrera and coworkers.[34]

Meso-halogenated BODIPYs are also important substrates for postderivatization. In the synthesis reported by Leen et al.,[36] halogen is introduced through deoxygenative substitution on a dipyrrylketone. Reaction with phosphorus oxychloride (or oxybromide) leads to rapid formation of a dipyrrinium salt, which is subsequently treated with $BF_3{\cdot}OEt_2$ in basic media to produce BODIPY. This methodology was not suitable for introducing iodine into *meso*-position, and the respective 8-iodo-BODIPY was obtained from 8-chloro-BODIPY by modified Finkelstein procedure (figure 1.14).

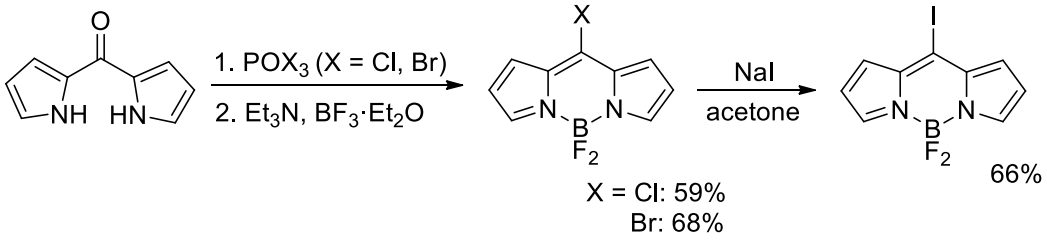

Figure 1.14. Synthesis of *meso*-halogenated BODIPYs by Dehaen and coworkers.[36]

It was shown[36-37] that (like for 8-thiomethyl BODIPY) halogen in *meso*-position can be substituted by various nucleophiles in S_NAr reactions; these substrates are also active in Pd-catalyzed Suzuki, Stille, and Sonogashira cross-couplings (figure 1.15).

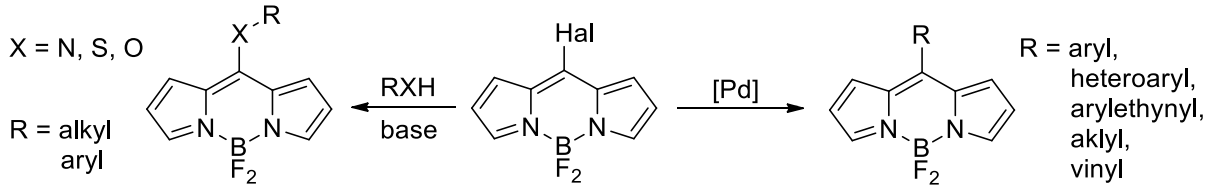

Figure 1.15. Reactivity of *meso*-halogenated BODIPYs.

Postfunctionalization at α position(s) of BODIPY core can be done by various techniques.[18] The most important ones include transformations of α-haloganated BODIPYs,[38] which can be prepared either from suitably halogenated pyrroles,[39] or by halogenation of dipyrromethane intermediate,[29, 40] or directly from BODIPY[41] (figure 1.16).

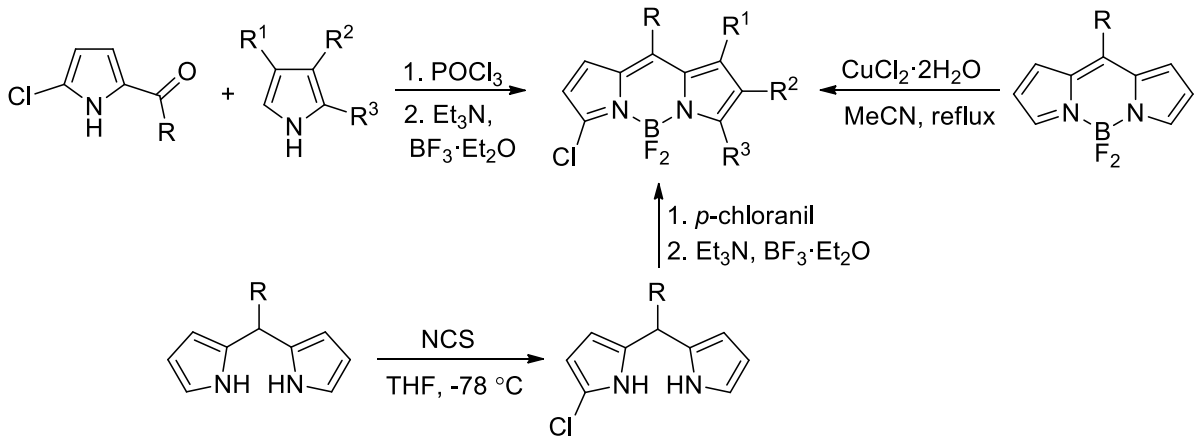

Figure 1.16. Synthetic pathways towards α-chloro-BODIPY.

Similar to *meso*-chloro-BODIPY, α-chlorinated BODIPYs readily undergo S_NAr substitution reactions (figure 1.17).[27b, 40, 42] Monosubstitution easily proceeds at room temperature, while for disubstitution higher temperatures and/or longer reaction times are required. A variety of substituents can be also introduced by Pd-catalyzed Stille, Suzuki, Heck, Sonogashira and Negishi cross-coupling reactions (figure 1.17).[43] Selectivity between monosubstitution and disubstitution in the latter case can be achieved by applying one or two equivalents of the respective coupling partner.

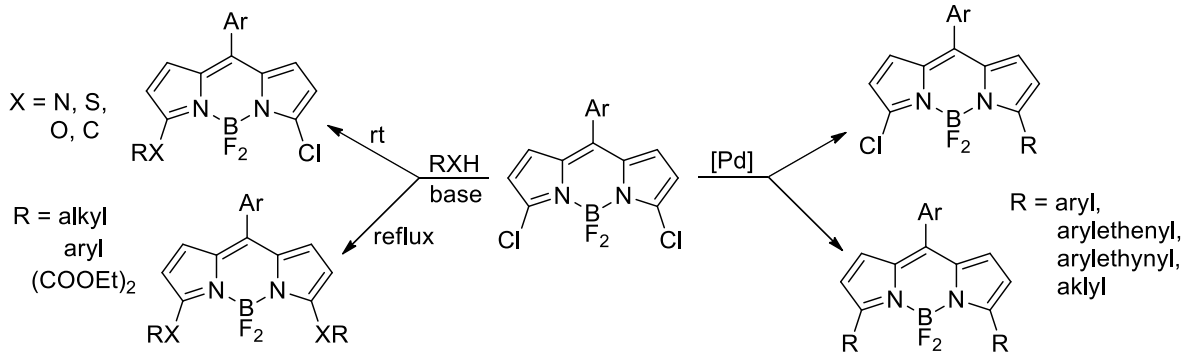

Figure 1.17. Reactivity of α-chlorinated BODIPYs.

To introduce different groups directly into α position(s) of 3,5-unsubstituted BODIPYs (avoiding halogenation step), some modern procedures have been developed: oxidative nucleophilic substitution,[44] vicarious nucleophilic substitution,[45] palladium-catalyzed C–H arylation,[46] radical C–H arylation.[47]

In contrast to others, the β position of BODIPY core is often modified via electrophilic aromatic substitution reactions (S_EAr): halogenation[48], formylation[49] and sulfonation[50] are the most typical examples. Also as in other cases, a special role is devoted to 2,(6)-halo-BODIPYs[38-39], which are active in Suzuki and Sonogashira cross-coupling reactions (figure 1.18).[39, 51] In the same time S_NAr processes for these substrates are not known.

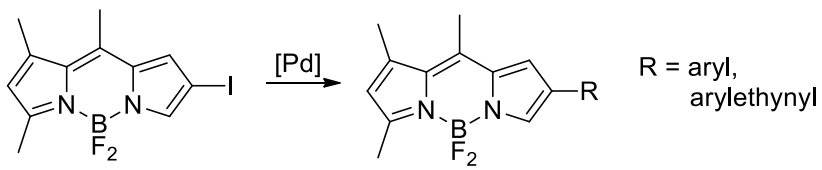

Figure 1.18. Pd-catalyzed cross-coupling reaction of 2-iodo-BODIPY described by Dehaen and coworkers.

1.3. Application of transition-metal complexes labeled with BODIPY

Being at the intersection of organic and inorganic chemistry, organometallic compounds are a crucial part of modern chemical science. The special role in this field is devoted to transition-metal complexes because of their exceptional chemical properties and reactivity.[52] Just as an example it is worth to mention the revolutionary impact of transition-metal catalysis on the development of modern organic chemistry awarded by various Nobel prizes. Nowadays, transition-metal organometallic complexes have found a wide variety of applications both in industry and academia.

This chapter describes various reactions and applications of well-defined transition-metal complexes, which are tagged with BODIPY fluorophore. Such species can combine useful properties of the organometallic compounds and light absorbing/emitting capability of the dye. Besides the outstanding photophysical properties (e.g. high brightness and photostability), BODIPY has other unique characteristics, which makes it preferable to combine with transition metals. First of all, BODIPY core doesn't contain functional groups suitable for complexation with transition metals and therefore remains sufficiently chemically inert to not interact with (active) transition-metal center. Another important point comes from the fact that the molecules of typical fluorophore and metal complex are in the same size range. The use of relatively small BODIPY ensures (or at least significantly reduced) possible steric interference between fluorophore part and transition-metal side. One more useful property of BODIPY is the possibility of versatile chemical modifications of its core, which facilitate tethering of this dye to a metal complex. Consequently, BODIPY is a very promising fluorophore for tagging transition-metal complexes.

1.3.1. Study of catalytic processes (ensemble experiments)

Understanding the mechanisms of catalytic processes is crucial for further improvements of catalytic systems towards better efficiency and selectivity. Nonetheless, direct observation of catalytically active species in solution represents a very challenging task, since the concentration level of such species is normally beyond the sensitivity range of common analytical techniques (for instance NMR). Being the most sensitive analytical tool, fluorescence spectroscopy is a promising method in the field of catalytic mechanisms study. For instance, it was used to clarify mechanistic details in ruthenium-mediated metathesis reactions[3a, 3b] or to observe palladium-catalyzed transformations.[3c] Dapoxyl and dansyl were used as fluorophores in these cases.

The application of BODIPY-tagged complexes in similar experiments was first reported by Lin and Blum.[53] The aim of their fundamental work was to show the applicability of two-ligand FRET method for the study of transition-metal systems. To achieve this task, palladium complex **1.3** tagged with donor and acceptor BODIPY fluorophores has been synthesized by reacting palladium dimer **1.1** with BODIPY-tagged phosphine **1.2** (figure 1.19). Both ligands in such complex are coordinated to one metal center, and therefore donor and acceptor fluorophores are close enough to each other for FRET to occur. Indeed, a decrease in emission intensity of donor BODIPY with simultaneous increase of acceptor intensity was observed, and a FRET efficiency of 92% was established. It was shown, that emission intensity of donor and acceptor was proportional to the concentration of the complex **1.3** over the range from 3×10^{-7} to 5×10^{-6} M. Measurements at lower concentration level were limited by the spectrometer sensitivity. At higher concentrations, the impact of intermolecular FRET or self-

quenching became significant. Thus, together with other additional experiments, it was proven that at the concentration range of the experiments the changes in fluorescence intensities of donor and acceptor fluorophores occurred exclusively due to intramolecular FRET within complex **1.3**.

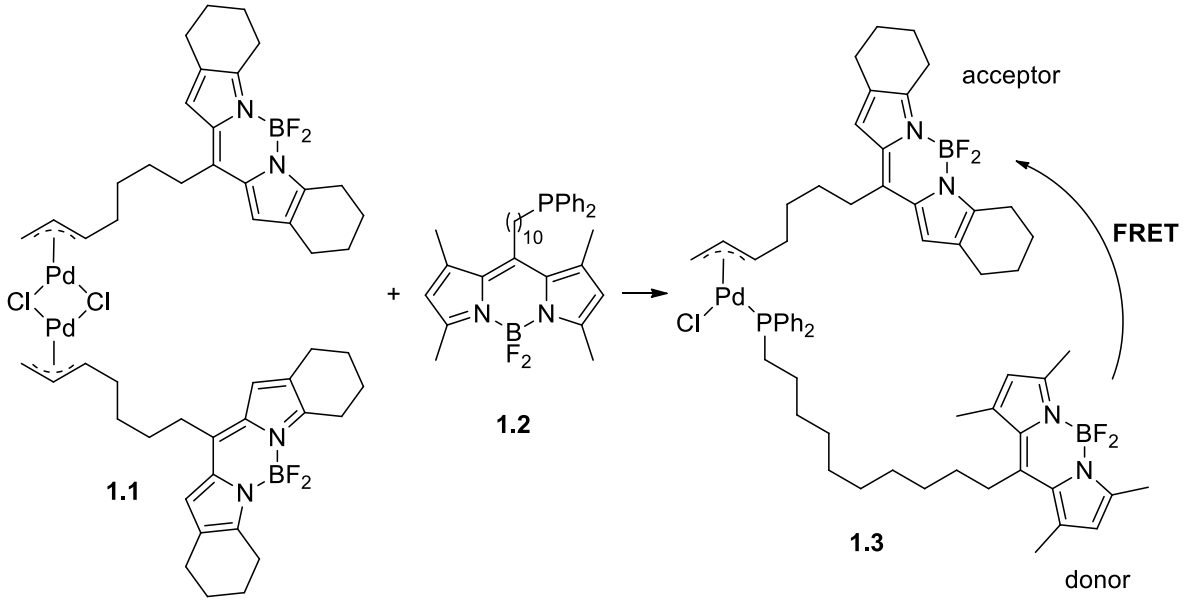

Figure 1.19. Synthesis of complex **1.3**.[53]

The formation of complex **1.3** can be observed directly in the cuvette of the spectrometer. Upon mixing of stoichiometric amounts of phosphine **1.2** and complex **1.1** in one portion, the rapid increase of acceptor emission intensity was observed. The final intensity level was almost the same as predicted for the full conversion. The addition of aliquots of phosphine **1.2** to the solution of complex **1.1** resulted only in a partial increase of fluorescence intensity respectively to the rate of conversion. The changes of fluorescence intensity were monitored in real-time. The authors also stressed that the proposed analytical method can be performed at much lower concentration level with faster resolution time than is accessible for NMR spectroscopy. Based on the elementary ligand-exchange reaction, this groundwork has shown that fluorescence spectroscopy is a suitable analytical technique for the observation and quantification of the transformations of transition-metal complexes at the micromolar concentration level.

Recently, Navarro et al. have shown[54] that cleavage of the triazolylidene palladium dimer **1.4** with acridine led to the moderate (around 8%) decrease of fluorescence intensity of BODIPY fluorophore (figure 1.20). Addition of DMAP, instead of acridine, didn't influence the fluorescent intensity, which defined DMAP as a spectator ligand. In the same time, being more donating, DMAP can substitute acridine in complex **1.5** to form complex **1.6**, which led to an increase of fluorescence intensity. Based on this observation, the authors have suggested that fluorescence spectroscopy can be used for monitoring other ligand-exchange reactions of the complex **1.5** and, more generally, for investigation of catalytic transformations caused by this precursor.

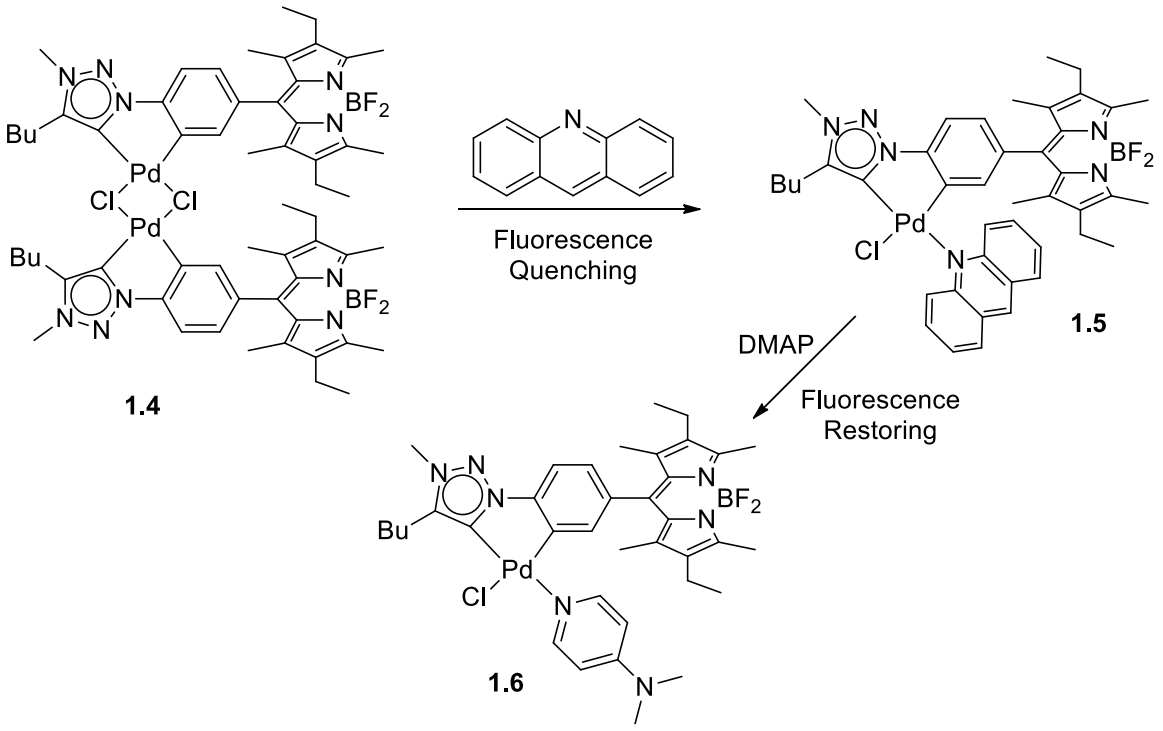

Figure 1.20. Transformations reported by Navarro et al..[54]

Blum and coworkers have used fluorescence microscopy techniques to study various organometallic transformations. By imaging the location of the nascent polymers relative to a solid surface of single crystals of Grubbs II catalyst, metathesis polymerization was revealed to be solely homogeneous rather than heterogeneous or both.[55] Two-fluorophore experiments revealed the "dumbbell" polymer morphology, which was shown to be originated from physical strand aggregation/precipitation rather than chemical attachment.[56] In more recent work,[57] fluorescence microscopy has been applied to study the oxidative addition of organohalides to metallic zinc powder. Upon mixing of the model alkyl iodide **1.7** with zinc, the appearance of bright fluorescent spots on the surface of zinc particles was observed (figure 1.21). It was unambiguously established that the observed fluorescence was due to the formation of an oxidative addition product rather than nonspecific physisorption or Lewis acid/base coordination. Moreover, the role of lithium chloride, which is known to facilitate the formation of organozinc reagents,[58] was also revealed. It was shown that the addition of lithium chloride led to the solubilization of the formed organometallic species and re-exposure of zinc surface for further substrate insertion. Concurrent complexation of both lithium and chloride was determined to be important for enhancing the solubility of the surface species. This work describes the first example of successful fluorescence spectroscopy application for the determination of the mechanistic role of a reagent in organic/organometallic synthesis.

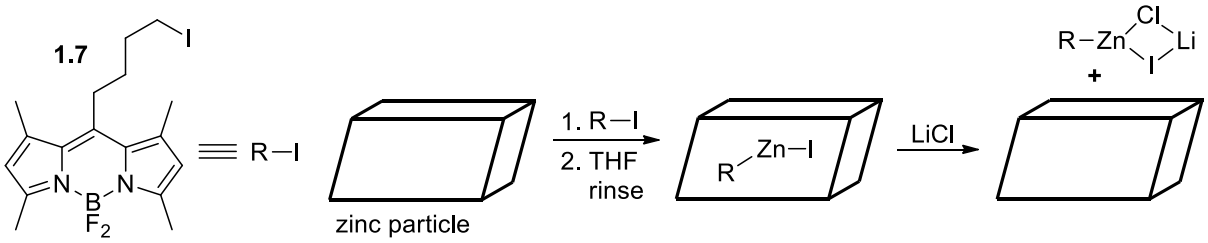

Figure 1.21. General schematic of the experiment reported by Feng et al..[57]

1.3.2. Study of catalytic processes (single-molecule experiments)

Compared to ensemble experiments, which provide averaged spectra of billions of molecules, the main fundamental advantage of single-molecule fluorescence microscopy (SMFM) is the chance to record signal evolution of individual fluorophores.[9] As a consequence, it is possible to study reaction kinetics avoiding high-speed mixing or other synchronization methods. Also, in the case of macromolecules, fluctuations of their structure can be seen directly using SMFM, which is not possible in ensemble-averaged measurements. However, most single-molecule techniques require immobilization of substrate, which limits SMFM application to the investigation of surface processes.

Even though the first applications of SMFM for studying biological systems were reported almost 30 years ago,[59] its usage for monitoring transition-metal transformations started developing only in the last decade.[60] Cordes and Blum in their perspective[4] identified the following reasons for this lag: lower substrate specificity of transition-metal complexes compare to biomolecules, which complicates the elimination of non-specific background signals; absence of commercially available fluorophores designed specifically to probe chemical systems; more strict requirements for the experimental conditions in case of air-sensitive transition-metal complexes, whereas biophysical systems normally tolerate ambient conditions. Despite the mentioned problems, noticeable progress in this area has been recently achieved.[4, 61]

The first SMFM imaging of fluorophore-tagged transition-metal complex outside of biological systems was reported by Canham et al. in 2008.[62] BODIPY-tagged palladium (II) complex **1.8** has been synthesized and immobilized on the surface of glass coverslip (figure 1.22). The covalent character of the immobilization was proven by polarization-modulation Fourier transform IR reflection-absorption spectroscopy (PM-FTIRRAS). Individual molecules of the complex **1.8** were successfully observed by using SMFM. This groundwork represents the first step in the development of the single-molecule study of transition-metal complexes.

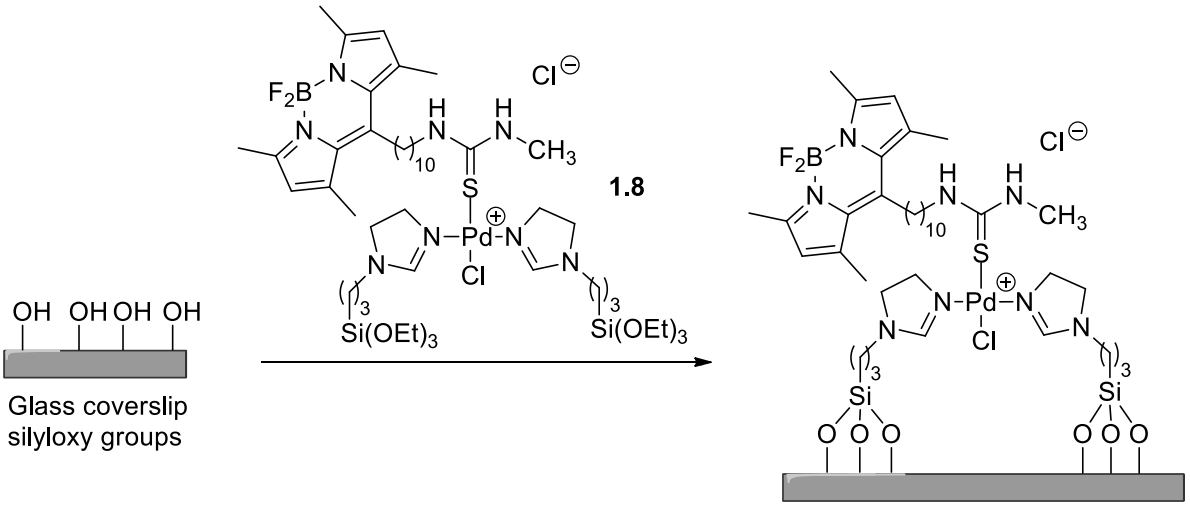

Figure 1.22. Immobilization of BODIPY-tagged palladium complex on a glass coverslip.[62]

The next obvious step to try would be observing by SMFM an elementary event of transition-metal catalysis – a ligand-exchange reaction. This was done by Esfandiari et al..[63] The concept, introduced by the authors, is shown in figure 1.23. The water molecule in BODIPY-tagged platinum complex **1.9** can be easily substituted by sulphur-containing ligand. In case

this ligand is bonded to the surface, the formation of Pt–S bond would result in bonding of complex **1.9** to the surface as well. In the conditions of total internal reflectance fluorescence (TIRF) excitation mode, only surface-bonded species can be observed by SMFM. Therefore, only ligand-exchange events would produce signals, which indeed were successfully monitored at single-molecule level in real time.

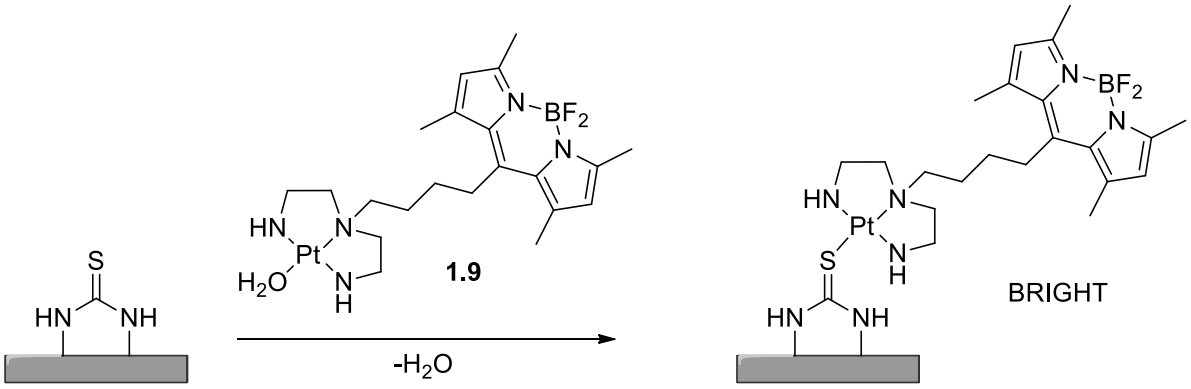

Figure 1.23. Schematic representation of the experiment reported by Esfandiari et al..[63]

These experiments have also provided useful information about reactivity distribution on triethoxysilane-modified surfaces, which are used in industry as a catalyst support. Such type of information is not available by other traditional methods. Superlocalization techniques allowed to localize chemical processes on the surface with accuracy up to ±11 nm, i.e. below the diffraction limit. It was shown that the observed chemical transformations are uncorrelated which means the chemical reaction of one metal complex did not influence the location of a future chemical reaction of another metal complex. By using SMFM it was also possible to determine the kinetics of ligand-exchange reactions on the surface, and the biexponential first-order profile was found. Deconvolution strategy was applied to obtain this result.

Surface-supported molecular catalysts attract the attention of chemists due to their ease of recovery and potential recyclability. However, kinetic investigations of this type of catalysts by common spectroscopic techniques are hampered because of surface heterogeneity and biphasic conditions. In 2016, Goldsmith and coworkers have shown[64] how SMFM can be applied to study the initiation dynamics of an operational surface-supported palladium catalyst. The prepared fluorescent complex **1.10** (figure 1.24) contained BODIPY moiety covalently bound to the pyridine ligand. Catalyst initiation upon base addition led to the release of the ligand, which then diffused quickly out of the excitation volume and didn't longer emit. Therefore, loss of the fluorescence signal at a single complex can be correlated with the start of initiation at that individual complex.

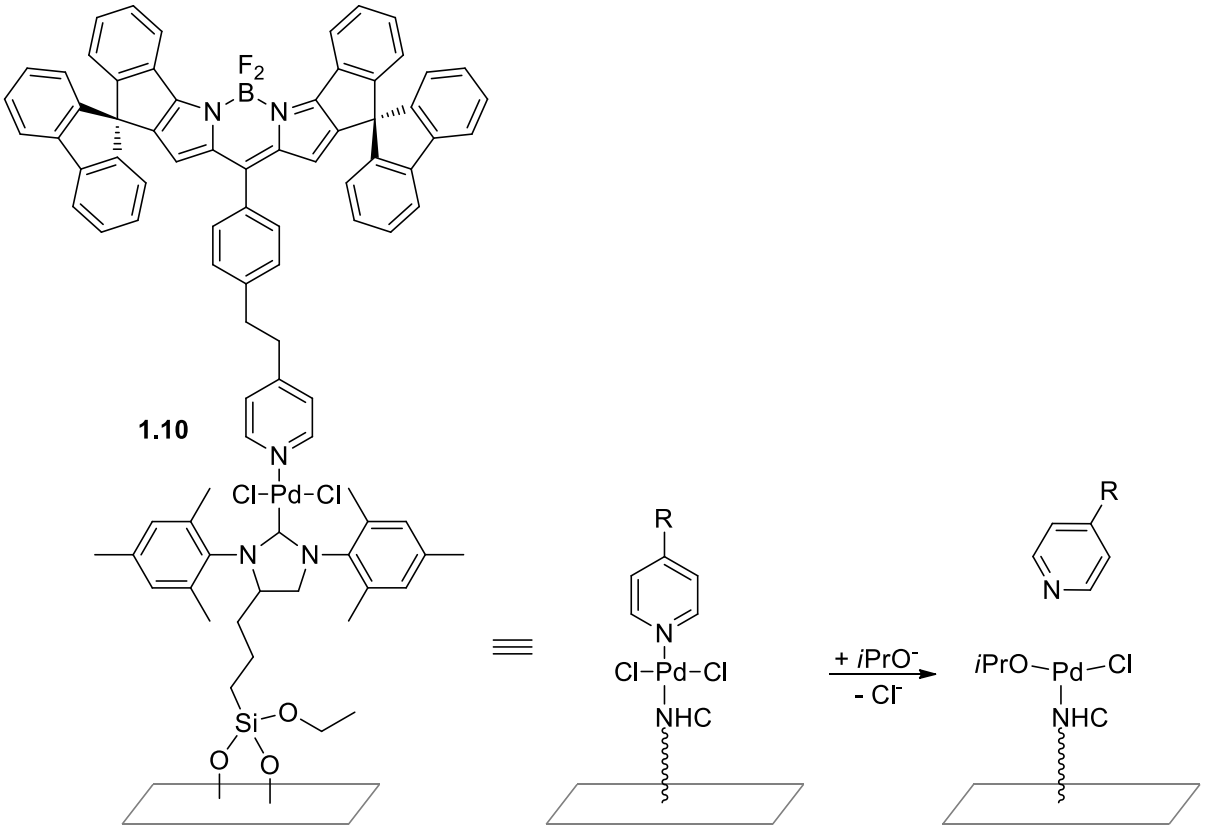

Figure 1.24. General schematic of the experiment reported by Goldsmith and coworkers.[64]

Analysis of the rate of signal loss during the catalyst initiation has revealed highly heterogeneous kinetics. This result was attributed to the presence of different local microstructures on the surface. Although their exact structures are still unknown, the obtained data allowed the evaluation of different hypotheses, resulting in a plausible structure−reactivity model. This work provided the first direct evidence that the many different physical surface microstructures detected in silyloxy tethered molecular complexes displayed different chemical reactivity.

Despite the obvious progress in the imaging of transition-metal complexes and simple ligand-exchange reactions, observation of subsequent catalytic transformations still remains a challenging goal.

1.3.3. Fluorescent chemosensors

The term fluorescent chemosensor describes abiotic compounds which are able to transform chemical information (e.g., presence and/or concentration of some particular species) into a useful fluorescence signal. BODIPY-based chemosensors have found a wide variety of applications in different areas of science.[13] Despite that, fluorophore-tagged transition-metal complexes have not been widely used for sensing purposes so far. One of the fields, where such compounds have promising sensing potential, is gas detection, in particular, carbon monoxide sensing.[5]

The development of new CO sensors is driven by the high toxicity of this gas. The need of detection at very low concentration level (less than 50 ppm) represents a challenging task. Application of highly sensitive fluorescence techniques seems to be a very promising strategy to tackle this problem. Fluorogenic probes based on luminescence transition-metal

complexes[65] are very attractive for the development of new CO chemosensors.[66] The first BODIPY-based CO probe was reported by Chang and coworkers.[67] The initially quenched BODIPY-tagged palladium dimer **1.11** fell apart upon reaction with CO (figure 1.25). The released free BODIPY showed very bright fluorescent emission, which can be easily detected.

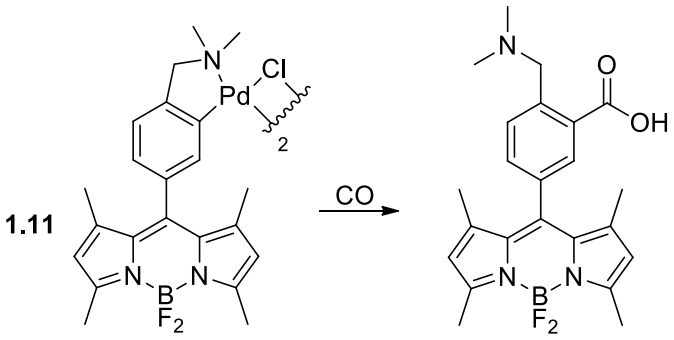

Figure 1.25. BODIPY-based CO probe reported by Chang and coworkers.[67]

BODIPY-tagged transition metal complexes for CO sensing, in which the fluorophore plays a spectator role, were developed by Plenio group. In 2015, Kos and Plenio have reported[68] [(NHC)MX(cod)] complexes **1.12**-**1.15** (M = Ir, Rh; X = Cl, I; figure 1.26), which contained a BODIPY moiety covalently bonded to the NHC ligand. Upon substitution of the labile cod ligand into stronger coordinated CO, the initially fluorescence quenched ("dark") cod complexes **1.12**-**1.15** were irreversibly transformed to the very bright carbonyl complexes **1.16**-**1.19**. Based on this observation the reported complexes were recognized to be suitable for CO detection. A similar sensing principle was used by Chung and coworkers,[66c] although $[Ru(phen)_3]^{2+}$-based subunits were used as luminescence labels in that case.

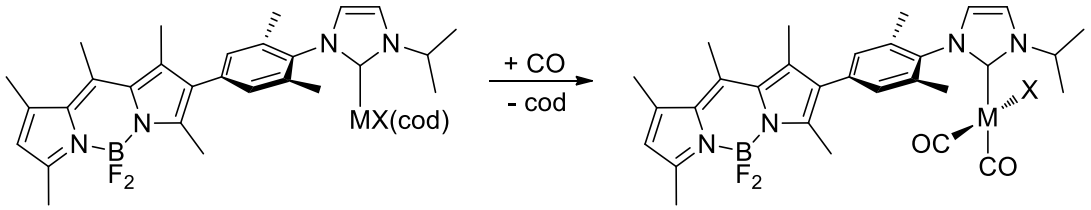

dark

	M=	X=
1.12:	Rh	Cl
1.13:	Rh	I
1.14:	Ir	Cl
1.15:	Ir	I

bright

	M=	X=
1.16:	Rh	Cl
1.17:	Rh	I
1.18:	Ir	Cl
1.19:	Ir	I

Figure 1.26. Fluorescence-based CO chemosensors reported by Kos and Plenio.[68]

High fluorescence emission of carbonyl complexes indicated that the heavy-atom effect was not a dominant quenching mechanism in this case. The authors proposed photoinduced electron transfer (PET) to be responsible for the observed fluorescence changes. This hypothesis was supported by cyclic voltammetry measurements, which established the metal center to be more electron-deficient in the case of the carbonyl rather than cod complexes. The best sensing results were observed for complex **1.14**. In case ethyl acetate was used as a solvent, bubbling of CO gas through the micromolar solution of **1.14** led to an 80-fold increase of fluorescent intensity. Moreover, the reaction was extremely fast and led to completion within few seconds. Complex **1.14** had shown high sensitivity while exposed to the atmospheric air containing less than 100 ppm of CO. It should be also noted that the final fluorescence intensity was proportional to the amount of CO in the sample.

The main disadvantage of this approach was the small Stokes shift of the complexes (no more than 25 nm), which meant very similar wavelength for the reflected excitation light and fluorescence emission. Difficulties in distinguishing emitted and reflected light can possibly cause serious problems while applying the probe for sensing in real situations. To increase the difference between excitation and emission wavelength, Halter and Plenio have recently utilized[69] a strategy based on fluorescence resonance energy transfer (FRET). Newly prepared iridium complex **1.20** (figure 1.27) contained two BODIPY units constituting the FRET pair. It has shown virtual Stokes shift of almost 100 nm, which meant green excitation and red emission light. Despite this improvement, the addition of carbon monoxide solution to the solution of complex **1.20** gave a fluorescent gain (the relationship between final and starting fluorescence intensities) of only 1.7, which is not ideal for CO sensing.

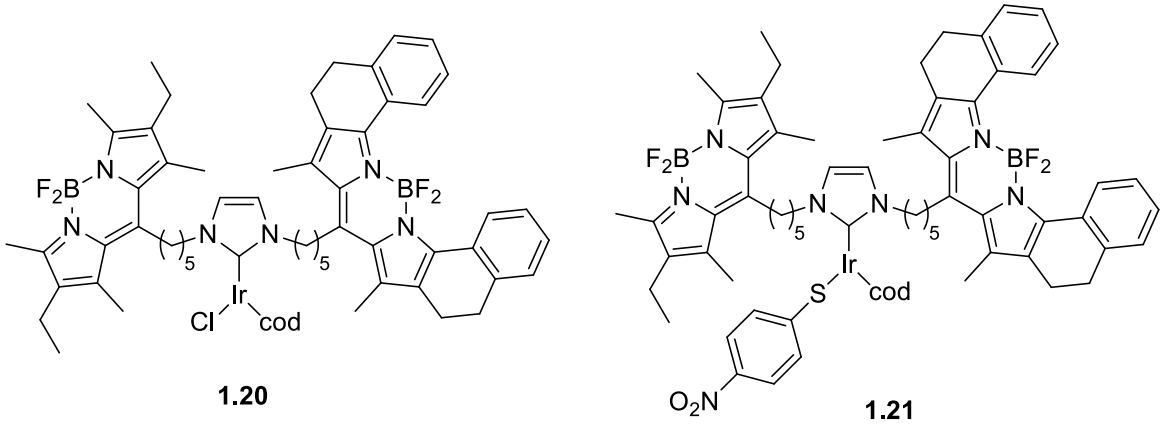

Figure 1.27. Fluorescence CO chemosensors reported by Halter and Plenio.[69]

Since PET was shown to be the dominant quenching mechanism in such systems, the authors have proposed that modulation of the electron density at the metal center could result in improved sensing properties. Thus, stable thiolato complex **1.21** (figure 1.27) was prepared by reacting of complex **1.20** with *para*-nitrothiophenol in the presence of a base, which led to the substitution of chloride into thiolato residue. Because of donating properties of thiolates, such substitution reaction caused an increase in electron density on iridium, which in turn led to quenching of the fluorescence. The emission intensity of compound **1.21** was almost three times lower than for the starting complex **1.20**, whereas upon reaction of **1.21** with CO fluorescence intensity has reached roughly the same level as in the case of **1.20** (figure 1.28). Hence, compared to complex **1.20**, the fluorescent gain for **1.21** was considerably improved and determined to be 4.3. Impregnation of an indicator paper strip with a solution of complex **1.21** allowed to obtain simple sensing device. Upon exposure to air containing 500 ppm of CO, a pronounced colour change of the fluorescent emission was observed within a few minutes. Chemosensor **1.21** has also shown excellent CO selectivity under ambient conditions. This work has introduced a fruitful strategy towards optimization of the fluorogenic probes, which is based on the fine-tuning of the electron density in fluorophore-tagged transition-metal complexes.

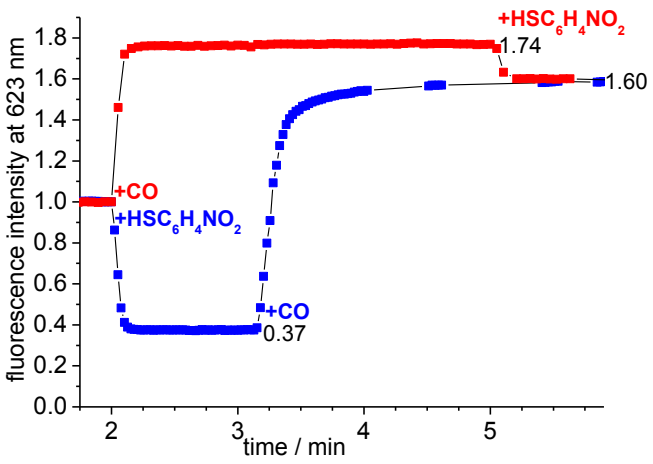

Figure 1.28. Fluorescence–time trace for the reactions of **1.20** (c = 1.0×10^{-6} molL^{-1} in 1,2-dichloroethane) with $HSC_6H_4NO_2$ (200 equiv) followed by CO (gain = 4.3; blue trace) or with CO (gain = 1.7) followed by $HSC_6H_4NO_2$ (red trace) in the presence of Hünig base (200 equiv). The fluorescence intensity of **1.20** has been set to 1.0. Taken from reference [69].

A fluorescence-based sensing approach can be also applied for detection of hydrogen. Development of hydrogen-based economy creates demand for hydrogen sensing to properly address safety issues. In 2015 Kos and Plenio reported[70] the first chemosensors for H_2 (compounds **1.22** and **1.23**, figure 1.29), which were based on Crabtree-type iridium complexes tagged with BODIPY fluorophore. As shown in figure 1.29 upon oxidative addition of hydrogen initially quenched complexes **1.22** and **1.23** were converted to much brighter **1.24** and **1.25**. The fluorescence gains were 11.7 and 9 respectively. Since oxidation state of iridium center increased during the reaction (from I to III), PET was established as the main quenching mechanism, which was in a good agreement with the above-mentioned works.

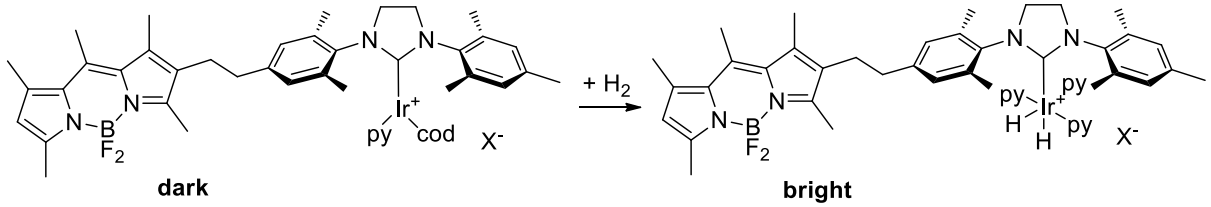

Figure 1.29. First hydrogen chemosensors described by Kos and Plenio.[70]

The impregnated paper strips have shown excellent sensitivity for hydrogen detection (figure 1.30). The distinguishable fluorescent brightness of paper strip was observed even at H_2 concentration of 4% – lower explosion limit. The fluorescent probes **1.22** and **1.23** were also used for monitoring of the catalytic hydrogenation reaction with different alkenes. The increase of fluorescence intensity during the reactions was very similar to the formation of dihydride species alone in the absence of alkene substrates. Based on this observation the authors assumed that the iridium dihydride species were the dominant ones in the catalytic reactions. Hence, probes **1.22** and **1.23** were shown to be not only efficient hydrogen chemosensors but also useful for the analysis of catalytic hydrogenation reactions.

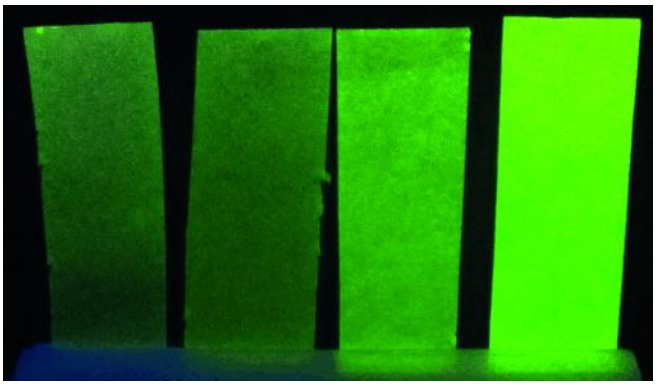

Figure 1.30. Hydrogen-sensitive paper strips.[70]

Nitroxyl (HNO), the one-electron reduced, protonated analogue of nitric oxide, is one of the reactive nitrogen species (RNS) relevant to biology.[71] Rosenthal and Lippard have reported[72] complex **1.26** (figure 1.31), which appeared to be the first fluorescent molecular probe with visible excitation and emission profiles for detecting HNO in living biological samples. Complex **1.26** was only weakly fluorescent (Φ = 0.01), which was attributed to PET from BODIPY to the bound Cu^{2+} ion. However, reduction of Cu^{2+} ion, for instance, with cysteine led to the restoring of fluorescence emission. Treatment of complex **1.26** with excess Angeli's salt, which generates an equimolar ratio of nitroxyl and nitrite under physiological conditions, resulted in a 4.3 ± 0.6-fold increase in fluorescence intensity, demonstrating fast HNO turn-on detection. The ability of complex **1.26** to operate in live cells was also studied and an excellent selectivity for HNO over other biologically relevant RNS, including NO, was observed.

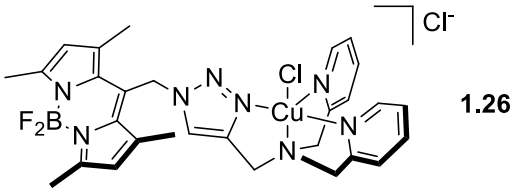

Figure 1.31. Fluorescent molecular probe for nitroxyl reported by Rosenthal and Lippard.[72]

Despite the need of further improvement, the BODIPY-tagged transition-metal complexes have been proven as promising fluorescent probes, in particular, for gas detection. It was shown that the changes in the electron density at the metal center, caused by ligand exchange, can be effectively translated into observable changes of the fluorophore brightness.

1.3.4. Triplet photosensitizers

Triplet photosensitizers (PSs) are compounds which upon photoexcitation efficiently generate a triplet excited state that is subsequently transferred to other compounds which have only a small intrinsic triplet state yield.[73] The main photophysical features of triplet PSs are the following: strong absorption of the excitation light; efficient intersystem crossing (ISC) from singlet to triplet states; a long triplet lifetime to ensure productive collisions with triplet energy acceptor. The unique properties of PSs have found wide application in photodynamic therapy (PDT),[74] photocatalytic reactions[75] and triplet-triplet annihilation (TTA) upconversion.[76]

Because of the excellent photophysical properties, BODIPY dyes are widely used as triplet photosensitizers.[77] The BODIPY core should be modified in order to enhance ISC to the triplet state. This is commonly achieved by introducing heavy atoms into its structure (bromine or iodine are typical examples),[14] although heavy-atom free photosensitizers are known as well.[78] Attachment of the BODIPY unit to the transition-metal complexes should also enhance formation of the triplet state.[6] The content of the current section is devoted to BODIPY-tagged transition-metal complexes, which show promising photosensitizing properties. The obtained conjugates were used for the singlet oxygen generation and TTA upconversion, so these topics are also briefly introduced.

The lowest energy excited state of the molecular oxygen (so-called “singlet oxygen”) demonstrates significantly different chemical behaviour from that in the ground triplet state.[79] The most convenient method of singlet oxygen generation is based on electronic energy transfer from an excited state of PS molecule to a ground state of oxygen. Because of its unique characteristics, singlet oxygen still remains at the forefront of a wide range of scientific research.[80] Cytotoxic properties of singlet oxygen have found broad application in medicine for cancer treatment. The methodology, called photodynamic therapy (PDT),[74] is based on the photosensitized singlet oxygen production and can be applied to remove ailing tissue. The application of PDT relies on a combination of three key elements: light, active photosensitizer and molecular oxygen. The PS drug is delivered to the ailing region, which is subsequently irradiated with light to generate reactive oxygen species (mainly singlet oxygen), which destroy target diseases. Because of the low half-life of singlet oxygen, its therapeutic effect can be highly localized.

Photon upconversion is defined as an anti-Stokes process in which the wavelength of emitted light is shorter than the excitation wavelength.[81] One of the possible mechanisms which allow upconversion to occur is triplet-triplet annihilation (TTA).[76] TTA upconversion is based on the combination of two different compounds: the triplet sensitizer (donor) and the triplet annihilator (acceptor). As shown in figure 1.32, at first light energy is accumulated in the triplet excited state of the sensitizer upon its excitation followed by ISC. Next, the acceptor is excited to the triplet state via triplet-triplet energy transfer (TTET) process from sensitizer. And finally, TTA occurs when excited acceptor molecules collide with each other to produce the singlet excited state of the acceptor, whose subsequent decay results in upconverted fluorescence. The efficiency of the described sequence critically relies on the relative arrangement of the energy levels both of donor and acceptor. The big advantage of TTA upconversion is the low energy density needed for sensitizing process. Even solar light can be used as the excitation source, which makes TTA upconversion very promising technique for application in various photophysical and photochemical processes.

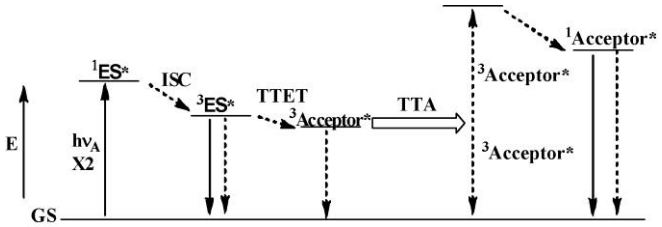

Figure 1.32. Generalized energy level diagram of the TTA upconversion processes. Solid lines represent radiative processes. GS is ground state, ES is excited state, ISC is intersystem crossing, TTET is triplet-triplet energy transfer, and TTA is triplet-triplet annihilation. Taken from reference [76b].

For the first time BODIPY-based phosphorescence was observed in the BODIPY-tagged Ru(II) polypyridine complexes (figure 1.33, compounds **1.27**-**1.29**), described by the research group of Raymond Ziessel.[82] Despite being hybrids of two well-known luminophores, the reported complexes **1.27**-**1.29** didn't show any luminescence in solution at room temperature. However, nanosecond transient absorption spectroscopy revealed the formation of a long-lived (microsecond timescale) excited state, which was identified as the BODIPY-based triplet state. In contrast to room temperature, at 77 K in a rigid matrix, the long-lived (millisecond lifetime) emission at about 770 nm was observed for these complexes. The authors have assigned the observed phosphorescence to be BODIPY-centered. It was proposed that BODIPY-based phosphorescence has occurred due to the presence of the heavy ruthenium metal and closely lying metal-based ^{3}MLCT level of the Ru(terpy)$_2$-type subunits. It should be noted that the low-temperature fluorescence of BODIPY subunit was also observed, albeit with reduced lifetimes in comparison to the corresponding free ligands.

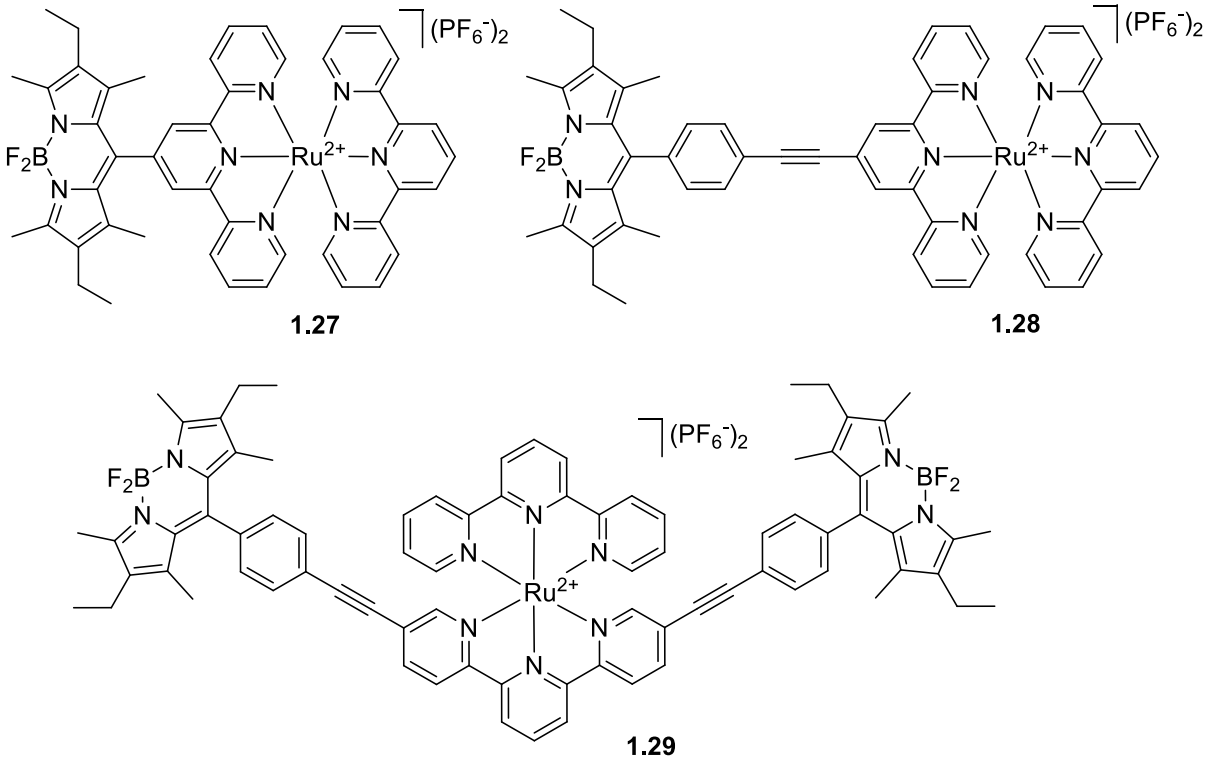

Figure 1.33. BODIPY-tagged ruthenium (II) complexes described by Galletta et al..[82]

The application of BODIPY as a visible light-harvesting ligand for Ru(II) complexes was further developed in the work of Wu et al..[83] They have reported the new complexes **1.30** and **1.31** (figure 1.34), which contain both Ru(II) polyimine and BODIPY subunits connected however by different types of linkers. Thus, in the complex **1.30** the luminophores are joined via C≡C bridge, which enables π-conjugation between BODIPY and Ru(II) polyimine subunits, whereas in the complex **1.31** the BODIPY is tethered to the coordination framework of ruthenium by phenylethynyl moiety; therefore, no conjugation is possible in the latter case.

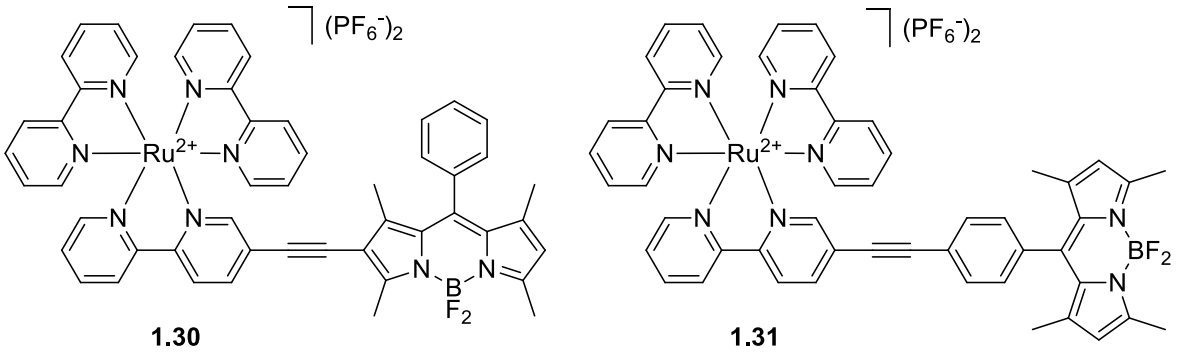

Figure 1.34. BODIPY-tagged ruthenium (II) complexes described by Wu et al..[83]

Both complexes **1.30** and **1.31** showed strong absorption of visible light. Nonetheless, only in the case of complex **1.30**, room temperature near IR (NIR) phosphorescence of BODIPY unit was observed (emission at 741 nm in deaerated solution). For Ru(II) complexes such a result was reported for the first time. It was proposed, that because of π-conjugation heavy atom effect in **1.30** was more significant than in **1.31**, which resulted in more efficient ISC in **1.30**. Fluorescence emission of both complexes was considerably quenched. In contrast, fluorescence of complex **1.30** totally disappeared at 77 K, although phosphorescence was preserved. For complex **1.30** no BODIPY phosphorescence emission was observed even at low temperature. This result is in agreement with previous work of Ziessel,[82] who observed low-temperature phosphorescence only with terpyridine-based complexes **1.27**-**1.29**, whereas analogous bipyridine-based complexes didn't show any phosphorescence.

Complexes **1.30** and **1.31** were tested as the triplet photosensitizers for singlet oxygen generation. Using 1,5-dihydroxynaphthalene as a scavenger, kinetics of singlet oxygen-mediated photooxidation was followed. Determined singlet oxygen quantum yield for complex **1.30** was 0.93, while for complex **1.31** only 0.64. The higher level of singlet oxygen production in case of compound **1.30** was associated with more efficient ISC. This result further supports that π-conjugation between BODIPY and ruthenium coordination center greatly facilitates ISC. The reported work serves a nice example to show how properties of BODIPY-tagged transition-metal complexes can be adjusted by choosing suitable linker between fluorophore and metal coordination framework. A very similar approach was used for the preparation of highly efficient triplet photosensitizers based on Pt(II) complexes[84] and cyclometalated Ir(III) complexes.[85]

Instead of Ru(II), other metal complexes were also linked to BODIPY. Nastasi et al. have reported[86] synthesis of novel BODIPY-tagged Pt(II) terpyridine complex **1.32** (figure 1.35). Compare to analogous Ru(II) species, the photophysical properties of the new complex were found to be different. In compound **1.32** fluorescence of BODIPY subunit is not significantly quenched both at room temperature and at 77 K. Although an oxidative photoinduced electron transfer is thermodynamically allowed, it is not so efficient, as in the case of Ru(II), because of unfavorable electronic factors due to the specific structural arrangement of the subunits. Under the same conditions, the luminescence of the Pt(terpy) part is almost quenched by energy transfer to the BODIPY triplet state. Analogously to Ru(II) complexes, compound **1.32** exhibited phosphorescence of BODIPY at 77 K. The reason for this is the presence of the heavy metal center.

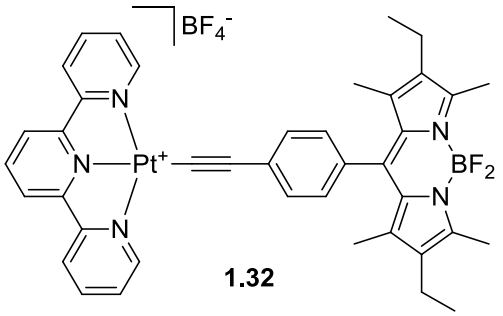

Figure 1.35. BODIPY-tagged platinum (II) complex reported by Nastasi et al..[86]

Based on the previous experience with Ru(II) complexes, Wu et al. have reported[87] new BODIPY-tagged Pt(II) complex, where the fluorophore and metal centers were connected directly with acetylide bonds in order to maximize the heavy-atom effect of platinum (figure 1.36, compound **1.33**). Complex **1.33** showed strong absorption in the visible-light range and a long-lived triplet excited state. Room-temperature NIR phosphorescence of BODIPY was also observed for this compound. The localization of triplet state on the BODIPY moiety was confirmed by steady-state and time-resolved spectroscopy, emission spectra at 77 K, and DFT calculations. Showing suitable photophysical properties, complex **1.33** was used as triplet photosensitizer for TTA upconversion. Upon excitation of compound **1.33** in the presence of a triplet acceptor (perylene), an intense blue emission can be observed even with naked eye. Irradiation of perylene alone did not produce the blue emission, which clearly supported the upconverted fluorescence. The upconversion quantum yield was determined as 5.2%. Concerning the intense absorption of complex **1.33**, its overall upconversion capability was significant.

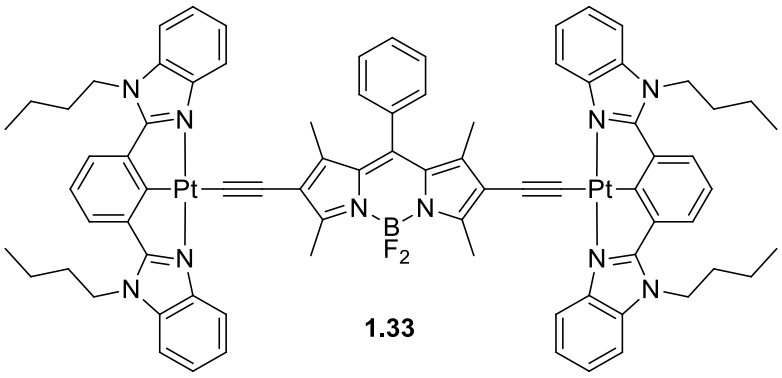

Figure 1.36. BODIPY-tagged platinum (II) complexes reported by Wu et al..[87]

In the following work Zhao and coworkers have described[88] symmetric and asymmetric BODIPY-tagged platinum(II) bis(phosphine) bis(aryleneethynylene) complexes **1.34**-**1.37** (figure 1.37). The prepared compounds have shown strong visible light absorption profile, which was red-shifted in the case of binuclear complexes **1.36** and **1.37** compared to mononuclear complexes **1.34** and **1.35**. The complexes **1.34**-**1.37** have exhibited fluorescence at room temperature, as well as weak phosphorescence. Nanosecond time-resolved transient difference absorption spectroscopy revealed long-lived BODIPY-localized triplet excited states for all complexes. This was supported by 77 K emission and spin density analysis. The compounds **1.34**-**1.37** were used as efficient triplet photosensitizers for TTA upconverted emission of perylene. Interestingly, for complexes **1.34** and **1.35** higher upconversion quantum yields were determined (19.0% and 14.3% respectively) than in the case of **1.36**

and **1.37** (3.0% and 3.5%). It was proposed the energy differences between triplet excited states of perylene and Pt(II) complexes matched better for TTA upconversion in the case of compounds **1.34** and **1.35**.

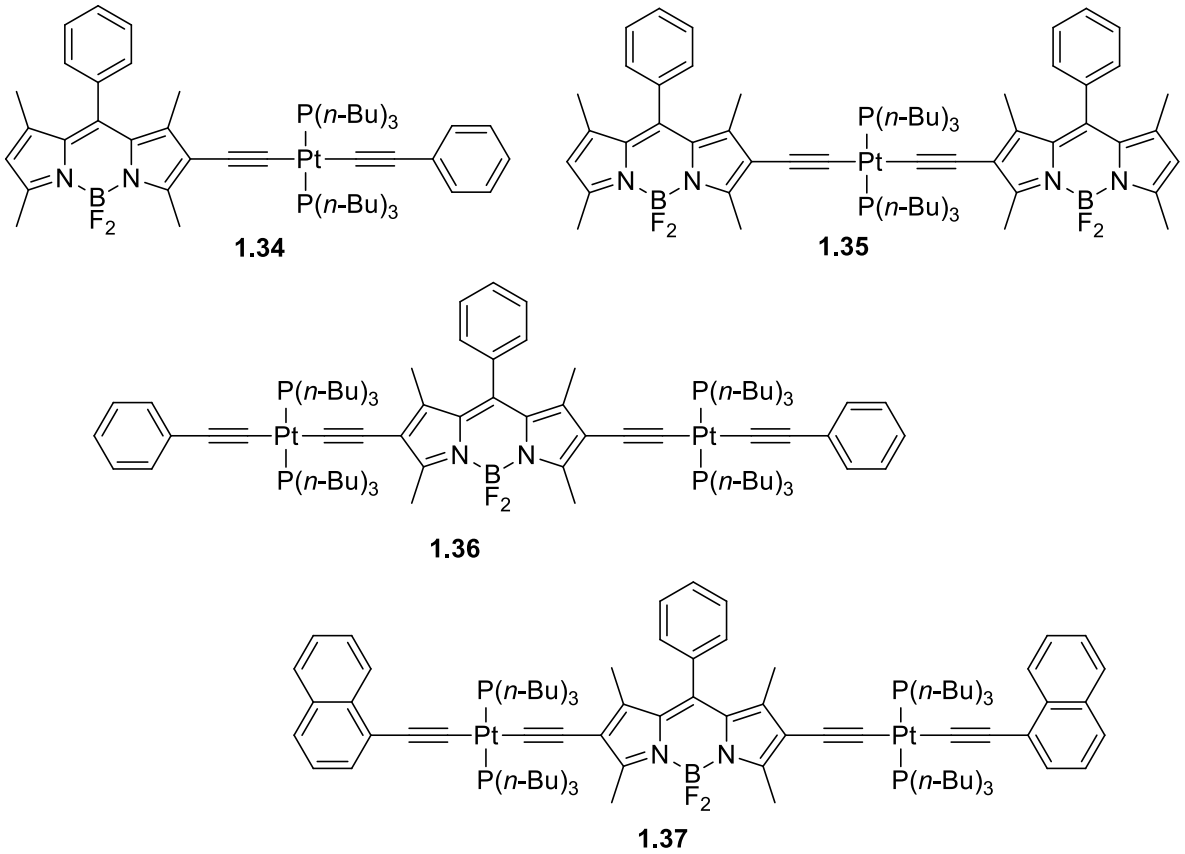

Figure 1.37. BODIPY-tagged platinum (II) complexes described by Zhao and coworkers.[88]

In order to expand the absorption wavelength range and thus additionally improve the sensitizer's efficiency, Jia et al. have further developed[89] the structure of BODIPY-tagged Pt(II) complexes (compounds **1.38** and **1.39**, figure 1.38). To achieve broadband absorption of visible light, a strategy was proposed to combine different fluorophores with different absorption profiles in one metal complex molecule. Complexes **1.38** and **1.39** contained three BODIPY subunits. Because of different coordination profiles, these subunits had different absorption wavelength. Indeed, for the complex **1.38**, the absorption band was observed in the range 450-700 nm, which was clearly much broader than for the previously reported complex **1.36** with only one BODIPY moiety attached. Complex **1.39** showed two well-separated absorption bands at 504 nm and 640 nm, which were assigned to the peripheral 4'-phenyl coordinated BODIPY and the central coordinated BODIPY subunits respectively. The absorbed photoexcitation energy was subsequently transformed into the triplet excited state energy through intramolecular resonance energy transfer (RET) followed by ISC. Complex **1.38** showed fluorescence emission and weak phosphorescence at room temperature. For complex **1.39** only fluorescence was observed. Long-lived triplet excited states were determined for both complexes. In the case of complex **1.38**, triplet excited state was distributed on all BODIPY subunits, whereas in **1.39** it was localized only on the central BODIPY ligand. Complexes **1.38** and **1.39** were used for singlet oxygen generation and showed high quantum yields (76% and 78% respectively). Successful application in multi-wavelength excitable TTA upconversion was also shown.

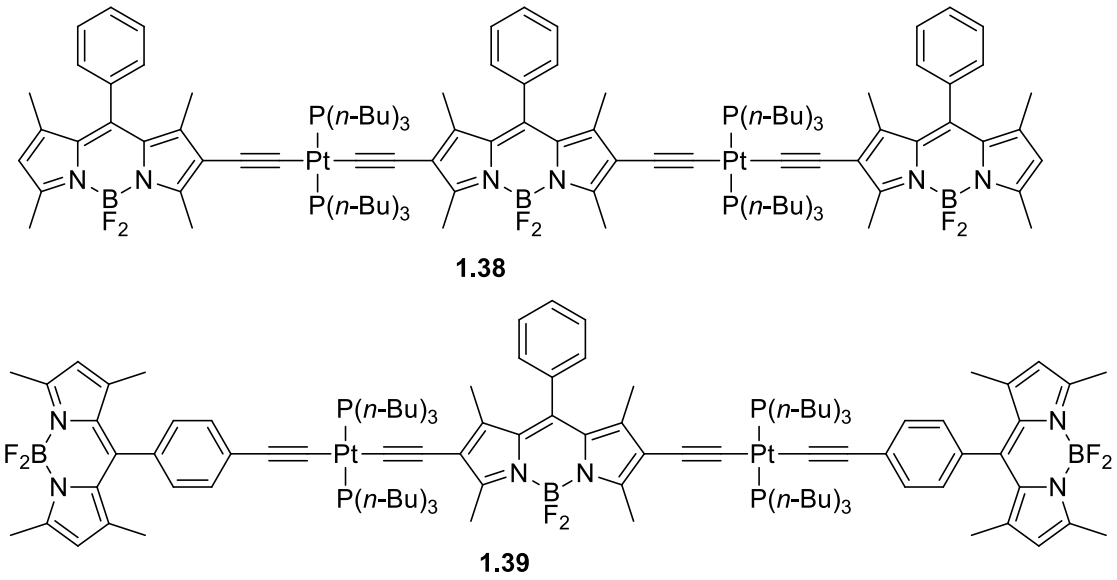

Figure 1.38. BODIPY-tagged platinum (II) complexes reported by Jia et al..[89]

Winter and coworkers have described[90] complexes **1.40** and **1.41** (figure 1.39), where platinum atom was directly attached to BODIPY ligand via its *meso*-position. Complexes *cis*-**1.40** and *cis*-**1.41** showed almost exclusively fluorescence (Φ values of 26% and 19.5%, respectively). The *trans*-configured complexes *trans*-**1.40** and *trans*-**1.41** showed dual emissions with bands centered at ca. 485 nm (fluorescence) and 640 nm (phosphorescence). The fluorescence quantum yield of *trans*-**1.41** was reduced to 7.2%, whereas the phosphorescence quantum yield reached a value of 14.2%. The data for *trans*-**1.40** were even more impressive: fluorescence quantum yield of 1.1% and phosphorescence quantum yield of 31.2% were established. More efficient ISC in case of *trans*-**1.40** and *trans*-**1.41** was attributed to the shorter distance between Pt and BODIPY in these complexes according to single crystal X-ray analyses. Since the intensity of phosphorescence emission was very sensitive to the presence of oxygen, complex *trans*-**1.40** appeared to be a very promising sensor for the ratiometric detection of oxygen up to the atmospheric level.

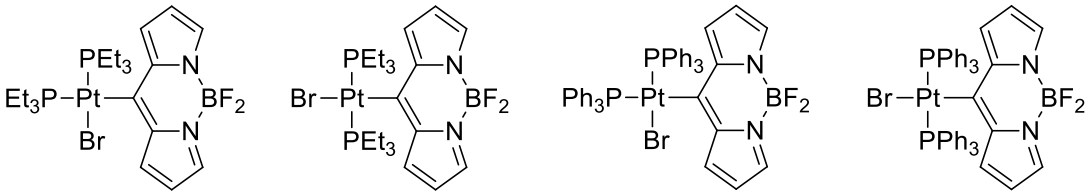

Figure 1.39. BODIPY-tagged platinum (II) complexes reported by Winter and coworkers.[90]

In the subsequent research, Winter and coworkers reported[91] new platinum (II) complexes **1.42**-**1.44** (figure 1.40), which all contained two different dye ligands connected to the platinum atom by a direct σ bond. Additional fluorophore was found to act as an antenna that funnels the light absorbed by the dye with the higher excitation energy to the one absorbing at lower energy, providing fast and efficient energy transfer. All complexes show dual fluorescence and phosphorescence emission with a maximum phosphorescence quantum yield of 41% for complex **1.43**, which is the highest value for room temperature phosphorescence from a BODIPY dye reported until now. Complex **1.43** was used for singlet oxygen generation and quantum yield of 36% for this process was found.

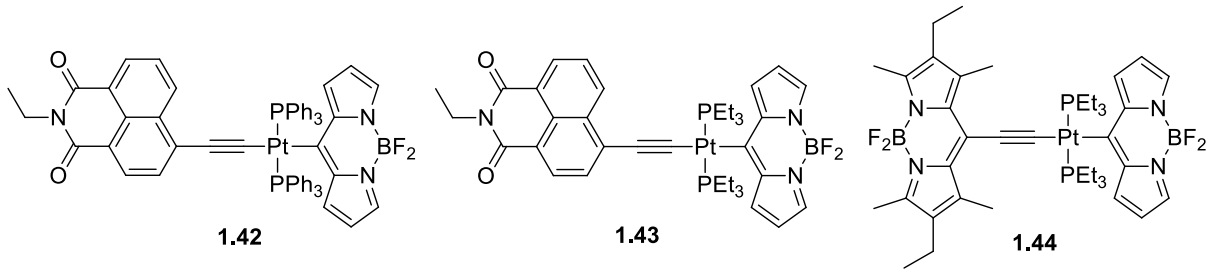

Figure 1.40. BODIPY-tagged platinum (II) complexes described by Geist et al..[91]

The first Re(I) tricarbonyl chloride complexes attached to BODIPY were reported[92] by Zhao and coworkers (figure 1.41). A π-conjugation linker, a C≡C triple bond, was used to ensure efficient ISC. Attachment of electron-donating substituent to BODIPY moiety in complex **1.46** resulted in the broader absorption band of this compound compared to complex **1.45**. In the prepared complexes only fluorescence of the ligand was observed upon excitation, not the phosphorescence of the Re(I) coordination center. However, long-lived triplet excited states were identified. Nanosecond time-resolved transient absorption spectroscopy and DFT calculations have proven the triplet excited states of **1.45** and **1.46** to be localized on the BODIPY ligands. The quantum yield of singlet oxygen production for complex **1.45** was established to be 88%, which was significantly higher than for complex **1.46** (0.06%). Most likely, less efficient ISC in **1.46** is due to ligand bulkiness. The overall TTA upconversion capability (proposed by the authors as the product of extinction coefficient and upconversion quantum yield) was 15 times higher for complex **1.45** than for complex **1.46**.

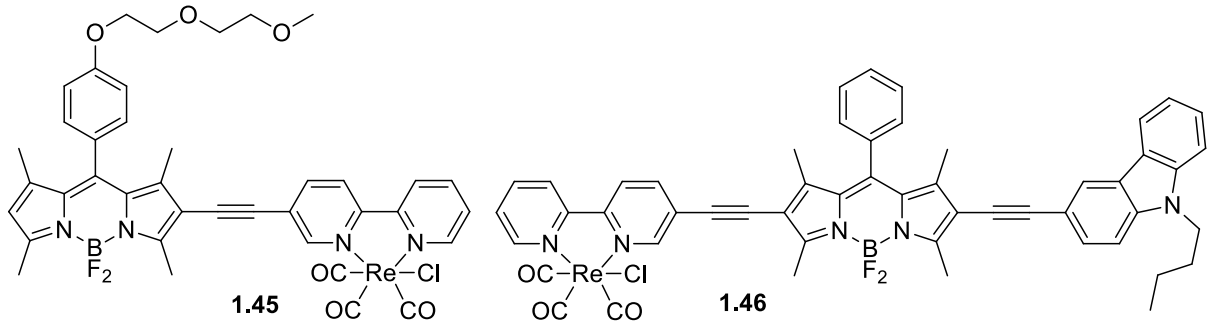

Figure 1.41. BODIPY-tagged Re(I) tricarbonyl chloride complexes reported by Zhao and coworkers.[92]

Rhenium bipyridine platforms were used for photocatalytic conversion of CO_2 to CO.[93] In order to expand the absorption profile of these compounds to visible region, Andrade et al. have prepared[94] BODIPY-tagged complex **1.47** (figure 1.42). However, photochemical activation of CO_2 mediated by **1.47** with light of $\lambda_{ex} \geq 495$ nm resulted only in trace levels of CO production. This outcome was attributed to very poor electronic coupling between the BODIPY moiety and Re center due to rather long distance between the two. This work has clearly demonstrated the importance of linker between BODIPY and metal moieties for the efficient sensitizing process.

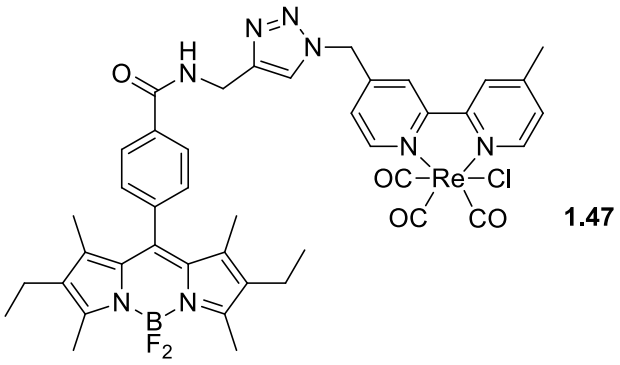

Figure 1.42. BODIPY-tagged Re(I) complex reported by Andrade et al..[94]

The first phosphorescence BODIPY-tagged iridium complex **1.48** (figure 1.43) was described by Rachford et al..[95] As expected, the luminescence of this complex at room temperature was mostly quenched due to ISC. However, at 77 K complex **1.48** showed phosphorescence at 730 nm, which was demonstrated to result from triplet state of BODIPY subunit. Such results were in a good agreement with previous investigations.[82]

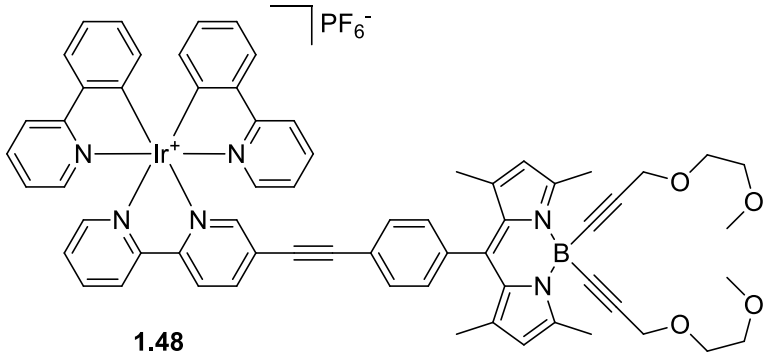

Figure 1.43. BODIPY-tagged iridium complex described by Rachford et al..[95]

An interesting approach towards NIR photosensitizers was reported by Zhou et al.,[96] who designed and synthesized hybrid organic–metal complexes **1.49**-**1.52** (figure 1.44). The implemented strategy was based on the combination of the complementary advantages of aza-BODIPY dyes and iridium (rhodium) porphyrin complexes. Thus, the obtained compounds showed strong NIR absorption of the aza-BODIPY moieties together with long-lived triplet states of transition metal porphyrins. The photosensitizing capabilities of the conjugates were investigated by applying them for the singlet oxygen production. Ir(III) complexes **1.49** and **1.50** showed high quantum yields of 0.85 and 0.79 respectively; efficiency of Rh(III) complexes **1.51** and **1.52** was lower, evaluated quantum yields were 0.27 for **1.51** and 0.19 for **1.52**. The authors have also noted remarkable photostability of the synthesized compounds. The reported results are very promising for the future developments. Thus, very recently, Xu et al. have reported[97] multi-dimensional Ni(II) and Zn(II) porphyrin-BODIPY hybrids, which might be suitable for mimicking the photosynthesis process or studying host-guest chemistry.

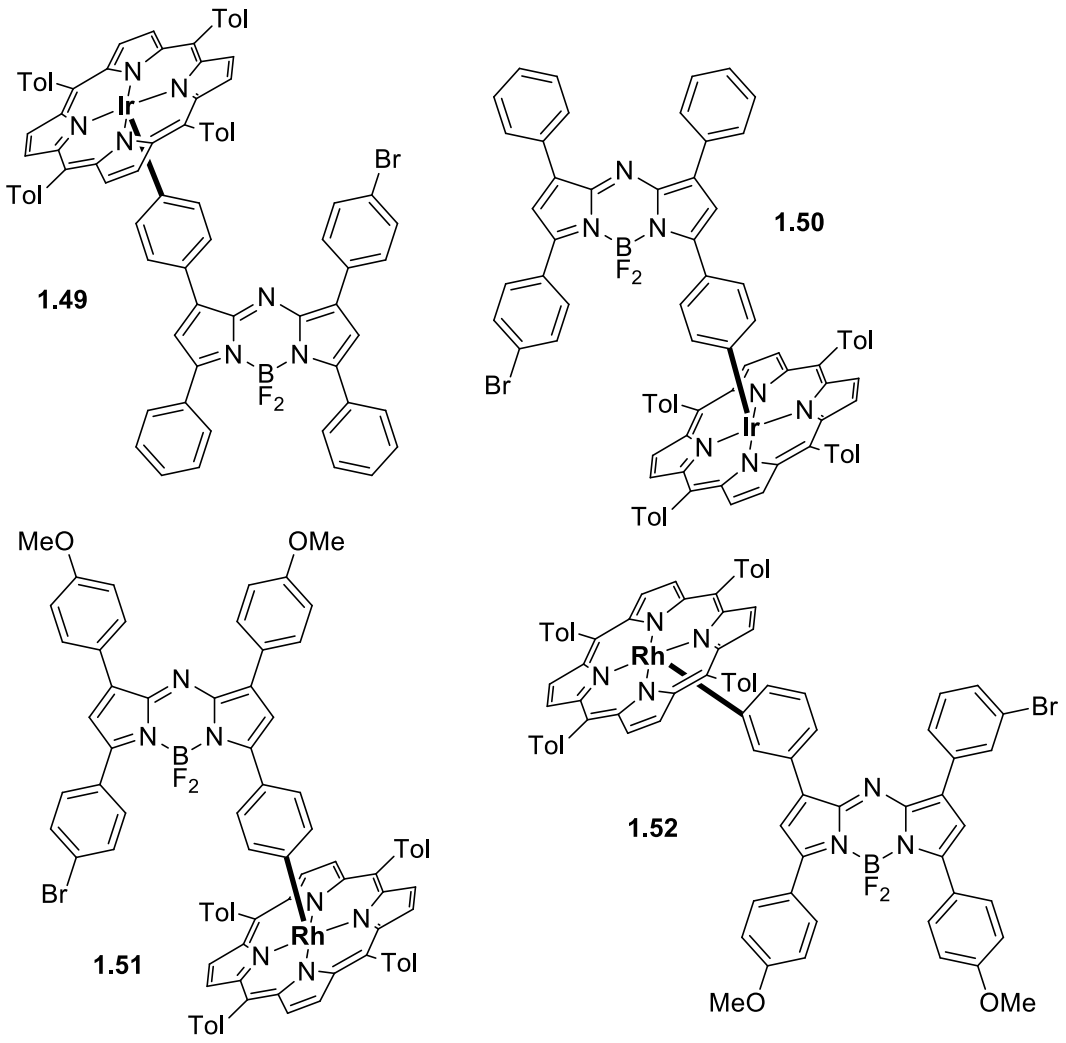

Figure 1.44. BODIPY-tagged iridium and rhodium complexes reported by Zhou et al..[96]

Very recently, Üçüncü et al. have shown[98] for the first time that BODIPY-tagged gold (I) complexes can be also used as photoactive triplet sensitizers. Absorption and emission bands of the complex **1.53** (figure 1.45) were significantly red-shifted compared to its metal-free analogue, which clearly indicated a perturbation on the π-conjugation. A significant decrease of fluorescence quantum yield (almost 12 times compare to BODIPY acetylene) for complex **1.53** as well as shorter fluorescence lifetime indicated ISC promoted by the internal heavy atom effect of Au(I). This was further proved in the singlet oxygen generation experiments. Quantum yield for the complex **1.53** was 0.84 – one of the highest values known so far. Such promising result has promoted investigation of cytotoxic properties of **1.53** *in vitro* against cancer cell lines. Significant decrease in viability was observed even at very low concentrations of complex **1.53** (EC_{50} = 2.5 nM). Weak fluorescence of **1.53** was sufficient for its visualization in the cellular medium. It was concluded that complex **1.53** passed through the cell membrane and localized particularly in the cytosol. The latter result was very interesting since it showed the reported gold complex can combine properties of both photosensitizer and theranostic (see section 1.3.6).

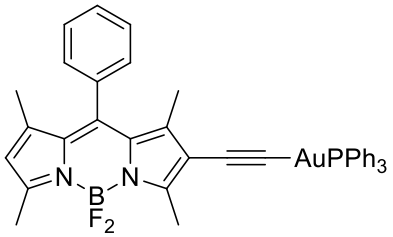

1.53

Figure 1.45. BODIPY-tagged gold complex prepared by Üçüncü et al..[98]

In general, attachment of BODIPY to certain transition-metal complexes – such as Ru(II), Pt(II), Ir(III), Rh(III) and Au(I) complexes – led in some cases to obtaining very efficient triplet photosensitizer. The main advantage of these compounds is intense absorption in the visible-light range, which is very crucial for their performance. Although the topic started to develop only recently, already obtained results showed huge potential for further development and application of this type of complexes.

1.3.5. Biological imaging

Radioimaging is a widely used technique for visualization of biological processes.[99] Although it allows sensitive detection of biological transformations deep within the body, its spatial resolution of a few millimeters is not suitable for imaging at cellular and subcellular levels. In contrast, another important imaging technique – fluorescence microscopy[100] – is characterized by the submicron resolution level, which allows accurate depiction of processes within cells. Therefore, a strategy, which is based on the complementary application of both methodologies, offers the unique opportunity to directly correlate *in vitro* and *in vivo* imaging studies. Implementation of this strategy critically relies on the development of novel radioimaging probes tagged with a fluorophore.[7]

Application of BODIPY for dual imaging purposes was substantially described by Higham and coworkers. In 2012, Davies et al. have reported[101] synthesis of the BODIPY-tagged primary phosphanes **1.54** and **1.55** (figure 1.46). As predicted by the DFT-based model,[102] these compounds were found to be air-stable both in solution and in the solid state. Moreover, the introduction of the phosphino group didn't alter significantly fluorescent properties of the BODIPY core. Variation of substituents at boron had a more pronounced effect. Fluorescence quantum yield of phosphane **1.55** was almost 8 times higher than of **1.54**, indicating the lower impact of methyl groups at boron on photophysical properties of the molecules than in the case of phenyl groups. In the subsequent research[103] synthetic routes towards **1.54** and **1.55** were optimized, which allowed multigram preparation of these compounds.

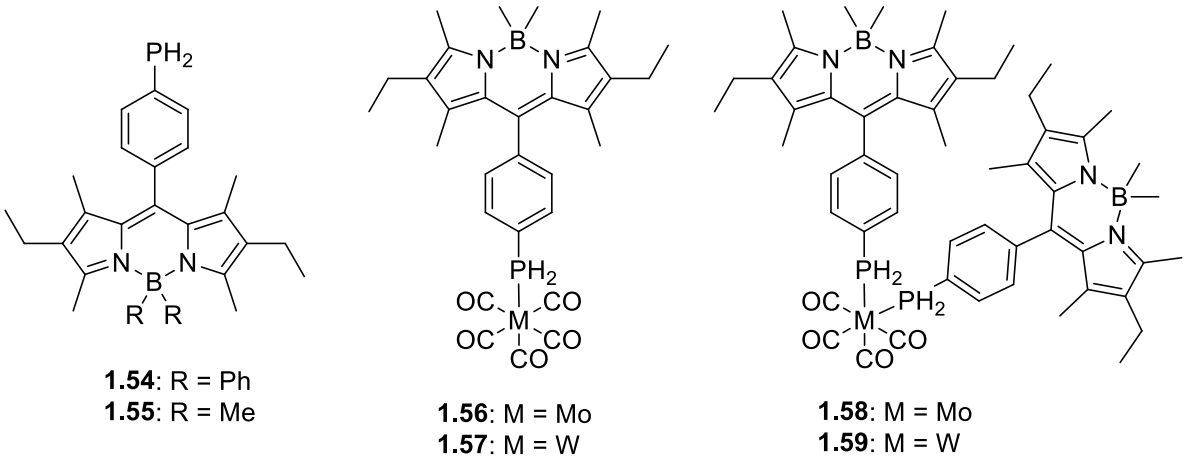

Figure 1.46. Chemical structures of phosphane **1.55**[101] and its molybdenum and tungsten complexes.[104]

Because of more favourable fluorescence properties phosphane **1.55** was chosen as the main substrate for further investigations. In order to determine how the BODIPY unit influenced the ability of phosphorus in **1.55** to coordinate to transition metals, and also to establish the effect of any complexation on photophysical properties of **1.55**, its molybdenum and tungsten complexes **1.56**-**1.59** were prepared (figure 1.46).[104] Monosubstituted complexes **1.56** and **1.57** were obtained by reacting **1.55** with $[Mo(CO)_6]$ and $[W(CO)_6]$ respectively in THF under UV irradiation. The disubstituted complex *cis*-**1.58** was obtained by refluxing *cis*-$[Mo(CO)_4(pip)_2]$ and **1.55** in dichloromethane; reaction of two equivalents of **1.55** with *cis*-$[W(CO)_4(pip)_2]$ in toluene at 75 °C for 20 h led to formation of *cis*-**1.59** as the major product. The complexes **1.56**-**1.59** were isolated and fully characterized. Structures of **1.56** and **1.58** were proven by X-ray crystallography. Spectroscopic and crystallographic properties of the prepared compounds were consistent with those found for complexes of other primary phosphanes. Fluorescence of the complexes **1.56**-**1.59** was only slightly (for **1.58** and **1.59**) or moderately (for **1.56** and **1.57**) quenched compared to **1.55**, despite the presence of the heavy metals. Hence, no essential influence of BODIPY incorporation on the reactivity of phosphane **1.55** and no significant changes of its photophysical properties upon complexation were observed.

In medicinal diagnoses the most widely used radionuclide is ^{99m}Tc.[105] Its complexes are utilized as imaging agents in single-photon emission computed tomography (SPECT).[106] Because of the similar coordination profile, rhenium is frequently used as a mimic of ^{99m}Tc.[107] To prepare fluorescent technetium and rhenium complexes Davies et al. have developed tridentate phosphine ligand **1.60** (figure 1.47).[101, 108] It was obtained by Pt-catalyzed reaction of **1.55** with two equivalents of vinyldiphenylphosphane. Observed reactivity of **1.55** in this reaction was typical for primary phosphanes. Fluorescence properties of **1.60** were only slightly changed compared to **1.55**, indicating no reductive PET (induced by the two additional phosphorus groups) has occurred. Upon refluxing of tripodal phosphane **1.60** and *mer*-$[ReCl(CO)_3(PPh_3)_2]$ in toluene, a mixture of three stereoisomers **1.61**-**1.63** was generated (figure 1.47).[108] Subsequently, it was found that reflux of the same reagents at a higher temperature, in mesitylene, led to the formation of isomer **1.61** exclusively. Fluorescent technetium complex **1.64** was synthesized from **1.60** and readily available radioactive synthon *fac*-$[^{99m}Tc(CO)_3(OH_2)_3]^+$.[109] To better correlate with the ^{99m}Tc experiments, additional rhenium complex **1.65** was synthesized by reaction of **1.60** and $[Re(CO)_5][OTf]$ in refluxing ethanol. The structures of all rhenium complexes were

characterized by X-ray diffraction. The fluorescence quantum yields of the complexes **1.61**-**1.65** were only slightly lowered in comparison to free ligand **1.60**, probably, due to ISC. Therefore, prepared probes appeared to have suitable photophysical properties for *in vitro* cell imaging.

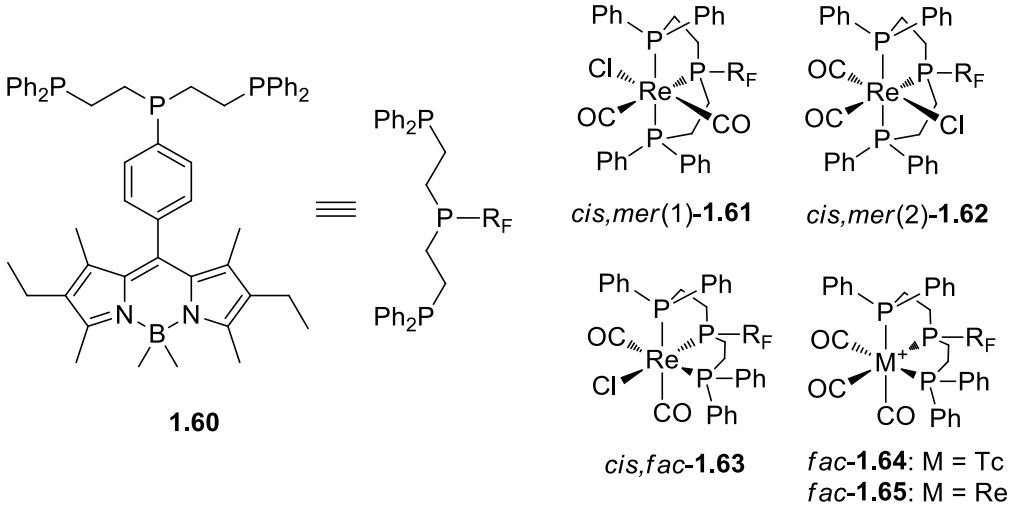

Figure 1.47. BODIPY-tagged phosphane **1.60**[101] and rhenium and technetium complexes derived from it.[108]

The authors reported that technetium complex **1.64** represented the first example of a phosphine-based, multi-functional imaging tool. The most prominent features of this complex are: a tridentate phosphine for kinetic stability; a fluorophore for *in vitro* imaging; a radioactive metal for *in vivo* imaging by SPECT.

For a preliminary screening, the rhenium complexes **1.61** and **1.65** were imaged in prostate carcinoma (PC-3) cells by epi-fluorescence microscopy. Complex **1.61** enabled visualization of organelles without any apparent cytotoxicity, whereas for **1.65** some cytotoxic effect was observed. Nonetheless, both complexes have shown negligible cytotoxicity at the concentrations required for SPECT. Therefore, these complexes were concluded to be highly appropriate for application as imaging agents.

Another imaging technique, used for tumor localization, is positron emission tomography. The copper isotope ^{64}Cu is an attractive positron emitter because of its relatively long half-life.[107, 110] Other group 11 metals radioisotopes – ^{199}Au and ^{111}Ag – have shown potential for medical application due to beta-emitting properties.[111] BODIPY-tagged coinage metals complexes were reported by Davies et al. (figure 1.48).[112] The authors have utilized fluorescent tertiary phosphines **1.66**-**1.69** as the ligands. Upon their complexation with $[Cu(CH_3CN)_4][PF_6]$ the copper(I) complexes **1.70**-**1.73** were formed. Interestingly, the metal center in these complexes is three-coordinated, although copper usually forms four-coordinated complexes.[113] Most probably, phosphine ligands **1.66**-**1.69** are too bulky for the four-coordinate structure in this case. Analogously, silver (**1.74**-**1.77**) and gold (**1.78**-**1.81**) complexes were obtained by reaction of the phosphines with $[Ag(\eta^2{:}\eta^2\text{-cod})(hfa)]$ (hfa – hexafluoroacetylacetonat) and [AuCl(tht)] (tht – tetrahydrothiophene) respectively. The structures of most substances have been additionally confirmed by X-ray crystallography. Similar to the above-mentioned BODIPY-tagged phosphines **1.55** and **1.60** and their complexes, the newly prepared compounds **1.66**-**1.81** have shown only slight variation (mostly decrease) of the fluorescence quantum yields upon incorporation of phosphine moiety and following complexation. The phenyl rings at boron lowered fluorescence much more

significantly than methyl groups. Favourable photophysical properties made these compounds very attractive for applications in medicinal imaging. The authors have also suggested that the newly prepared fluorescent complexes **1.70**-**1.81** might display cytotoxic activity. Development and application of compounds, which combines both imaging and therapeutic modalities, is disclosed in more detail in the next section.

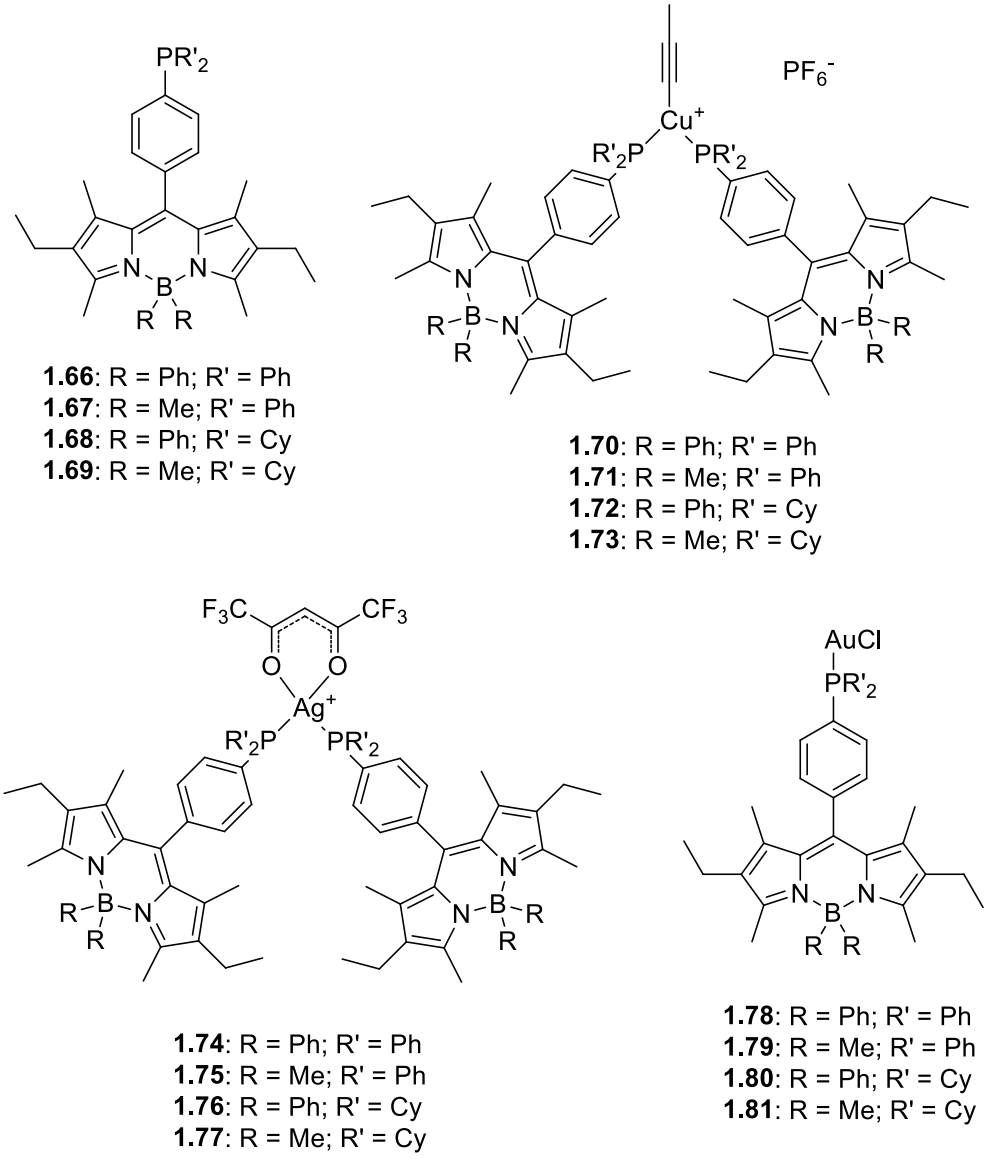

Figure 1.48. BODIPY-tagged tertiary phosphines and derived complexes.[112]

1.3.6. Theranostics

Developing new drugs and improving existing ones can be largely facilitated if the mechanisms of their action are known. This knowledge can be obtained from a combination of various biological experiments. One of the recently developed strategies for solving this problem provides the tracking of therapeutic compounds directly in biological systems. This is possible due to the tagging of drugs with imaging probes (fluorophores or radionuclides). The newly obtained compounds are commonly called “theranostics”, or trackable therapeutic agents. Thus, theranostic is a single molecule, which enables both diagnosis and therapy.

Organometallic complexes, which have been widely used in medicine (for example, for cancer treatment[114]) are one of the most suitable targets in the context of this strategy.[8, 115] Organic fluorophores[116], luminescent complexes[117] or radioisotopes[118] can be used as imaging probes.

Being very promising anticancer agents, organometallic-arene[119] and gold[120] complexes are very interesting substrates for theranostics development. In 2013, Bodio and coworkers reported the synthesis of new BODIPY-labeled phosphane **1.82**.[121] By reacting this ligand with suitable metal precursors, respective Ru(II), Os(II) and Au(I) transition-metal complexes were obtained (figure 1.49). The syntheses of complexes **1.83**-**1.85** have been optimized to give an overall yield of 28-30% in 10 steps. Quantum yields of prepared compounds remained quite high, although being partially quenched in the case of ruthenium and osmium derivatives.

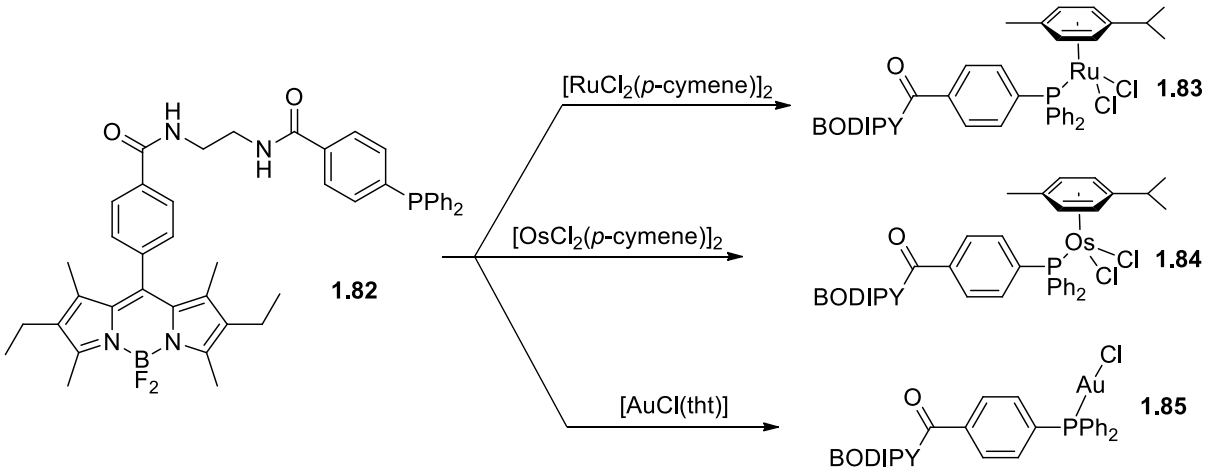

Figure 1.49. Synthesis of theranostic agents reported by Tasan et al..[121]

All three synthesized complexes have shown moderate cytotoxic properties compared to cisplatin but were much more active than posphane **1.82**. The most active was gold complex **1.85**. Bearing BODIPY residue and being water soluble, complexes **1.83**-**1.85** were suitable for detection by fluorescence microscopy *in vitro*. They were shown to rapidly bind to the biological membranes, with no clear specificity. The authors suggested such distribution properties were defined mainly by BODIPY moiety. Thus, BODIPY-tagged transition-metal complexes were shown for the first time to be promising theranostic agents for optical imaging, worthy of further development.

Based on the results above, Bodio and coworkers have continued to design new BODIPY-tagged metal complexes[122] in order to obtain theranostics with improved properties. At first, previous research has shown the gold complexes possessing the best anticancer activity as well as the highest emission intensity. Therefore, for further developments only gold complexes were used. Secondly, the linker between the fluorophore and transition-metal moieties was changed in order to improve water solubility. And thirdly, different biovectors were introduced in order to target the compounds selectively on tumors and also to further improve water solubility.

The reported new theranostics are shown in the figure 1.50. The gold complex **1.86** was easier to synthesize (three steps less and simpler purification) than one reported before (compound **1.85**). It was further modified by introduction of vectors via metallic center: two

sugar derivatives (thioglucose analogues) and a peptide (modified bombesin). In this way, three theranostic agents **1.87**-**1.89** were easily obtained, by reacting complex **1.86** with the corresponding thiolate derivatives. The obtained gold complexes showed high fluorescence quantum yield (>85%), except the complex **1.89** (Φ = 21%). The authors have suggested the origin of this quenching effect is PET between the tryptophan residue of peptide and the BODIPY unit.

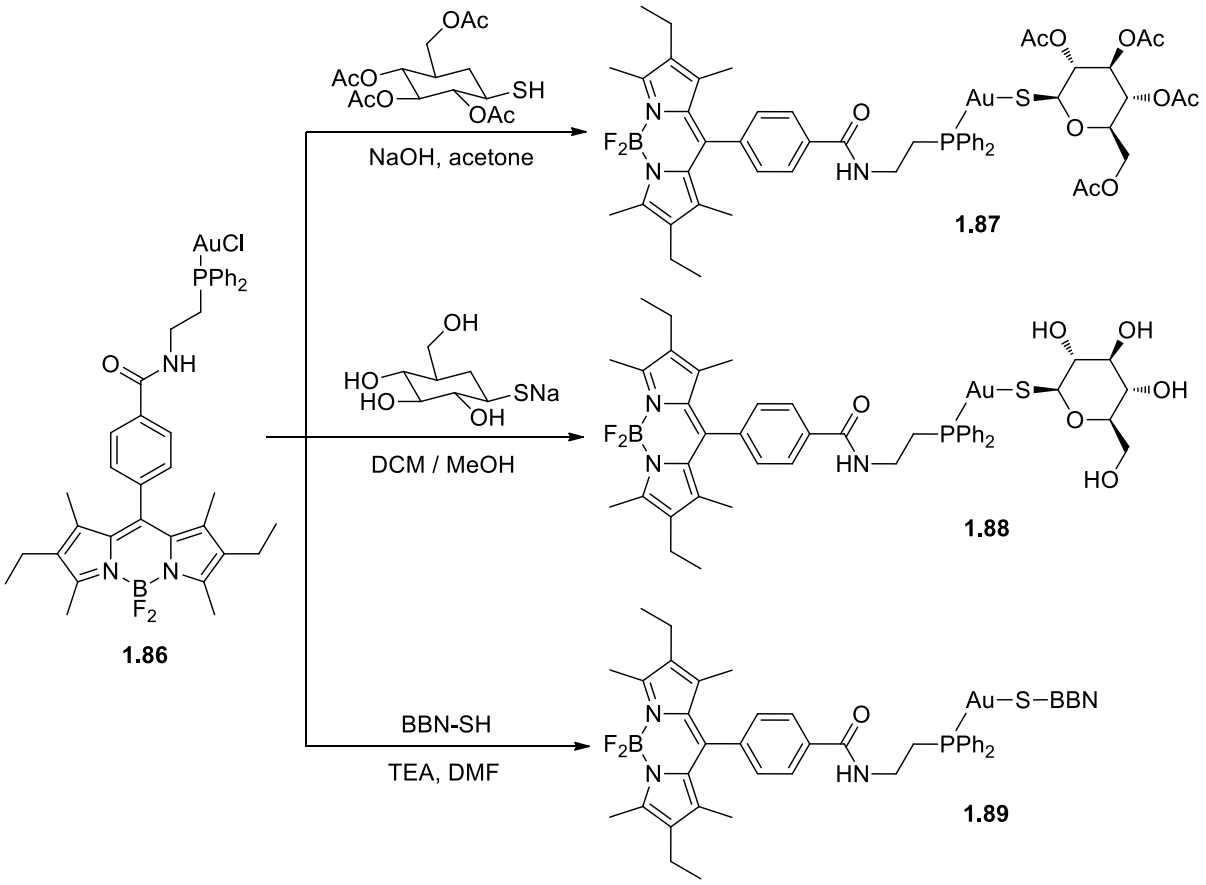

Figure 1.50. New theranostics reported by Doulain et al. (BBN-SH – a bombesin-analog agonist).[122]

The synthesized compounds appear to be cytotoxic. The authors suggested that application of biovectors allows selective targeting between cancer and healthy tissues. Despite the promising results, the application of theranostics for studies *in vivo* still remains a challenging task.

Further improvement of theranostics, based on BODIPY-tagged gold complexes, was published recently.[123] The fluorescence brightness of the reported complexes (figure 1.51) was high enough to be suitable for detection even at a very low concentration. Compounds **1.90** and **1.91** have shown strong cytotoxicity against breast, prostate, and colon cancer cell lines, and were much more active than previously reported complex **1.86**, even though they contained two Au(I) centers. An investigation by confocal microscopy showed that complexes **1.90** and **1.91** are accumulated and homogeneously distributed in the cytoplasm. Moreover, in addition to anticancer activity, compound **1.90** was also proven to be a promising anti-inflammatory agent. Further research is directed towards introducing a vector on its gold atoms or on the BODIPY core in order to induce a selective targeting of tumors.

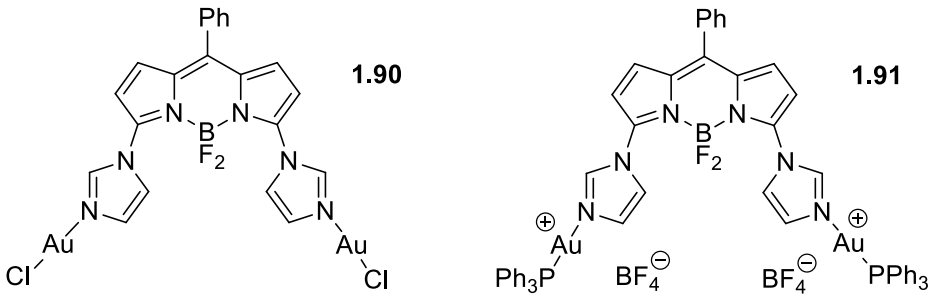

Figure 1.51. New theranostics reported by Trommenschlager et al..[123]

Another class of organometallic compounds, interesting for theranostics development, are platinum-based complexes, which have been used as anticancer drugs for decades.[124] Sun et al. have prepared[125] BODIPY-tagged platinum complex **1.92** (figure 1.52) and studied its cellular distribution and cytotoxicities in human cervical carcinoma and human breast cancer cell lines. It was shown that the cytotoxic activity of complex **1.92** was lower than that of cisplatin. Nonetheless, by using fluorescence microscopy it was possible to image the distribution of platinum complex in living cells. Compound **1.92** was found to localize predominantly in the mitochondria. Thus, the synthesized platinum theranostic agent **1.92** showed both cytostatic and imaging functionalities.

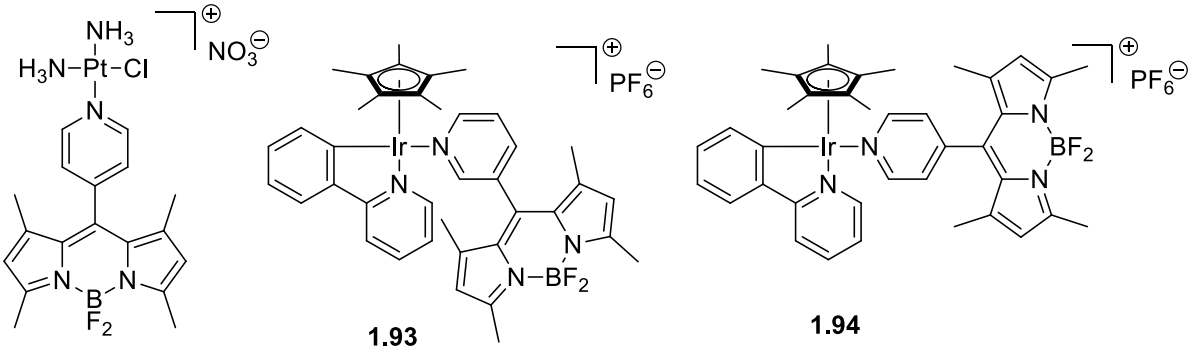

Figure 1.52. Theranostics based on BODIPY-pyridyl ligands.

It was shown recently that organometallic iridium (III) complexes also exhibit anticancer activity.[126] Zimbron et al. have described[127] synthesis and properties of new theranostic agents, based on cyclometalated half-sandwich iridium(III) complexes. Their structures are shown in figure 1.52 (compounds **1.93** and **1.94**). Due to the potentially labile bond between BODIPY-pyridyl unit and iridium metal center, the stability of the complexes **1.93** and **1.94** was tested. Full dissociation of both complexes was observed in the solution of DMSO (good coordinated solvent) after 2 days, whereas in the case of a weaker coordinated solvent such as methanol no solvolysis was noticed after 7 days. Compared to the emission intensity of free BODIPY-pyridyl ligand, fluorophores in complexes **1.93** and **1.94** were partially quenched due to complexation with iridium. Nonetheless, both complexes still displayed relatively high quantum yields (29% for **1.93** and 14% for **1.94**). Being brighter (also in water medium), complex **1.93** was chosen for further investigations. Its photostability was tested: only negligible photodissociation and photobleaching were observed upon continuous irradiation, which confirms the suitability of this compound for cellular imaging studies by fluorescence microscopy. Complex **1.93** exhibited high antiproliferative activity on a range of cancer cell lines. Authors suggested the high cancer cell cytotoxicity of **1.93** can arise from its high

lipophilicity and stability toward hydrolysis. Cell imaging studies revealed very rapid cell internalization, which indicates the complex **1.93** was membrane-permeating. As in previous examples, application of a BODIPY tag provided useful information about the dynamics of cell uptake, accumulation, and distribution of the metallodrug in living cells.

Silver has long been used as an antimicrobial agent for the treatment and prevention of infections of burns and difficult-to-treat wounds.[128] In order to follow the extent of active silver released to the wound, Mascharak and coworkers have developed[129] BODIPY-tagged silver complex **1.95** (figure 1.53). Fluorescence emission of BODIPY in this complex is quenched. However, the release of silver led to the restoring of fluorescence intensity. Therefore, complex **1.95** appeared to be suitable for tracking the delivery of silver to bacteria through turn-on fluorescence. Accompanied antibacterial efficacy arisen from silver delivering by complex **1.95** was comparable to that of silver nitrate. The authors have suggested that complex **1.95** can potentially be incorporated into a bandage material to treat burn wound infections with the advantage of real-time tracking of silver release.

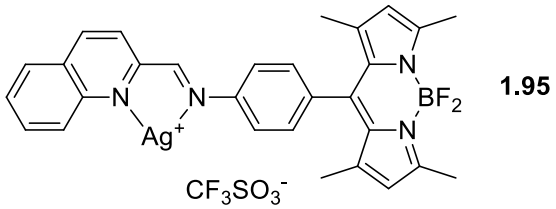

1.95

Figure 1.53. Silver complex reported by Pinto et al..[129]

The field of trackable therapeutic metal-based drugs has started to grow only very recently. That's why the current research in this area is still at its early stage, and the known theranostics are far from clinical application. Nonetheless, the observed results are very promising, which indicates a huge potential of this strategy. It should be noted, that tethering of a probe results in the formation of a new compound with modified therapeutic properties. Therefore, implementation of theranostics strategy should be done at the beginning of the research followed by the optimization process, which should be performed with the already tagged therapeutic compound. The wide variability of theranostics approach is likely to enhance the fast development of this research area.

2. Scope of the Dissertation

The aim of this dissertation was to discover the potential of fluorescence spectroscopy for the investigation of transition-metal catalyzed transformations and to reveal mechanistic insights into such processes. The current work covers the synthesis of novel BODIPY-tagged transition-metal complexes and their application in the ensemble fluorescence experiments as shown in the following scheme:

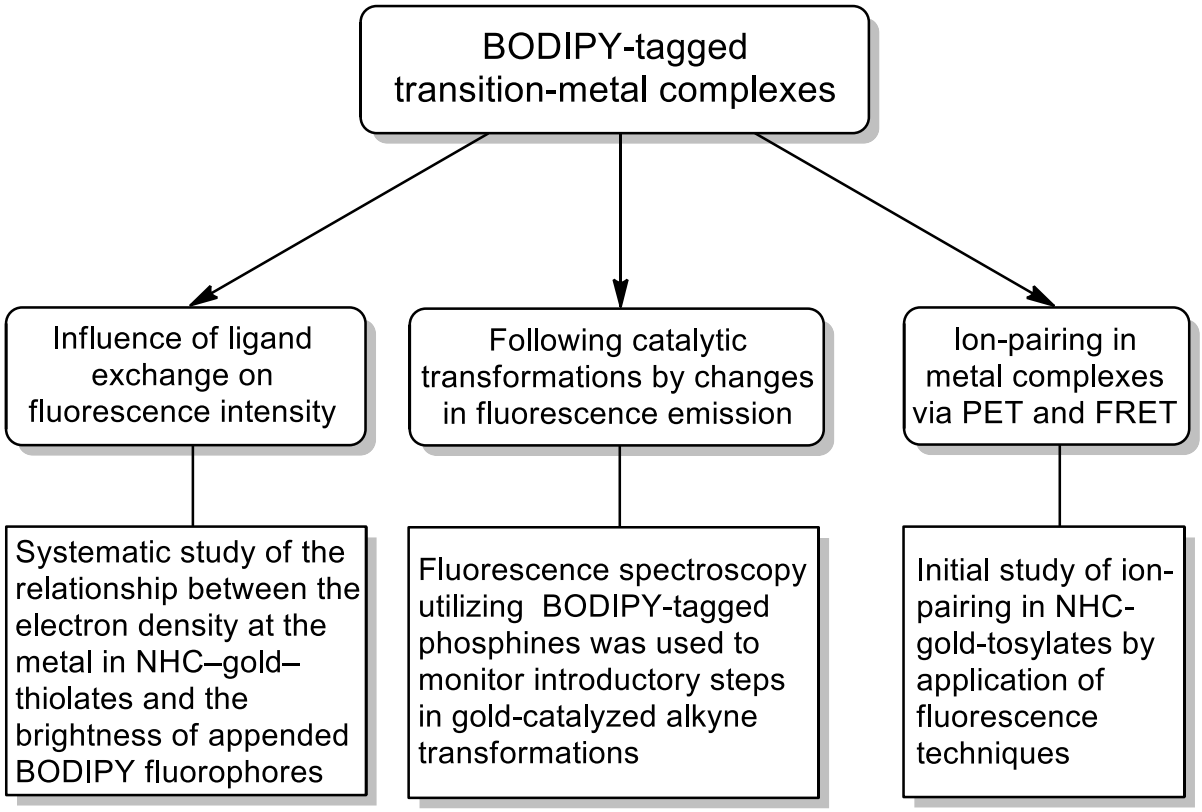

Ligand-exchange reactions constitute elementary steps in catalytic transformations and are crucial in the chemistry of metal complexes. It was previously shown in our lab that substitution of cyclooctadiene ligand with CO molecules in BODIPY-tagged iridium complexes led to the increase in the fluorescence brightness. Concerning the fundamental importance of such observation, we decided to conduct the systematic study of this phenomenon. Chapter 3.1 describes the application of various BODIPY-tagged NHC-gold complexes for the investigation of the relationship between electron density on metal center and fluorescence intensity of the attached fluorophore. The obtained results allowed us to establish the fundamental principle, which connects ligand exchange events and the intensity of fluorescence signal.

Based on the knowledge gained in the first part we were able to design and prepare novel fluorescent complexes, which appeared to be very sensitive probes for the fluorescence investigations. Chapter 3.2 covers the synthesis of BODIPY-tagged phosphine ligands and the respective metal complexes. Sufficient stability and intermediate level of fluorescence intensity of gold(I) phosphine complexes made them very attractive tools for catalyst activation study. They were used for monitoring introductory steps in gold-catalyzed alkyne

transformations by means of fluorescence spectroscopy in a catalytically relevant concentration range.

Ion-pairing plays an important role in catalytic processes of transition-metal complexes. A deeper understanding of counterion effect would greatly facilitate the development of novel catalytic systems with improved activity and selectivity. However, structure investigation of ion pairs is normally limited to NMR experiments. In this respect, we suggest the development of a novel approach based on fluorescence spectroscopy. The basic concept of application of fluorescence techniques for ion-pairing study is introduced in chapter 3.3. The initial experiments with BODIPY-tagged gold(I)-sulfonates have supported the idea and demonstrate the great potential of the proposed approach.

3. Results and Discussion

3.1. Systematic modulation of the fluorescence brightness in boron-dipyrromethene (BODIPY)-tagged N-heterocyclic carbene (NHC)–gold–thiolates

3.1.1. Modulation of the emission intensity

During the last four decades,[130] a very large number of fluorescent molecular probes for the detection of cations, anions and small molecules have been developed.[131] To obtain potent molecular probes with excellent sensitivity, the interaction within the receptor-fluorophore pair needs to be optimized.[132] In this sense, Nagano et al. had shown for fluorescein and boron-dipyrromethene (BODIPY)[11a, 19] derivatives that the systematic manipulation of the electronic nature of an appended quencher enables excellent control over the brightness of the fluorophore (figure 1).[133]

Based on this knowledge, the precise adjustment of the relative HOMO-LUMO energies of a 1,2-diaminobenzene and a BODIPY dye led to the construction of a highly responsive bioimaging fluorescence probe for the detection of NO.[133c] In a conceptually related approach Park et al.[134] were able to rationally perturb the fluorescence quantum yield in emission-tunable fluorophores (Seoul-Fluors).[135] However, with a view to the structures displayed in figure 1, it is understandable that the covalent modification of organic fluorophores can be a tedious process, involving extensive synthetic work.

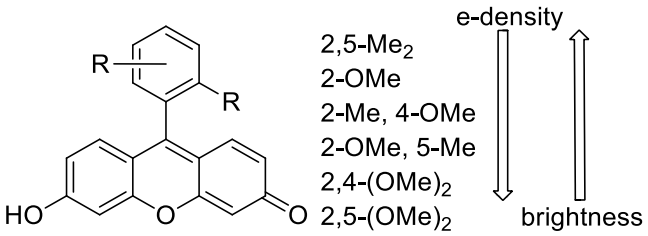

Figure 1. Systematic modulation of substituents and electron density of a fluorescein and the influence on fluorescence brightness.

Transition metal complexes with appended fluorophores can also experience significant changes in the fluorescence properties.[136] Chu et al. have reported[137] BODIPY-Fischer carbene dyads, where the fluorophore was attached to the metal-carbene group by an ethylenic bridge (figure 2a). The photophysical properties of such system depend on the extent of π-conjugation between BODIPY unit and carbene. In case of electron-deficient alkoxycarbene (X = OMe), the π-conjugation was maximized, which resulted in very pronounced quenching of fluorescence emission. In contrast, for electron-rich aminocarbene (X = NMe_2) π-conjugation was diminished and the photophysical properties of BODIPY moiety were not altered significantly. Thus, it was demonstrated that fluorescence of BODIPY can be tuned by modifying electron-accepting properties of the metal-carbene unit. In the subsequent work[138] Chu et al. have shown that emissive properties of the system can be efficiently modulated even if the transition-metal fragment is not directly attached to the BODIPY core. Fluorescence intensity of BODIPY-Fischer carbene diads (figure 2b) experienced a noticeable substituent (R) effect. For π-donor groups (R = OMe, NMe_2) higher emission intensities were observed than for π-acceptor groups (R = Br, CF_3). The fluorescence properties of BODIPY can also be affected by cyclometallated Rh (Ir) fragments[139] (figure 2c). When the fluorophore and transition-metal part are in close proximity to each other (n = 0), BODIPY emission was completely suppressed. At a bigger distance (n = 1) the quenching

effect was less pronounced. The origin of the quenching was attributed to an acceptor-excited PET.

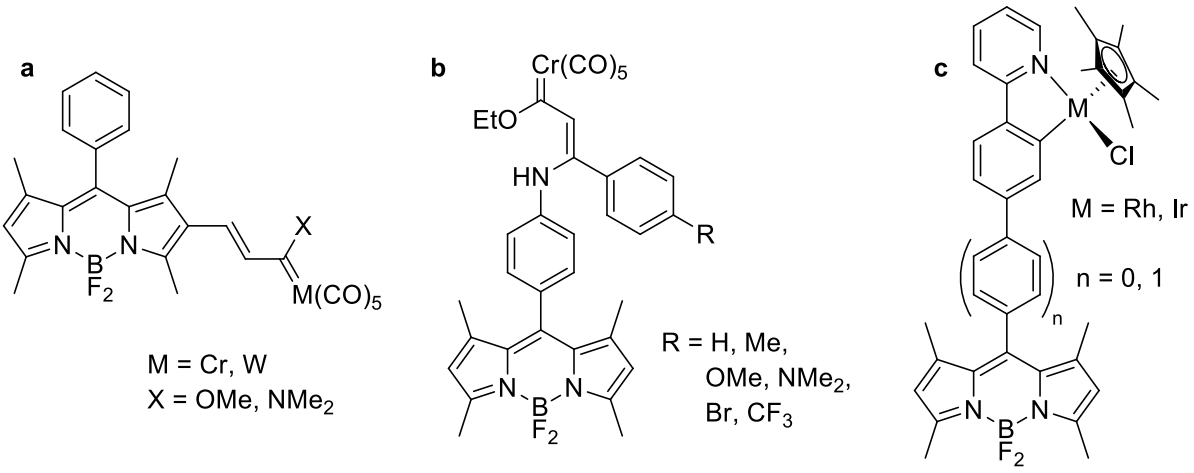

Figure 2. BODIPY-tagged complexes used in the research of Sierra and coworkers.

Modulation of fluorescence intensity of the fluorophore-tagged transition-metal complexes was used for monitoring cross-coupling reactions[3c] and olefin metathesis catalyst initiation.[3b] BODIPY-tagged complexes can be applied as molecular probes for the sensing of small molecules such as CO[68] or H_2.[70] In such complexes changes in the coordination sphere of the metal lead to diagnostic changes in the fluorescence brightness of the BODIPY fluorophore. This fluorescence modulation appeared to be related to the electron density at the transition metal.[68] This chapter represents the systematic study of the relationship between the electron density in a gold complex and the brightness of appended BODIPY fluorophores using a combined experimental and computational approach.

3.1.2. Synthesis of BODIPY-substituted NHC-gold complexes

The various [(NHC-BODIPY)AuX] (X = Cl, I) complexes **1**, **2**, **3a** and **3b** used in this study are displayed in figure 3. They are characterized by different distances between the BODIPY unit and the gold. Thus, in complex **1**, fluorophore and imidazole ring of NHC ligand are separated with a phenyl ring. In the complex **2**, this distance is extended by an additional CH_2–CH_2 chain, whereas complexes **3a** and **3b** represent an extreme case: the BODIPY unit is connected directly to the imidazole.

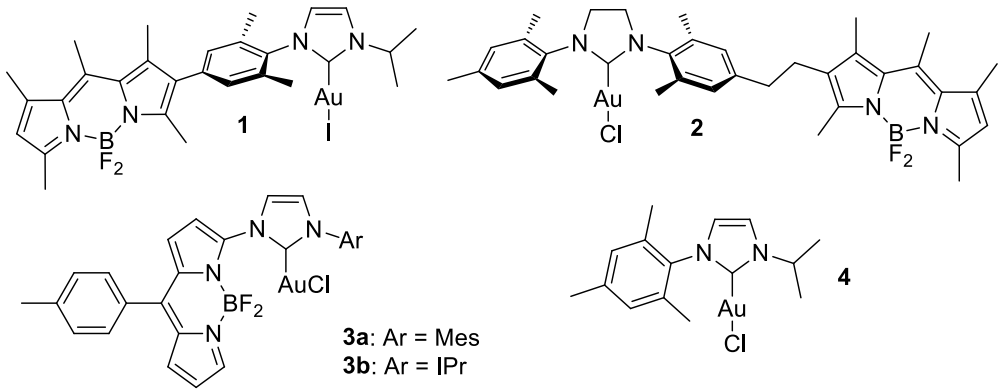

Figure 3. BODIPY-tagged NHC-gold complexes employed in thiol fluorescence experiments.

Complex **1** was reported previously.[68] To obtain complex **2**, at first azolium salt **5** was prepared by cyclization of the known diamine[70] (figure 4). Subsequent in situ formation of

[(NHC)AgCl] species and transfer of the carbene to [AuCl(Me_2S)] yielded complex **2**.[140] Due to the low solubility of salt **5** in CH_2Cl_2, acetonitrile was used as a solvent to generate intermediate silver complex; also prolonged reaction time was needed for complete conversion of the starting materials.

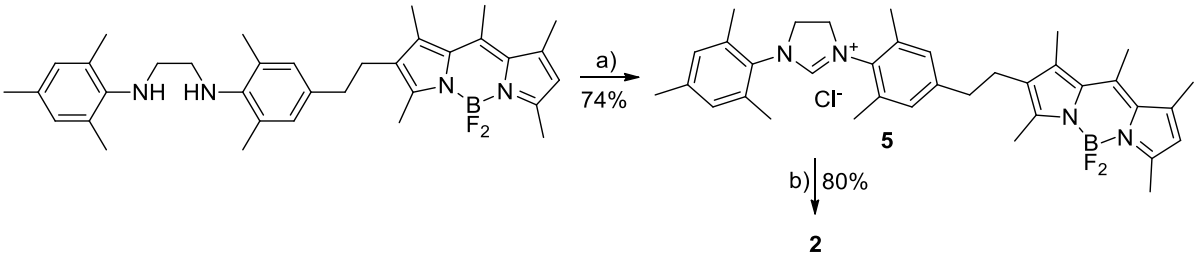

Figure 4. Synthesis of the complex **2**. Reaction conditions: a) NH_4BF_4, $HC(OEt)_3$, HCOOH, 120°C, 24 h, then amberlite IRA, Cl-form; b) Ag_2O, MeCN, 40°C, 3 h, then [AuCl(Me_2S)], RT, 24 h.

Synthesis of the complexes **3a** and **3b** appeared not to be a trivial task. All of the proposed synthetic approaches towards these compounds were based on the same starting material – 3-chloro-BODIPY **6**, which was prepared by the reaction of 2,2'-(p-tolylmethylene)bis(1*H*-pyrrole)[28b] with *N*-chlorosuccinimide followed by chloranil and $BF_3{\cdot}Et_2O$. A three step, one-pot procedure involving two chromatographic purifications provides compound **6** in an acceptable overall yield of 19% (figure 5). An experimental procedure and spectroscopic data for this compound were reported only very recently.[41] Our procedure reported herein is based on the synthesis of the closely related 3,5-dichloro-BODIPY.[29] In the latter compound, the chlorine atoms are highly activated towards Pd-catalyzed cross-coupling reactions and nucleophilic substitution[46] and can be replaced with various nucleophiles (amines, alcohols, thiols, etc.) in good yields employing mild reaction conditions.[141] Hence, the diamine **7** was smoothly obtained by the reaction shown in figure 5. Attempts of its cyclization either by refluxing in triethyl orthoformate or by reacting with pentafluorobenzaldehyde were not successful. Most likely, decreased nucleophilicity of nitrogen atom attached directly to electron-withdrawing BODIPY restricts the cyclization reaction, whereas instability of unsubstituted BODIPY core facilitates alternative decomposition pathways to be realized.

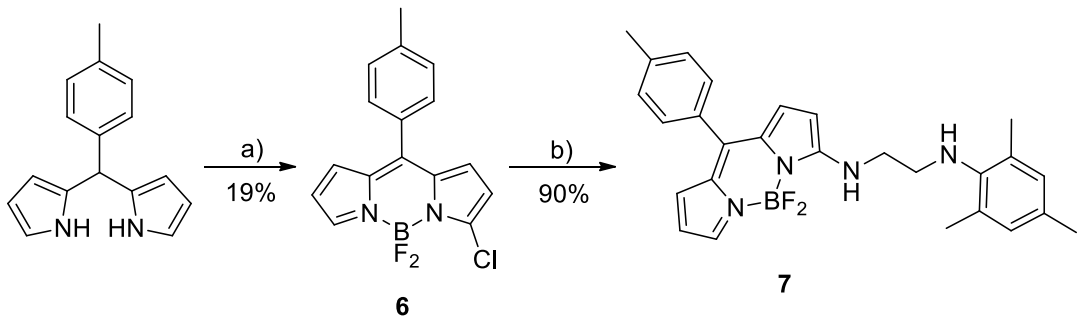

Figure 5. Synthesis of the diamine **7**. Reaction conditions: a) *N*-chlorosuccinimide, -78 °C, THF, followed by chloranil, followed by $BF_3{\cdot}Et_2O$, NEt_3; b) N^1-mesitylethane-1,2-diamine, NEt_3, CH_2Cl_2, 40 °C, 1 h.

Therefore, it became clear, that imidazolium ring should be introduced directly into the BODIPY unit. Similarly to the reported procedure,[142] azolium salt **9** was smoothly prepared by reaction of **6** with imidazole and subsequent alkylation with isopropyl iodide (figure 6). Unfortunately, this approach was also not successful: the transfer of the respective carbene on gold via silver complex occurred only in a poor yield and, moreover, this synthesis was poorly

reproducible. Most probably, the key problem was the instability of the formed complexes due to insufficient steric bulk around metal center created by isopropyl group.

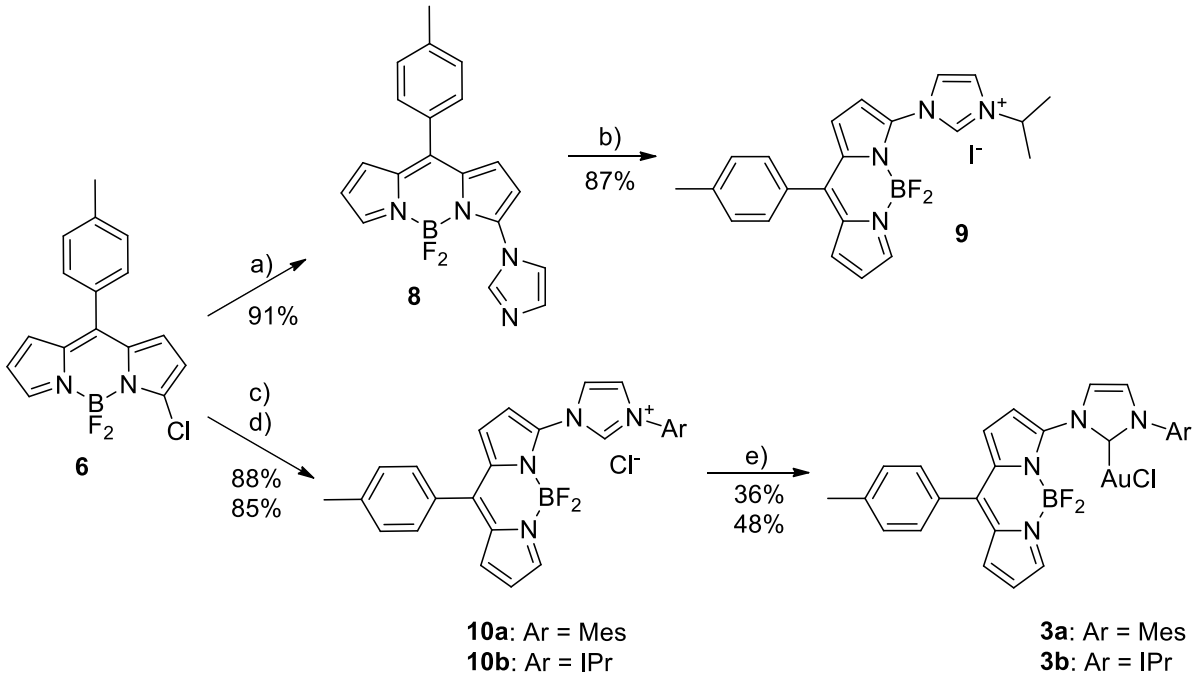

Figure 6. Synthesis of complexes **3a** and **3b**. Reaction conditions: a) imidazol, MeCN, RT, 40 h; b) 2-iodopropane, MeCN, 70 °C, 48 h; c) 1-mesityl-1*H*-imidazole, MeCN, RT, 60 h; d) 1-(2,6-diisopropylphenyl)-1*H*-imidazole, MeCN, RT, 60 h; e) Ag_2O, CH_2Cl_2, 40 °C, 1 h, then [AuCl(Me_2S)], RT, 2 h.

To increase the stability of the metal complexes, aryl groups were introduced. Niu et al. have reported[143] the direct formation of azolium salt by the substitution reaction of α-chlorine of BODIPY with *N*-methyl imidazole. Using analogous one-step procedure, azolium salts **10a** and **10b** were easily obtained from BODIPY **6** and 1-mesityl-1*H*-imidazole or 1-(2,6-diisopropylphenyl)-1*H*-imidazole respectively (figure 6). In this case, silver salt approach led to the successful formation of the respective gold complexes **3a** and **3b**. The better yield of **3b** reflects the higher bulkiness of 2,6-diisopropylphenyl group compared to mesityl.

Simple chloro-to-thiolato ligand exchange at the transition metal enables the systematic manipulation of electron density with minimal synthetic effort.[68] Aryl thiolates are strong electron donors but were also chosen with a view to the high affinity of sulfur to gold. Nine different 4-substituted aryl thiols with R = NO_2, CF_3, COMe, Cl, H, Me, *t*Bu, OMe, and NMe_2 were employed, covering the range from strongly electron-withdrawing groups (EWG) to strongly electron-donating groups (EDG).[144] For the monitoring of the fluorescence evolution, the full range of gold thiolates was generated in the cuvette only. In order to verify the identity of the respective [(NHC-BODIPY)Au(SC_6H_4R)] species, some of these complexes were isolated. Following the reported procedure,[145] the desired gold thiolates were synthesized by reaction of the respective [(NHC)AuX] (X = Cl, I) complexes with the different thiols in the presence of base (figure 7). The resulting gold thiolates are air-stable complexes. The identity of the gold thiolates was confirmed by NMR spectroscopy, and HR mass spectra and for [**1**($SC_6H_4NO_2$)] by X-ray diffraction analysis as well.[146]

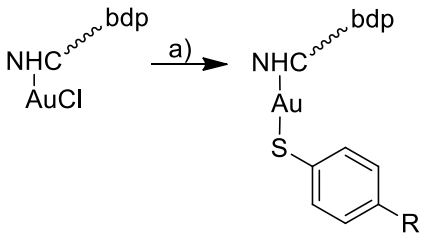

Figure 7. General synthesis of NHC-gold thiolates. Reaction conditions: a) thiol (1.1 equiv) and NaOH (1.2 equiv) in ethanol added to [(NHC-BODIPY)AuCl] (1.0 equiv) in CH_2Cl_2.

3.1.3. Spectroscopic properties of the synthesized compounds

As listed in table 1, the complexes **1**, **2** and their derivatives display typically for BODIPY fluorophore absorption band near 510 nm.[68] Transformation of azolium salt **5** into complex **2** doesn't alter significantly emission and absorbance maxima of BODIPY. The same is true for the gold complexes and the corresponding thiolato derivatives. The latter compounds show lower quantum yields compared to the starting halide complexes. Such decrease of fluorescence emission qualitatively correlates with the intensity changes observed in the in situ generated fluorescence-time traces (see next section).

Compound	Φ	Absorbance λ_{max} [nm]	Emission λ_{max} [nm]
1	0.61[a]	509	533
2	0.50	509	523
5	0.50	510	523
[**1**($SC_6H_4NO_2$)]	0.44	509	533
[**2**($SC_6H_4NO_2$)]	0.41	509	524
6	0.093[b]	506	519
7	0.018	490 (broad)	532
8	0.036	518	533
9	0.12	497	521
10a	0.13	496	522
10b	0.14	496	522
3a	0.072	508	529
3b	0.078	508	530

[a] For this compound and below Φ values were determined in 1,2-dichloroethane versus rhodamine 6G (Φ = 0.95 in EtOH) at RT with a concentration range of 0.25–1 μM;

[b] For this compound and below Φ values were determined in 1,2-dichloroethane versus rhodamine 101 (Φ = 1.0 in EtOH) at RT with a concentration range of 0.25–1 μM.

Table 1. Spectroscopic properties of BODIPY derivatives.

Substituents in the α-position of BODIPY core have a strong influence on its optical properties. Derivatives of BODIPY **6** have diverse values of absorbance and emission maxima. Substitution of Cl with imidazole leads to a long-wave shift of the absorbance maximum, whereas for the compound **7** short-wave shift was observed. Introduction of the *N*-substituents results in a decrease of quantum yield, most probably due to the PET quenching induced by nitrogen lone pair. In the case of derivative **8**, the fluorescence quenching is less pronounced due to the lower donating properties of the imidazole nitrogen; tilting of the imidazole ring also reduces its interaction with BODIPY.

BODIPY-azolium salts exhibit short-wave shift. Electron-accepting properties of the positively charged imidazole ring diminish PET, which leads to restoring of fluorescence. This situation is partially maintained for the complexes **3a** and **3b**, which are characterized by lower but still high enough fluorescence brightness to enable the fluorescence-time measurements with these complexes.

3.1.4. Monitoring the fluorescence during the formation of the gold-thiolates

To probe the effect of the halide-to-thiolate substitution in solution, the brightness of gold complexes **1**, **2** and **3a**[147] was monitored during the substitution reaction. The respective thiols were added to the 1,2-dichloroethane solutions of the respective gold halide complex ($c = 1.0 \cdot 10^{-6}$ mol·L^{-1}) containing Hünig base. This approach is more precise than the determination of the fluorescence quantum yield of the isolated gold thiolates.[148] The formation of the gold thiolates always leads to a decrease in the brightness relative to the respective complexes **1**–**3**. In table 2 the normalized intensities of the respective thiolato complexes are listed.

complex	**1**	**2**	**3a**
R=	I_{AuS}/I_{AuX}	I_{AuS}/I_{AuX}	I_{AuS}/I_{AuX}
NMe_2	0.0148	0.0668	-
OMe	0.0274	0.323	-
*t*Bu	0.0711	0.687	-
Me	0.0542	0.607	-
H	**0.127**	**0.820**	**<0.001**
Cl	0.199	0.903	-
COMe	0.496	0.990	-
CF_3	0.961	0.999	<0.001
NO_2	0.750	0.814	-

Table 2. Fluorescence intensities of the respective [(NHC-BODIPY)Au(SC_6H_4R)] complexes relative to the fluorescence level of the respective complexes **1**–**3**.

A typical set of fluorescence-time traces is shown in figure 8 for the reactions of complex **1**. The rate of the halide-to-thiolate substitution depends on the nature of the R substituent. For electron-deficient and more acidic thiols the formation of the gold thiolates is ca. 20-50 times faster than for electron-rich thiols. The final intensities, which correspond to the complete conversion of the starting gold complex, also greatly depend on the nature of the thiol. For the gold thiolate with 4-R = CF_3 derived from complex **1**, the brightness is nearly the same as that of the halide complex with I(AuS)/I(AuX) = 0.96, while for R = NMe_2 the fluorescence is 65-times weaker. The fluorescence intensities of complex **1** derived [(NHC-BODIPY)Au(SC_6H_4R)] nicely correlate with the Hammett parameters of the respective substituents R (figure 9). A linear fit was applied in this case.

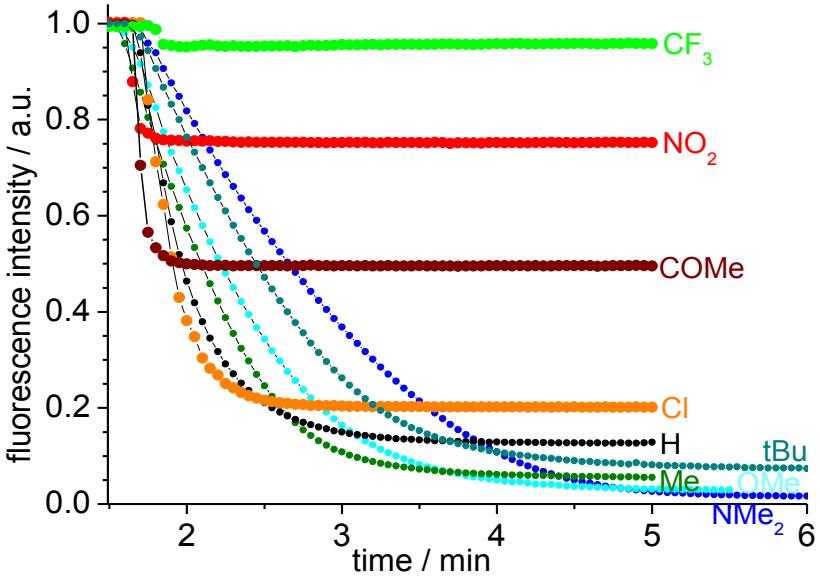

Figure 8. Fluorescence-time traces upon addition of 100 equivalents of RC_6H_4SH (R = NO_2, CF_3, COMe, Cl, H, Me, *t*Bu, OMe and NMe_2) to complex **1** ($c = 1.0 \cdot 10^{-6}$ mol·L^{-1}) and Hünig base (100 equiv) in 1,2-dichloroethane solvent leading to the formation of the respective complexes [**1**(SC_6H_4R)]. The fluorescence intensity of complex **1** is set to 1.0.

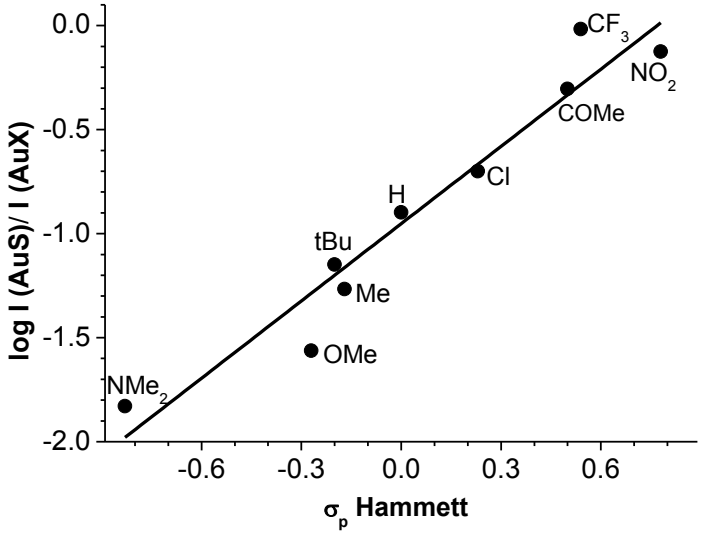

Figure 9. The plot of the σ_p-Hammett plot and the relative fluorescence brightness of complexes [**1**(SC_6H_4R)].

Analogous fluorescence-time traces were obtained for the complex **2** (figure 10). The general trends are very similar to the previous example. Nonetheless, compared to complex **1**, the brightness of the thiolato derivatives of complex **2** appeared to be less sensitive to the nature of R substituent. For instance, the formation of the gold thiolate with 4-R = CF_3 derived from complex **2** is not accompanied by any changes in fluorescence brightness (I(AuS)/I(AuX) = 0.999). Relative fluorescence intensities of the gold thiolates obtained from electronic-rich thiols are also much higher than for the complex **1** (table 2). The Hammett plot for the thiolates of complex **2** is fitted with an exponential function, with the log I(AuS)/I(AuX) values converging towards zero for the electron-deficient thiolates (figure 11). Most likely the bending of the fit only occurs for thiolates with highly EWG and is not visible in the data set.

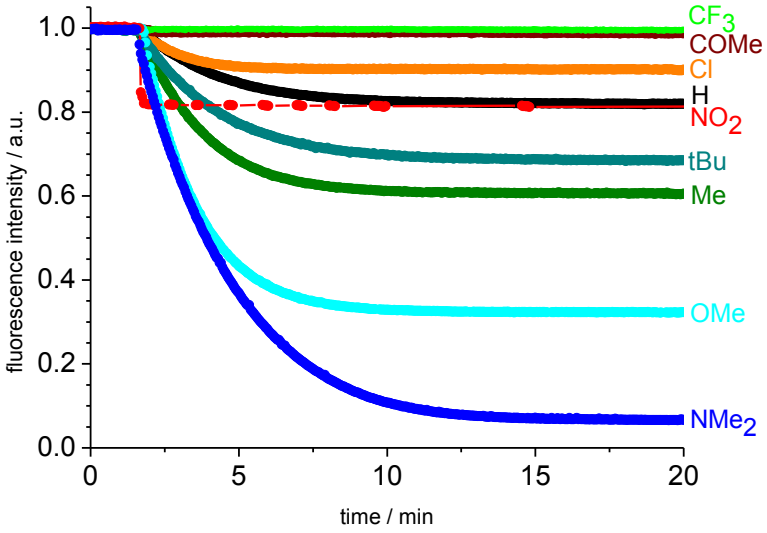

Figure 10. Fluorescence-time traces upon addition of 100 equivalents of RC_6H_4SH (R = NO_2, CF_3, COMe, Cl, H) or 500 eq of RC_6H_4SH (R = Me, *t*Bu, OMe, NMe_2) to complex **2** ($c = 1.0 \cdot 10^{-6}$ mol·L^{-1}) and Hünig base (100 equiv) in 1,2-dichloroethane solvent leading to the formation of the respective complexes [**2**(SC_6H_4R)]. The fluorescence intensity of complex **2** is set to 1.0.

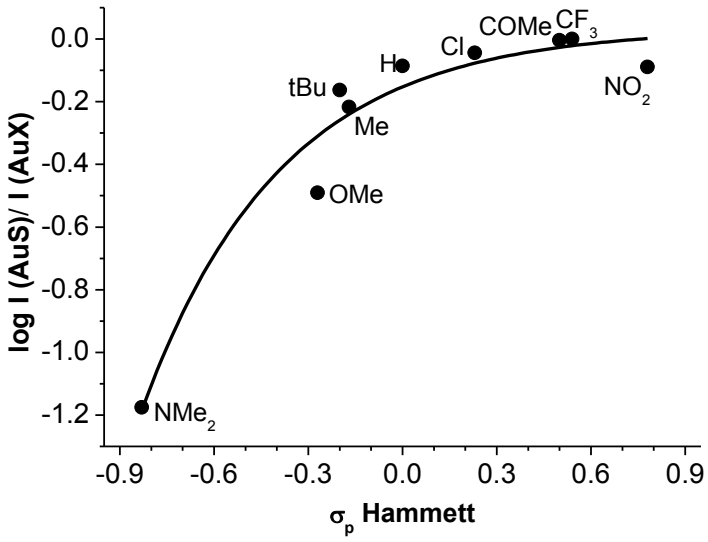

Figure 11. The plot of the σ_p-Hammett plot and the relative fluorescence brightness of complexes [**2**(SC_6H_4R)].

The reaction of complex **3a** with thiophenol leads to the complete quenching of fluorescence (figure 12). Moreover, even addition of electron deficient 4-$CF_3C_6H_4SH$, which forms the brightest gold thiolates in case of complexes **1** and **2**, leads to the same result (I(AuS)/I(AuX) was estimated at 0.001). Obviously, the addition of any other thiol would show the same pattern. This result indicates the very high sensitivity of the fluorescence brightness of complex **3a** to the substituents on gold center. Unfortunately, it also prevents any rationalization of the relationship between fluorescence brightness and the nature of thiols.

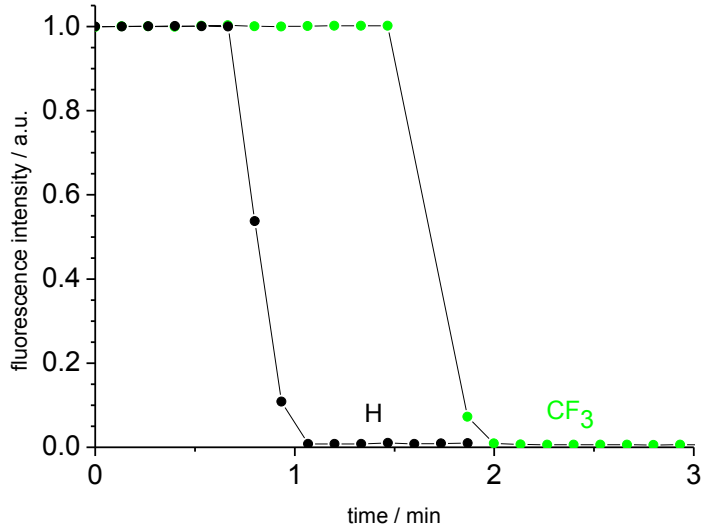

Figure 12. Fluorescence-time traces upon addition of 100 equivalents of RC_6H_4SH (R = CF_3, H) to complex **3a** (c = $1.0 \cdot 10^{-6}$ mol·L^{-1}) and Hünig base (100 equiv) in 1,2-dichloroethane solvent leading to the formation of the respective complexes [**3a**(SC_6H_4R)]. The fluorescence intensity of complex **3a** is set to 1.0.

The quantum yields of the complexes **1** and **2** were found to be independent of the nature of halide in the AuX unit. With the view to the exceptional sensitivity of the complex **3a**, halide exchange reaction was tested. Chloro-to-iodo substitution in the complex **3a** after excess addition of tetrabutylammonium iodide led to ca. 23% decrease in fluorescent intensity (figure 13). Most probably, electron-donating nature of iodide is responsible for this result.

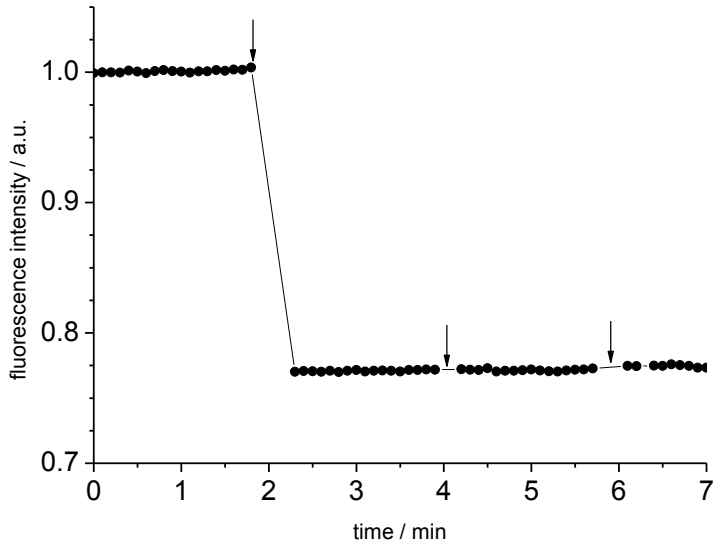

Figure 13. Fluorescence-time traces upon addition of three aliquots of NBu_4I (100 equiv; denoted by arrows) to a solution of **3a** (c = $1.0 \cdot 10^{-6}$ mol·L^{-1}) in 1,2-dichloroethane. The fluorescence intensity of complex **3a** is set to 1.0.

In general, for thiols having EWG, the fluorescence level of the gold-thiolates derived from complexes **1** and **2** is close to that of the respective halide complex. The thiolates derived from complex **3a** are characterized by very strong interactions of quencher and fluorophore, which was expected based on the very short distance of quencher and fluorophore.

Based on the data for complexes **1**, **2** and **3a** and the derived thiolato complexes, the electron-density at the gold thiolates appears to be the dominant factor determining the fluorescence intensity. The lack of overlap between the absorption spectrum of the gold-thiolate and the emission spectrum of the BODIPY renders Förster and Dexter quenching unlikely.[9] In the complexes **1** and **2**, the emission wavelength of the BODIPY unit is virtually independent of the nature of the NHC-metal complex.[68] The dominant quenching mechanism in the gold complexes thus appears to be photoinduced electron transfer (PET) instead.[9],[149]

3.1.5. DFT-calculations

The hypothesis described is supported by the results of the DFT calculations.[150] Thus, the occurrence of the PET mechanism can be roughly estimated by comparing the relative energies of the frontier molecular orbitals (FMO) of the fragments present in the dyads.[133c, 139] As shown in figure 14, the HOMO of the thiolate fragment of complex **1** is higher in energy than that of the corresponding BODIPY moiety regardless of the R substituent. Therefore, upon photoexcitation, the BODIPY fragment behaves as an electron acceptor and its fluorescence is quenched by the acceptor-excited PET (a-PET) process. The extent of this quenching is directly related to the energy difference (ΔE) between the involved orbitals (figure 14). Indeed, a similar linear correlation to that shown in figure 9 is found when plotting the ΔE values versus the corresponding σ-Hammett substituent constants (figure 15). Concerning the fluorescence-time plots of complexes **1** and **2** a minor anomaly concerning the thiophenolato ligand with R = NO_2 becomes apparent since the brightness of the respective thiolato complexes (table 2) is slightly lower than expected (based on the respective Hammett parameters). The nitro group is known to be a fluorescence quencher.[151] However, our DFT calculations do not support a d-PET mechanism for these complexes.

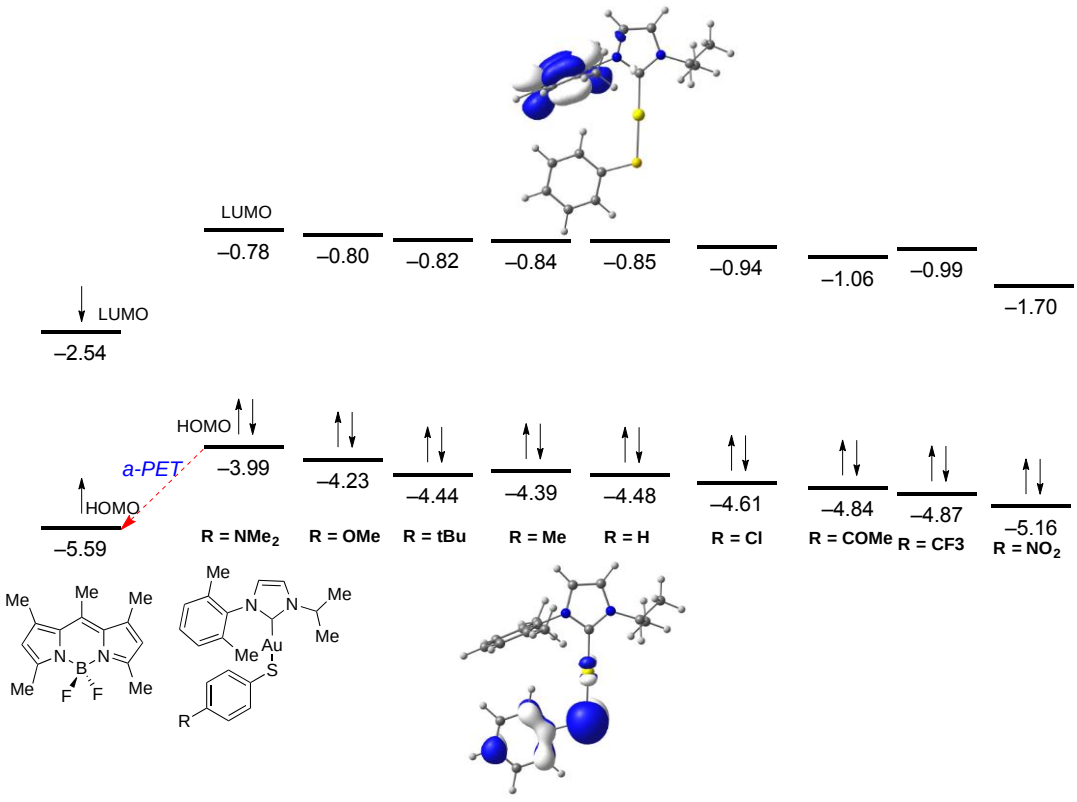

Figure 14. Computed frontier molecular orbitals of the isolated chromophores present in compounds [**1**(SC_6H_4R)] (orbital energies are given in eV).

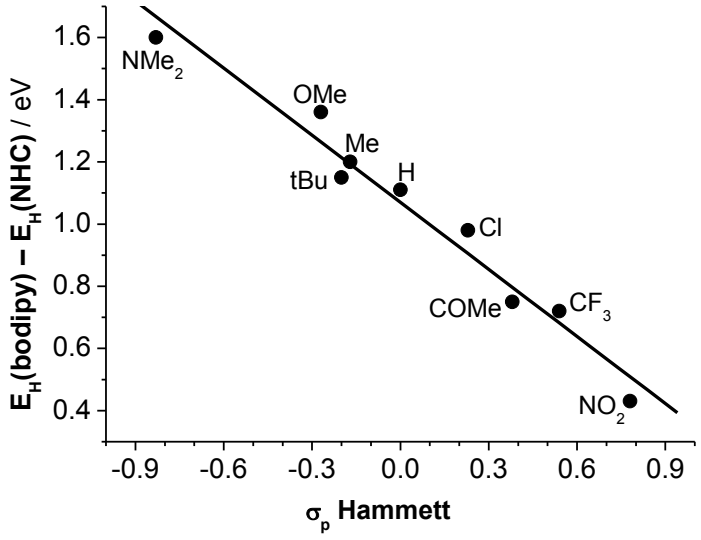

Figure 15. Plot (R^2= 0.98) of the σ_p-Hammett constants and the energy difference (ΔE) between the HOMO of the BODIPY and thiolate fragments in complexes [**1**(SC_6H_4R)].

3.1.6. The distance between fluorophore and quencher

Förster resonance energy transfer (FRET) and photoinduced electron transfer (PET) are two distance-dependent processes which can modulate fluorescence brightness through interaction between a fluorophore and a quencher. FRET, being a dipolar, nonradiative process, is effective over long distances, typically between 2–8 nm. PET involves an electron transfer between fluorophore and quencher and requires contact interaction between the two. Therefore, PET is limited to much shorter distances of around 1 nm.[152]

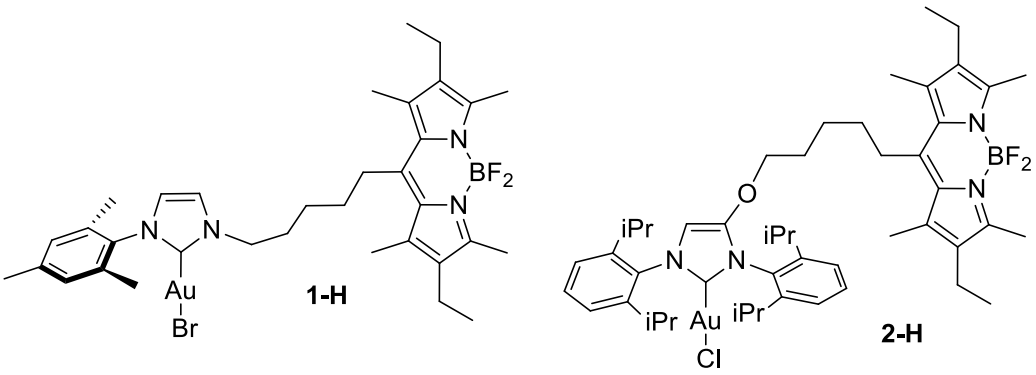

Figure 16. BODIPY-tagged gold complexes prepared by O. Halter.

To better understand the effect of the distance between fluorophore and quencher on the fluorescence attenuation, additional gold complexes were prepared in our group by O. Halter (figure 16). In the gold thiolates derived from complexes **1**, **2**, **1-H** and **2-H**, the relative fluorescence brightness for R = H (table 2, bold, for **1** and **2**; 0.612 for **1-H**, 0.995 for **2-H**) was plotted versus the distance of sulfur and boron atoms (d(B···S)) in the respective BODIPY. The choice of sulfur is justified since according to the DFT calculations the HOMO of the gold-thiolate complexes is sulfur centered, whereas the boron atom is located close to the center of the BODIPY. Note that the d(B···S) values coming from DFT calculations are only approximate due to the conformational flexibility of the gold thiolates. Nonetheless, the data in figure 17

can be fitted reasonably well with an exponential function. Up to d(B···S) of 1.0 nm, the fluorescence attenuation due to the gold–thiolate quencher is pronounced, whereas for d(B···S) > 1.5 nm, the BODIPY fluorescence is virtually unperturbed. Both results make sense in the context of PET, the rate of which shows an exponential dependence of the distance between fluorophore and quencher.[152-153]

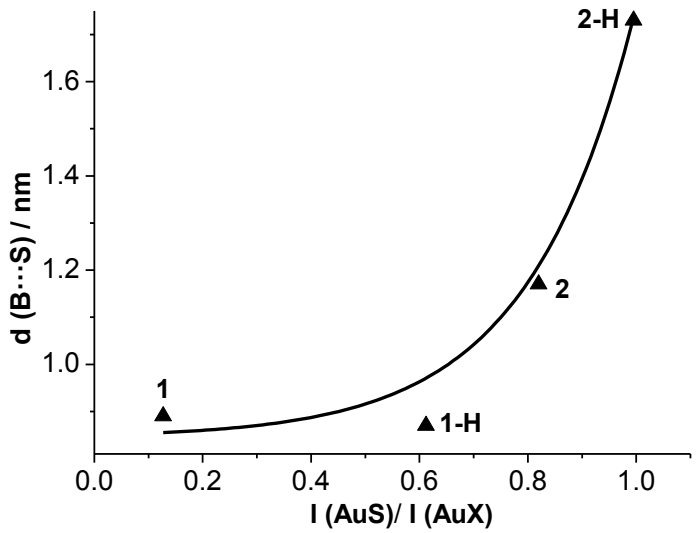

Figure 17. Plot of the distance between fluorophore and quencher (d(B···S)) versus the fluorescence attenuation.

Obviously, the d(B···S) in the complex **3a** is shorter than in **1**. Complete suppression of fluorescence brightness in [**3a**(SPh)] additionally supports PET mechanism. Nonetheless, unlike the complexes **1** and **2**, where electron transfer occurs through space since no conjugation between BODIPY and metal center is possible, in case of **3a** through-bond mechanism can be also realized. As shown in table 1 the quantum yields of BODIPY-imidazole derivatives greatly depend on the electron-withdrawing character of the imidazole ring. Chloro-to-thiolato substitution reduces electron-accepting properties of gold center, which results in releasing of electron density in NHC-ligand. This, in turn, facilitates PET quenching of BODIPY. Although the overall outcome is the same, in case of complex **3a** PET occurs rather in an indirect manner.

3.1.7. Redox potentials

We attempted to determine the redox potentials of the model gold thiolates [**4**(SC_6H_4R)] (R = NO_2, H, OMe) by cyclic voltammetry. Concerning the coordination sphere of gold, complex **4** (figure 3) is similar to complex **1** but contains a 4-Me instead of the 4-(2-BODIPY) substituent to avoid overlap of the Au-thiolate and BODIPY oxidations. For the complexes studied, the oxidation of the gold thiolate was irreversible (only the oxidation wave was observed). Nonetheless, the observed oxidation potentials exhibit a very pronounced dependence on the nature of the thiolato ligand: E_{ox} = +1.15 V (R = NO_2), E_{ox} = +0.81 V (R = H), E_{ox} = +0.58 V (R = OMe) (figure 18). The observed electrochemical trend correlates with the computed energy of the corresponding HOMO: –5.23 eV (R = NO_2) > –4.67 eV (R = H) > –4.46 eV (R = OMe), indicating that a less stabilized (i.e., less negative) HOMO is translated into a lower oxidation potential. Based on these data, the estimated free energy for the electron transfer was calculated using the Rehm-Weller equation.[154] This calculation is based on the assumption that the observed oxidation potentials E(ox) – 57/2 mV correspond to the reversible redox potentials $\Delta E_{1/2}$. The ΔG_{PET} for [**1**(SC_6H_4R)] (ΔG_{PET} = –0.02 eV (R =

NO_2), –0.36 eV (R = H), –0.59 eV (R = OMe)) and [**2**(SC_6H_4R)] (ΔG_{PET} = 0.04 eV (R = NO_2), –0.30 eV (R = H), –0.53 eV (R = OMe)) were calculated by employing the experimentally determined potentials for the oxidation of [**4**(SC_6H_4R)] (figure 18), the redox potential for the reduction of the BODIPY and the excitation energy (the electrostatic term can be neglected in 1,2-dichloroethane solvent). The four ΔG_{PET} for R = H and OMe are negative, while it is close to zero or even positive for R = NO_2. This underlines the special behavior of the nitro-substituted complexes.

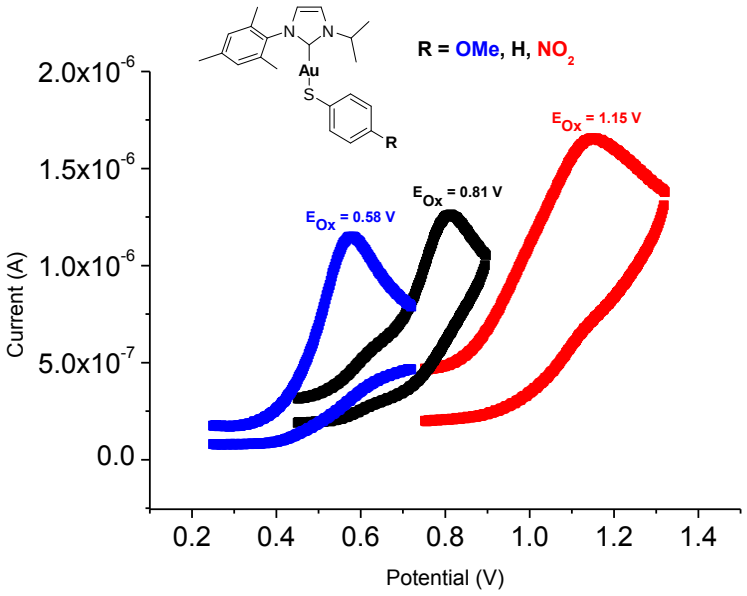

Figure 18. Fragments of cyclic voltammograms representing oxidation potentials in [**4**(SC_6H_4R)] (R = NO_2, H, OMe).

3.2. Observing initial steps in gold-catalyzed alkyne transformations by utilizing BODIPY-tagged phosphine-gold complexes

3.2.1. Application of fluorescence spectroscopy for observing ligand-exchange reactions in metal complexes

Understanding catalytic processes is of essential importance for enhancing catalysts and catalytic transformations.[155] Acquiring such an understanding critically relies on spectroscopic techniques, which are able to probe the status of the species under study with sufficient precision and sensitivity.[156] In this respect, fluorescence spectroscopy, due to its exceptional sensitivity, can be a useful method.[9]

Ligand exchange reactions constitute elementary steps in the chemistry of metal complexes and are crucial in catalytic transformations. It thus appears highly interesting to synthesize a fluorescent reporter ligand for catalytically active metals, whose fluorescence properties are modulated by such elementary reactions. Only a few examples related to catalysis in single molecule studies[4, 60, 157] and in ensemble measurements in solution have been realized,[3c, 158] despite the fact that related approaches are very popular in photoluminescent sensing.[159]

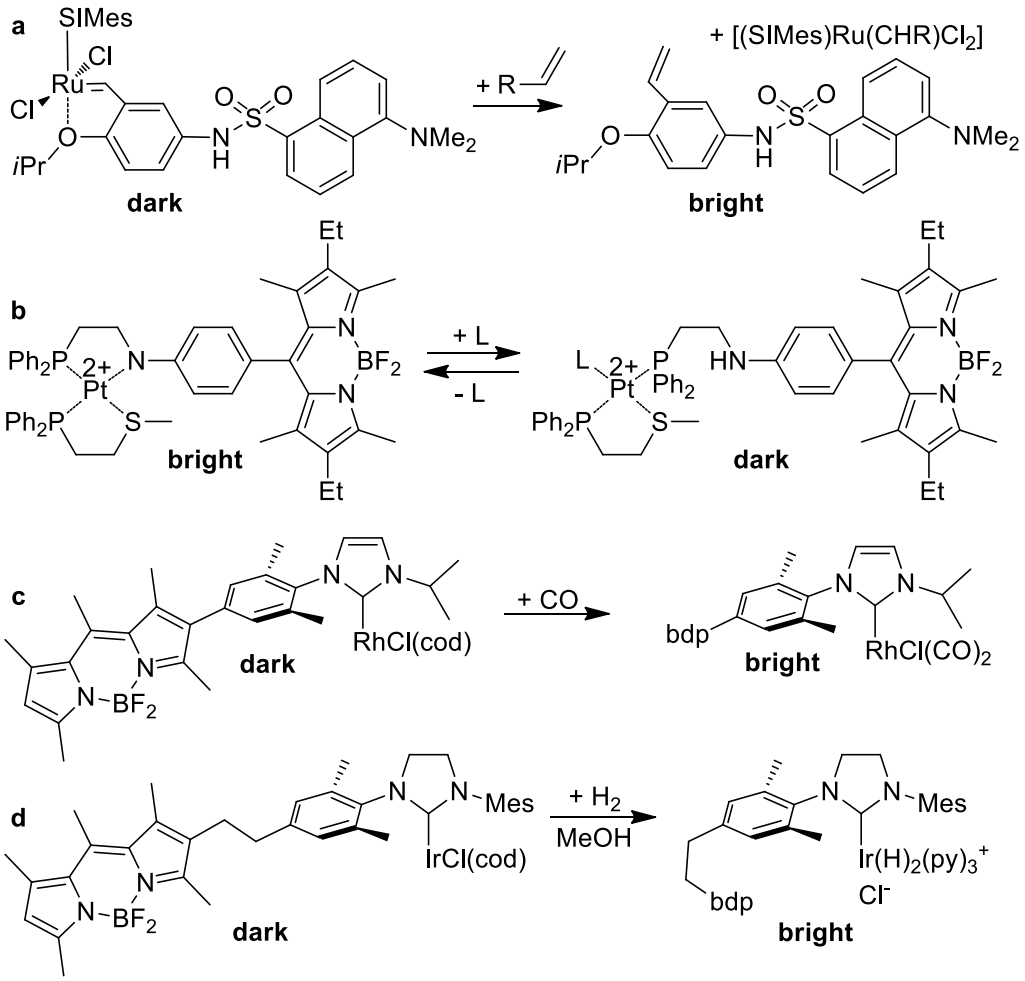

Figure 19. Examples for switched fluorescence (on/off) in transition metal complexes with an appended fluorophore (Mes = 2,4,6-trimethylphenyl, bdp = BODIPY, SIMes = 1,3-bis(2,4,6-trimethyl)phenyl-4,5-dihydroimidazol-2-ylidene).

The detection processes in such complexes so far are relatively simple, in that only two states are considered (signal on/off) depending on the presence or the absence of quencher. A transition metal and a ligand tagged with a fluorescent dye associate to form a fluorescent or a non-fluorescent complex whose brightness is reversed by some reaction. This principle has been put to good use to clarify mechanistic issues concerning the postulated release-return mechanism in olefin metathesis (figure 19a).[3b] Mirkin et al.[136a] reported a Pt-complex, whose BODIPY-centered fluorescence is reversibly modulated by an added ligand L (figure 19b). This ligand L releases a nitrogen donor from the coordination sphere of platinum, which then quenches the fluorophore. It was recently shown that changes in the fluorescence signal of BODIPY-tagged *N*-heterocyclic carbene metal complexes also occur as a consequence of changes in the coordination sphere of a metal, despite the fact that the spatial relationship of fluorophore and transition metal remains unchanged. In this case, the substitution of a cod (1,5-cyclooctadiene) ligand in an Ir-complex by two CO molecules, converts an initially dark complex into a brightly fluorescent complex (figure 19c).[68] This modulated fluorescence intensity was attributed to changes in the electron-density at the transition metal and indicates that the PET mechanism appears to be primarily responsible for fluorescence quenching. The oxidative addition of H_2 to a fluorophore-tagged Crabtree-type complex is another example of a fluorogenic reaction (figure 19d) useful for the detection of H_2.[70]

It was shown in the previous chapter that sensitivity of such probes critically relies on the distance between the fluorophore and the metal center. In order to enhance sensitivity, this distance should be minimized. This chapter is devoted to the synthesis of metal complexes of BODIPY-tagged phosphines, in which one phosphorus donor is directly connected to the BODIPY core. Thus, the BODIPY fluorophore and the metal center are separated by just one atom (phosphorus) – the smallest possible linker. The resulting phosphine should be dark, due to PET quenching by the phosphorus lone pair. However, coordination of this lone pair to a transition metal should restore fluorescence, when using metals which do not open other quenching pathways (for example heavy atom effect or via minor changes in the electronic structure).[131a, 160] Such a partially quenched fluorescence signal can be sensitive to subtle changes in the coordination sphere of the metal and translate such changes into an increase or a decrease of the BODIPY fluorescence.

3.2.2. Synthesis of BODIPY-tagged phosphines

Only a few examples of such phosphines have been reported in the literature.[161] Higham et al. recently synthesized several BODIPY-phosphines as well as metal complexes with coinage metals ions such as Cu, Ag, Au and with Re.[101, 112] Bodio et al. also reported such phosphines and the derived Ru, Os, and Au complexes[121] and Blum et al. a related Pd complex.[53] Most of the metal complexes previously reported are highly fluorescent, because the distance between the phosphorus (or the transition metal) quencher and the BODIPY is rather large. Our strategy is different, in that the phosphorus donor and the BODIPY core are to be connected directly, to initially generate fluorescence-quenched BODIPY-phosphines.

We first tested the known 8-Ph_2P-BODIPY (figure 20).[16d] However, we learnt that this ligand and the respective gold complex show unfavourable properties (low fluorescence quantum yields, very broad emission band, and instability). Therefore, another synthetic approach leading to different BODIPY-phosphines was required.

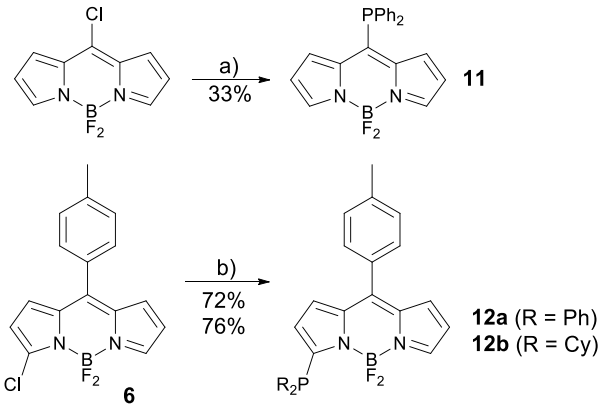

Figure 20. Synthesis and reaction conditions for BODIPY-phosphines: a) Ph_2PH, CH_2Cl_2, 15 min; b) R_2PH (R = Ph, Cy), $Pd(OAc)_2$, Et_3N, toluene.

Reactions of 3-chloro-BODIPY **6** with Ph_2PH or Cy_2PH and base (Et_3N) provide the respective BODIPY-phosphines **12a** and **12b**, but better yields (72–76%) were obtained, when the same reactions were carried out in the presence of catalytic amounts of $Pd(OAc)_2$[162] (figure 20). Additional phosphine for the activation of the palladium catalyst was not required and we assume that the secondary phosphine used as a reagent forms a sufficiently active cross-coupling catalyst.[163] The BODIPY-phosphines **12a** and **12b** are slightly sensitive towards

oxidation and in a few reactions under ambient atmosphere, small amounts of phosphine oxide **13a** were formed and separated by chromatography.

3.2.3. Metal complexes of BODIPY-phosphines

The new metal complexes of BODIPY-phosphines (figure 21), like [AuCl(**11**)] and [MX(**12b**)] (M = Cu, Ag, Au) were synthesized following established procedures for Ph_3P-metal complexes for copper (X = I),[164] silver (X = Cl)[165] and gold (X = Cl).[166] The copper and the silver complexes with **12a** and **12b** are significantly less stable than the respective gold complexes. Solutions of the copper complexes decompose within a few hours, the silver complexes decompose once the solutions are exposed to ambient atmosphere. The most stable complexes are formed with the electron-rich phosphine **12b** and gold. Nonetheless, NMR spectra of all Cu^+, Ag^+ and Au^+ complexes could be recorded. However, based on the optical data, which are the same as those of phosphine **12a**, [CuI(**12a**)] appears to dissociate at the low concentrations (c = 1.0·10^{-6} mol·L^{-1}) used to record such spectra. Complex [$PdCl_2$(**12b**)$_2$] was synthesized from [$PdCl_2$(MeCN)$_2$] and **12b** in 88% yield.[167]

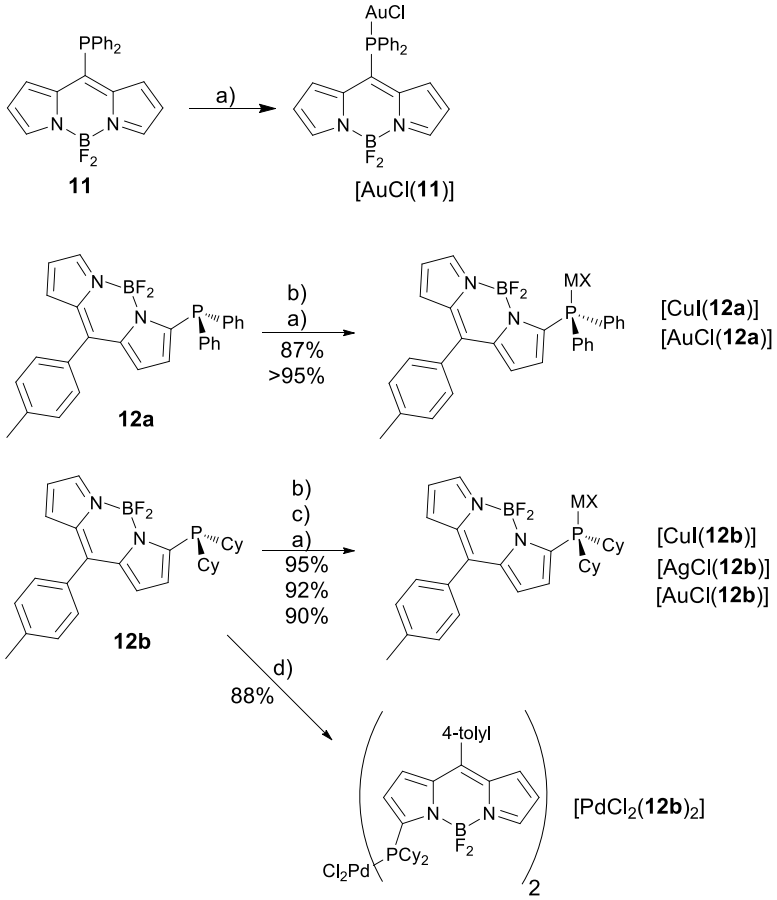

Figure 21. Synthesis and reaction conditions for metal complexes of BODIPY-phosphines: a) [AuCl(Me_2S)], CH_2Cl_2, rt, 30 min; b) CuI, MeCN, rt, 1 h; c) $AgNO_3$, KCl, water/thf, rt, 3 h; d) [$PdCl_2$(MeCN)$_2$], CH_2Cl_2, rt, 12 h.

3.2.4. NMR spectra

The BODIPY-phosphines are characterized by the presence of several NMR active nuclei and, in particular, the ^{31}P NMR spectra display interesting features. In the ^{31}P spectra of **12a** and **12b**, large $^4J(^{31}P\text{-}^{19}F)$ coupling constants are observed (**12a**: J = 45.5 Hz; **12b**: J = 52.4 Hz;

figure 22).[168] The same corresponding $^{4}J(^{31}P\text{-}^{19}F)$ values are much smaller in the respective phosphine-metal complexes; for example, in the gold complex [AuCl(**12a**)], J is 15.4 Hz, and it is even smaller in [AuCl(**12b**)] (J < 2 Hz; figure 22). Our explanation for this observation is based on the Fermi contact term mechanism, which accounts for the coupling between ^{19}F and ^{31}P and the efficiency of which increases with increasing s-orbital participation in the bonds connecting the two nuclei.[169] In the phosphine, the phosphorus lone pair is partially delocalized into the electron deficient BODIPY π-system. This leads to increased s-content in the respective P–C(BODIPY) bond. In the gold complexes, as well as in the other metal complexes, this lone pair is donated to the transition metal rather than to the BODIPY, leading to a decrease in the s-content of the P–C(BODIPY) bond and consequently to a decrease in the coupling constant. A related phenomenon concerning $^{19}F\text{-}^{13}C$ coupling constants was observed in fluorine-containing crown ether complexes, in which the magnitude of the coupling constants turned out to be an effective gauge of the fluorine-metal interactions.[170]

In [AgCl(**12b**)] a $^{107,109}Ag\text{-}^{31}P$ coupling is detected, with a typical value for Ag-phosphine complexes of J = 617 Hz.[171] The ^{31}P signal is severely broadened ($\nu_{1/2}$ = 150 Hz) and this line broadening prevents the determination of the individual ^{107}Ag or ^{109}Ag coupling with ^{31}P. Such signal broadening is also observed for [CuI(**12a**)] and [CuI(**12b**)] and potential $^{31}P\text{-}^{19}F$ coupling could not be resolved. Such exchange-broadened ^{31}P NMR signals are typical for Ag- and Cu-phosphine complexes and reflect the lability of such species in solution.[171]

The coordination of BODIPY phosphines **12a** and **12b** to Au led to a significant deshielding of the ^{31}P resonance from δ = -20.3 ppm for **12a** to δ = 20.2 for [AuCl(**12a**)] and from δ = -14.7 ppm for **12a** to δ = 47.5 for [AuCl(**12b**)]. The more pronounced deshielding of the ^{31}P NMR resonance in **12b** (compared to **12a**) upon metal coordination is in line with a more efficient donation of the phosphorus lone pair in [AuCl(**12b**)] to gold.

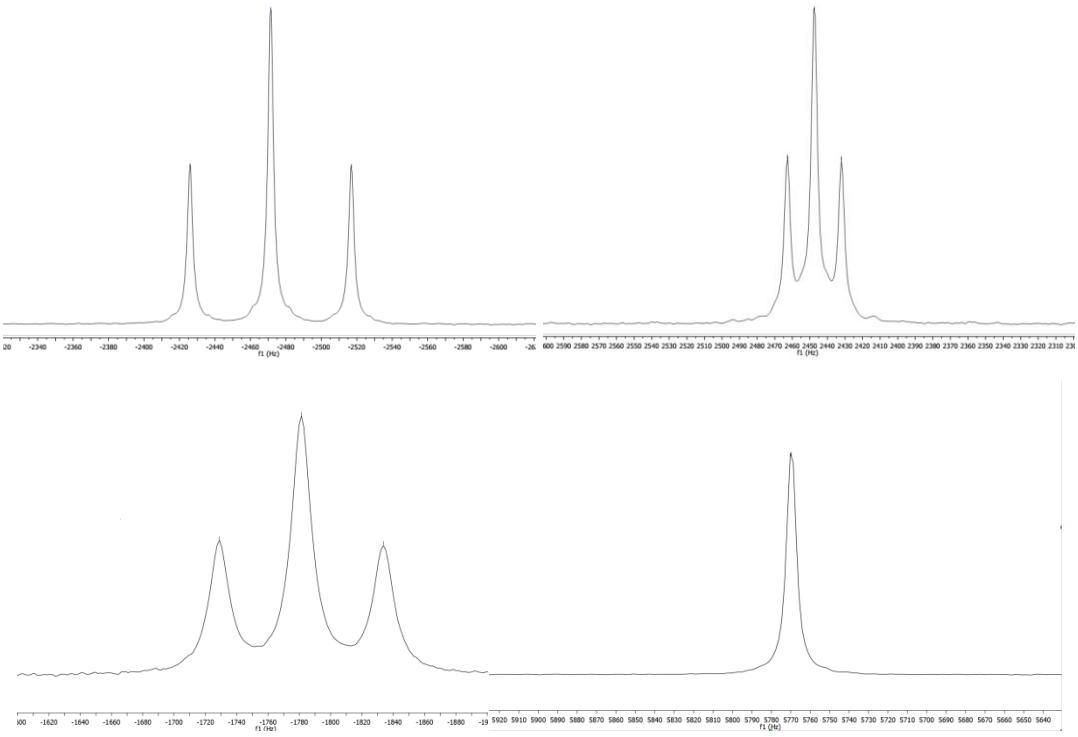

Figure 22. $^{31}P\{^{1}H\}$-NMR spectra of phosphines **12a** (left up) and **12b** (left down) and for complexes [AuCl(**12a**)] (right up) and [AuCl(**12b**)] (right down). Total range displayed for each spectrum is 300 Hz.

3.2.5. X-ray crystal structure analysis of [AuCl(12a)]

Single crystals of [AuCl(**12a**)] were grown by slow evaporation of a cyclohexane/CH_2Cl_2 solution (figure 23). The geometrical features of the complex are very similar to those of the related [AuCl(PPh_3)] complex (Au–P 223.08(5) pm, Au–Cl 229.15(5) pm).[172] Gold has a coordination number of two and adopts linear coordination geometry. The distance from gold to the nearest fluorine atom is 325.3(5) pm, which is too long to consider a significant Au···F interaction.[170a]

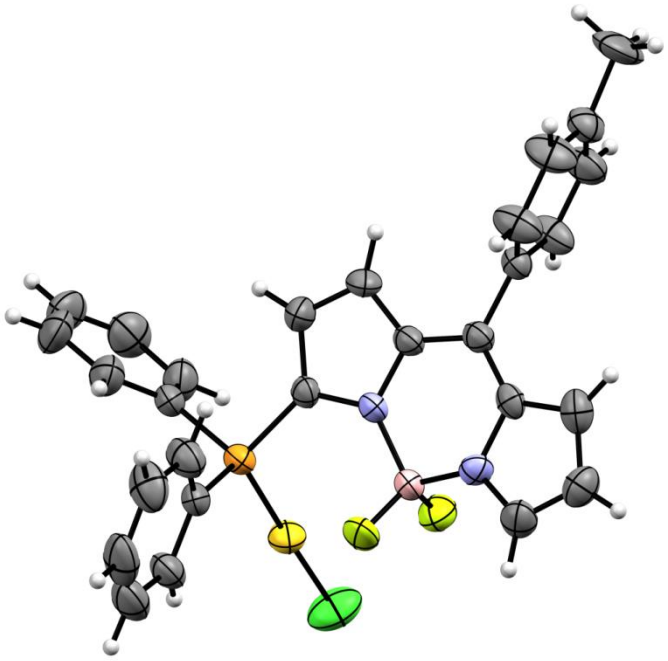

Figure 23. X-ray crystal structure analysis[173] and ORTEP representation of X-ray crystal structure of [AuCl(**12a**)]. Thermal ellipsoids are set at 50 % probability (color coding: Au yellow, P orange, F greenish yellow, B pink, Cl green, N blue). Important bond lengths (pm) and angles (°): Au–P 222.7(2), Au–Cl 229.8(3), Au···F 325.3(5), 377.1(6), P–Au–Cl 174.88(8). CCDC-1055648 contains the supplementary crystallographic data for this structure.

3.2.6. Optical properties

Fluorescence quantum yields and absorbance and emission maxima of the newly synthesized BODIPY compounds are summarized in table 3. All fluorophores reported herein display a strong UV/Vis absorbance at 506–552 nm and are characterized by small Stokes shift of approximately 15 nm. The small Stokes shifts point to a similar geometry of the excited and the ground state of the fluorophore.[11a] Replacing Cl with PPh_2 or PCy_2 leads to a long-wave shift of the absorbance maximum ($\Delta\lambda = +13$ or $+25$ nm); complexation of the phosphorus by group 10 metals leads to short-wave shift in the absorbance (and emission) maxima of approximately 10 nm. Like other 3-heteroatom-substituted BODIPY compounds, such as the 3-amino-substituted BODIPY,[141] the BODIPY-phosphines **12a** and **12b** are essentially non-fluorescent with fluorescence quantum yields $\Phi < 0.001$. It is likely that the phosphorus lone pair engages in PET quenching of the excited state.[9] In case this is true, the respective complexes of **12a** and **12b** with transition metals coordinated through the phosphine electron lone pair can be expected to display brighter fluorescence unless the presence of the metal opens new relaxation pathways. Indeed, the respective metal complexes of Ag^+ and Au^+ are fluorescent with Φ close to 0.1, while that of Pd^{2+} is non-fluorescent. Spectroscopic reporter

groups are important since the d^{10} ions Cu^+, Ag^+, and Au^+ do not show d-d transitions in the UV/Vis spectrum. Interestingly, the phosphine oxide **13a** is fluorescent (Φ = 0.026) but less so than the metal complexes, which is consistent with the results of a study on fluorescent phospholes.[174]

Compound	Φ[a]	Absorbance λ_{max} [nm]	Emission λ_{max} [nm]
11	<0.001	529	-
6	0.093	506	519
12a	<0.001	531	-
12b	<0.001	519	-
13a	0.026	508	524
[AuCl(**11**)]	0.008	552	567
[CuI(**12b**)]	0.016	516	527
[AgCl(**12b**)]	0.073	515	528
[AuCl(**12a**)]	0.087	515	531
[Au(NTf_2)(**12b**)]	0.11	508	523
[AuCl(**12b**)]	0.096	510	526
[Au(CCPh)(**12b**)]	0.070[b]	510	526
[$PdCl_2$(**12b**)$_2$]	<0.001	540	-

[a] Φ values were determined in 1,2-dichloroethane versus rhodamine 101 (Φ = 1.0 in EtOH) at RT with a concentration range of 0.25–1 μM.

[b] estimated value, see experimental part.

Table 3. Optical properties of BODIPY derivatives.

3.2.7. Monitoring ligand substitution reactions by fluorescence spectroscopy

In contrast to the bright BODIPY-NHC conjugates recently reported,[68, 70] the fluorescence in the BODIPY-phosphines described herein is largely quenched, probably due to PET-type quenching of the fluorophore. However, once the phosphorus lone pair is donated to a metal, an increase in the fluorescence quantum yields is likely, unless the metal itself opens new quenching pathways. Au(I) is normally a non-quenching metal ion and we, therefore, decided to study different ligand substitution reactions in the stable complex [AuCl(**12b**)]. This is especially interesting with a view to the prominent role that closely related complexes have played in homogeneous catalysis.[175]

Gold-thiolato complexes. The addition of an alkanethiol (1-dodecanethiol) to [AuCl(**12b**)] leads to an exponential decrease in the fluorescence intensity within approximately two minutes; upon addition of base (Et_3N), the fluorescence of this complex nearly vanishes (figure 24).[176] Upon addition of an arylthiol (thiophenol or thiocresol) to [AuCl(**12b**)] the

decrease in fluorescence is more pronounced, leading to an almost quenched complex; the addition of base produces only a small additional decrease in the brightness (figure 25). The addition of Et_3N alone to [AuCl(**12b**)] does not have a significant influence on the fluorescence intensity, the fluorescence is only quenched once the thiol is added. This shows that the addition of thiol and Et_3N leads to the formation of the well-established gold thiolato complexes,[177] with a significantly increased electron density at the gold. It is likely that this increase in electron density enhances the PET quenching of the fluorophore because the electron-rich gold is less willing to accept the phosphorus lone pair.[131a] Such conclusion is in line with the research on NHC–gold–thiolates described in the previous chapter. This hypothesis is additionally supported by work from Nagano et al. on organic fluorophores, who established a qualitative relationship between the electron density (rather the energy of the HOMO) of a quencher and the fluorescence quantum yield.[133a]

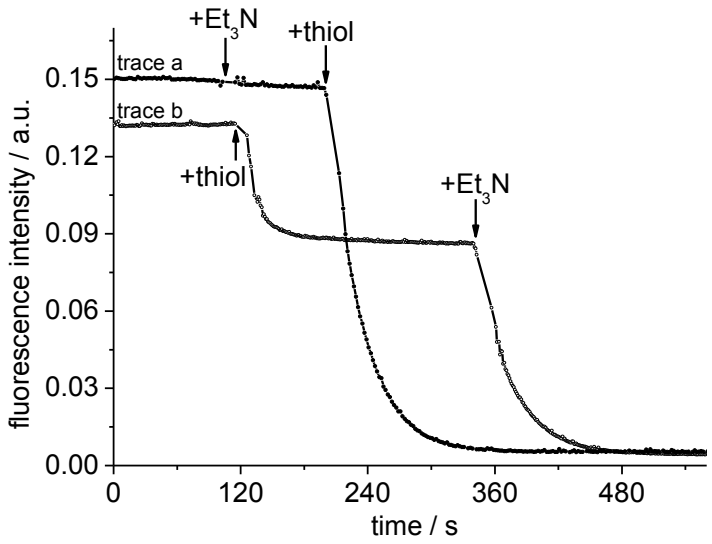

Figure 24. Fluorescence intensity vs. time plot for the reaction of thiol (dodecanethiol) with [AuCl(**12b**)] in 1,2-dichloroethane ($c = 1.0 \cdot 10^{-6}$ mol·L^{-1}) and base (Et_3N). Order of addition of reactants: [AuCl(**12b**)] + Et_3N then thiol (trace a) or [AuCl(**12b**)] + thiol then Et_3N (trace b).

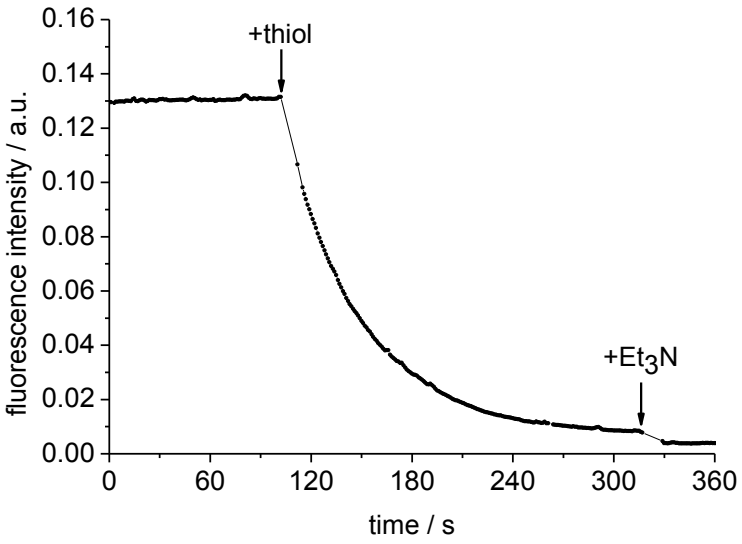

Figure 25. Fluorescence intensity vs. time plot for the reaction of thiol (thiophenol) with [AuCl(**12b**)] in 1,2-dichloroethane (c = 1.0·10^{-6} mol·L^{-1}) and base (Et_3N). Order of addition of reactants: [AuCl(**12b**)] + thiol then Et_3N.

It is not clear why the addition of alkanethiol leads to a smaller decrease in the fluorescence intensity than with the arylthiol, but the different acidities of alkanethiol and arylthiol might play an important role. Two explanations are considered: a) the thiol replaces the chloro ligand forming a cationic complex of the type [Au(RSH)(**12b**)]$^+$Cl$^-$; b) alternatively, an equilibrium of the type [AuCl(**12b**)] + RSH = [Au(SR)(**12b**)] + HCl is established. In order to probe hypothesis (a), the reaction of [AuCl(**12b**)] with thiophene was studied in the fluorescence spectrometer. No change in the fluorescence was observed upon addition of thiophene (figure 26) and therefore coordination of the thiol is less likely.

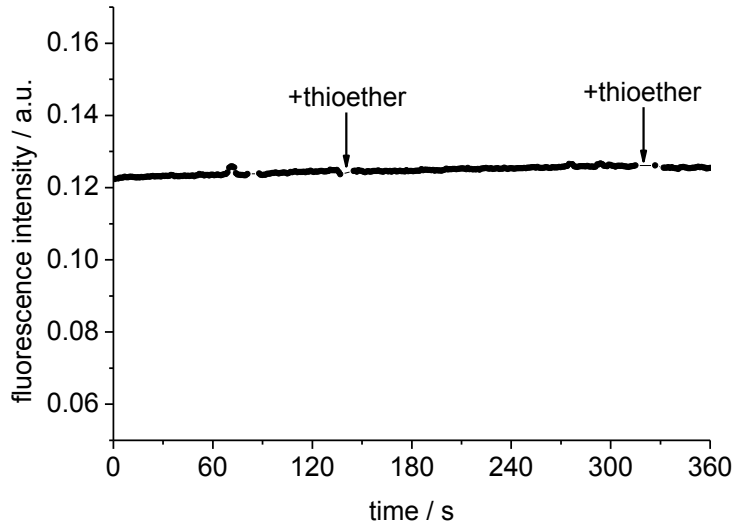

Figure 26. Fluorescence intensity vs. time plot for the reaction of thioether (tetrahydrothiophene) with [AuCl(**12b**)] in 1,2-dichloroethane (c = 1.0·10^{-6} mol·L^{-1}). Order of addition of reactants: [AuCl(**12b**)] + thioether.

To verify hypothesis (b), different amounts of thiol (50, 100, 200, 400 equiv) were added to [AuCl(**12b**)]. Depending on the amount of added thiol, a corresponding decrease in the fluorescence intensity was observed, with more thiol leading to successively weaker

fluorescence (figure 27). The fluorescence is always fully quenched upon addition of base to this reaction mixture. This observation is in line with shifting the equilibrium [according to (b)] upon addition of more alkanethiol to the product side. Based on this equilibrium, the much larger initial drop of brightness with aryl thiols as compared to alkyl thiols can be explained based on the much higher acidity of aryl thiols.

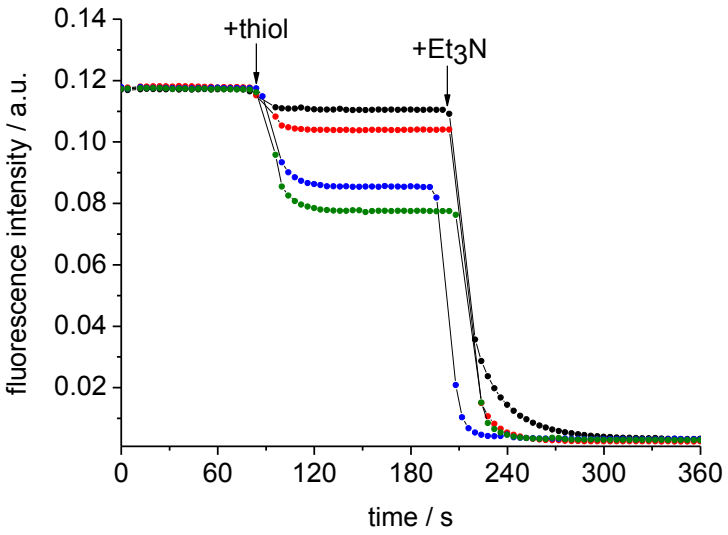

Figure 27. Fluorescence intensity vs. time plot for the reactions of [AuCl(**12b**)] (c = 1.0·10^{-6} mol·L^{-1}) in 1,2-dichloroethane with different amounts of dodecanethiol, added after ca. 80 s (black: +50 equiv dodecanethiol; red: +100 equiv; blue: +200 equiv; green: +400 equiv) to [AuCl(**12b**)], followed by addition of excess of triethylamine.

The analogous experiments (addition of 1 equiv thiol and 1 equiv Et_3N to [AuCl(**12b**)], albeit at ca. 10000 times higher concentration of gold complex) were carried out in NMR tubes. Resonances detected in the ^{31}P NMR spectra of the nonfluorescent solutions show the clean transformation of [AuCl(**12b**)] (δ= 47.5 ppm) into [Au($SC_{12}H_{25}$)(**12b**)] (δ= 49.6 ppm) or into [Au(SPh)(**12b**)] (δ= 50.5 ppm); no other peaks are observed in the ^{31}P NMR spectra (figure 28).

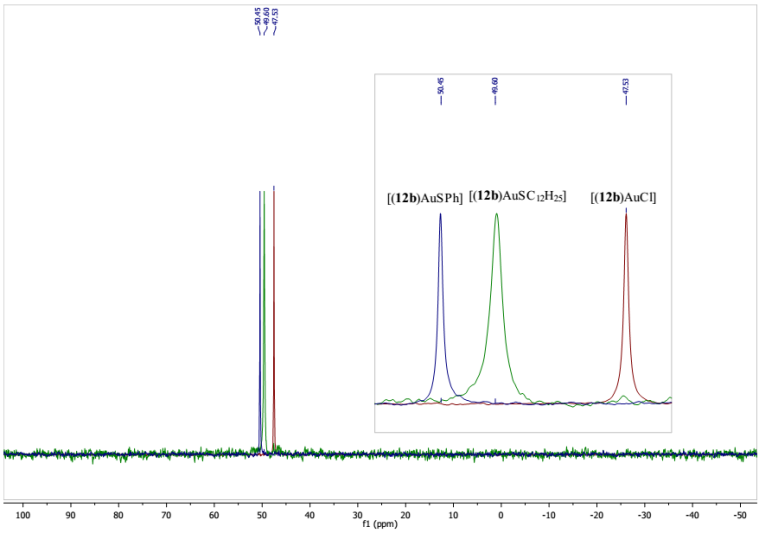

Figure 28. ^{31}P-NMR spectra of [(**3b**)AuCl], and its thiol derivatives [(**3b**)Au$SC_{12}H_{25}$] and [(**3b**)AuSPh], formed directly in NMR tube upon addition of 1 equiv of the respective thiol and 1 equiv of Et_3N to the solution of [(**3b**)AuCl] in $CDCl_3$.

Gold complexes with weakly coordinating anions. Based on the results with Au thiolates, a decrease in the electron density at the transition metal could lead to enhanced brightness. We were therefore interested, whether it is possible to study the formation of "cationic" gold complexes at catalytically relevant concentrations using fluorescence spectroscopy. This was tested by replacing the strongly coordinating chloride in [AuCl(**12b**)] with weakly coordinating (donating) anions (wca), with the help of silver salts.[178] Such reactions are very important in gold catalysis, often constituting the crucial activating step in numerous gold-catalyzed transformations.[179] Complexes such as [LAu(wca)] are generated in situ from [LAuX] (X = Cl, Br, I) through silver salt metathesis involving precipitation of AgX,[180] but may also be isolated and then used in catalysis.[181] The nature of the anion and of the solvent, in which such reactions are carried out, exert a very significant influence on the formation of solvent-separated ions (vs. close ion-pairs) and consequently on catalytic activity.[182]

To a solution of [AuCl(**12b**)] in 1,2-dichloroethane were added aliquots corresponding to 0.5 equivalents of [Ag(ONf)] (ONf = $C_4F_9SO_3^-$) in the same solvent (figure 29). The fluorescence intensity of the solution increases following the addition of each aliquot and reaches saturation after adding approximately 2.5 equivalents of silver salt, corresponding to an increase in fluorescence brightness of approximately 20%.[183],[184] Addition of more silver salt (up to 20 equiv) does not lead to significant change in the fluorescence intensity. It is likely that the fluorescence increase is due to ONf^- being less electron-donating than chloride. To test this, [Au(NTf_2)(**12b**)] was synthesized and the fluorescence intensity was found to be almost the same as that of the in situ prepared gold nonaflate. However, for both [Au(wca)(**12b**)] complexes, the change in the fluorescence intensities is rather modest compared to those seen in the other reactions described herein. This may well mean that in the 1,2-dichloroethane solvent, cation and anion still form fairly close ion pairs, which is reasonable with a view to the very low donicity of 1,2-dichloroethane.[185],[186] The experiments clearly show that the reaction of the gold complex with [Ag(ONf)] requires superstoichiometric amounts of silver salt to form the gold nonaflate complex. When smaller amounts of silver salt intermediate species are used, presumably Au···Cl···Au species are formed.[187] This fits well with results reported by Echavarren et al., who showed that a significant excess of [Ag(OTf)] is required to produce the related [(JohnPhos)Au(OTf)] from [(JohnPhos)AuCl], as demonstrated by NMR studies.[187] Our studies confirm the results from Echavarren's group; however, in our study, such information is obtained at catalytically relevant concentrations.[188]

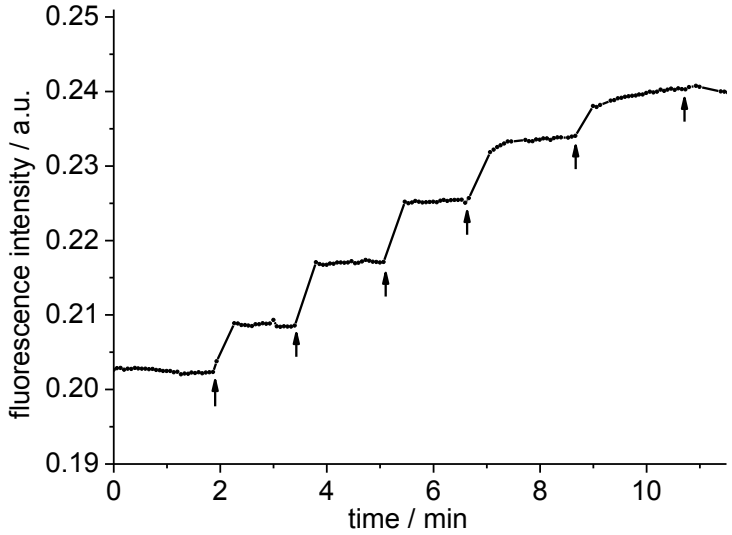

Figure 29. Fluorescence intensity vs. time plot for the addition of six times 0.5 equiv aliquots of [Ag(ONf)] (denoted by arrows) to a solution of [AuCl(**12b**)] ($c = 1.0 \cdot 10^{-6}$ mol·L^{-1}) in 1,2-dichloroethane.

Gold-acetylene complexes. Next, we were interested to learn, whether the modulation of brightness could be used to probe the initial steps defining gold-catalyzed reactions with acetylenes. Key species in such reactions are η^2-bonded acetylenes,[189] σ-bonded acetylides,[190] and the cationic digold species $[(LAu)_2(CCR)]^+$.[190-191] Changes in the coordination sphere should influence the electron density at gold and lead to the characteristic modulation of the fluorescence intensity.

To a solution of [AuCl(**12b**)] in 1,2-dichloroethane were added 1–30 equivalents of [Ag(ONf)]. The formation of [Au(ONf)(**12b**)] is accompanied by a modest increase in the fluorescence intensity (figures 29 and 30). To the in situ generated gold nonaflate were added 1000 equivalents of phenyl acetylene, leading to a very pronounced increase in the brightness (figure 30). The amount of silver in the reaction mixture has a significant influence on the evolution of the fluorescence intensity. In the presence of large amounts of [Ag(ONf)] (> 10 equiv) a very fast increase in the brightness is observed. When applying less silver salt, the reaction with acetylene is sluggish or does not take place. The need for a large excess of silver salt is not obvious since our previous experiments had shown that [Au(ONf)(**12b**)] is already formed with approximately 2.5 equivalents of silver salt. However, it is well known that for many Au-catalyzed reactions, a significant rate acceleration occurs in the presence of a large excess of silver salt.[180b, 182a, 192] Based on these results, we conclude that the coordination of the alkyne to the gold and alkyne deprotonation are critical steps. Consequently, the coordination of alkyne to excess silver salt appears to activate this substrate for the reaction with gold, leading to an overall faster reaction.

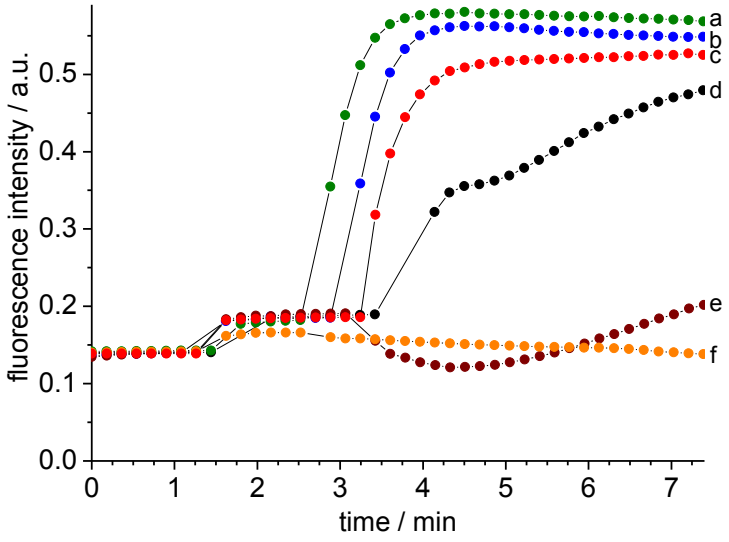

Figure 30. Fluorescence intensity vs. time plot for the reactions of [AuCl(**12b**)] (c = 1.0·10^{-6} mol·L^{-1}) in 1,2-dichloroethane with different amounts of [Ag(ONf)], added after ca. 1.5 min (trace f: +1 equiv [Ag(ONf)]; trace e: +5 equiv; trace d: +10 equiv; trace c: +15 equiv; trace b: +20 equiv; trace a: +30 equiv) to [AuCl(**12b**)], followed by addition of phenyl acetylene (1000 equiv added after 2.5–3.4 min). Traces a-f denote the fluorescence-time changes after addition of alkyne to gold complexes activated with different amounts of [Ag(ONf)].

The reactions of acetylenes with cationic gold complexes can lead to several different species, including a side-on bound complex [LAu(PhCCH)], a terminal acetylide complex [LAu(CCPh)], and a dinuclear species [(LAu)$_2$(CCPh)]$^+$.[193] Based on the fluorescence intensity alone, it is not possible to identify the formed species. Nonetheless, we were able to gather sufficient evidence to overcome this problem. The side-on complex is a fragile species and only a few examples of such complexes have been reported.[189a] In the presence of a base, this complex is easily converted into the terminal acetylide.[194] However, in the reactions presented herein, the addition of an excess of base (Et_3N) does not lead to significant changes in the brightness. The side-on complexes with PhCCH are characterized by modest formation constants,[190, 195] which render their presence in the 10^{-6} mol·L^{-1} solutions of Au complex less likely. To probe the potential formation of a side-on bound complex, the cationic gold complex was exposed to 1000 equivalents of 4-octyne, which is known to form more stable complexes with LAu$^+$ than PhCCH.[195] However, no change in the fluorescence brightness was observed (figure 31) and based on this evidence we conclude that the side-on acetylene-gold complex is not formed in such dilute solutions.

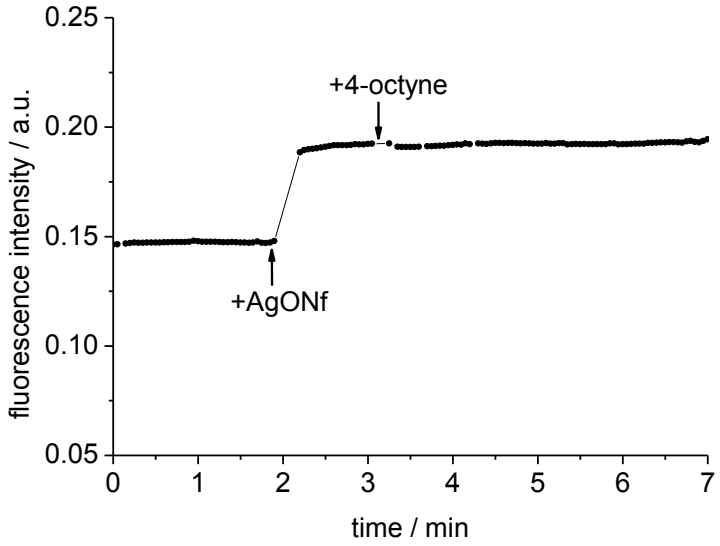

Figure 31. Fluorescence intensity vs. time plot for the reaction of [AuCl(**12b**)] (c = 1.0·10^{-6} mol·L^{-1}) in 1,2-dichloroethane with [Ag(ONf)] (15 equiv) and 4-octyne (1000 equiv).

The terminal acetylide complex is another potential reaction product. However, this neutral complex should not lead to the observed pronounced increase in the fluorescence level, but instead to a significant decrease. To further clarify this, [Au(CCPh)(**12b**)] was synthesized and the fluorescence quantum yield determined, which is much lower than that of [AuCl(**12b**)] (table 3). For this reason, we believe the species formed in our fluorescence experiments to be the dinuclear [((**12b**)Au)$_2$(CCPh)]$^+$.[190-191] Closely related species with SIPr-type NHC ligands instead of **12b** are well known.[189a] The cationic nature of this complex is in accord with the pronounced increase in fluorescence intensity. A reaction mixture containing the dinuclear species, based on a procedure by Widenhoefer et al.,[190] was probed by NMR spectroscopy (albeit at much higher concentration than in the fluorescence experiment). This experiment provides clear evidence for the formation of the dinuclear species. However, we were not able to isolate this complex in its pure state due to its instability. The phosphine ligand **12b** is most likely insufficiently bulky to render a stable dinuclear complex. Furthermore, NMR signals are observed for the known vinyl triflate, which is the addition product of PhCCH and TfOH. Based on the fluorescence intensity of the in situ formed [((**12b**)Au)$_2$(CCPh)], the fluorescence quantum yield of this complex is estimated to be close to Φ = 0.4.

Finally, we were interested to find out whether the modulation of the electronic nature of the phenyl acetylene has an influence on the fluorescence intensity of the remote BODIPY unit. This was tested by using phenyl acetylenes with electron-withdrawing (R = NO_2) and electron-donating groups (R = NMe_2) in the 4-position. The respective digold complexes [((**12b**)Au)$_2$(CCC$_6$H$_4$-R)]$^+$ were generated with the aid of Hünig's base in the cuvette and the fluorescence intensity measured (figure 32). The fluorescence experiment proved to have excellent sensitivity, since even the remote 4-NMe_2 substituent led to a significant decrease in the fluorescence brightness of the peripheral BODIPY unit, while the 4-NO_2 group caused a small increase in the (already high) brightness of the fluorescence emission.

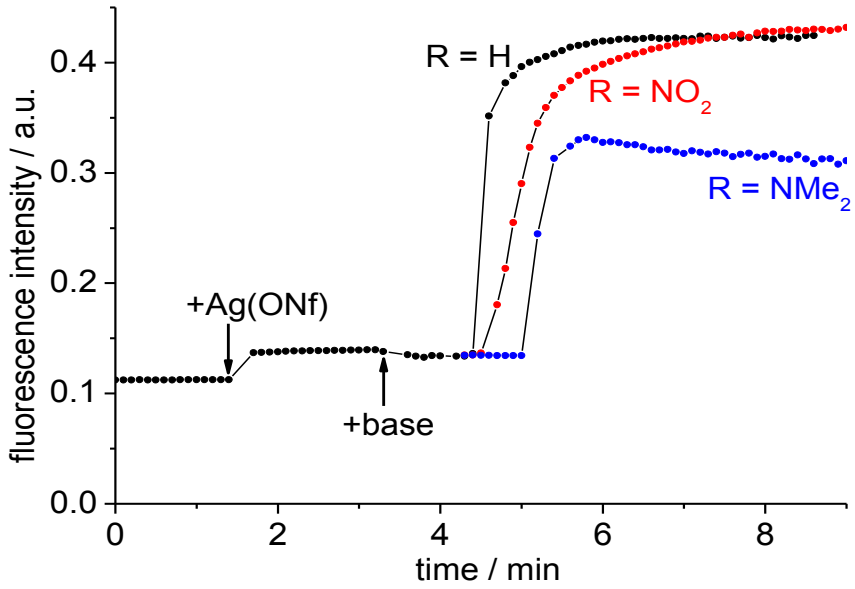

Figure 32. Fluorescence intensity vs. time plot for the reactions of [AuCl(**12b**)] (c = 1.0·10^{-6} mol·L^{-1}) with [Ag(ONf)], Hünig's base, and three different phenyl acetylene derivatives HCCC$_6$H$_4$R (1000 equiv; R = NO$_2$, H, NMe$_2$) yielding [((**12b**)Au)$_2$(CCC$_6$H$_4$R)]$^+$ ONf$^-$ complexes in 1,2-dichloroethane.

3.3. Ion-pairing in transition-metal complexes via PET and FRET

3.3.1. Ion pairs in transition-metal catalysis

The phenomenon of ion-pairing plays an important role in catalytic processes of transition-metal complexes.[196] Nowadays, it is a matter of fact that the nature of weakly coordinating anion has a great influence on the activity of catalyst, as well as on its chemo-, regio- and stereoselectivity, which was observed in a variety of chemical transformations such as olefin polymerization,[197] Diels-Alder,[198] Heck,[199] hydrogenation,[200] carbonylation,[201] and many other catalytic reactions.[202] Concerning activity, in most cases, it has been found that the weaker the coordinating power of the anion, the higher the reactivity for a given cation.[203] The reason for such trend is that both the substrate and the anion compete for the reactive site of the cation, and the less coordinating anion would facilitate the coordination of substrate and subsequent catalytic transformations. At the same time, the influence of the counterion on the selectivity of the catalyst is still often the matter of debate.

In reactions of transition-metal complexes, contact ion pairs play a decisive role. They are divided into two types: outer-sphere ion pairs (OSIPs) and inner-sphere ion pairs (ISIPs) (figure 33).[196] Since catalytic processes normally take place in solution, X-ray analysis may be only suitable for investigation of ISIPs, where strong interaction between cation and anion can be responsible for identical ionic orientation in the solid state and in solution; the structures of solvated OSIPs can be considerably different from that in the solid state. Therefore, the main tools used for the ion-pairing study in solution are NMR techniques, such as PGSE (pulsed field gradient spin-echo) and NOE (homo- and hetero-nuclear) NMR experiments.[204]

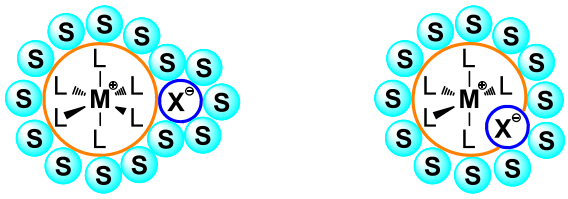

Figure 33. Schematic representation of OSIP (left) and ISIP (right).

By using PGSE experiments it is possible to determine the hydrodynamic volume of the diffusing particles. Based on this, the degree of aggregation of catalytic species can be established, i.e. whether they exist as free ions, or ion pairs, quadruples, etc. Typically, the type of ionic species present in solution strongly depends on the nature of solvent and concentration of complexes.[205]

NMR techniques based on NOE, which acts directly through space, can be used to establish the structures of ion pairs of transition-metal complexes in solution.[206] Although NOE is limited to the distance of max. 0.5 nm, it is suitable for investigation of intimate ion pairs, which affect the reactivity of catalysts the most. The obvious requirement for NOESY is that both ionic counterparts should contain magnetically nonequivalent NMR-active nuclei with high receptivity, for example, ^{1}H and ^{19}F nuclei. By investigation of ^{1}H-NOESY and ^{19}F,^{1}H-HOESY NMR spectra of several Fe(II),[207] Ru(II),[208] Os(II),[209] Pd(II),[210] Pt(II)[211] and Ir(III)[212] complexes ion pairs, Macchioni and coworkers have shown that in most cases there is a predominant relative anion-cation orientation, determined mainly by a gain in electrostatic interaction energy. Despite the successful qualitative NMR investigations, quantitative determination of the average interionic distances by NOESY faces some limitations. For a quantitative analysis, the correlation times of the reference distance and the distances of interest must be the same. This is not necessarily the case if we compare a pair of nuclei belonging only to one of the ions constituting ion pair (intramolecular distance) and the nuclei of the cation and those of the anion (interionic distance). Nonetheless, Zuccaccia et al. have shown[213] that in some cases quantification of interionic NOEs can be successfully carried out with the consequent possibility of estimating average interionic distances.

Catalytic activity[214] and selectivity[215] of gold(I) cationic complexes are also greatly affected by the nature of counterion. For example, Macchioni and coworkers have shown[216] that properties of anion influence the catalytic performance of gold complexes in the alkoxylation reaction of alkynes by two reasons: on the one hand, the anion facilitates the reaction by deprotonation of methanol during the nucleophilic attack; on the other hand, its coordination to the metal center suppresses the catalytic activity by preventing alkyne coordination. Both of these factors have opposite dependence on basicity of the anion, and the medium basic OTs^{-} was found to show the best catalytic activity. These results were further supported by the computational study.[217] In more general research, Zhdanko and Meier have shown[178b] that the overall anion effect is generally determined as superposition of the elementary effects such as hydrogen bond acceptor power, coordinating ability to gold, and affinity for a proton (basicity). The authors suggested OTf^{-} to be an optimal counterion for the majority of cases in gold(I)-catalyzed hydroalkoxylation of alkynes. In another comprehensive study, Zuccaccia and coworkers have shown[218] that efficiency of gold(I) catalysts for a given process depends not only on the properties of anion and ligand alone but rather on their combination.

Since gold(I)-alkene and -alkyne complexes are important intermediates in gold-catalyzed transformations,[219] Macchioni and coworkers have investigated ion-pairing in cationic

gold(I) catalysts bearing unsaturated hydrocarbons by combining NMR experiments with theoretical modelling.[189d, 220] Depending on the nature of ligand three specific anion-cation orientations were identified for most of the complexes[221] (figure 34): for phosphine ligands the anion preferentially located close to the substrate (orientation C) and/or above and below the metal (orientation B); in the case of NHC complexes the anion tends to stay near the ligand (orientation A). Within this general pattern, the ion-pairing can be finely tuned by the introduction of functional groups in the ligand.

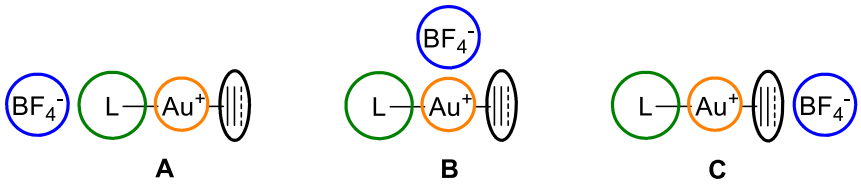

Figure 34. Three orientations, A, B, and C, of the counterion in gold(I)-alkene (-alkyne) complexes.

In the subsequent work, Zuccaccia and coworkers have investigated[222] a relationship between the anion-cation relative orientation and the catalytic activity of gold complexes. For this reason, the authors have compared the structures of *in situ* prepared complexes P1, P2 and P3 (figure 35) with their activity in the alkoxylation reaction of 3-hexyne directly in NMR tube. The difference in the number and the position of the OH and NH moieties (hydrogen bond donors) and also in the steric hindrance around them was designed with the deliberate purpose of influencing the ion pair structure of the catalyst. Thus, the anion in complex P1 in $CDCl_3$ was found to localize predominantly near the ligand; the relationship of the relative orientations A and C (figure 34) was established to be 97:3. In fact, the interaction between BF_4^- and the ligand in P1 was so strong that ion-pairing was not affected even by using more polar CD_3OD as a solvent. Substitution of one NH hydrogen with bulky isopropyl group weakened the interaction between the anion and the ligand, so that for the complex P2 A:C = 79:21, which indicates a higher relative abundance of the anion in the orientation C (closer to the alkyne side) compared to P1. In complex P3 the anion was predominantly localized near OH group; the impact of orientation A and C was negligible.

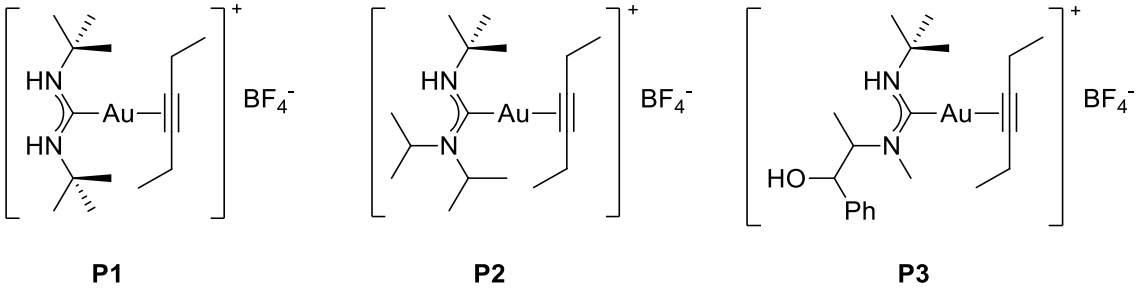

Figure 35. Different *N*-acyclic carbene (NAC) gold complexes prepared by Biasiolo et al.

The highest catalytic activity was observed for the complex P2 (catalyst loading 1 mol%), which showed 59% conversion of alkyne in 90 min using $CDCl_3$ as a solvent, whereas for P1 and P2 conversion was only 24-30% at the same time. This is consistent with the previously reported works,[178b, 216-217] according to which the anion has a beneficial role in activating the methanol by lowering the activation barrier of the attack: if a specific interaction keeps the anion far from the catalytic center, it cannot play its role of activator and the reaction slows down. By using methanol as a solvent for the reaction, catalytic activity of the complexes P2 and P3 was found to be almost the same, since in more polar solvent both complexes exist as

free ions. Hence, tuning of the preferential position of the counterion by careful ligand design opens the way to greater control over the properties and activity for the gold-mediated reactions in which the anion plays an important role during the catalysis.

Concerning the important role of counterions in transition-metal catalysis, we decided to explore whether fluorescence spectroscopy can be used for the ion-pairing study. Compare to NMR techniques, it can operate at much lower concentration range – more relevant to the catalytic processes; also it requires relatively simple equipment, which can provide fast measurements, thus making possible "live" observation of chemical transformations. In the previous chapters, the design and application of PET-based molecular probes were shown. Another distance-dependent effect – FRET – is widely used in biology as a "spectroscopic ruler"[223] to measure the distances between different parts of macromolecules, etc. In this chapter, we have focused on designing transition metal complexes suitable for ion-pairing study by employing either PET or FRET quenching mechanisms.

3.3.2. Ion-pairing via PET

At first, we decided to probe whether PET effect is suitable for ion-pairing study. The general idea is schematically represented in figure 36. The lone pair(s) of the anion, connected to the fluorophore, should quench the fluorescence brightness because of PET. Once the anion is coordinated to the transition metal, the negative charge should be withdrawn towards the metal center, which plays a role of Lewis acid. As a consequence, fluorescence emission should increase. In contrast, the breakup of ion pair should lead to the quenching of fluorescence due to releasing of electron density on the anion. Hence, the intensity level of fluorescence emission was expected to provide useful information about the extent of association of counterions and their spatial arrangement.

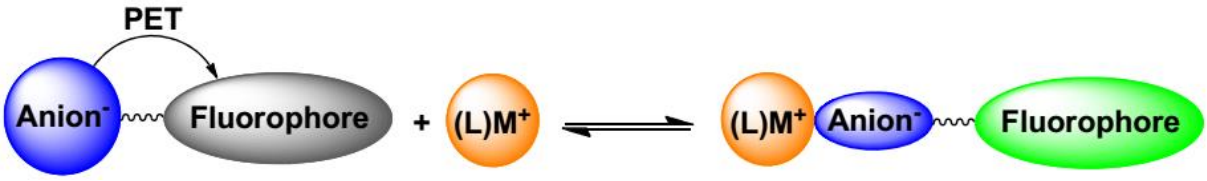

Figure 36. Investigation of ion-pairing based on PET effect.

Gold(I) complexes are widely used in catalysis and were also chosen for our study because of non-quenching nature of gold metal. NHC-gold(I) complexes containing medium-coordinating tosylate counterion appeared to be very efficient in catalysis, for example, in alkoxylation of alkynes.[216-217] Therefore, to test our concept, we have synthesized gold sulfonate complex [AuIPr(**14**)] (figure 37). Since SO_3 group is directly connected to the BODIPY core in this molecule, the influence of anion on the emission brightness of the fluorophore should be maximized. This complex was obtained from IPrAuCl and silver salt **14**·Ag by the halide abstraction reaction. The salt **14**·Ag was prepared in a similar way to the known BODIPY sulfonate sodium salts,[50] by using silver carbonate instead of sodium carbonate to quench the intermediate BODIPY sulfonic acid. Purification of the silver salt **14**·Ag by silica column leads to an unclear result: although NMR shifts fit the ones observed in the spectrum of the crude product, the "purified" material doesn't react with IPrAuCl anymore. Based on this we have concluded, that interaction with silica during purification leads to some chemical transformation, most probably, cation exchange. Therefore, salt **14**·Ag was purified by precipitation with diethyl ether from DCM solution, thus avoiding silica column.

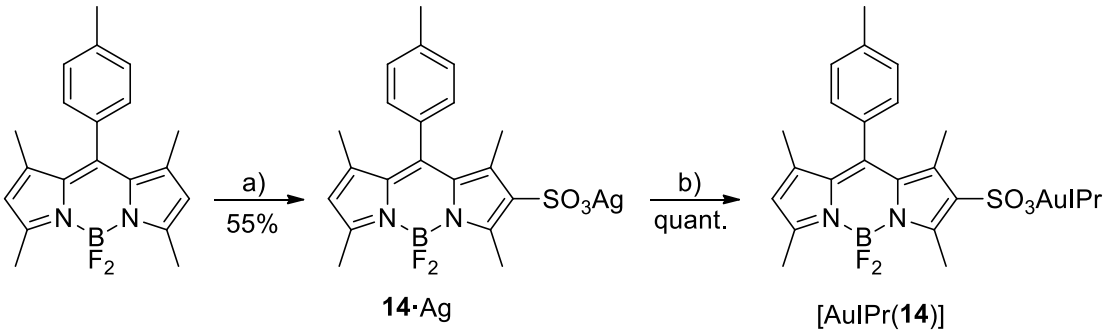

Figure 37. Synthesis of gold sulfonato complex [AuIPr(**14**)]. Reaction conditions: a) $ClSO_3H$, DCM, -78 °C, 30 min, then RT, 1h, then MeOH, Ag_2CO_3, 12 h; b) IPrAuCl, DCM, RT, 12 h.

We suggest that complex [AuIPr(**14**)] in toluene should exist predominantly in the form of intimate ion pairs. The increase of solvent polarity by addition of acetonitrile should lead to another extreme case – complete dissociation of ion pairs. Such chemical transformation should be characterized by the maximum change of fluorescence intensity. In other words, a difference of fluorescence emission between two states would define the range of values that can be useful for ion-pairing study.

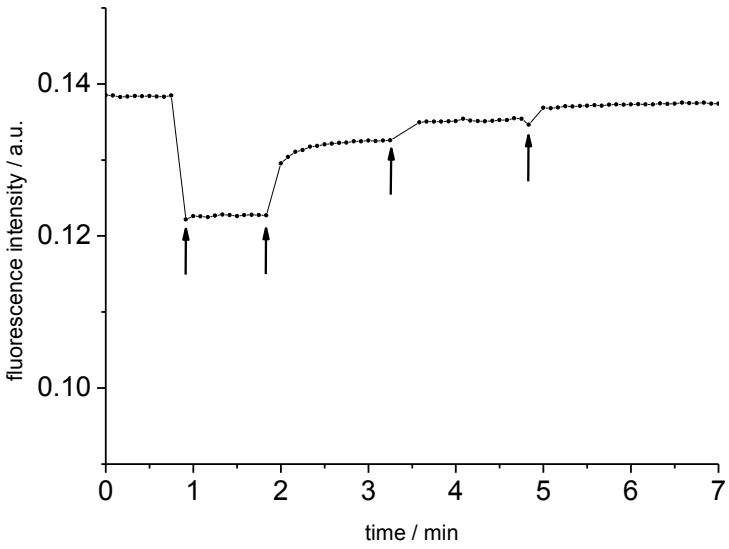

Figure 38. Fluorescence intensity vs. time plot for the addition 50 µl aliquots of acetonitrile (denoted by arrows) to a solution of [AuIPr(**14**)] ($c = 1.0 \cdot 10^{-6}$ mol·L^{-1}) in toluene.

As shown in figure 38, the addition of acetonitrile to the solution of the complex [AuIPr(**14**)] in toluene led indeed to decrease of fluorescence intensity, which was in line with our prediction. Further increase of polarity has caused restoring of emission intensity, indicating suppression of PET at higher acetonitrile content. Most probably, it happened due to stabilization of the negative charge of the anion by solvation with a polar solvent. Nonetheless, the initial drop of fluorescence intensity was only *ca*. 11%, which shows the rather low sensitivity of the PET-based probe. Any other transformations should lead to even smaller intensity change, which can be difficult to detect. For example, the addition of phenyl acetylene was not accompanied by any observable change of emission intensity. Concerning the low stability of complex [AuIPr(**14**)] in solution, which limits its full characterization, we

have concluded that the PET-based probe is not suitable for ion-pairing study. Therefore, another quenching mechanism was considered.

3.3.3. Ion-pairing via FRET: general concept

FRET is another fluorescence quenching mechanism, which can be used for distance measurements in chemical systems. An interesting example of FRET application was described by Diederich and coworkers,[224] who have used fluorescence techniques for investigation of the vase–kite switching process in the quinoxaline-bridged resorcin[4]arene cavitands. In their research, the authors have prepared BODIPY-substituted cavitands shown in figure 39. Addition of trifluoroacetic acid caused the transition of cavitands from the vase state to the kite state, which was clearly demonstrated by FRET measurements: the donor intensity strongly increased and the acceptor intensity almost disappeared due to the increased distance between the two dyes. FRET was also applied for the determination of the average opening angle α of the cavitands in the vase conformation in solution. In general, to calculate the distance between the donor and acceptor fluorophores from the measured FRET efficiency, knowledge of Förster radius R_0 is needed. Since R_0 value depends on many factors, it should be determined for any particular system independently. Prepared cavitands (figure 39) were different by the number of phenylethynyl units (n) in the linker which connects the fluorophores and the rest of the molecule. Assuming that α is constant for all cavitands at a certain temperature, the distance between the donor and acceptor BODIPYs (R) was expressed as a function of α and n. The brief mathematical description is given below. It should be also noted, that cavitand with $n = 0$ was not suitable for the investigations, since R_0 value for this compound was different than in the others cases ($n = 1, 2, 3$). Most probably, it was caused by the hindered rotation of the fluorophores, which resulted in a different orientation factor.

The FRET efficiency can be calculated by the formula (1):

$$E = 1 - \frac{I_{DA}}{I_D} \quad (1)$$

where I_{DA} – measured emission intensity of the donor fluorophore in the presence of the acceptor fluorophore and I_D – in the absence of the acceptor fluorophore. The dependence on distance is defined by the equation (2):

$$E = \frac{1}{1+\left(\frac{R}{R_0}\right)^6} \quad (2)$$

which can be rewritten in the following manner:

$$\sqrt[6]{\frac{1}{E} - 1} = \frac{R}{R_0} \quad (3)$$

where R is a distance between two fluorophores, R_0 – Förster radius. The distance R was also defined through trigonometric transformations:

$$R = 2d + a = 2c\sin(\alpha) + a = 2[(nb + e)\sin(\alpha)] + a = 2e\sin(\alpha) + \mathrm{a} + 2b\sin(\alpha)n \quad (5)$$

where values a, b, c, d and α are defined as shown in figure 39, n – is a number of connecting phenylethynyl units, $e = c$ when $n = 0$. When the expression for R from equation (5) was

substituted into equation (3), the authors have obtained an expression (6) for R/R_0 that was a linear function of n.

$$\sqrt[6]{\frac{1}{E}-1}=\frac{R}{R_0}=\frac{2e\sin(\alpha)+a}{R_0}+\frac{2b\sin(\alpha)}{R_0}n \qquad (6)$$

The values of a, b and e were obtained from X-ray analysis. The values of R_0 and α were unknown but were easily obtained by plotting R/R_0 versus n. The plot was fitted linearly with a good correlation and from the slope and y-intercept of this line, values for the Förster radius and the average opening angle were calculated: $R_0 = 37$ Å and $\alpha = 16°$.

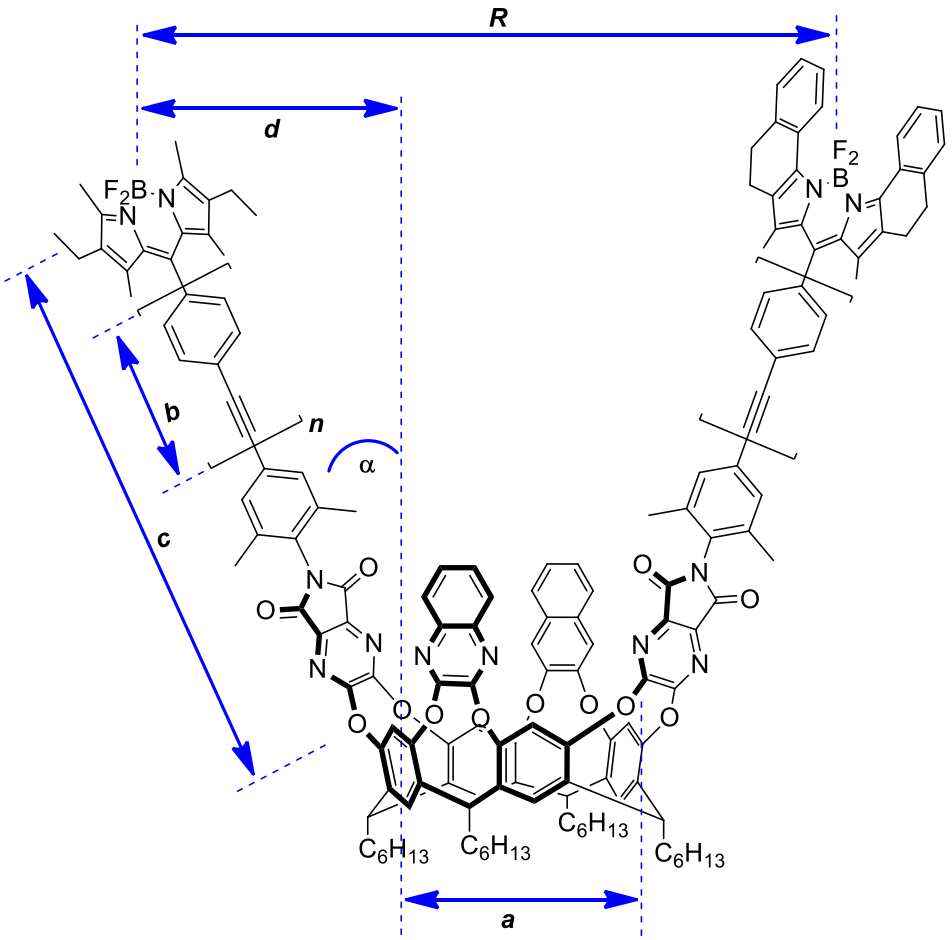

Figure 39. BODIPY-substituted cavitands reported by Diederich and coworkers.

We suggest that the similar approach as described above can be also applied for the ion-pairing study. The very general concept is represented in figure 40. The FRET efficiency in the system, which consists of two counterions labeled with the FRET pair fluorophores, should depend on the average distance between the cation and anion. Hence, the ISIP should be characterized by the maximum FRET efficiency: the high intensity of acceptor fluorophore and almost absent emission of donor fluorophore (figure 40, a). In the case of OSIP, when cationic metal species are coordinated to the substrate, FRET efficiency should decrease leading to intermediate intensity values for both donor and acceptor fluorophores (figure 40, b). And, finally, solvation of ion pairs by a polar solvent and formation of free ions should lead to the complete disappearance of FRET and full restoring of donor emission (figure 40, c). The choice to connect acceptor fluorophore to cation and donor fluorophore to anion was arbitrary; the contrary connection doesn't affect the overall concept.

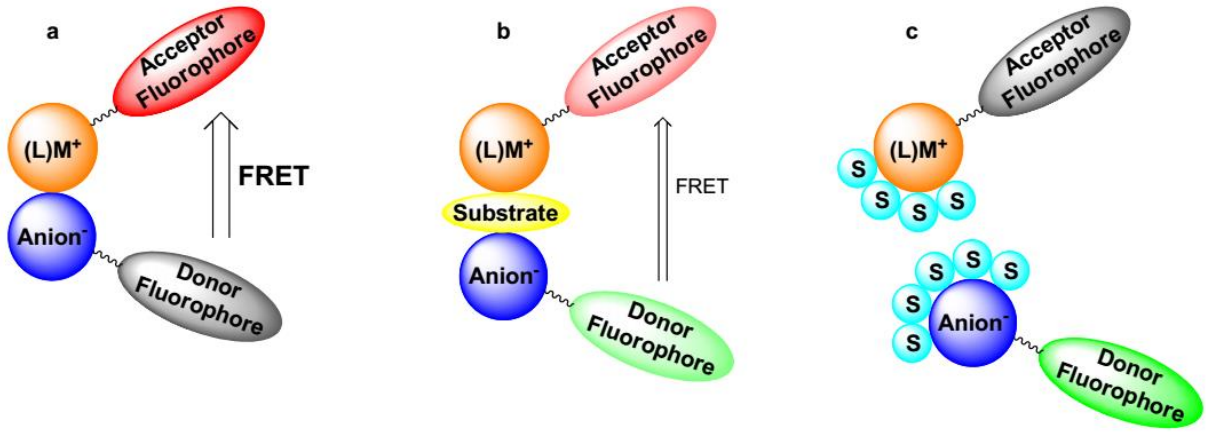

Figure 40. The general concept of the FRET application for ion-pairing study: a) ISIP is characterized by the maximum FRET efficiency; b) OSIP – intermediate FRET efficiency; c) free ions – disappearance of FRET.

More details of the proposed approach are revealed in figure 41. An acceptor fluorophore is connected to the ancillary ligand and a donor fluorophore to the anion moiety through properly designed linkers (figure 41, a). We can characterize relative 3D arrangement of ion pair components by using Cartesian coordinates and putting the origin on the metal center as shown in figure 41, b. In this case, we can define the average position of acceptor fluorophore by a vector $\vec{A}$, which points from the origin to the fluorophore (strictly speaking to the middle of its transition dipole). To simplify the concept we assume that the value of vector $\vec{A}$ depends only on the chemical structure of ligand and linker (and other macroscopic parameters such as solvent, temperature, etc.) and doesn't depend on the type of ion pair (i.e. position of anion). In general, it is not necessarily true but can be achieved by careful design of the linker between ligand and acceptor fluorophore. Analogously to $\vec{A}$, we can define position of donor fluorophore as a vector $\vec{D}$ (figure 41, b), although in this case some additional requirements should be fulfilled. At first, positions of anion moiety and donor fluorophore can be easily correlated only if they are connected by a rigid (preferably straight) linker. And second, for such representation to be correct the whole anion should point towards the metal center. This requirement is more specific and must be considered separately for each particular case.

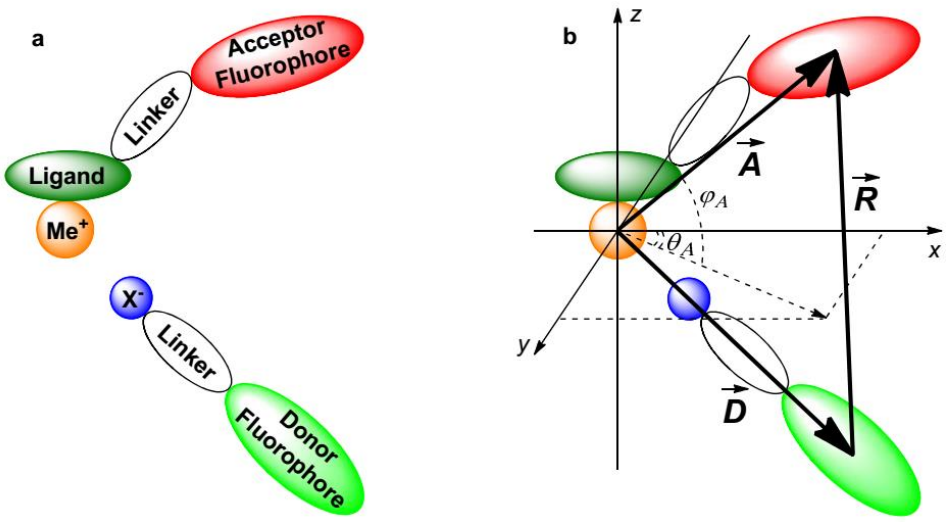

Figure 41. Schematic representation of fluorophores-tagged ion pair (a); position determination of ion pair components using vectors (b).

The distance between two fluorophores R can be defined as a module of vector $\vec{R}$ (figure 41, b), which equals to the difference between vectors $\vec{A}$ and $\vec{D}$. Based on equation (3) we can derive the following expression (7) for our system:

$$\sqrt[6]{\frac{1}{E}-1} = \frac{|\vec{A}-\vec{D}|}{R_0} \quad (7)$$

A vector can be defined through three parameters. For example, in spherical coordinates $\vec{A}$ is completely characterized if its length $|\vec{A}|$, azimuthal angle θ_A, and polar angle ϕ_A are known (figure 41, b). To fully characterize the ion pair system we need to define two vectors $\vec{A}$ and $\vec{D}$, each of which is determined by three parameters, and establish Förster radius R_0 – in total 7 unknown parameters. Hence, in most general case, it is necessary to determine FRET efficiency of at least 7 systems differing in the length of the linker(s) of donor and/or acceptor fluorophores by known length. This should be enough to make a system of 7 independent equations of general view as expression (7) and to solve it. Obviously, it is a very tedious work, especially from synthetic point of view. Also, in case of 7 different systems, which are characterized by 7 different distances R, it can be difficult to avoid the situation when for one of the systems R value appears to be too different from R_0. In this case, FRET measurements may not be sensitive enough to determine the distance R with necessary accuracy. Therefore, we suggest that any particular ion pair system can be reasonably simplified. An example is described below.

Our research was focused on NHC-gold(I) tosylate ion pairs. The coordinate system was chosen such that origin was located on metal center, z-axis was perpendicular to the line between two nitrogen atoms, and imidazole ring was lying in xz plane (figure 42). At first, we considered a situation without any substrate. Tosylate is known for its high affinity to gold,[178b] therefore, in a non-polar solvent like toluene, gold(I) tosylate should exist predominantly in a form of ISIP. Considering the linear structure of most gold(I) complexes,[188] we assume that in the chosen coordinate system anion is located along the z-axis as shown in figure 42, a (vector $\vec{D}$ is marked in green). In this case, $\theta = \phi = 0$, and $|\vec{D}|$ can be estimated with good accuracy by using computational methods as distance between gold and boron atoms. The acceptor fluorophore ($BODIPY_A$) we propose to connect directly to imidazole ring of NHC ligand through alkoxy chain. Such connection ensures unhindered rotation of $BODIPY_A$ and is favourable synthetically. It is also important that linker is long enough to avoid any influence of metal center on the fluorescence intensity of $BODIPY_A$ via PET. Despite the flexibility of alkyl chain, we assume that $BODIPY_A$ is located in average in the plane of imidazole ring, i.e. in xz plane. Based on this we can reduce amount of unknown parameters by establishing $\theta_A = 0$. Therefore, to define vector $\vec{A}$ (marked in red in figure 42) we need to determine only its length $|\vec{A}|$ and polar angle ϕ_A. Together with R_0 we have only 3 unknown parameters, which can be found by investigating 3 systems differing in value of n = 1, 2, 3 (figure 42, a).

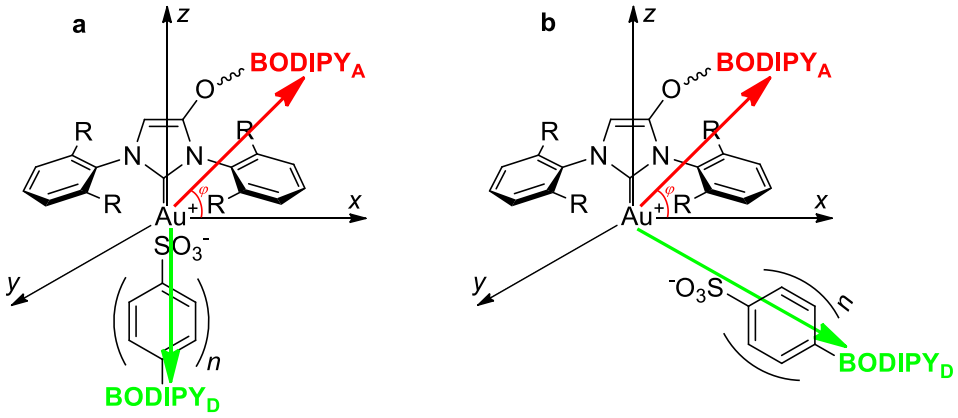

Figure 42. Ion-pairing in NHC-gold(I) tosylates: a) in the absence of substrate – ISIP; b) in the presence of substrate – OSIP (a substrate is omitted for clarity).

In the next situation, when a substrate is coordinated to gold (figure 42, b), the position of anion ($\vec{D}$) is no longer well-defined. Assuming the localization of $\vec{A}$ has not been changed and all the parameters found in the previous situation remain the same, there are again only 3 parameters to determine: $|\vec{D}|$, θ_D, ϕ_D. Using the same systems (n = 1, 2, 3), it is possible to figure out the spatial structure of ion pair also in this case. Comparing to seven-component, such three-component approach seems to be more applicable and realistic. If all the simplifications were correct, it is possible to determine gold(I) tosylate ion pairs structures for variety of substrates using simple measurements of fluorescent intensity in three different systems.

3.3.4. Synthesis of the complexes

Our strategy towards BODIPY sulfonates was based on the condensation of sulfonated aromatic aldehydes with pyrroles. In this way, the target BODIPY sulfonates can be straightforwardly obtained in a couple of steps. For the monophenyl derivative, we have started from sodium 3-formylbenzenesulfonate **15**·Na, which can be easily obtained by sulfonation of benzaldehyde. To increase the solubility in organic solvents sodium was exchanged by tetrabutylammonium cation (figure 43). Following the common procedure for the synthesis of BODIPYs, compound **16**·NBu$_4$(Et*i*Pr$_2$NH) was prepared in 30% yield. Finally, employment of ion-exchange resin yielded the target acid **16**·H. It should be noted, that application of acidic resin leads to partial decomposition of BODIPY moiety. Fortunately, acid **16**·H can be easily purified by short silica column.

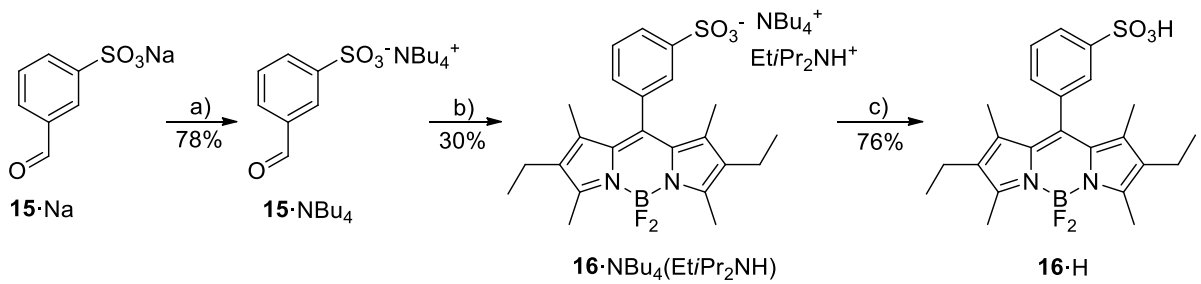

Figure 43. Synthesis of BODIPY sulfonic acid **16**·H. Reaction conditions: a) NBu$_4$Br, DCM, H$_2$O; b) 3-ethyl-2,4-dimethylpyrrole, chloranil, *i*Pr$_2$NEt, BF$_3$·Et$_2$O, DCM; c) Amberlite IR-120 hydrogen form cation exchange resin, MeOH.

To avoid additional step with silver carbonate, we decided to use the acid **16**·H directly for the synthesis of NHC-gold(I) sulfonates. For this reason, we have prepared acetate complex [(**17**)-O-IPrAu(OAc)] by reaction of the respective halide complex [(**17**)-O-IPrAuCl] (prepared in our laboratory before by O. Halter) with silver acetate. Being much less acidic, acetate in [(**17**)-O-IPrAu(OAc)] was easily substituted by sulfonate in quantitative yield (figure 44). Analogously [IPrAu(**16**)] was prepared from **16**·H and [IPrAu(OAc)].

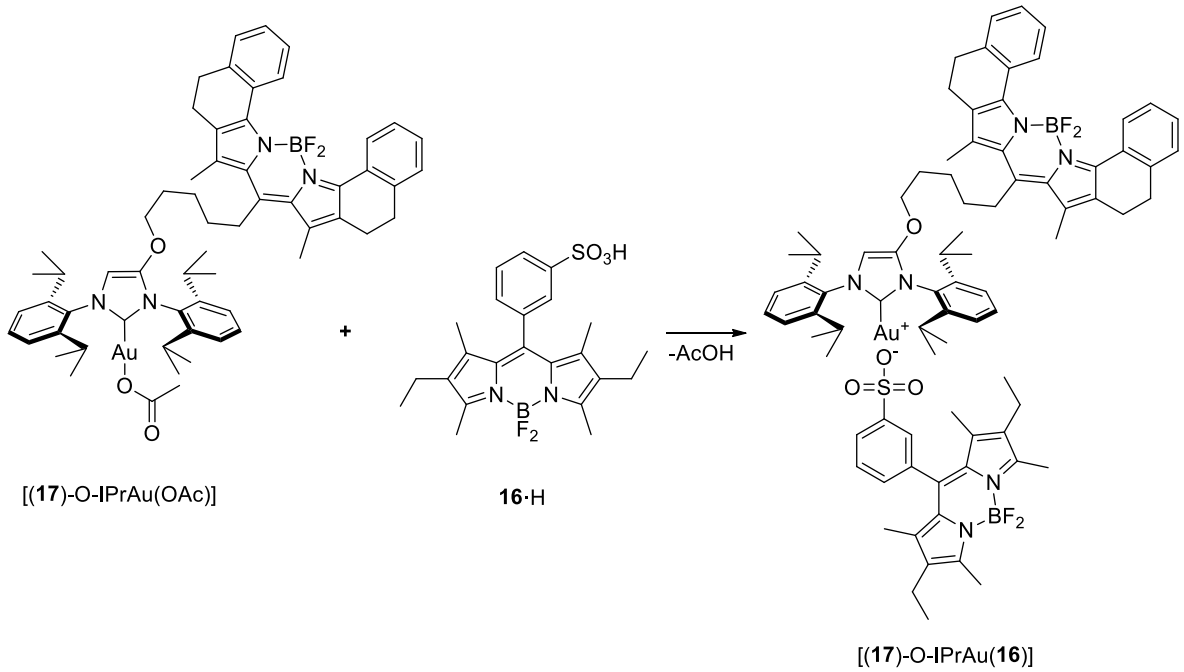

Figure 44. Synthesis of BODIPYs-tagged NHC-gold(I) tosylate. Reaction conditions: DCM, RT, overnight.

The synthesis of biphenyl sulfonates was started from the commercially available biphenyl-4-carboxaldehyde, which can be selectively sulfonated as shown in figure 45. Subsequent cation exchange and condensation with 3-ethyl-2,4-dimethylpyrrole, followed by complexation with $BF_3{\cdot}OEt_2$, led to the formation of BODIPY sulfonate **19a**·Et*i*Pr$_2$NH. As in the case of the monophenyl sulfonate, employment of ion-exchange resin led to the partial decomposition, so the crude acid should be purified additionally by silica column. Unfortunately, in the case of biphenyl sulfonates, the "purified" product didn't react with NHC-gold(I) acetate. At first, we concluded the low solubility of biphenyl moiety was the reason for such unexpected result. However, application of more soluble sulfonate **19b**·NBu$_4$ with longer hexyl side chains in the same reactions eventually led to a similar outcome. At this point, we realized that purification by silica column was the source of the problem. Most probably, the presence of some minor impurities in silica caused the substitution of the proton. We have already observed similar problem for the silver salt **14**·Ag. Unlike the monophenyl acid **16**·H, separation of the biphenyl acids from the byproducts was more complicated and the longer column was needed. Therefore, suppressing of undesirable effects by decreasing amount of silica was not possible in this case. To avoid decomposition during the ion-exchange step, we decided to try a less polar solvent. Application of DCM instead of methanol also led to the partial decomposition, although the byproduct, in this case, was different according to NMR spectra. Hence, preparation of pure biphenyl sulfonic acids and respective NHC-gold(I) sulfonates still remains a challenging task.

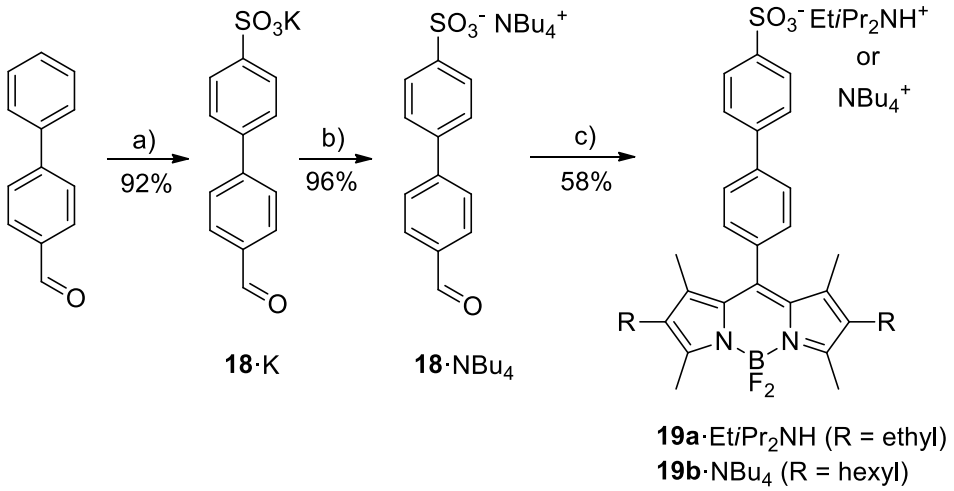

Figure 45. Synthesis of BODIPY biphenyl sulfonates. Reagents and conditions: a) oleum, 40°C; b) NBu_4Br, DCM, H_2O; c) pyrrole, chloranil, iPr$_2$NEt, $BF_3{\cdot}Et_2O$, DCM.

3.3.5. FRET measurements

To ensure the existence of sufficient amount of intimate ion pairs of complex [(**17**)-O-IPrAu(**16**)] in the dilute solution we decided to use non-polar toluene as a solvent for our measurements. Upon excitation at 527 nm (absorbance maxima of donor fluorophore), we have clearly observed the emission band of acceptor fluorophore at 627 nm, which was 11.9 times more intense than the donor emission band at 539 nm (figure 46). Furthermore, by measuring the fluorescence intensity of complex [IPrAu(**16**)] (which is lacking acceptor fluorophore) under the same conditions and using equation (1), the FRET efficiency was established to be 96%. The appearance of strong FRET clearly indicates the existence of ISIPs in toluene solution, which is fully consistent with the proposed concept (figure 40, a).

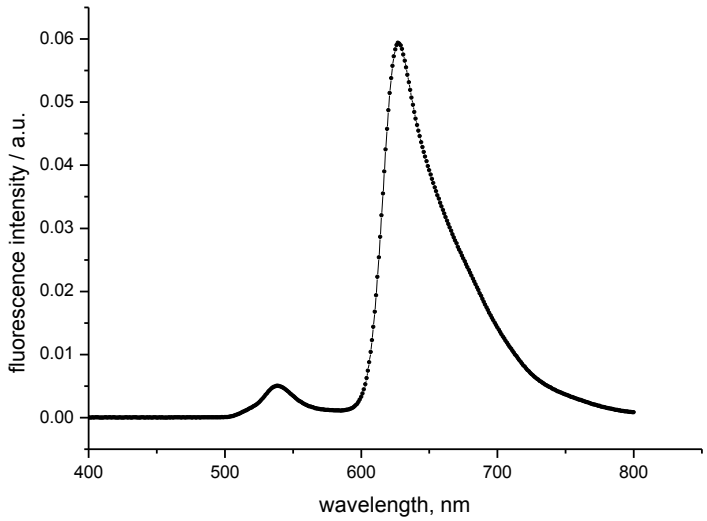

Figure 46. Emission spectrum of complex [(**17**)-O-IPrAu(**16**)] (c = 1.0·10^{-6} mol·L^{-1}) in toluene (λ_{exc} = 527 nm).

Next, we have examined the influence of more polar solvents on the system. Addition of acetonitrile led to a steep decrease of acceptor to donor intensity relationship (figure 47, left).

Combining the results of measurements for both complexes [(**17**)-O-IPrAu(**16**)] and [IPrAu(**16**)] we were able to plot FRET efficiency versus acetonitrile content (figure 47, right). The obtained results clearly showed that at acetonitrile content of 25 vol% there are no ion pairs anymore in solution, which was indicated by full disappearance of the FRET.

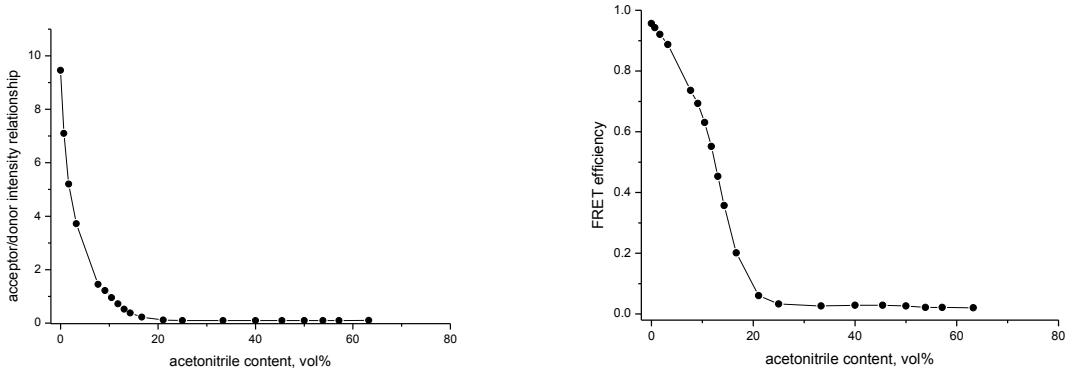

Figure 47. FRET measurements of toluene solutions of complex [(**17**)-O-IPrAu(**16**)] (c = 1.0·10^{-6} mol·L^{-1}). Left: dependence of acceptor to donor intensity relationship on acetonitrile content. Right: dependence of FRET efficiency on acetonitrile content.

Addition of 1,2-dichloroethane (DCE) also led to decrease of FRET efficiency (figure 48). However, it was not so steep in this case and the full disappearance of FRET was achieved at higher solvent content – approximately 63 vol%. Although it can be predicted based on the different polarity of the solvents, this result quantitatively showed higher solvation power of acetonitrile relative to 1,2-dichloroethane towards gold cationic species.

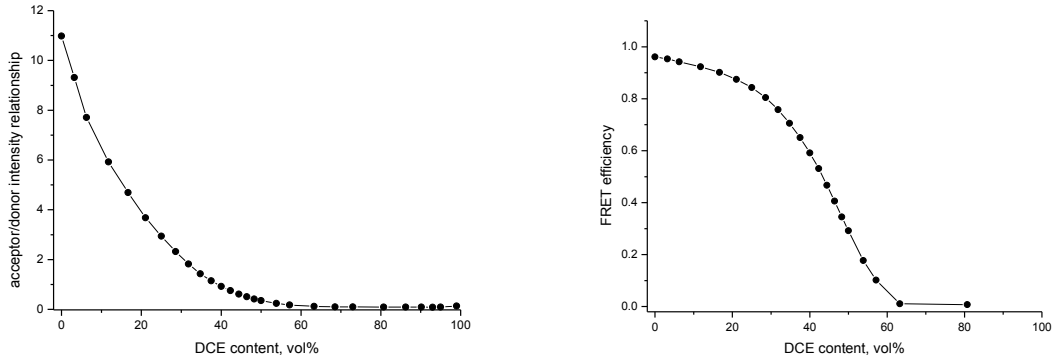

Figure 48. FRET measurements of toluene solutions of complex [(**17**)-O-IPrAu(**16**)] (c = 1.0·10^{-6} mol·L^{-1}). Left: dependence of acceptor to donor intensity relationship on 1,2-dichloroethane content. Right: dependence of FRET efficiency on 1,2-dichloroethane content.

Dependence of energy transfer efficiency on polar solvent content (figures 47 and 48, right) is very similar to the FRET dependence on distance (equation (2)). It can be understood in the way that the higher polar solvent content corresponds to the larger average distance between counterions because of ion pairs dissociation to free ions.

Finally, we have explored the reaction of complex [(**17**)-O-IPrAu(**16**)] with the alkyne substrate. Addition of excess amount of phenyl acetylene led to the increase of donor intensity with the simultaneous decrease of acceptor intensity (figure 49). It is reflected in the overall decrease of acceptor to donor intensity relationship, which becomes close to zero after

approximately 10 min. The most probable outcome of the reaction is the formation of gold dinuclear species, which were observed in the fluorescence experiments described in chapter 3.2.7. The complete disappearance of FRET means that the digold species and tosylate anions exist as separated ions rather than ion pairs at a concentration level of the experiment. Remote localization of anion can be a reason of the high cationic character of gold dinuclear species, which explains a significant increase of fluorescence intensity shown in figure 30 (chapter 3.2.7).

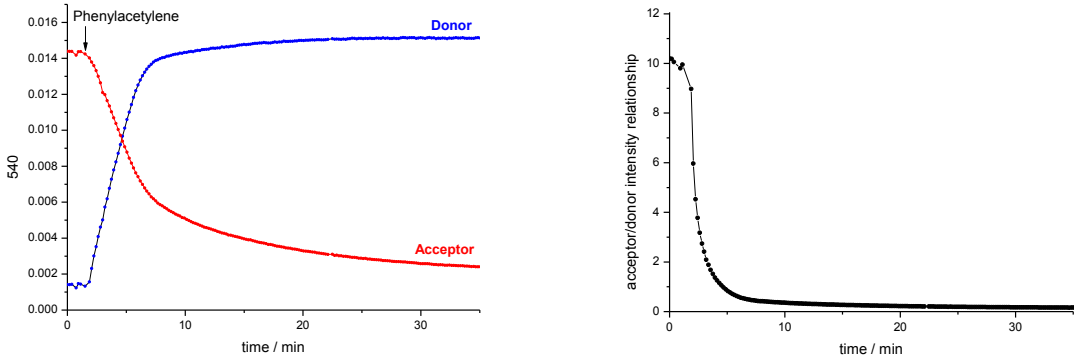

Figure 49. Left: fluorescence intensity vs. time plot for the reaction of complex [(**17**)-O-IPrAu(**16**)] (c = 1.0·10^{-6} mol·L^{-1}) in toluene with phenyl acetylene (1000 equiv). Right: dependence of acceptor to donor intensity relationship on time over the course of the reaction.

4. Summary and Conclusions

In the following paragraphs, the most important aspects of my work are presented as a short summary.

1. The reaction of the newly synthesized NHC-gold complexes **1**, **2** and **3a** with various aryl thiolates was monitored in situ by means of fluorescence spectroscopy (figure 50).

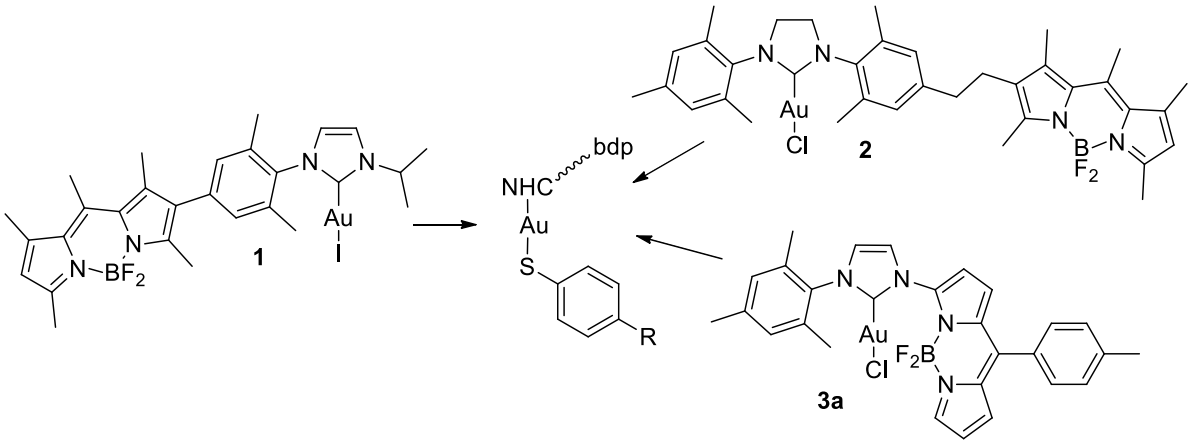

Figure 50. NHC-gold complexes used in reactions with various thiophenols.

2. The substitution of halide by various substituted aryl thiolates at the gold leads to a decrease in the brightness of the appended fluorophore. The extent of the decrease depends on the electronic nature of the thiol: the reaction with electron-rich thiolates leads to a strong decrease of fluorescence emission, whereas with electron-deficient thiolates the intensity drop was much less pronounced (figure 51).

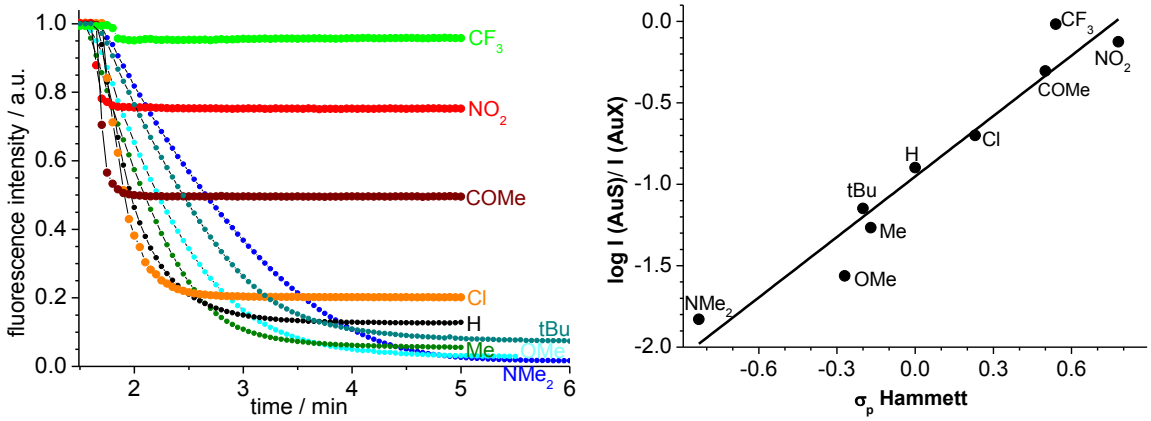

Figure 51. Left: fluorescence-time traces upon addition of 100 equivalents of RC_6H_4SH (R = NO_2, CF_3, COMe, Cl, H, Me, *t*Bu, OMe and NMe_2) to complex **1** ($c = 1.0 \cdot 10^{-6}$ mol·L^{-1}) and Hünig base (100 equiv) in 1,2-dichloroethane solvent leading to the formation of the respective complexes [**1**(SC_6H_4R)]. Right: the plot of the σ_p-Hammett parameter and the relative fluorescence brightness of complexes [**1**(SC_6H_4R)].

The fluorescence brightness of a BODIPY fluorophore attached to NHC–gold complexes can be easily tuned by changing the electron density at the transition metal.

3. DFT calculations, conducted in cooperation with Prof. Dr. Israel Fernandez (Universidad Complutense de Madrid), suggest that fluorescence quenching occurs predominantly by the a-PET-mechanism, despite the presence of a 5d transition metal ion and heavy atom halides (figure 52).

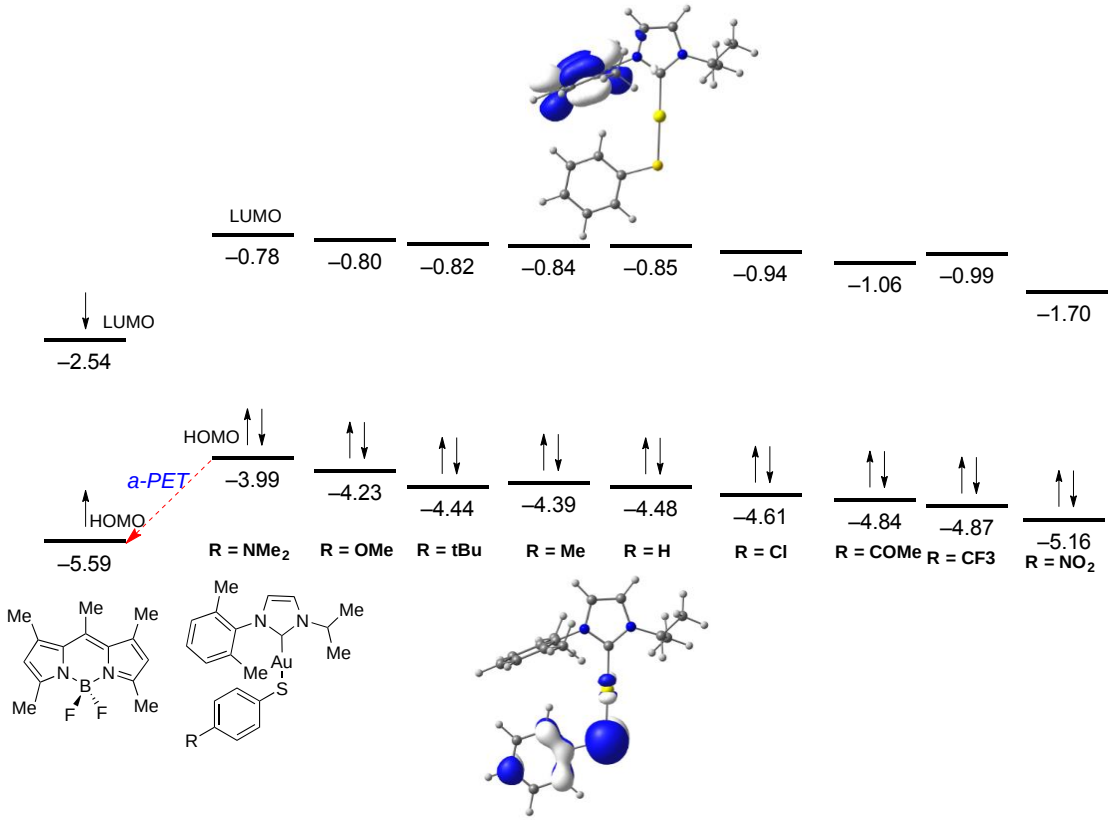

Figure 52. Computed frontier molecular orbitals of the isolated chromophores present in compounds [**1**(SC_6H_4R)] (orbital energies are given in eV).

It was firmly established that fluorescent dyes can be used as highly sensitive probes for the determination of electron density at transition metals, thus being valuable tools for investigations in organometallic chemistry and homogeneous catalysis.

4. Novel BODIPY-tagged phosphines **12a** and **12b** and the derived transition-metal complexes were prepared (figure 53).

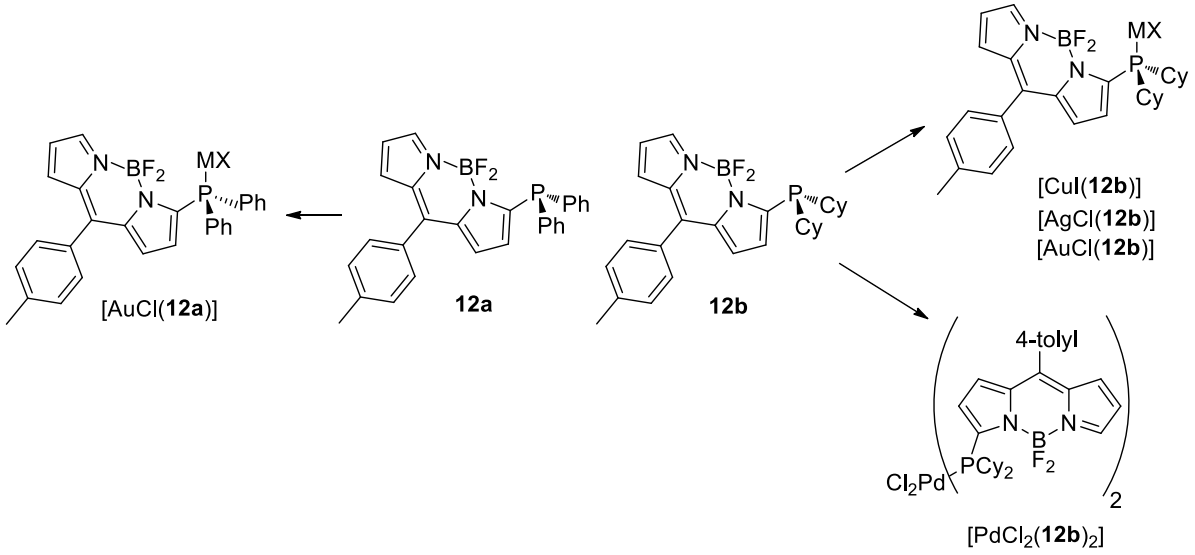

Figure 53. Transition-metal complexes containing BODIPY-tagged phosphine ligands.

The synthesized compounds are characterized by very different fluorescence properties: phosphines **12a** and **12b** and the respective Pd complex are strongly quenched ($\Phi < 0.001$);

the Cu complex was only partially quenched (Φ = 0.016), whereas Au and Ag complexes exhibited an intermediate level of fluorescence intensity ($\Phi \approx 0.10$).

5. It was demonstrated that fluorescence spectroscopy on BODIPY-tagged phosphines can be used to monitor introductory steps in gold-catalyzed alkyne transformations in a catalytically relevant concentration range. The reactions involving [AuCl(**12b**)] show that changes in the electron density at the transition metal, resulting from ligand substitution reactions, translate into characteristic changes in the brightness of the BODIPY reporter group. An increase in the electron density at gold leads to a decrease in the brightness, whereas lower electron density at gold results in an increase in the fluorescence brightness. In suitably designed complexes, the fluorophore is highly sensitive to changes in the environment of the gold and even remote substituents in the periphery lead to pronounced changes in the brightness (figure 54).

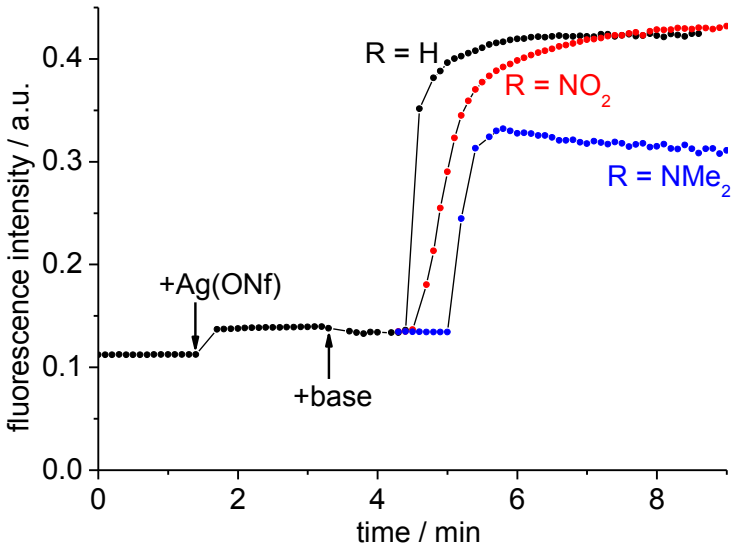

Figure 54. Fluorescence intensity vs. time plot for the reactions of [AuCl(**12b**)] (c = 1.0·10^{-6} mol·L^{-1}) with [Ag(ONf)], Hünig's base, and three different phenyl acetylene derivatives $HCCC_6H_4R$ (1000 equiv; R = NO_2, H, NMe_2) yielding $[((\mathbf{12b})Au)_2(CCC_6H_4R)]^+ ONf^-$ complexes in 1,2-dichloroethane.

6. The in situ fluorescence spectroscopic studies reveal subtle details of the reaction of [AuCl(**12b**)] with [Ag(ONf)] and different acetylenes. It was shown that activation of gold complexes through silver salt metathesis requires superstoichiometric amounts (approximately 2.5 equivalents) of [Ag(ONf)]. However, to accelerate the subsequent reaction with the alkyne even a larger excess (>15 equiv) of silver salt is needed (figure 55, traces a-c); addition of less silver salt leads to sluggish or no reaction (figure 55, traces d-f). This may explain why several gold-catalyzed reactions perform better in the presence of excess silver salt – even though the "cationic" species are already formed with approximately 2.5 equivalents of silver salt. Hence, the nature of the silver additive appears to be important both as an activator to generate the "cationic" gold complex and as an activator of the alkyne.

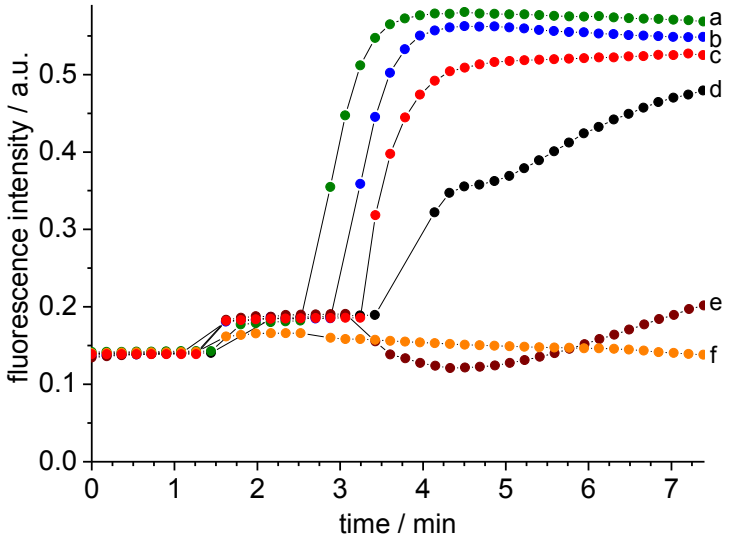

Figure 55. Fluorescence intensity vs. time plot for the reactions of [AuCl(**12b**)] (c = 1.0·10^{-6} mol·L^{-1}) in 1,2-dichloroethane with different amounts of [Ag(ONf)], added after ca. 1.5 min (trace f: +1 equiv [Ag(ONf)]; trace e: +5 equiv; trace d: +10 equiv; trace c: +15 equiv; trace b: +20 equiv; trace a: +30 equiv) to [AuCl(**12b**)], followed by addition of phenyl acetylene (1000 equiv added after 2.5–3.4 min).

7. The general concept of the application of fluorescence spectroscopy for the investigation of ion-pairing in transition metal catalysis was introduced. The proposed approach is based on the distance-dependent FRET effect. Measurement of FRET efficiency in suitably fluorophore-tagged metal complexes is suggested to provide useful information about ion-pairing at catalytically relevant concentration range.

8. A pair of NHC-gold(I) tosylate complexes suitable for FRET efficiency measurements was prepared (figure 56).

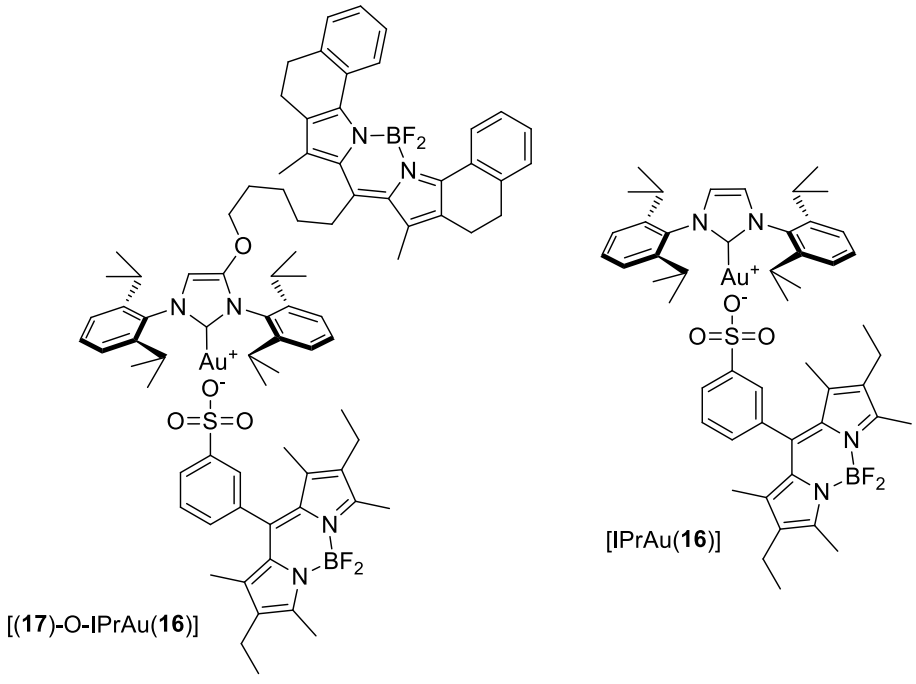

Figure 56. BODIPY-tagged NHC-gold(I) tosylates.

9. Energy transfer efficiency in complex [(**17**)-O-IPrAu(**16**)] appeared to be very sensitive to the average distance between counterions. Thus, the addition of acetonitrile or 1,2-dichloroethane to the toluene solutions of [(**17**)-O-IPrAu(**16**)] led to the dissociation of ion pairs to free ions, which was nicely indicated by the decrease of FRET efficiency (figure 57). The initial measurements revealed the great potential of fluorescence spectroscopy for ion-pairing study.

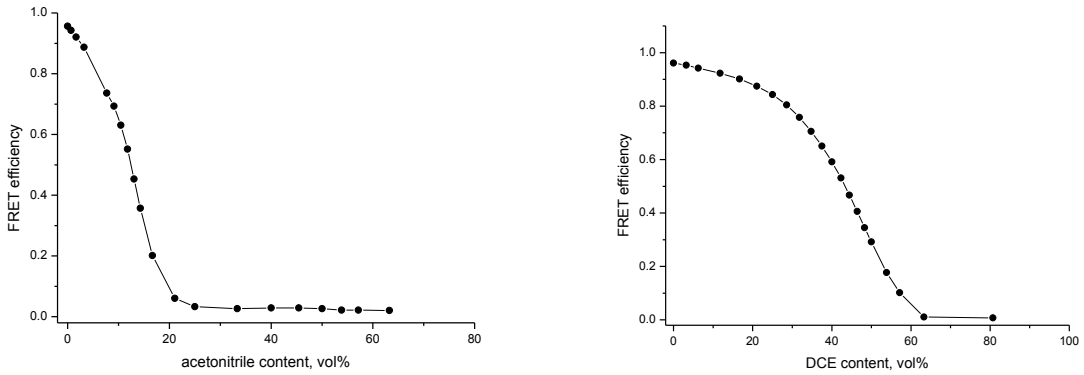

Figure 57. Dependence of FRET efficiency of toluene solutions of complex [(**17**)-O-IPrAu(**16**)] ($c = 1.0 \cdot 10^{-6}$ mol·L^{-1}) on acetonitrile content (left) or 1,2-dichloroethane content (right).

In this thesis, it was shown that the observation of the modulated fluorescence intensity in (catalytically active) transition metal complexes with suitable fluorescent tags renders a highly useful tool for the analysis of chemical transformations.

5. Zusammenfassung der Ergebnisse

In den folgenden Abschnitten werden die wichtigsten Aspekte meiner Arbeit als kurze Zusammenfassung dargestellt.

1. Die neuartigen NHC-Gold-Komplexe **1**, **2** und **3a** wurden mit diversen Arylthiolverbindungen umgesetzt. Fluoreszenz-Spektroskopie wurde dabei in situ eingesetzt, um den Reaktionsfortschritt zu überwachen (Abbildung 58).

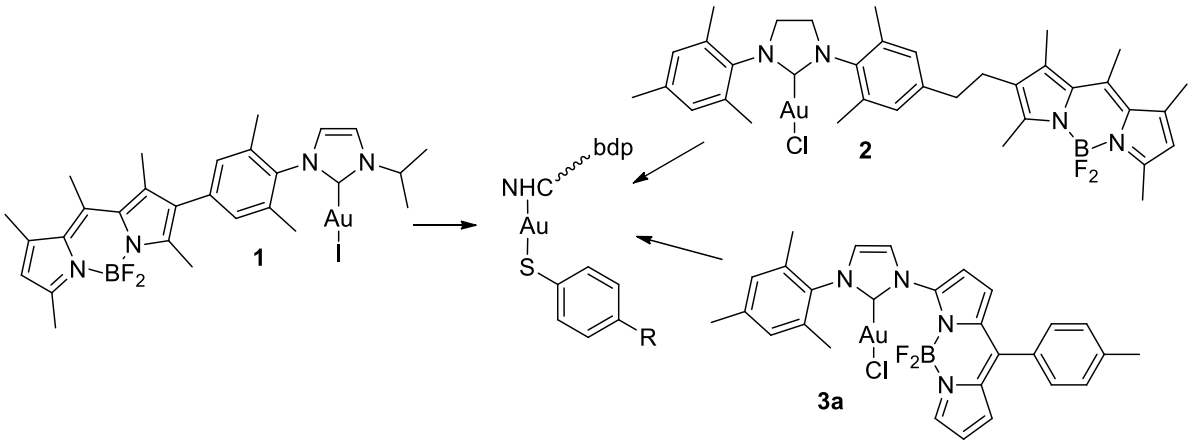

Abbildung 58. Umsetzung der NHC-Gold-Komplexe mit diversen Thiophenolen.

2. Werden die Halogenliganden am Goldzentrum durch diverse substituierte Arylthiole ersetzt, beobachtet man eine Abnahme der Helligkeit des an die Komplexe gebunden Fluorophors. Das Maß der Helligkeitsabnahme korreliert mit den elektronischen Eigenschaften des Thiols: Während der Umsatz mit elektronenreichen Thiolen zu einer signifikanten Abnahme der Fluoreszenz-Emission führt, wird bei elektronenarmen Thiolen lediglich ein geringer Intensitätsabfall beobachtet (Abbildung 59).

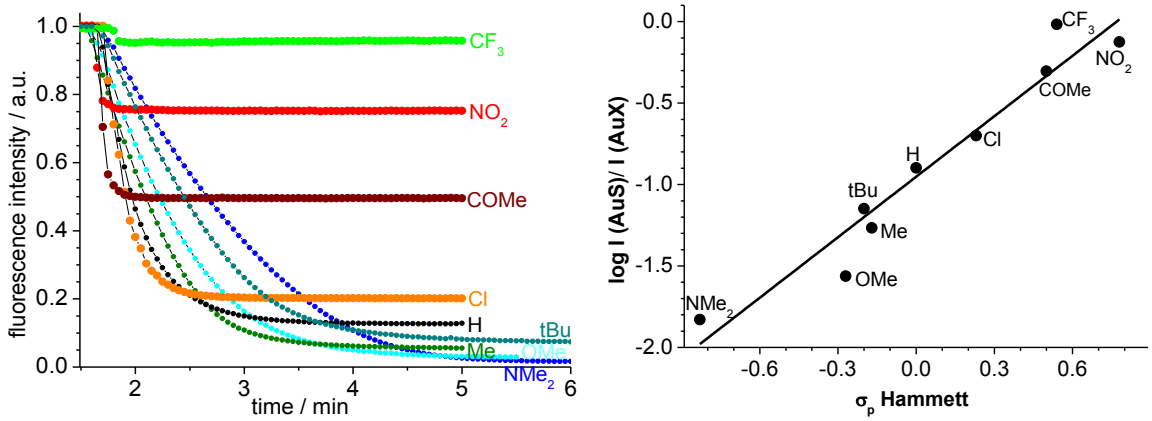

Abbildung 59. Links: Fluoreszenz-Zeit-Verläufe nach Zugabe von 100 Äquivalenten RC_6H_4SH (R = NO_2, CF_3, COMe, Cl, H, Me, *t*Bu, OMe and NMe_2) zum Komplex **1** (c = $1.0 \cdot 10^{-6}$ mol·L^{-1}), welcher in 1,2-Dichlorethan gelöst und mit Hünig-Base (100 eq) versetzt wurde. Bei den Umsätzen werden die entsprechenden Komplexe [**1**(SC_6H_4R)] gebildet. Rechts: Auftragung des Hammett-Parameters σ_p gegen die relative Fluoreszenz-Helligkeit des entsprechenden Komplexes [**1**(SC_6H_4R)].

Die Fluoreszenzhelligkeit des BODIPY-Fluorophors, welches an den NHC-Gold-Komplex gebundenen ist, lässt sich leicht einstellen, indem die Elektronendichte am Übergangsmetall variiert wird.

3. DFT-Berechnungen, die in Zusammenarbeit mit Prof. Dr. Israel Fernandez (Universidad Complutense de Madrid) durchgeführt wurden, weisen darauf hin, dass trotz der Gegenwart eines 5d-Übergangmetallions und schwerer Halogenatome die Löschung der Fluoreszenz hauptsächlich nach dem a-PET-Mechanismus abläuft (Abbildung 60).

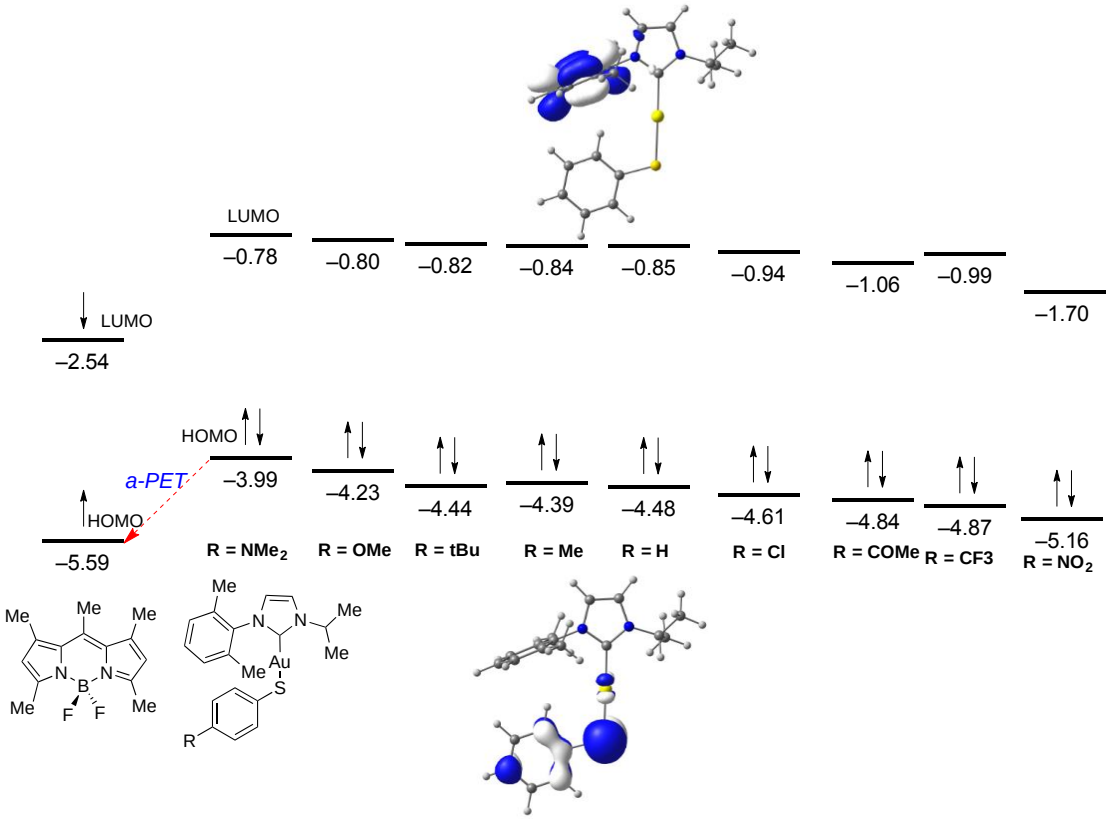

Abbildung 60. Berechnete Grenzmolekülorbitale des isolierten Chromophors, welcher in den Verbindungen [**1**(SC_6H_4R)] enthalten ist (Orbitalenergien sind in eV angegeben).

Es wurde dezidiert bewiesen, dass Fluoreszenzfarbstoffe als hochsensible Sonden verwendet werden können, um die Elektronendichte am Übergangsmetall zu bestimmen. So erweisen sich die Fluorophore als wertvolle Werkzeuge für Untersuchungen in der Organometallchemie und der homogenen Katalyse.

4. Die bislang literaturunbekannten BODIPY-markierten Phosphine **12a** and **12b** und die davon abgeleiteten Übergangsmetall-Komplexe wurden synthetisiert (Abbildung 61).

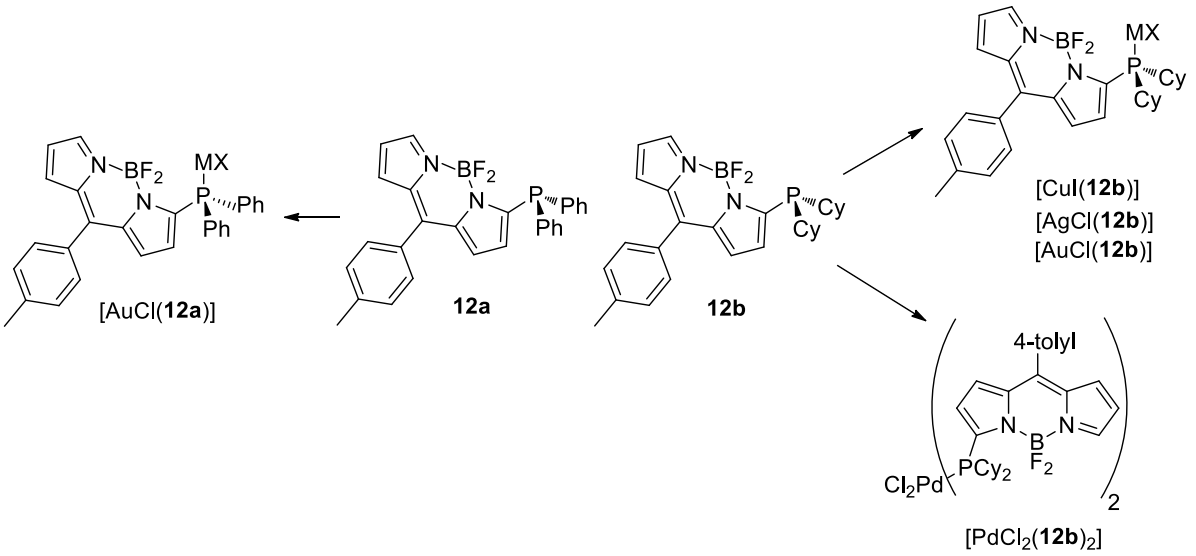

Abbildung 61. Übergangsmetall-Komplexe mit BODIPY-markierten Phosphin-Liganden.

Die hergestellten Verbindungen zeichnen sich durch signifikant unterschiedliche Fluoreszenz-Eigenschaften aus: So weisen die Phosphine **12a** and **12b** und die entsprechenden Palladiumkomplexe eine weitgehend gelöschte Fluoreszenz auf ($\Phi < 0.001$). Die Fluoreszenz des Kupferkomplexes wurde hingegen lediglich abgeschwächt ($\Phi = 0.016$), wohingegen die Gold- und Silberkomplexe ein mittlere Fluoreszenzintensität aufweisen ($\Phi \approx 0.10$).

5. Es wurde nachgewiesen, dass die Fluoreszenz-Spektroskopie BODIPY-markierter Phosphine genutzt werden kann, um die einführenden Schritte goldkatalysierter Alkin-Transformationen im für die Katalyse relevanten Konzentrationsbereich zu verfolgen. Bei Reaktionen mit dem Komplex [AuCl(**12b**)] wurde die Elektronendichte am Übergangsmetall durch Substitution von Liganden variiert. Dabei konnte gezeigt werden, dass eine Variation der Elektronendichte am Übergangsmetall mit einer charakteristischen Änderung der Helligkeit der BODIPY-Gruppe einhergeht. Ein Anstieg der Elektronendichte am Gold führt zu einer Abnahme der Fluoreszenzhelligkeit, wohingegen eine geringere Elektronendichte am Gold einen Anstieg der Helligkeit bewirkt. In entsprechenden Komplexen ist das Fluorophor hochsensibel für Änderungen in der Umgebung des Goldzentrums. Sogar der Austausch von Substituenten, die sich in der Peripherie des Komplexzentrums befinden, führt zu einer signifikanten Änderung der Helligkeit (Abbildung 62).

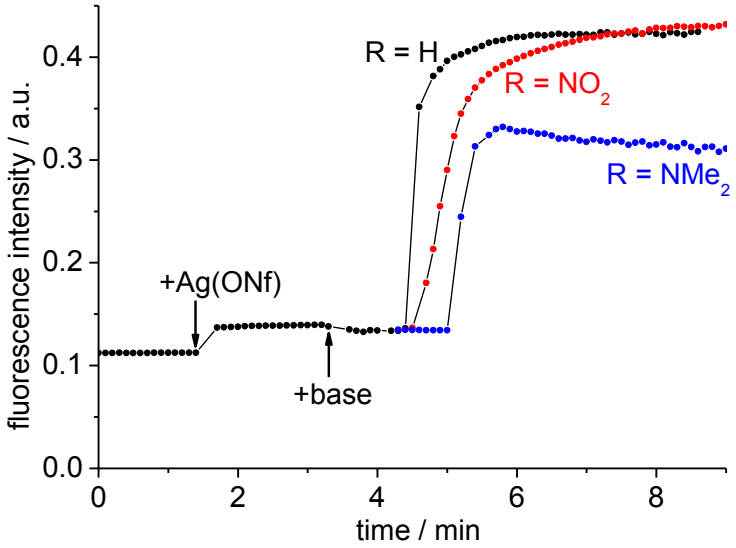

Abbildung 62. Auftragung der Fluoreszenz-Intensität gegen die Zeit für die Reaktionen, bei denen [AuCl(**12b**)] (c = $1.0 \cdot 10^{-6}$ mol·L^{-1}) mit [Ag(ONf)], Hünig-Base und drei verschiedenen Phenylacetylenderivativen $HCCC_6H_4R$ (1000 eq; R = NO_2, H, NMe_2) in 1,2-Dichloroethan zu $[((\mathbf{12b})Au)_2(CCC_6H_4R)]^+$ ONf$^-$-Komplexen umgesetzt werden.

6. Die Studien mittels in situ Fluoreszenzspektroskopie liefern Erkenntnisse zu subtilen Details der Reaktionen von [AuCl(**12b**)] mit [Ag(ONf)] und verschiedenen Acetylenverbindungen. Es wurde gezeigt, dass zur Aktivierung von Goldkomplexen durch Silbersalz-Metathese überstöchiometrische Mengen (etwa 2.5 Äquivalente) von [Ag(ONf)] benötigt werden. Ein noch größerer Überschuss (>15 Äquivalente) von Silbersalz ist erforderlich, um die Folgereaktion mit dem Alkin zu beschleunigen (Abbildung 63, Spuren a-c). Wird der Goldkomplex mit weniger Silbersalz versetzt, findet die Reaktion nicht oder nur verlangsamt statt (Abbildung 63, Spuren d-f). Dies würde erklären, warum diverse goldkatalysierte Reaktionen in der Gegenwart eines Überschusses an Silbersalzen besser ablaufen – auch wenn „kationische“ Spezies schon bei etwa 2.5 Äquivalenten Silbersalzen vorliegen. Folglich scheint die Natur des Silberadditivs eine wichtige Rolle zu spielen, da es sowohl den „kationischen“ Goldkomplex generiert, als auch das Alkin aktiviert.

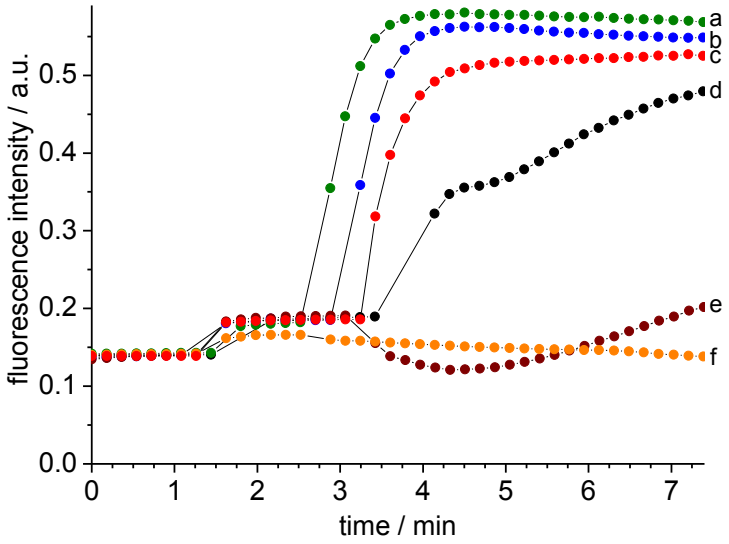

Abbildung 63. Auftragung der Fluoreszenz-Intensität gegen die Zeit für jene Reaktionen, bei denen [AuCl(**12b**)] (*c* = $1.0 \cdot 10^{-6}$ mol·L^{-1}) in 1,2-Dichlorethan mit verschiedenen Mengen an [Ag(ONf)] umgesetzt wurde. [AuCl(**12b**)] wurde nach etwa 1.5 Minuten mit Ag(ONf) versetzt (Spur f: +1 eq [Ag(ONf)]; Spur e: +5 eq; Spur d: +10 eq; Spur c: +15 eq; Spur b: +20 eq; Spur a: +30 eq). Nach 2.5–3.4 min erfolgte die Zugabe von 1000 Äquivalenten Phenylacetylen.

7. Die Anwendung der Fluoreszenz-Spektroskopie für die Untersuchung von Ionenpaaren in der Übergangsmetall-Katalyse wurde als grundlegendes Konzept neu eingeführt. Die Messung der FRET-Effizienz in geeigneten Fluorophor-markierten Metallkomplexen könnten Aufschluss über die Ionenpaarung in katalytisch relevanten Konzentrationsbereichen geben.

8. Zwei literaturunbekannte NHC-Gold(I)-Tosylat-Komplexe, die sich für die FRET-Effizienz-Messungen eignen, wurden hergestellt (Abbildung 64).

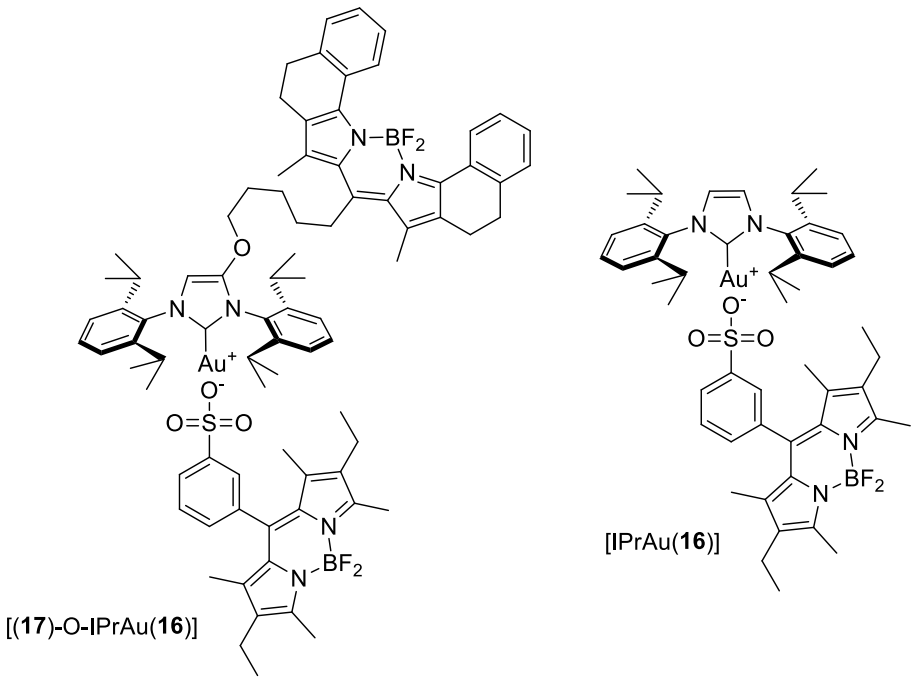

Abbildung 64. BODIPY-markierte NHC-Gold(I)-Tosylate.

9. Die Effizienz des Energietransfers im Komplex [(**17**)-O-IPrAu(**16**)] scheint sehr sensibel für die durchschnittliche Distanz zwischen zwei Gegenionen zu sein. Demzufolge führte die Zugabe von Acetonitril beziehungsweise 1,2-Dichlorethan zu den Toluol-Lösungen von [(**17**)-O-IPrAu(**16**)] zur Dissoziation der Ionenpaare zu freien Ionen. Anhand der Abnahme der FRET-Effizienz konnte die Dissoziation eindeutig nachgewiesen werden (Abbildung 65). Diese ersten Messungen im Rahmen meiner Arbeit weisen auf das große Potential der Fluoreszenzspektroskopie hin, um die Ionenpaarbildung zu untersuchen.

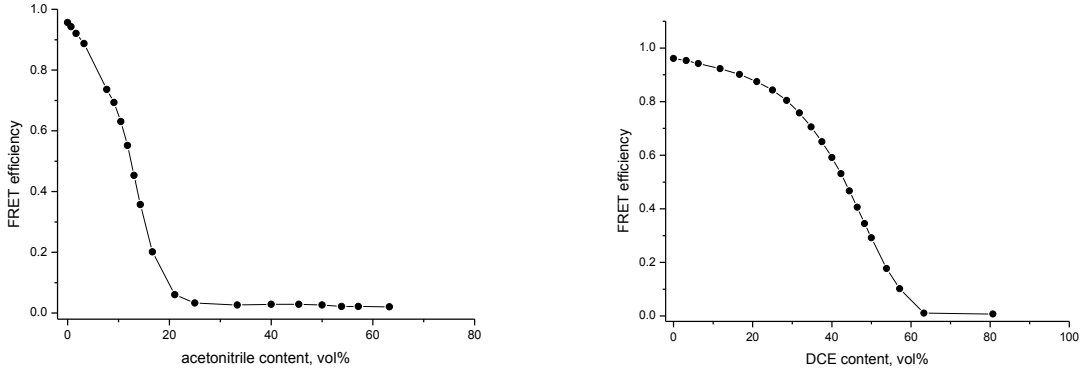

Abbildung 65. Abhängigkeit der FRET-Effizienz der in Toluol gelösten Komplexe [(**17**)-O-IPrAu(**16**)] (c = 1.0·10^{-6} mol·L^{-1}) vom Acetonitril- (links) beziehungsweise 1,2-Dichlorethan-Gehalt (rechts).

In dieser Arbeit konnte gezeigt werden, dass die Beobachtung modulierter Fluoreszenzintensitäten in (katalytisch aktiven) Übergangsmetall-Komplexen mittels geeigneter Fluoreszenzmarker ein sehr nützliches Werkzeug darstellt, um chemische Transformationen zu analysieren.

6. Experimental Part

General experimental. All reactions involving transition metal complexes were conducted in oven-dried glassware. Reactions were performed in Schlenk flasks under a positive pressure of argon or nitrogen. The flasks were fitted with rubber septa and gas-tight syringes with stainless steel needles or double-cannula were used to transfer air- and moisture-sensitive liquids.

Materials. All chemicals were purchased as reagent grade from commercial suppliers and used without further purification unless otherwise noted. CH_2Cl_2 (99.5) and pentane (99) were obtained from Grüssing GmbH, toluene from Sigma-Aldrich (Lab. Reagent grade, 99.3%). These solvents were dried and degassed by using a column purification system from Innovative Technology Inc. Tetrahydrofuran was dried under sodium and distilled under argon atmosphere. All solvents were stored over molecular sieves (4 Å). Preparative chromatography was performed using Merck silica 60 (0.063–0.2 mm).

Instrumentations. ^{1}H, ^{19}F, ^{31}P and ^{13}C-NMR spectra were recorded on a Bruker DRX 500 or Bruker ARX 300 spectrometer. The chemical shifts are given in parts per million (ppm) on the delta scale (δ) and are referenced to tetramethylsilane (^{1}H, ^{13}C-NMR = 0.0 ppm), the residual peak of $CDCl_3$ (^{1}H-NMR = 7.26 ppm, ^{13}C-NMR = 77.23 ppm), DMSO-d_6 (^{1}H-NMR = 2.50 ppm, ^{13}C-NMR = 39.51 ppm), C_6D_6 (^{1}H-NMR = 7.16 ppm, ^{13}C-NMR = 128.39 ppm), CD_2Cl_2 (^{1}H-NMR = 5.32 ppm), hexafluorobenzene (^{19}F-NMR = -164.90 ppm) or H_3PO_4 (^{31}P-NMR = 0.0 ppm). Abbreviations for NMR data: s = singlet; d = doublet; t = triplet; q = quartet; sep = septet; m = multiplet; bs = broad signal. Mass spectra were recorded on the Finnigan MAT95 spectrometer using electron ionization (EI). UV-Vis spectra were recorded on Analytik Jena Specord 600 UV-Vis spectrometer, fluorescence spectra were recorded on J&M TIDAS S700/CCD UV/NIR 2098 spectrometer combined with J&M TIDAS LSM monochromator with 75 W Xenon light source and thermo-controlled cuvette holder. Samples for emission and absorption measurements were contained in 1 cm × 1 cm quartz cuvette (Hellma Analytics, Lot.: 111-10-40). Cyclic voltammetry was performed using a standard electrochemical instrumentation consisted of an EG&G 273A-2 potentiostat-galvanostat. A three-electrode configuration was employed. The working electrode was a Pt disk (diameter 1 mm) sealed in the soft glass with a Pt wire as a counter electrode. The pseudo reference electrode was a Ag wire. Potentials were calibrated internally against the formal potential of ferrocene (+0.46 V vs. Ag/AgCl) or octamethylferrocene (-0.01 V vs. Ag/AgCl). All cyclic voltammograms were recorded in dry CH_2Cl_2 under an atmosphere of argon, supporting electrolyte N*n*Bu$_4$PF$_6$ (c = 0.1 mol/L).

6.1. Experimental Procedures and Compounds Characterization

Synthesis of salt 5

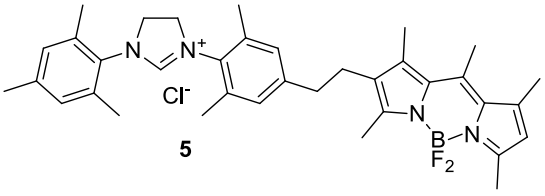

5

BODIPY-C_2H_4-diamine (50 mg, 0.088 mmol, 1 eq) and ammonium tetrafluoroborate (9.2 mg, 0.088 mmol, 1 eq) were suspended in triethyl orthoformate (3 ml) and 2 drops of formic acid were added. The reaction mixture was stirred at 120 °C for 24 h. After cooling down to room

temperature the content of the flask was poured into 10 ml of diethyl ether and the mixture stirred for 1 h. The formed precipitate was collected by filtration, washed with diethyl ether and dried. The product was dissolved in acetone/methanol mixture and amberlite IRA, Cl-form (1 g) was added. The mixture was stirred overnight and the ion-exchange resin was removed by filtration. The volatiles were evaporated under reduced pressure. The residue was triturated with diethyl ether, filtered, washed with diethyl ether and dried in vacuo. Product was obtained as an orange powder (40 mg, 74% yield).

^{1}H NMR (500 MHz, DMSO-d_6) δ 9.04 (s, 1H), 7.15 (s, 2H), 7.09 (s, 2H), 6.19 (s, 1H), 4.46 (s, 4H), 2.64 (s, 3H), 2.63 (s, 3H), 2.42 (s, 3H), 2.39 (s, 3H), 2.38–2.34 (m, 16H), 2.33 (s, 3H), 2.29 (s, 3H). ^{13}C NMR (126 MHz, DMSO-d_6) δ 160.21, 152.57, 151.42, 143.36, 141.75, 140.48, 139.60, 138.24, 135.44, 135.32, 131.30, 131.18, 131.09, 130.82, 129.85, 129.39, 128.95, 120.70, 50.89, 35.39, 25.38, 20.50, 17.17, 17.13, 16.78, 16.34, 14.05, 13.92, 12.14. ^{19}F NMR (282 MHz, DMSO-d_6) δ -145.50 – -146.50 (m). HRMS (ESI): m/z calcd. for $C_{36}H_{44}BF_2N_4^+$ $[M\text{-}Cl]^+$ 581.3622, found 581.3632.

Synthesis of complex 2

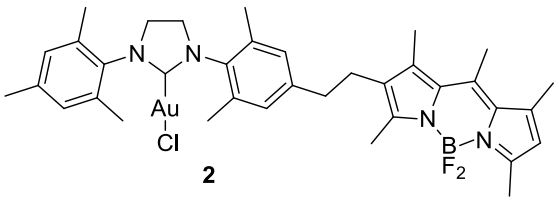

2

A 10 ml flame-dried Schlenk flask equipped with a stirring bar was charged with the salt **5** (20 mg, 0.032 mmol, 1 eq), Ag_2O (4.1 mg, 0.018 mmol, 0.55 eq) and acetonitrile (2 ml). The reaction mixture was stirred at 40 °C for 3 h. $[AuCl(SMe_2)]$ (9.5 mg, 0.032 mmol, 1 eq) was added and the obtained suspension was stirred at room temperature for 24 h. Insoluble material was removed by filtration and the volatiles were evaporated under reduced pressure. Product was obtained as an orange powder (21 mg, 80% yield).

^{1}H NMR (500 MHz, $CDCl_3$) δ 6.95 (s, 2H), 6.86 (s, 2H), 6.02 (s, 1H), 3.99 (s, 4H), 2.70–2.64 (m, 4H), 2.60 (s, 3H), 2.51 (s, 3H), 2.43 (s, 3H), 2.41 (s, 3H), 2.32 (s, 6H), 2.31 (s, 6H), 2.30 (s, 3H), 2.12 (s, 3H). ^{13}C NMR (126 MHz, $CDCl_3$) δ 195.34, 153.49, 152.43, 142.47, 141.49, 140.31, 139.22, 138.92, 135.97, 135.69, 135.46, 134.76, 132.27, 132.07, 130.04, 129.94, 129.64, 120.93, 50.91, 36.37, 25.99, 21.29, 18.18, 17.56, 17.17, 15.02, 14.57, 12.68. ^{19}F NMR (282 MHz, $CDCl_3$) δ -149.55 (q, J (^{19}F-^{11}B) = 32.2 Hz). HRMS (APCI): m/z calcd. for $C_{36}H_{43}AuBClFN_4$ $[M\text{-}F]^+$ 793.2914, found 793.2949 (100%); m/z calcd. for $C_{36}H_{43}AuBF_2N_4$ $[M\text{-}Cl]^+$ 777.3209, found 777.3242 (20%).

Synthesis of complex 4

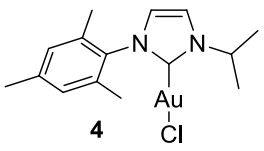

4

3-isopropyl-1-mesityl-1*H*-imidazol-3-ium iodide (100 mg, 0.281 mmol, 1 eq) was dissolved in CH_2Cl_2 (5 ml) and Ag_2O (32.5 mg, 0.141 mmol, 0.5 eq) was added. The reaction mixture was stirred for 1 h at 40 °C. $[AuCl(SMe_2)]$ (83 mg, 0.281 mmol, 1 eq) was added and the stirring was continued for another 1 h at room temperature. The formed precipitate was removed by filtration and the filtrate was evaporated under reduced pressure. Product was obtained as a white powder (110 mg, 85% yield).

^{1}H NMR (500 MHz, $CDCl_3$) δ 7.18 (d, J = 1.8 Hz, 1H), 6.95 (s, 2H), 6.87 (d, J = 1.7 Hz, 1H), 5.20 (hept, J = 6.7 Hz, 1H), 2.32 (s, 3H), 2.00 (s, 6H), 1.55 (d, J = 6.8 Hz, 6H). ^{13}C NMR

(126 MHz, $CDCl_3$) δ 171.38, 139.82, 135.16, 135.00, 129.60, 122.52, 116.71, 53.78, 23.64, 21.31, 17.98. HRMS (EI): m/z calcd. for $C_{15}H_{20}N_2Au^{35}Cl$ $[M]^+$ 460.0975, found 460.0977.

Synthesis of gold-thiolate complexes

General procedure. The respective thiol (1.1 eq) was dissolved in ethanol and 0.1 M NaOH in ethanol (1.2 eq) was added. The formed mixture was added to the solution of gold complex ((NHC)AuCl, 1 eq) in CH_2Cl_2. The reaction mixture was stirred for 3 h at room temperature. The volatiles were evaporated under reduced pressure. The residue was dissolved in CH_2Cl_2 and the remaining insoluble material was removed by filtration. The solvent was evaporated under reduced pressure and the crude product was triturated with a small amount of methanol, filtered and dried.

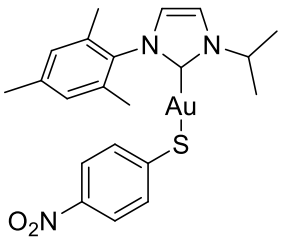

[**4**($SC_6H_4NO_2$)]

Complex [**4**($SC_6H_4NO_2$)] was obtained as a yellow powder (23 mg, 73% yield) from complex **4** (25 mg, 0.054 mmol), 4-nitro-thiophenol (9.3 mg, 0.060 mmol) and 0.1 M NaOH in ethanol (650 μl, 0.065 mmol).

^{1}H NMR (500 MHz, $CDCl_3$) δ 7.70 (d, J = 8.9 Hz, 2H), 7.22 (d, J = 1.9 Hz, 1H), 7.15 (d, J = 8.8 Hz, 2H), 7.06 (s, 2H), 6.95 (d, J = 1.9 Hz, 1H), 5.09 (hept, J = 6.8 Hz, 1H), 2.43 (s, 3H), 2.06 (s, 6H), 1.60 (d, J = 6.8 Hz, 6H). ^{13}C NMR (126 MHz, $CDCl_3$) δ 181.60, 158.06, 143.56, 140.15, 135.47, 135.36, 131.84, 129.57, 122.74, 122.41, 116.95, 53.59, 23.74, 21.42, 18.00. HRMS (EI): m/z calcd. for $C_{21}H_{24}O_2N_3AuS$ $[M]^+$ 579.1249, found 579.1255.

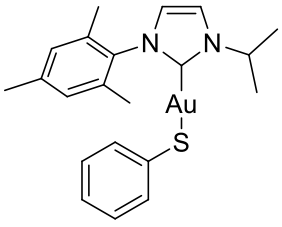

[**4**(SPh)]

Complex [**4**(SPh)] was obtained as a white powder (19 mg, 65% yield) from complex **4** (25 mg, 0.054 mmol), thiophenol (6.1 μl, 0.060 mmol) and 0.1 M NaOH in ethanol (650 μl, 0.065 mmol).

^{1}H NMR (500 MHz, CD_2Cl_2) δ 7.27–7.21 (m, 1H), 7.09 (d, J = 6.9 Hz, 2H), 7.05 (s, 2H), 6.97–6.93 (m, 1H), 6.91–6.80 (m, 3H), 5.12 (hept, J = 7.0 Hz, 1H), 2.38 (s, 3H), 2.06 (s, 6H), 1.58 (d, J = 6.7 Hz, 6H). ^{13}C NMR (126 MHz, $CDCl_3$) δ 182.84, 143.33, 139.65, 135.47, 135.37, 132.34, 129.49, 127.65, 122.65, 122.17, 116.62, 53.39, 23.70, 21.41, 18.04. HRMS (EI): m/z calcd. for $C_{21}H_{25}N_2AuS$ $[M]^+$ 534.1398, found 534.1397.

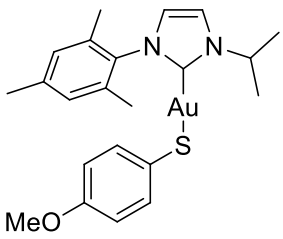

[**4**(SC_6H_4OMe)]

Complex [**4**(SC_6H_4OMe)] was obtained as a white powder (18 mg, 59% yield) from complex **4** (25 mg, 0.054 mmol), 4-methoxy-thiophenol (7.4 μl, 0.060 mmol) and 0.1 M NaOH in ethanol (650 μl, 0.065 mmol).

^{1}H NMR (500 MHz, CD_2Cl_2) δ 7.23 (d, J = 1.9 Hz, 1H), 7.05 (s, 2H), 6.96 (d, J = 7.6 Hz, 2H), 6.95 (d, J = 1.8 Hz, 1H), 6.49 (d, J = 8.5 Hz, 2H), 5.11 (hept, J = 6.8 Hz, 1H), 3.70 (s, 3H), 2.39 (s, 3H), 2.06 (s, 6H), 1.57 (d, J = 6.8 Hz, 6H). ^{13}C NMR (126 MHz, CD_2Cl_2) δ 182.88, 156.67, 140.04, 136.06, 135.86, 133.14, 129.71, 122.64, 117.28, 113.95, 55.77, 53.87, 23.79, 21.56, 18.14. HRMS (EI): m/z calcd. for $C_{22}H_{27}ON_2AuS$ $[M]^+$ 564.1504, found 564.1518.

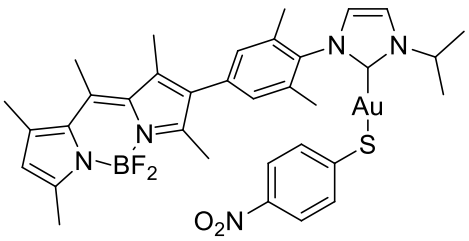

[**1**($SC_6H_4NO_2$)]

Complex [**1**($SC_6H_4NO_2$)] was obtained as an orange powder (5 mg, >95% yield) from complex **1** (5 mg, 0.006 mmol), 4-nitro-thiophenol (1.1 mg, 0.007 mmol) and 0.1 M NaOH in ethanol (80 μl, 0.008 mmol).

^{1}H NMR (500 MHz, $CDCl_3$) δ 7.71 (d, J = 8.8 Hz, 2H), 7.31 (d, J = 8.8 Hz, 2H), 7.28 (d, J = 1.8 Hz, 1H), 7.09 (s, 2H), 7.04 (d, J = 1.7 Hz, 1H), 6.11 (s, 1H), 5.16 (hept, J = 6.5 Hz, 1H), 2.64 (s, 3H), 2.55 (s, 3H), 2.48 (s, 3H), 2.45 (s, 3H), 2.26 (s, 3H), 2.16 (s, 6H), 1.63 (d, J = 6.8 Hz, 6H). ^{13}C NMR (126 MHz, $CDCl_3$) δ 181.54, 158.02, 154.95, 151.07, 143.62, 142.42, 142.13, 136.88, 136.55, 136.33, 135.65, 133.04, 132.00, 131.79, 130.87, 122.93, 122.36, 122.05, 117.22, 53.75, 23.78, 18.24, 17.73, 17.12, 15.77, 14.76, 13.49. ^{19}F NMR (282 MHz, $CDCl_3$) δ -149.64 (q, J (^{19}F-^{11}B) = 32.1 Hz). HRMS (ESI): m/z calcd. for $C_{34}H_{37}AuBF_2N_5NaO_2S$ $[M+Na]^+$ 848.2287, found 848.2283.

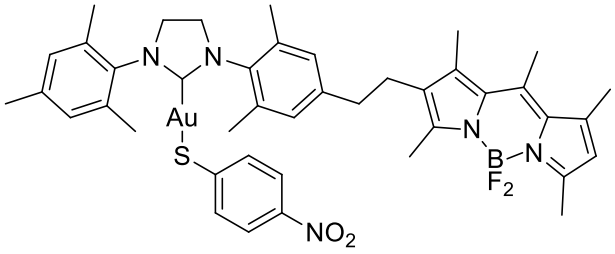

[**2**($SC_6H_4NO_2$)]

Complex [**2**($SC_6H_4NO_2$)] was obtained as an orange powder (6 mg, 81% yield) from complex **2** (6.5 mg, 0.008 mmol), 4-nitro-thiophenol (1.4 mg, 0.009 mmol) and 0.1 M NaOH in ethanol (96 μl, 0.0096 mmol).

^{1}H NMR (500 MHz, $CDCl_3$) δ 7.60 (d, J = 8.6 Hz, 2H), 7.03 (s, 2H), 6.93–6.88 (m, 4H), 6.03 (s, 1H), 4.04 (s, 4H), 2.70 (s, 4H), 2.60 (s, 3H), 2.51 (s, 3H), 2.41 (s, 3H), 2.39 (s, 3H), 2.37 (s, 6H), 2.35 (s, 6H), 2.34 (s, 3H), 2.21 (s, 3H). ^{13}C NMR (126 MHz, $CDCl_3$) δ 204.22, 153.49, 152.72, 143.45, 142.65, 141.24, 140.43, 139.49, 138.36, 136.23, 136.16, 135.39, 134.82, 131.67, 130.01, 129.58, 126.66, 122.58, 121.06, 51.22, 51.10, 36.39, 26.05, 21.37, 18.21, 17.58, 17.11, 14.81, 14.59, 12.58. ^{19}F NMR (282 MHz, $CDCl_3$) δ -149.57 (q, J (^{19}F-^{11}B) = 32.2 Hz). HRMS (APCI): m/z calcd. for $C_{42}H_{47}AuBFN_5O_2S$ $[M-F]^+$ 912.3188, found 912.3197.

Synthesis of 3-chloro-BODIPY 6

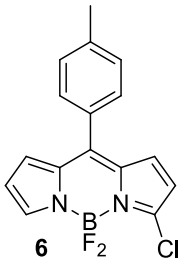

6

2,2'-(p-tolylmethylene)bis(1*H*-pyrrole) (4.00 g, 16.93 mmol) was dissolved in 150 ml of THF and cooled to -78 °C. To the cooled solution *N*-chlorosuccinimide (2.26 g, 16.93 mmol) was added in one portion and reaction mixture was stirred at -78°C for 3 h. The reaction mixture was left in a fridge (-40°C) overnight. After warming to room temperature water (100 ml) was added and the reaction mixture was extracted with CH_2Cl_2 (3 × 100 ml). The combined organic layers were dried over anhydrous $MgSO_4$, filtered, and evaporated under reduced pressure. The crude product was dried and dissolved in CH_2Cl_2 (200 mL). Chloranil (5.0 g, 20.34 mmol) was added to the solution in one portion and the mixture was stirred for 2 h at room temperature. Triethylamine (23.6 ml, 169.20 mmol) was added and the mixture was stirred for an additional 30 min. $BF_3{\cdot}Et_2O$ (31.3 ml, 253.61 mmol) was added dropwise over 30 min and the resulting mixture was stirred for 4 h at room temperature. The resulting dark solution was washed with water (3 × 100 ml), dried over anhydrous $MgSO_4$, filtered, and evaporated under reduced pressure. The crude product was charged on top of a flash chromatography

column (400 × 40 mm, 0.015-0.040 mm silica gel). Using cyclohexane / CH_2Cl_2 (1:1) mixture as the eluent, the desired product was collected as the second orange band (TLC: R_f = 0.30). A second chromatography is needed to obtain higher than 98% purity product (without di- and unsubstituted by-products). Evaporation of solvent afforded product as an orange powder (1.02 g, 19% yield).

^{1}H-NMR (500 MHz, $CDCl_3$) δ 7.92 (s, 1H), 7.42 (d, J = 8.0 Hz, 2H), 7.33 (d, J = 7.9 Hz, 2H), 6.92 (d, J = 4.1 Hz, 1H), 6.90 (d, J = 4.3 Hz, 1H), 6.57–6.54 (m, 1H), 6.41 (d, J = 4.3 Hz, 1H), 2.47 (s, 3H). ^{13}C-NMR (126 MHz, $CDCl_3$) δ 146.26, 144.32, 141.69, 134.91, 134.18, 131.97, 131.62, 130.77, 130.51, 129.45, 118.95, 118.43, 21.66. ^{19}F-NMR (282 MHz, $CDCl_3$) δ -150.26 (q, J (^{19}F-^{11}B) = 28.3 Hz). HR-MS (EI), m/z: 316.07758 $[M]^{+\bullet}$, calcd. 316.0746 (Δ= 3.0 mmu).

Synthesis of BODIPY-diamine 7

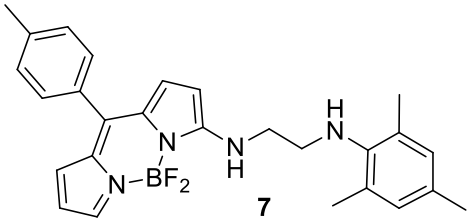

7

To the solution of 3-chloro-BODIPY **6** (50 mg, 0.158 mmol, 1 eq) in DCM (5 ml) N^1-mesitylethane-1,2-diamine (56 mg, 0.316 mmol, 2 eq) and triethylamine (110 μl, 0.790 mmol, 5 eq) were added. The reaction mixture was stirred at 40°C for 1 h. The crude product was purified by column chromatography using DCM as an eluent. The product was obtained as an orange powder (65 mg, 90%).

^{1}H NMR (300 MHz, $CDCl_3$) δ 7.46 (s, 1H), 7.39 (d, J = 8.0 Hz, 2H), 7.27 (d, J = 8.0 Hz, 2H), 6.96 (d, J = 4.9 Hz, 1H), 6.84 (s, 2H), 6.66 (s, 1H), 6.48 (d, J = 3.4 Hz, 1H), 6.35 (dd, J = 3.6, 2.4 Hz, 1H), 6.15 (d, J = 5.0 Hz, 1H), 3.58 (q, J = 5.9 Hz, 2H), 3.23 (t, J = 5.8 Hz, 2H), 2.44 (s, 3H), 2.28 (s, 6H), 2.24 (s, 3H). ^{13}C NMR (126 MHz, $CDCl_3$) δ 161.77, 139.48, 136.25, 134.08, 133.56, 132.92, 131.96, 131.69, 130.92, 130.52, 129.97, 129.12, 120.60, 113.75, 110.09, 48.37, 44.74, 21.57, 20.81, 18.47. HRMS (ESI): m/z calcd. for $C_{27}H_{29}BF_2N_4Na$ $[M+Na]^+$ 481.23455, found 481.23558 (100%); m/z calcd. for $C_{27}H_{30}BF_2N_4$ $[M+H]^+$ 459.25261, found 459.25349 (10%).

Synthesis of BODIPY-imidazole 8

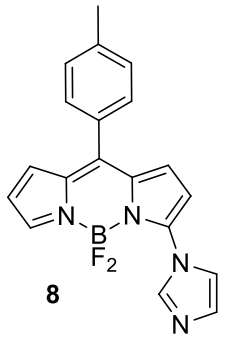

8

To the solution of 3-chloro-BODIPY **6** (50 mg, 0.158 mmol, 1 eq) in acetonitrile (5 ml) imidazol (54 mg, 0.790 mmol, 5 eq) was added and the reaction mixture was stirred at room temperature for 40 h. After evaporation of the solvent under reduced pressure the crude product was purified by column chromatography (eluent: DCM/methanol 50:1). The product was obtained as a pink powder (50 mg, 91% yield).

^{1}H NMR (500 MHz, $CDCl_3$) δ 8.22 (s, 1H), 7.90 (s, 1H), 7.69 (s, 1H), 7.46 (d, J = 8.1 Hz, 2H), 7.35 (d, J = 7.8 Hz, 2H), 7.23 (s, 1H), 7.00 (d, J = 4.4 Hz, 1H), 6.96 (d, J = 4.1 Hz, 1H), 6.58 (dd, J = 4.2, 1.8 Hz, 1H), 6.49 (d, J = 4.4 Hz, 1H), 2.48 (s, 3H). ^{13}C NMR (126 MHz, $CDCl_3$) δ 147.82, 147.27, 144.08, 141.78, 138.13, 134.62, 133.39, 132.72, 131.43, 130.81, 130.71, 130.46, 129.50, 120.37, 119.21, 112.22, 21.68. ^{19}F NMR (282 MHz, $CDCl_3$) δ -144.41 (q, J (^{19}F-^{11}B) = 30.2 Hz). HRMS (APCI): m/z calcd. for $C_{19}H_{16}BF_2N_4$ $[M+H]^+$ 349.14306, found 349.14340.

Synthesis of imidazolium salt 9

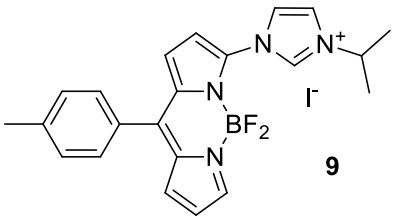

9

To the solution of BODIPY-imidazole **8** (50 mg, 0.144 mmol, 1 eq) in acetonitrile (5 ml) 2-iodopropane (144 μl, 1.44 mmol, 10 eq) was added and the reaction mixture was stirred at 70 °C for 48 h. After evaporation of the solvent under reduced pressure the crude product was purified by column chromatography (eluent: DCM/methanol 20:1). The product was obtained as a red powder (65 mg, 87% yield).

^{1}H NMR (500 MHz, $CDCl_3$) δ 10.52 (s, 1H), 8.13 (s, 1H), 8.01 (s, 1H), 7.60 (s, 1H), 7.48 (d, J = 7.8 Hz, 2H), 7.42–7.35 (m, 3H), 7.15 (d, J = 3.8 Hz, 1H), 7.02 (s, 1H), 6.70 (d, J = 3.0 Hz, 1H), 5.25 (hept, J = 6.5 Hz, 1H), 2.50 (s, 3H), 1.74 (d, J = 6.1 Hz, 6H). ^{13}C NMR (126 MHz, $CDCl_3$) δ 149.85, 148.00, 142.93, 140.59, 136.98, 136.04, 134.96, 133.44, 131.23, 131.06, 130.02, 129.82, 123.95 (t, J = 6.9 Hz), 121.31, 119.87, 114.16, 54.58, 23.23, 21.77. ^{19}F NMR (282 MHz, $CDCl_3$) δ -143.52 (q, J (^{19}F-^{11}B) = 30.5 Hz). HRMS (ESI): m/z calcd. for $C_{22}H_{22}BF_2N_4$ $[M\text{-}I]^+$ 391.19001, found 391.19061.

Synthesis of imidazolium salts 10a and 10b.

General procedure. To the solution of 3-chloro-BODIPY **6** (1 eq) in acetonitrile, the respective *N*-aryl imidazole (5 eq) was added and the reaction mixture was stirred at room temperature for 60 h. After evaporation of the solvent under reduced pressure, the crude product was purified by column chromatography (eluent: DCM/methanol 10:1).

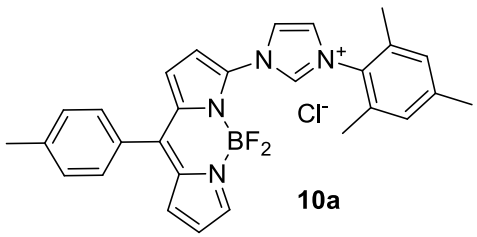

10a

Imidazolium salt **10a** was obtained as a dark orange powder (70 mg, 88% yield) from BODIPY **6** (50 mg, 0.158 mmol) and 1-mesityl-1*H*-imidazole (147 mg, 0.790 mmol) in acetonitrile (5 ml).

^{1}H NMR (500 MHz, , $CDCl_3$) δ 10.36 (s, 1H), 8.82 (t, J = 1.8 Hz, 1H), 7.97 (s, 1H), 7.65 (d, J = 4.4 Hz, 1H), 7.53 (t, J = 1.8 Hz, 1H), 7.45 (d, J = 8.1 Hz, 2H), 7.35 (d, J = 7.8 Hz, 2H), 7.12 (d, J = 4.0 Hz, 1H), 7.05–6.99 (m, 3H), 6.68 (dd, J = 4.4, 1.8 Hz, 1H), 2.47 (s, 3H), 2.32 (s, 3H), 2.18 (s, 6H). ^{13}C NMR (126 MHz, $CDCl_3$) δ 149.78, 147.76, 142.81, 141.76, 140.54, 138.26, 135.92, 134.85, 134.52, 133.43, 131.46, 130.98, 130.57, 130.10, 129.96, 129.72, 125.42, 124.04, 121.21, 114.72, 21.68, 21.26, 17.76. ^{19}F NMR (282 MHz, $CDCl_3$) δ -143.39 (q, J (^{19}F-^{11}B) = 31.0 Hz). HRMS (ESI): m/z calcd. for $C_{28}H_{26}BF_2N_4$ $[M\text{-}Cl]^+$ 467.22131, found 467.22225.

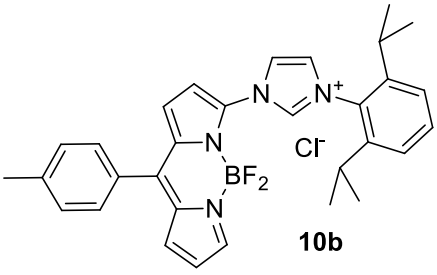

10b

Imidazolium salt **10b** was obtained as a dark orange powder (73 mg, 85% yield) from BODIPY **6** (50 mg, 0.158 mmol) and 1-(2,6-diisopropylphenyl)-1*H*-imidazole (180 mg, 0.790 mmol) in acetonitrile (5 ml).

^{1}H NMR (500 MHz, $CDCl_3$) δ 10.10 (s, 1H), 9.49 (s, 1H), 7.96 (s, 1H), 7.86 (s, 1H), 7.57 (t, J = 7.7 Hz, 1H), 7.52 (s, 1H), 7.47 (d, J = 7.5 Hz, 2H), 7.38–7.29 (m, 4H), 7.13 (d, J = 3.4 Hz, 1H), 7.08 (s, 1H), 6.69 (d, J = 2.2 Hz, 1H), 2.55–2.45 (m, 5H), 1.26 (d, J = 6.3 Hz, 6H), 1.20 (d, J = 6.3 Hz, 6H). ^{13}C NMR (126 MHz, $CDCl_3$) δ 149.85, 147.57,

145.65, 142.88, 140.73, 137.38, 135.87, 134.82, 133.55, 132.39, 131.90, 131.01, 130.03, 129.98, 129.76, 126.34, 125.19, 125.04, 123.68, 121.17, 115.00, 28.91, 24.46, 21.72. ^{19}F NMR (282 MHz, $CDCl_3$) δ -143.27 (q, J (^{19}F-^{11}B) = 31.3 Hz). HRMS (ESI): m/z calcd. for $C_{31}H_{32}BF_2N_4$ [M-Cl]$^+$ 509.26826, found 509.26859.

Synthesis of complexes 3a and 3b

General procedure. A 10 ml flame-dried Schlenk flask equipped with a stirring bar was charged with the respective imidazolium salt **10a** or **10b** (1 eq), Ag_2O (0.5 eq) and dichloromethane. The reaction mixture was stirred at 40 °C for 1 h. [$AuCl(SMe_2)$] (1 eq) was added and the obtained suspension was stirred at room temperature for 2 h. Insoluble material was removed by filtration and the volatiles were evaporated under reduced pressure. The crude product was purified by column chromatography using DCM as an eluent.

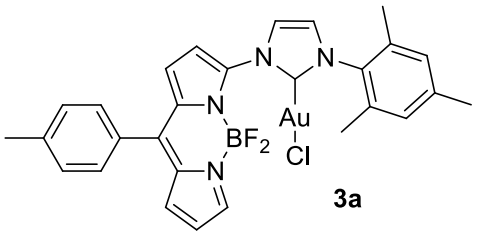

3a

Complex **3a** was obtained as an orange powder (15 mg, 36% yield) from **10a** (30 mg, 0.060 mmol), Ag_2O (6.9 mg, 0.030 mmol) and [$AuCl(SMe_2)$] (17.6 mg, 0.060 mmol) in DCM (2 ml).

^{1}H NMR (500 MHz, $CDCl_3$) δ 7.96 (s, 1H), 7.95 (d, J = 2.0 Hz, 1H), 7.52 (d, J = 8.0 Hz, 2H), 7.38 (d, J = 7.8 Hz, 2H), 7.09 (d, J = 4.2 Hz, 1H), 7.06 (d, J = 2.0 Hz, 1H), 7.02 (d, J = 4.3 Hz, 1H), 7.00 (d, J = 4.5 Hz, 1H), 6.99 (s, 2H), 6.64 (dd, J = 4.3, 1.7 Hz, 1H), 2.50 (s, 3H), 2.34 (s, 3H), 2.12 (s, 6H). ^{13}C NMR (126 MHz, $CDCl_3$) δ 174.54, 149.13, 146.70, 146.28, 142.26, 140.14, 135.65, 135.00, 134.67, 133.59, 133.28, 130.98, 130.47, 129.73, 129.62, 123.55 (t, J = 6.4 Hz), 122.05, 120.26, 115.66, 21.75, 21.35, 17.98. ^{19}F NMR (282 MHz, $CDCl_3$) δ -145.18 (q, J (^{19}F-^{11}B) = 29.9 Hz). HRMS (APCI): m/z calcd. for $C_{28}H_{25}AuBClFN_4$ [M-F]$^+$ 679.15050, found 679.15079.

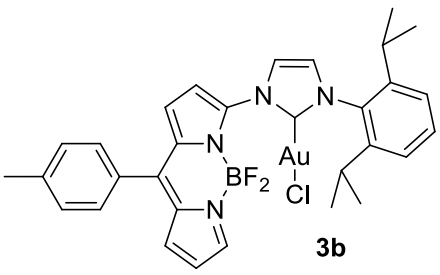

3b

Complex **3b** was obtained as an orange powder (13 mg, 48% yield) from **10b** (20 mg, 0.037 mmol), Ag_2O (4.3 mg, 0.018 mmol) and [$AuCl(SMe_2)$] (10.8 mg, 0.037 mmol) in DCM (2 ml).

^{1}H NMR (500 MHz, $CDCl_3$) δ 7.99 (s, 1H), 7.98 (d, J = 2.0 Hz, 1H), 7.52 (d, J = 8.0 Hz, 2H), 7.49 (t, J = 7.8 Hz, 1H), 7.38 (d, J = 7.8 Hz, 2H), 7.28 (d, J = 7.8 Hz, 2H), 7.10 (d, J = 2.0 Hz, 1H), 7.09 (d, J = 4.2 Hz, 1H), 7.06 (d, J = 4.3 Hz, 1H), 7.01 (d, J = 4.3 Hz, 1H), 6.65 (dd, J = 4.3, 1.7 Hz, 1H), 2.57 (hept, J = 6.7 Hz, 2H), 2.50 (s, 3H), 1.33 (d, J = 6.8 Hz, 6H), 1.19 (d, J = 6.9 Hz, 6H). ^{13}C NMR (126 MHz, $CDCl_3$) δ 175.22, 149.08, 146.64, 146.28, 145.94, 142.25, 135.61, 134.09, 133.58, 133.29, 130.95, 130.45, 129.62, 124.55, 123.28, 123.18, 120.26, 115.69, 28.68, 24.63, 24.53, 21.76. ^{19}F NMR (282 MHz, $CDCl_3$) δ -145.20 (q, J(^{19}F-^{11}B) = 30.0 Hz). HRMS (APCI): m/z calcd. for $C_{31}H_{31}AuBClFN_4$ [M-F]$^+$ 721.19745, found 721.19914.

Synthesis of BODIPY-phosphine 11

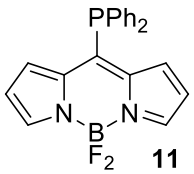

11

meso-ChloroBODIPY (50 mg, 0.221 mmol) was loaded into a 25 mL flame-dried Schlenk flask equipped with a stirring bar, followed by addition of CH_2Cl_2 (5 mL). Ph_2PH (46.11 μl, 0.265 mmol) was added and the reaction mixture was stirred for 10 min at room temperature. Solvent was evaporated under reduced pressure and the crude product was purified by short silica column using cyclohexane / CH_2Cl_2 (1:1) mixture as the eluent. The BODIPY-phosphine was collected as the red band (TLC: R_f = 0.22). Evaporation of the solvent afforded product as a red powder (27 mg, 33% yield). The obtained phosphine is slowly oxidized in air and should be stored under an inert atmosphere.

^{1}H-NMR (500 MHz, $CDCl_3$) δ 7.81 (s, 2H), 7.51–7.46 (m, 4H), 7.44–7.37 (m, 6H), 6.89 (d, J = 4.2 Hz, 2H), 6.33 (dd, J = 4.2, 1.2 Hz, 2H). ^{13}C-NMR (126 MHz, $CDCl_3$) δ 150.37 (d, J = 36.8 Hz), 144.04, 138.63 (d, J = 15.5 Hz), 134.64 (d, J = 9.5 Hz), 133.97 (d, J = 21.1 Hz), 131.98 (d, J = 11.9 Hz), 130.19, 129.40 (d, J = 7.8 Hz), 118.64. ^{19}F-NMR (282 MHz, $CDCl_3$) δ -148.70 (q, J (^{19}F-^{11}B) = 28.8 Hz). ^{31}P-NMR (121 MHz, $CDCl_3$) δ -7.62. HR-MS (EI), m/z: 376.1114 $[M]^{+\bullet}$, calcd. 376.1113 (Δ = 0.1 mmu).

Synthesis of complex [AuCl(11)]

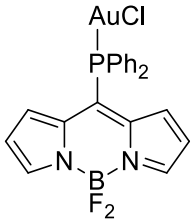

[AuCl(**11**)]

The BODIPY-phosphine **11** (6.0 mg, 0.016 mmol) was dissolved in CH_2Cl_2 (3 ml) and [AuCl(SMe_2)] (4.7 mg, 0.016 mmol) was added to the solution. After 30 min of stirring the solvent was evaporated under reduced pressure. The residue was dissolved in a small amount of CH_2Cl_2 (0.1 ml) and poured into pentane (3 ml). The formed precipitate was filtered, washed with pentane (3 × 1 ml) and dried. The product was obtained as a purple powder (9.0 mg, 93% yield).

^{1}H-NMR (500 MHz, $CDCl_3$) δ 7.87 (s, 2H), 7.84–7.77 (m, 4H), 7.66–7.61 (m, 2H), 7.57–7.52 (m, 4H), 6.63 (d, J = 4.4 Hz, 2H), 6.33 (d, J = 4.3 Hz, 2H). ^{13}C-NMR (126 MHz, $CDCl_3$) δ 146.64, 137.14 (d, J = 45.1 Hz), 136.66 (d, J = 12.4 Hz), 135.05 (d, J = 15.4 Hz), 133.52 (d, J = 1.7 Hz), 132.45, 130.17 (d, J = 12.7 Hz), 128.66 (d, J = 63.3 Hz), 120.13. ^{19}F-NMR (282 MHz, $CDCl_3$) δ -148.99 (q, J (^{19}F-^{11}B) = 27.8 Hz). ^{31}P-NMR (121 MHz, $CDCl_3$) δ 27.94. MS (EI): calcd for $C_{21}H_{16}BF_2N_2PClAu$ (M) 608, found 608. (HR-MS could not be obtained).

Synthesis of BODIPY-phosphine 12a

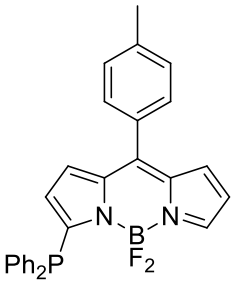

12a

3-Chloro-BODIPY **6** (150 mg, 0.474 mmol), $Pd(OAc)_2$ (10.6 mg, 0.047 mmol) and Ph_2PH (164.9 μl, 0.948 mmol) were loaded into 25 mL flame-dried Schlenk flask equipped with a stirring bar, followed by addition of toluene (10 mL). The mixture was degassed (2 cycles of freeze-pump-thaw). Triethylamine (330.5 μl, 2.369 mmol) was added and the reaction mixture was stirred overnight at room temperature. After evaporation of solvent under reduced pressure, the residue was filtered through a short silica gel pad using cyclohexane/CH_2Cl_2 (1:1) mixture for eluting. The collected deeply colored fractions were evaporated under reduced pressure and the crude product was purified by flash chromatography column (400 × 20 mm, 0.015-0.040 mm silica gel), using cyclohexane / CH_2Cl_2 (1:2) mixture as the eluent. The desired product was collected as the pink band (TLC: R_f = 0.25). Evaporation of the solvent

afforded product as a dark red powder (159 mg, 72% yield). The obtained phosphine is oxidized in air and should be stored under an inert atmosphere.

^{1}H-NMR (500 MHz, $CDCl_3$) δ 7.88 (s, 1H), 7.47–7.40 (m, 6H), 7.38–7.34 (m, 6H), 7.32 (d, J = 7.8 Hz, 2H), 6.90 (d, J = 4.0 Hz, 1H), 6.85 (d, J = 4.1 Hz, 1H), 6.51 (d, J = 3.2 Hz, 1H), 6.13 (d , J = 4.1 Hz, 1H), 2.47 (s, 3H). ^{13}C-NMR (126 MHz, $CDCl_3$) δ 159.68 (d, J = 23.4 Hz), 146.54, 144.71, 141.41, 138.84, 136.08 (d, J = 9.0 Hz), 135.42, 134.09 (d, J = 20.6 Hz), 131.45, 131.33, 130.79, 130.48, 129.32 (d, J = 5.6 Hz), 128.74 (d, J = 7.3 Hz), 125.32, 118.97, 21.66. ^{19}F-NMR (282 MHz, $CDCl_3$) δ -143.89 (dq, J (^{19}F-^{31}P) = 45.5 Hz, J (^{19}F-^{11}B) = 30.5 Hz). ^{31}P-NMR (121 MHz, $CDCl_3$) δ -20.34 (t, J (^{31}P-^{19}F) = 45.5 Hz). HR-MS (EI), m/z: 466.15601 $[M]^+$, calcd. 466.1582 (Δ = -2.2 mmu).

Synthesis of BODIPY-phosphine 12b

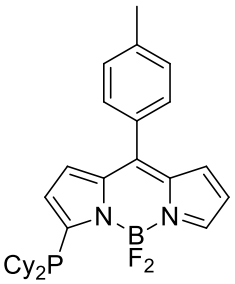

12b

3-Chloro-BODIPY **6** (150 mg, 0.474 mmol), $Pd(OAc)_2$ (10.6 mg, 0.047 mmol) and Cy_2PH (191.8 μl, 0.948 mmol) were loaded into 25 mL flame-dried Schlenk flask equipped with a stirring bar, following by addition of toluene (10 mL). The mixture was degassed (two cycles of freeze-pump-thaw). Triethylamine (330.5 μl, 2.369 mmol) was added and the reaction mixture stirred for 8 h at 50 °C. After evaporation of solvent under reduced pressure, the residue was filtered through a short silica gel pad using cyclohexane/CH_2Cl_2 (1:1) mixture for eluting. The collected deeply colored fractions were evaporated under reduced pressure and the crude product was purified by flash chromatography column (400 × 20 mm, 0.015-0.040 mm silica gel), using cyclohexane/CH_2Cl_2 (1:2) mixture as the eluent. The desired product was collected as the red band (TLC: R_f = 0.27). The evaporation of solvent afforded product as an orange powder (172 mg, 76% yield). The obtained phosphine is oxidized in air and should be stored under an inert atmosphere.

^{1}H-NMR (500 MHz, $CDCl_3$) δ 7.90 (s, 1H), 7.46 (d, J = 8.0 Hz, 2H), 7.31 (d, J = 7.8 Hz, 2H), 6.93 (d, J = 4.2 Hz, 1H), 6.86 (d, J = 4.0 Hz, 1H), 6.69 (d, J = 4.2 Hz, 1H), 6.50 (d, J = 3.0 Hz, 1H), 2.47 (s, 3H), 2.03–1.90 (m, 4H), 1.83–1.76 (m, 2H), 1.75–1.61 (m, 6H), 1.37–1.15 (m, 10H). ^{13}C-NMR (126 MHz, $CDCl_3$) δ 162.39 (d, J = 34.1 Hz), 145.60, 143.65, 141.10, 137.57, 134.88, 131.41, 130.71, 130.51 (d, J = 14.9 Hz), 129.18, 123.74, 118.38, 35.14 (d, J = 12.6 Hz), 30.38 (d, J = 26.8 Hz), 30.35, 27.33 (d, J = 8.0 Hz), 27.29 (d, J = 12.0 Hz), 26.48, 21.58. ^{19}F-NMR (282 MHz, $CDCl_3$) δ -140.21 (dq, J (^{19}F-^{31}P) = 52.7 Hz, J (^{19}F-^{11}B) = 30.1 Hz). ^{31}P-NMR (121 MHz, $CDCl_3$) δ -14.66 (t, J (^{31}P-^{19}F) = 52.4 Hz). HR-MS (EI), m/z: 478.24988 $[M]^{+\bullet}$, calcd. 478.2521 (Δ = -2.2 mmu).

Synthesis of complex [AuCl(12a)]

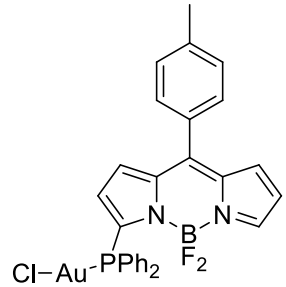

[AuCl(**12a**)]

BODIPY-phosphine **12a** (50 mg, 0.107 mmol) and [$AuCl(SMe_2)$] (31.5 mg, 0.107 mmol) were loaded into 25 mL Schlenk flask equipped with a stirring bar, followed by addition of CH_2Cl_2 (5 mL). After 30 min of stirring the solvent was evaporated under reduced pressure. The residue was dissolved in CH_2Cl_2 (0.5 ml) and poured into excess of pentane (5 ml). The formed precipitate was filtered, washed with pentane (3 × 1 ml) and dried. The product was obtained as a red powder (65 mg, 87% yield).

^{1}H-NMR (500 MHz, $CDCl_3$) δ 8.01 (s, 1H), 7.74–7.64 (m, 4H), 7.57–7.52 (m, 2H), 7.50–7.43 (m, 6H), 7.35 (d, J = 7.8 Hz, 2H), 7.06 (d, J = 4.1 Hz, 1H), 6.78 (d, J = 3.6 Hz, 1H), 6.62 (d, J = 4.1 Hz, 1H), 6.09–6.04 (m, 1H), 2.48 (s, 3H). ^{13}C-NMR (126 MHz, $CDCl_3$) δ 150.07, 148.47, 142.32 (d, J = 65.02 Hz), 142.29, 140.12 (d, J = 7.2 Hz), 137.04, 134.88, 134.76 (d, J = 14.9 Hz), 132.25, 130.91, 130.75, 129.60, 129.20 (d, J = 12.4 Hz), 129.03, 128.51, 128.15 (d, J = 7.3 Hz), 126.13 (d, J = 9.8 Hz), 121.79, 21.73. ^{19}F-NMR (282 MHz, $CDCl_3$) δ -139.97 (dq, J (^{19}F-^{31}P) = 15.5 Hz, J (^{19}F-^{11}B) = 30.7 Hz). ^{31}P-NMR (121 MHz, $CDCl_3$) δ 20.15 (t, J (^{31}P-^{19}F) = 15.4 Hz). MS (EI): calcd for $C_{28}H_{22}BF_2N_2PAuCl$ 698 (M), found 698. (HR-MS could not be obtained).

Synthesis of complex [AuCl(12b)]

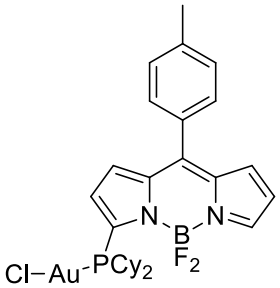

[AuCl(**12b**)]

BODIPY-phosphine **12b** (50 mg, 0.105 mmol) and [AuCl(SMe_2)] (31 mg, 0.105 mmol) were loaded into a 25 mL Schlenk flask equipped with a stirring bar, followed by addition of CH_2Cl_2 (5 mL). After 30 min of stirring the solvent was evaporated under reduced pressure. The residue was dissolved in small amount of CH_2Cl_2 (0.5 ml) and poured into pentane (5 ml). The formed precipitate was filtered, washed with pentane (3 × 1 ml) and dried. The product was obtained as an orange powder (67 mg, 90% yield).

^{1}H-NMR (500 MHz, $CDCl_3$) δ 8.09 (s, 1H), 7.47 (d, J = 8.1 Hz, 2H), 7.36 (d, J = 7.9 Hz, 2H), 7.29 (t, J = 4.7 Hz, 1H), 7.11 (d, J = 4.3 Hz, 1H), 6.86 (d, J = 3.8 Hz, 1H), 6.70 (d, J = 4.1 Hz, 1H), 2.99–2.89 (m, 2H), 2.49 (s, 3H), 2.14–2.07 (m, 2H), 1.89–1.82 (m, 2H), 1.73–1.63 (m, 6H), 1.53–1.40 (m, 4H), 1.35–1.23 (m, 6H). ^{13}C-NMR (126 MHz, $CDCl_3$) δ 148.91, 148.45, 142.75, 142.37, 140.45 (d, J = 4.1 Hz), 136.42, 134.61, 133.59 (d, J = 24.3 Hz), 130.94, 130.62, 129.55, 128.64 (d, J = 11.0 Hz), 121.43, 36.64 (d, J = 33.2 Hz), 32.67 (d, J = 5.2 Hz), 30.63, 26.44 (d, J = 11.6 Hz), 26.32 (d, J = 9.4 Hz), 25.70, 21.67. ^{19}F-NMR (282 MHz, $CDCl_3$) δ -143.29 (q, J (^{19}F-^{11}B) = 31.0 Hz). ^{31}P-NMR (121 MHz, $CDCl_3$) δ 47.49 (s). HR-MS (EI), m/z: 710.18508 $[M]^{+\bullet}$, calcd. 710.1872 (Δ = -2.1 mmu).

Synthesis of complex [Au(NTf_2)(12b)]

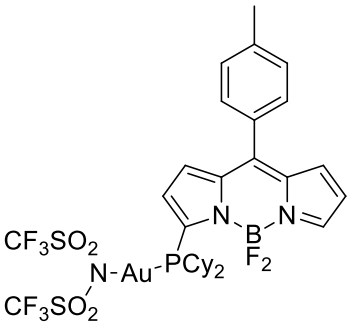

[Au(NTf_2)(**12b**)]

[Ag(NTf_2)] (8.6 mg, 0.022 mmol) and [AuCl(**12b**)] (15 mg, 0.021 mmol) were loaded into a 10 mL Schlenk flask equipped with a stirring bar, followed by addition of CH_2Cl_2 (2 mL). The mixture was stirred for 1 h at room temperature protected from light. Formed precipitate of silver chloride was separated by centrifuge and the solvent was evaporated under reduced pressure. Obtained material was carefully washed with pentane (3 × 0.2 ml) and dried. The product was obtained as a light orange powder (19 mg, 94% yield).

^{1}H-NMR (500 MHz, CD_2Cl_2) δ 8.14 (s, 1H), 7.50 (d, J = 8.1 Hz, 2H), 7.39 (d, J = 7.9 Hz, 2H), 7.19 (d, J = 4.4 Hz, 1H), 7.13 (t, J = 4.4 Hz, 1H), 6.93 (d, J = 3.5 Hz, 1H), 6.76 (d, J = 4.3 Hz, 1H), 2.93–2.82 (m, 2H), 2.49 (s, 3H), 2.19–2.11 (m, 2H), 1.94–1.85 (m, 2H), 1.77–1.66 (m, 4H), 1.63–1.57 (m, 2H), 1.52–1.35 (m, 4H), 1.31–1.17 (m, 6H). ^{13}C-NMR (126 MHz, CD_2Cl_2) δ 149.87, 149.59, 143.18, 141.02, 139.57, 139.11, 137.28,

135.74, 132.76 (d, J = 21.6 Hz), 131.50, 130.95, 130.01, 128.94 (d, J = 10.9 Hz), 122.41, 120.03 (q, J = 322.6 Hz), 36.86 (d, J = 34.4 Hz), 33.10 (d, J = 3.6 Hz), 31.28, 26.91 (d, J = 11.0 Hz), 26.79 (d, J = 9.0 Hz), 26.22, 21.85. ^{19}F-NMR (282 MHz, CD_2Cl_2) δ -78.31 (s), -141.81 (q, J (^{19}F-^{11}B) = 28.3 Hz). ^{31}P-NMR (121 MHz, CD_2Cl_2) δ 45.06 (s). Mass spectrum could not be obtained.

Synthesis of complex [AuCCPh(12b)]

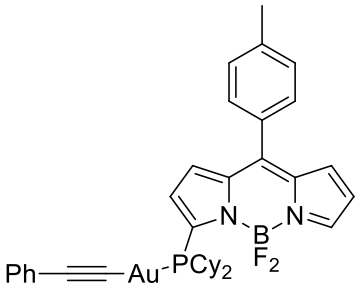

[AuCCPh(**12b**)]

10 ml flame-dried Schlenk flask equipped with a stirring bar was charged with 3 ml of THF, followed by addition of phenylacetylene (139 μl, 1.266 mmol). The obtained mixture was cooled down to -78 °C and *n*-BuLi (507 μl of 2.5 M solution in hexane, 1.268 mmol) was added in one portion. The reaction mixture was stirred at low temperature for 30 min. The cooling bath was removed allowing mixture warming up to room temperature. After 1 h of additional stirring the solution of lithium phenylacetylide (0.42 M) was obtained. [(**12b**)AuCl] (20 mg, 0.028 mmol) was loaded into Schlenk flask, followed by addition of THF (2 ml). The reaction mixture was cooled down to -78 °C and the previously prepared lithium phenylacetylide solution (75 μl, 0.032 mmol) was added in one portion. Stirring was continuing for 1 h. After removing of cooling bath reaction mixture was stirred for additional 30 min. The reaction was stopped by adding 3 drops of water. The solvent was evaporated under reduced pressure. The remaining residue was dissolved in CH_2Cl_2 (5 ml) and washed with water (3 × 3 ml). The organic layer was dried over anhydrous $MgSO_4$, filtered, and evaporated under reduced pressure. The remaining product was carefully washed with pentane, filtered and dried. The obtained red precipitate appears to be the mixture of product and starting material (ratio 3/1 according to ^{31}P-NMR). Further purification was not possible due to the instability of product.

^{19}F-NMR (282 MHz, CD_2Cl_2) δ -142.08 (q, J (^{19}F-^{11}B) = 30.6 Hz). ^{31}P-NMR (121 MHz, CD_2Cl_2) δ 49.57 (s). MS (APCI): calcd for $C_{36}H_{39}BF_2N_2PAu$ (M) 776.3, found 777.5 (M + H). (HR-MS could not be obtained).

Synthesis of complex [$PdCl_2$(12b)$_2$]

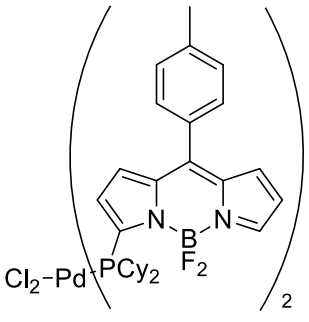

[$PdCl_2$(**12b**)$_2$]

BODIPY-phosphine **12b** (25 mg, 0.052 mmol) and [$PdCl_2(CH_3CN)_2$] (7.0 mg, 0.027 mmol) were loaded into a 25 mL Schlenk flask equipped with a stirring bar, following by addition of CH_2Cl_2 (5 mL). The reaction mixture was stirred overnight and the solvent was evaporated under reduced pressure. The residue was dissolved in small amount of CH_2Cl_2 (0.5 ml) and poured into excess of pentane (5 ml). The formed precipitate was filtered, washed with pentane and dried. The product was obtained as a red powder (26 mg, 88% yield).

^{1}H-NMR (500 MHz, $CDCl_3$) δ 7.98 (s, 1H), 7.47 (d, J = 7.9 Hz, 2H), 7.30 (d, J = 7.7 Hz, 2H), 7.09–7.03 (m, 1H), 6.91 (d, J = 3.6 Hz, 1H), 6.87 (d, J = 3.8 Hz, 1H), 6.56–6.51 (m, 1H), 3.12–3.03 (m, 2H), 2.58–2.50 (m, 2H), 2.46 (s, 3H), 2.10–2.02 (m, 2H), 1.86–1.58 (m, 12H), 1.46–1.35 (m, 4H). ^{13}C-NMR (126 MHz, $CDCl_3$) δ 150.28 (t, J = 14.1 Hz), 146.64, 144.79, 141.24, 139.21, 135.23, 131.43 (d, J = 4.9 Hz), 130.95, 130.26,

129.58, 129.12, 119.18, 34.95 (d, J = 9.3 Hz), 34.87 (d, J = 10.0 Hz), 30.95, 29.91, 27.72 (d, J = 4.6 Hz), 27.68 (d, J = 5.1 Hz), 27.52 (d, J = 6.2 Hz), 27.47 (d, J = 6.3 Hz), 26.56, 21.61. ^{19}F-NMR (282 MHz, $CDCl_3$) δ -140.88 (q, J (^{19}F-^{11}B) = 26.2 Hz). ^{31}P-NMR (121 MHz, $CDCl_3$) δ 28.34 (s). MS (ESI): calcd for $C_{56}H_{68}B_2F_4N_4P_2Pd$ (M – 2Cl) 1062.4, found 1063.6 (M – 2Cl + H). (HR-MS could not be obtained).

Phosphine oxide 13a

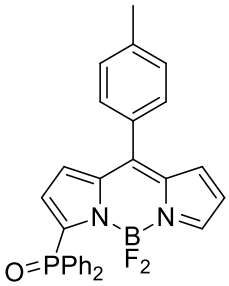

13a

The phosphine oxide was obtained as the by-product from other reactions involving phosphine **12a**. Different fractions were collected and purified by flash chromatography using ethyl acetate as the eluent. The residue was dissolved in small amount of CH_2Cl_2 and poured into an excess of pentane. The precipitate was filtered, washed with pentane and dried. The product was obtained as an orange powder.

^{1}H-NMR (500 MHz, $CDCl_3$) δ 8.00 (s, 1H), 7.88–7.75 (m, 4H), 7.59–7.52 (m, 2H), 7.51–7.42 (m, 6H), 7.34 (d, J = 7.6 Hz, 2H), 7.08–7.01 (m, 1H), 6.80 (s, 1H), 6.62–6.56 (m, 1H), 6.47 (s, 1H), 2.48 (s, 3H). ^{13}C-NMR (126 MHz, $CDCl_3$) δ 149.56, 148.87, 147.21, 146.34, 142.03, 139.37 (d, J = 9.9 Hz), 136.85, 134.46, 132.98, 132.37 (d, J = 10.1 Hz), 132.11, 130.97, 130.87, 129.45, 128.35 (d, J = 12.8 Hz), 127.93 (d, J = 9.2 Hz), 126.81 (d, J = 15.5 Hz), 121.40, 21.65. ^{19}F-NMR (282 MHz, $CDCl_3$) δ -143.01 (q, J (^{19}F-^{11}B) = 29.0 Hz). ^{31}P-NMR (121 MHz, $CDCl_3$) δ 20.03 (s). HR-MS (EI), m/z: 482.15183 $[M]^{+\bullet}$, calcd. 482.1531(Δ = -1.3 mmu).

Synthesis of complex [CuI(12b)]

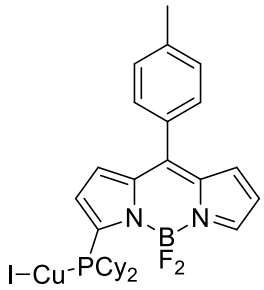

[CuI(**12b**)]

To a stirred solution of CuI (2.0 mg, 0.010 mmol) in CH_3CN (1 ml) the BODIPY-phosphine **12b** (5.0 mg, 0.011 mmol) dissolved in 1 ml of CH_3CN was added. Stirring was continued for 1 h. After evaporation of the solvent under reduced pressure, product was obtained as a violet powder (7.0 mg, >95% yield).

^{1}H-NMR (500 MHz, $CDCl_3$) δ 8.02 (s, 1H), 7.46 (d, J = 8.1 Hz, 2H), 7.37–7.30 (m, 3H), 7.00 (d, J = 4.1 Hz, 1H), 6.88 (d, J = 3.8 Hz, 1H), 6.60 (dd, J = 4.2, 1.4 Hz, 1H), 2.87–2.74 (m, 2H), 2.48 (s, 3H), 2.13–2.06 (m, 2H), 1.86–1.76 (m, 4H), 1.71–1.63 (m, 4H), 1.60–1.56 (m, 2H), 1.44–1.24 (m, 8H). ^{13}C-NMR (126 MHz, $CDCl_3$) δ 149.47, 147.63, 146.64, 141.79, 139.49, 135.85, 132.99, 131.14, 130.97, 130.59 (d, J = 16.9 Hz), 129.94 (d, J = 7.1 Hz), 129.40, 129.02, 120.20, 35.91 (d, J = 19.4 Hz), 30.83 (d, J = 9.9 Hz), 29.81, 27.08 (d, J = 27.0 Hz), 27.07, 26.07, 21.71. ^{19}F-NMR (282 MHz, $CDCl_3$) δ -141.99 (br s). ^{31}P-NMR (121 MHz, $CDCl_3$) δ1.91 (br s). MS (ESI): calcd for $C_{28}H_{34}BCuF_2N_2P$ (M – I) 541.2, found 541.5. (HR-MS could not be obtained).

Synthesis of complex [AgCl(12b)]

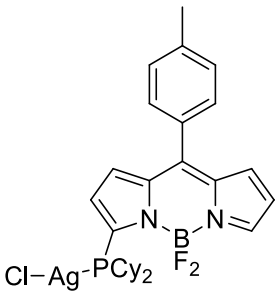

[AgCl(**12b**)]

BODIPY-phosphine **12b** (5.0 mg, 0.010 mmol) was loaded into a 10 mL Schlenk flask equipped with a stirring bar, following by addition of THF (1 mL) and saturated aqueous solution of KCl (1 ml). To the vigorously stirred two-phase mixture $AgNO_3$ (17 mg, 0.10 mmol) was added in few portions. After 3 h of stirring protected from light reaction mixture was filtered from AgCl and extracted with CH_2Cl_2 (3 × 2 ml). Combined organic fractions were dried over anhydrous $MgSO_4$, filtered, and evaporated under reduced pressure, giving product as a red powder (6.0 mg, 92% yield).

^{1}H-NMR (500 MHz, C_6D_6) δ 8.20 (br s, 1H), 7.73 (s, 1H), 6.83 (d, J = 8.1 Hz, 2H), 6.78 (d, J = 7.9 Hz, 2H), 6.65 (d, J = 3.8 Hz, 1H), 6.50 (d, J = 4.2 Hz, 1H), 5.92 (dd, J = 4.2, 1.2 Hz, 1H), 3.26 (br s, 2H), 2.30–2.09 (m, 4H), 2.00 (s, 3H), 1.91–1.76 (m, 6H), 1.68–1.63 (m, 2H), 1.58–1.46 (m, 4H), 1.41–1.32 (m, 4H). ^{13}C-NMR (126 MHz, C_6D_6) δ 147.76, 146.21, 141.24, 140.83, 135.96, 132.19, 131.72, 131.26, 130.99 (d, J = 9.4 Hz), 129.31, 119.96, 36.52 (d, J = 12.4 Hz), 32.67 (d, J = 14.3 Hz), 31.20 (d, J = 4.6 Hz), 27.63 (d, J = 4.6 Hz), 27.52, 26.53, 21.53. ^{19}F-NMR (282 MHz, C_6D_6) δ -141.99 (br s). ^{31}P-NMR (121 MHz, C_6D_6) δ 36.49 (d, J = 617.0 Hz). MS (ESI): calcd for $C_{28}H_{34}AgBF_2N_2P$ (M – Cl) 585.2, found 585.5. (HR-MS could not be obtained).

Synthesis of complex [CuI(12a)]

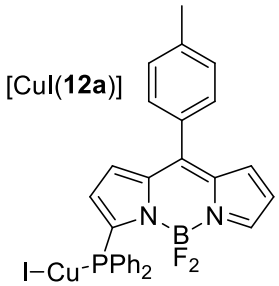

[CuI(**12a**)]

To a stirred solution of CuI (2.0 mg, 0.011 mmol) in CH_3CN (1 ml) the BODIPY-phosphine **12a** (5.0 mg, 0.011 mmol) dissolved in 1 ml of CH_3CN was added. Stirring was continued for 1 h. After evaporation of the solvent under reduced pressure, product was obtained as a deep purple powder (7.0 mg, >95% yield).

^{1}H-NMR (500 MHz, $CDCl_3$) δ 7.72 (br s, 1H), 7.61 (br s, 4H), 7.45 (d, J = 8.0 Hz, 2H), 7.40–7.30 (m, 8H), 6.90 (d, J = 4.1 Hz, 1H), 6.81 (d, J = 3.9 Hz, 1H), 6.46 (d, J = 2.9 Hz, 1H), 6.11 (d, J = 4.0 Hz, 1H), 2.46 (s, 3H). ^{13}C-NMR (126 MHz, $CDCl_3$) δ 146.96, 141.49, 139.24, 135.76, 134.55 (d, J = 17.2 Hz), 132.40, 132.09, 131.30, 130.85, 129.88, 129.36, 128.66 (d, J = 8.3 Hz), 125.60, 119.39, 21.69. ^{19}F-NMR (282 MHz, $CDCl_3$) δ -142.92 (br s). ^{31}P-NMR (121 MHz, $CDCl_3$) δ -18.42 (br s). MS (ESI): calcd for $C_{28}H_{22}BCuF_2N_2P$ (M – I) 529.1, found 529.5. (HR-MS could not be obtained).

Synthesis of silver salt 14·Ag

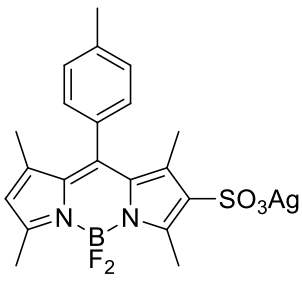

14·Ag

Tetramethyl-*meso*-(*p*-tolyl)-BODIPY (100 mg, 0.296 mmol, 1.0 eq) was loaded into 10 mL flame-dried Schlenk flask equipped with a stirring bar, followed by addition of DCM (4 mL). The obtained solution was cooled down to -78 °C and 1 M solution of chlorosulfonic acid in acetonitrile (355 μL, 0.355 mmol, 1.2 eq) was added dropwise. After stirring for 30 min the cooling bath was removed and the stirring was continued at room temperature for additional 1 h. The content of the flask was diluted with methanol (4 ml) and silver carbonate was added (82 mg, 0.296 mmol, 2.0

eq). The reaction mixture was stirred overnight protected from light. The excess of silver carbonate was removed by filtration. The filtrate was centrifuged and filtered again for complete removal of silver carbonate. After evaporation of the solvents under reduced pressure, the crude residue was dissolved in minimum amount of DCM. Excess addition of diethyl ether (5 mL) caused the precipitation of the pure silver salt, which was collected by filtration as an orange powder (85 mg, 55% yield).

^{1}H-NMR (500 MHz, CD_3OD) δ 7.39 (d, J = 7.7 Hz, 2H), 7.19 (d, J = 8.0 Hz, 2H), 6.15 (s, 1H), 2.76 (s, 3H), 2.51 (s, 3H), 2.45 (s, 3H), 1.68 (s, 3H), 1.42 (s, 3H). ^{13}C-NMR (126 MHz, CD_3OD) δ 159.92, 153.56, 147.04, 145.39, 141.35, 140.98, 134.29, 133.17, 131.50, 131.46, 131.29, 130.73, 129.20, 123.72, 21.53, 15.05, 14.88, 14.30, 13.37. HRMS (ESI, negative mode): m/z calcd. for $C_{20}H_{20}BF_2N_2O_3S$ $[M\text{-}Ag]^-$ 417.12612, found 417.12675.

Synthesis of complex [AuIPr(14)]

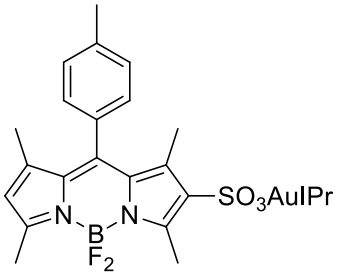

[AuIPr(**14**)]

BODIPY silver sulfonate (8.5 mg, 0.016 mmol, 1.0 eq) and IPrAuCl (10.0 mg, 0.016 mmol, 1.0 eq) were loaded into flame-dried Schlenk flask equipped with a stirring bar, followed by addition of DCM (2 mL). The reaction mixture was vigorously stirred overnight. The insoluble materials were removed by filtration. After evaporation of solvent the product was obtained as an orange powder in quantitative yield.

^{1}H-NMR (500 MHz, $CDCl_3$) δ 7.48 (t, J = 7.8 Hz, 2H), 7.29 (d, J = 7.7 Hz, 2H), 7.27 (d, J = 7.0 Hz, 4H), 7.20 (s, 2H), 7.08 (d, J = 7.7 Hz, 2H), 6.02 (s, 1H), 2.56 (s, 3H), 2.51–2.43 (m, 10H), 1.37 (s, 6H), 1.30 (d, J = 6.9 Hz, 12H), 1.21 (d, J = 6.9 Hz, 12H).

Synthesis of compound 15·NBu_4

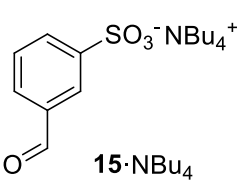

15·NBu_4

Sodium 3-formylbenzenesulfonate (2.8 g, 13.4 mmol) was dissolved in distilled water (10 mL) and to the obtained solution was added the solution of tetrabutylammonium bromide (3.6 g, 11.1 mmol) in dichloromethane (20 mL). The two-phase mixture was vigorously stirred for 2 h and transferred into a separatory funnel. The mixture was repeatedly shaken few times. The organic layer was separated and water phase washed few times with dichloromethane. The combined extracts were washed with brine and dried over magnesium sulfate. After evaporation of the solvent, the residue was purified by column chromatography (silica, acetone:dichloromethane, 1:10) affording the product as a colorless viscous oil (3.72 g, 78% yield).

^{1}H NMR (500 MHz, $CDCl_3$) δ 9.98 (s, 1H, CHO), 8.37 (t, J = 1.7 Hz, 1H, H_{Ar}), 8.17 – 8.14 (m, 2H, H_{Ar}), 7.81 (dt, J = 7.7, 1.4 Hz, 1H, H_{Ar}), 7.46 (t, J = 7.6 Hz, 1H,H_{Ar}), 3.27 – 3.21 (m, 8H, NCH_2), 1.64 – 1.55 (m, 8H, CH_2), 1.37 (sex, J = 7.4 Hz, 8H, CH_2), 0.93 (t, J = 7.3 Hz, 12H, CH_3). ^{13}C NMR (126 MHz, $CDCl_3$) δ 192.19 (CHO), 148.62, 136.18, 132.33, 129.16, 128.76, 128.59, 58.91 (NCH_2), 24.09 (CH_2), 19.80 (CH_2), 13.72 (CH_3). HR-MS (ESI, positive mode): m/z calcd. for $C_{16}H_{36}N^+$ $[M]^+$ 242.2842, found 242.2843. HR-MS (ESI, negative mode): m/z calcd. for $C_7H_5O_4S^-$ $[M]^-$ 184.9914, found 184.9914.

Synthesis of BODIPY sulfonate 16·NBu$_4$(Et*i*Pr$_2$NH)

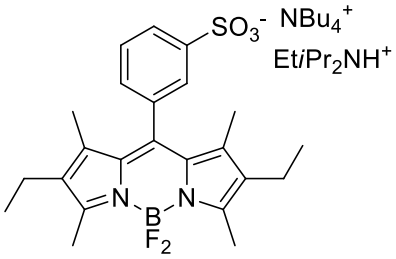

16·NBu$_4$(Et*i*Pr$_2$NH)

Compound **15**·NBu$_4$ (990 mg, 2.31 mmol), 3-ethyl-2,4-dimethylpyrrole (624.7 μL, 4.63 mmol) were dissolved in dichloromethane (100 mL) under nitrogen atmosphere. Trifluoroacetic acid (3 drops) was added and the mixture stirred overnight at RT in a dark. Next, DDQ (525.7 mg, 2.31 mmol) was added and the mixture stirred for 1.5 h at RT. After this the mixture was cooled to 0 °C and *N,N*-diisopropylethylamine (2.01 mL, 11.5 mmol) was added dropwise. After few minutes boron trifluoride diethyl etherate (2.0 mL, 16.1 mmol) was added dropwise and the mixture stirred for 1 h at r.t. Next, the mixture was washed with water, the organic layer was separated, dried over magnesium sulfate and the solvent evaporated under reduced pressure. The residue was purified by column chromatography (silica, acetone:dichloromethane, 1:1 to 2:1) affording the dye **16**·NBu$_4$(Et*i*Pr$_2$NH) with mixed cations (448.5 mg, 30% yield).

^{1}H NMR (500 MHz, $CDCl_3$) δ 8.04 (d, J = 7.8 Hz, 1H, H_{Ar}), 7.83 (s, 1H, H_{Ar}), 7.48 (t, J = 7.7 Hz, 1H, H_{Ar}), 7.26 (d, J = 8.3 Hz, 1H, H_{Ar}), 3.69 (hept, J = 6.6 Hz, 1H, *i*Pr$_2$CH), 3.34 – 3.27 (m, 2H, NCH_2, NBu_4), 3.11 (q, J = 7.5 Hz, 1H, NCH_2, *i*Pr$_2$NEt), 2.52 (s, 6H, CH_3, bodipy), 2.28 (q, J = 7.5 Hz, 4H, CH_2, bodipy), 1.70 – 1.61 (m, 4H, CH_2, NBu_4), 1.50 – 1.36 (m, 12H), 1.30 (s, 6H, CH_3, bodipy), 1.00 – 0.93 (m, 12H, CH3, bodipy+NBu_4). ^{13}C NMR (126 MHz, $CDCl_3$) δ 153.68, 147.80, 139.95, 138.74, 135.30, 132.79, 130.90, 129.14, 128.89, 126.76, 126.15, 59.00, 54.35, 42.67, 29.41, 24.16, 19.85, 18.77, 17.51, 17.15, 14.72, 13.74, 12.60, 12.34, 12.24. ^{19}F NMR (471 MHz, $CDCl_3$) δ -148.61 – -149.00 (m). HR-MS (ESI, positive mode): m/z calcd. for $C_{16}H_{36}N^+$ $[M]^+$ 242.2842, found 242.2838; m/z calcd. for $C_8H_{20}N^+$ $[M]^+$ 130.1590, found 130.1587. HR-MS (ESI, negative mode): m/z calcd. for $C_{23}H_{26}BF_2N_2O_3S^-$ $[M]^-$ 459.1730, found 459.1733.

Synthesis of BODIPY sulfonic acid 16·H

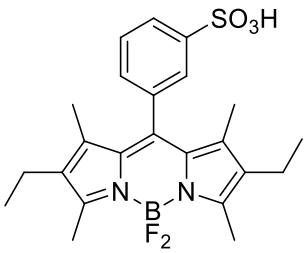

16·H

BODIPY sulfonate **16**·NBu$_4$(Et*i*Pr$_2$NH) (100 mg, 0.22 mmol) was dissolved in methanol and the solution was passed through Amberlite IR-120 hydrogen form cation exchange resin. The solvent was evaporated under reduced pressure and the residue purified by flash chromatography (silica, methanol:dichloromethane, 1:5) affording acid **16**·H (54.2 mg, 76% yield).

^{1}H NMR (500 MHz, DMSO-d_6) δ 7.77 (dt, J = 7.8, 1.3 Hz, 1H, H_{Ar}), 7.53 (t, J = 7.7 Hz, 1H, H_{Ar}), 7.49 (t, J = 1.7 Hz, 1H, H_{Ar}), 7.31 (dt, J = 7.5, 1.5 Hz, 1H, H_{Ar}), 2.44 (s, 6H, CH_3), 2.30 (q, J = 7.5 Hz, 4H, CH_2), 1.25 (s, 6H, CH_3), 0.95 (t, J = 7.5 Hz, 6H, CH_3). ^{13}C NMR (126 MHz, DMSO-d_6) δ 153.22, 149.43, 140.06, 137.92, 133.94, 132.64, 129.86, 128.74, 127.98, 126.05, 125.00, 16.36, 14.46, 12.22, 11.51. ^{19}F NMR (471 MHz, DMSO-d_6) δ -145.01 – -145.49 (m).

Synthesis of complex [(17)-O-IPrAu(OAc)]

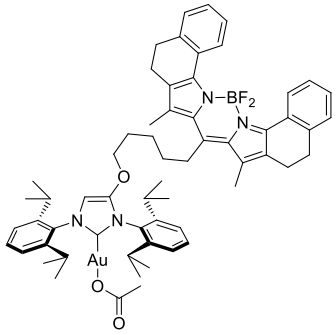

[(**17**)-O-IPrAu(OAc)]

Silver acetate (4.4 mg, 0.027 mmol, 1 eq) and the respective complex [(**17**)-O-IPrAuCl] (30.0 mg, 0.027 mmol, 1 eq) were loaded into a 10 mL Schlenk flask equipped with a stirring bar, followed by addition of CH_2Cl_2 (3 mL). The mixture was stirred for 3 h at room temperature protected from light. Formed precipitate of silver chloride was separated by centrifuge and the solvent was evaporated under reduced pressure. Obtained material was carefully washed with pentane and dried. The product was obtained in a quantitative yield as a deep blue powder.

^{1}H NMR (500 MHz, $CDCl_3$) δ 8.73 (d, J = 8.0 Hz, 2H), 7.48 (q, J = 7.6 Hz, 2H), 7.39 (t, J = 7.6 Hz, 2H), 7.30–7.22 (m, 8H, overlapped with solvent residual peak), 6.42 (s, 1H), 4.01 (t, J = 6.2 Hz, 2H), 3.12–3.01 (m, 2H), 2.89 (t, J = 7.0 Hz, 4H), 2.68–2.56 (m, 8H), 2.33 (s, 6H), 1.81–1.72 (m, 2H), 1.76 (s, 3H), 1.70–1.62 (m, 2H), 1.53–1.49 (s, 2H), 1.38 (d, J = 6.9 Hz, 6H), 1.36 (d, J = 6.9 Hz, 6H), 1.24 (d, J = 6.9 Hz, 6H), 1.20 (d, J = 6.9 Hz, 6H). ^{13}C NMR (126 MHz, $CDCl_3$) δ 176.50, 163.61, 149.85, 148.67, 146.36, 145.99, 143.77, 140.57, 135.01, 134.26, 133.22, 132.25, 130.87, 130.77, 130.63, 129.45, 128.77, 128.56, 128.19, 127.48, 124.41, 124.22, 99.55, 72.33, 32.04, 30.79, 29.36, 29.07, 28.80, 26.40, 24.83, 24.46, 24.29, 24.11, 23.97, 20.89, 14.15.

Synthesis of NHC-gold(I) sulfonato complexes [IPrAu(16)] and [(17)-O-IPrAu(16)]

General procedure. Corresponding NHC-gold(I) acetate complex (1 eq) and acid **16**·H (1 eq) were dissolved in DCM and stirred at room temperature overnight. The solvent was removed under reduced pressure and the residue was washed with pentane to give a pure product.

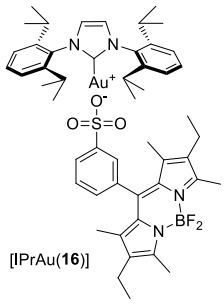

[IPrAu(**16**)]

Complex [IPrAu(**16**)] was quantitatively obtained from [IPrAu(OAc)] (10 mg, 0.016 mmol) and acid **16**·H (7 mg, 0.016 mmol).

^{1}H NMR (500 MHz, $CDCl_3$) δ 7.69 (d, J = 5.4 Hz, 1H), 7.52 (br s, 1H), 7.42–7.33 (m, 4H), 7.25 (d, J = 7.8 Hz, 4H), 7.22 (s, 2H), 2.56 (s, 6H), 2.48 (hept, J = 6.7 Hz, 4H), 2.30 (q, J = 7.5 Hz, 4H), 1.28 (d, J = 6.8 Hz, 12H), 1.19 (d, J = 6.9 Hz, 12H), 1.16 (s, 6H), 1.00 (t, J = 7.5 Hz, 6H). ^{13}C NMR (126 MHz, $CDCl_3$) δ 164.38, 154.06, 145.77, 144.47, 139.28, 138.85, 135.84, 133.82, 133.03, 131.15, 130.96, 130.53, 129.01, 126.99, 126.58, 124.51, 123.66, 29.09, 24.47, 24.30, 17.28, 14.87, 12.74, 12.25.

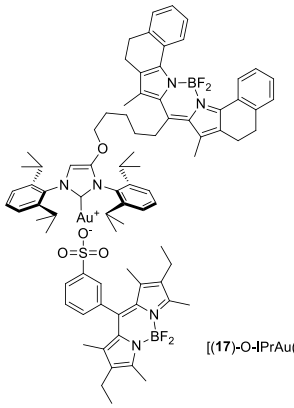

[(**17**)-O-IPrAu(**16**)]

Complex [(**17**)-O-IPrAu(**16**)] was quantitatively obtained from [(**17**)-O-IPrAu(OAc)] (20 mg, 0.017 mmol) and acid **16**·H (8 mg, 0.017 mmol).

^{1}H NMR (500 MHz, CD_2Cl_2) δ 8.68 (d, J = 8.0 Hz, 2H), 7.57 (d, J = 7.4 Hz, 1H), 7.44–7.35 (m, 6H), 7.33–7.25 (m, 9H), 6.53 (s, 1H), 4.05 (t, J = 6.2 Hz, 2H), 3.14–3.06 (m, 2H), 2.92 (t, J = 7.0 Hz, 4H), 2.69–2.55 (m, 8H), 2.53 (s, 6H), 2.36 (s, 6H), 2.33 (q, J = 7.6 Hz, 4H), 1.83–1.75 (m, 2H), 1.72–1.64 (m, 2H), 1.58–1.50 (m, 2H), 1.29 (d, J = 7.0 Hz, 6H), 1.27 (d, J = 6.9 Hz, 6H), 1.23

(d, J = 6.8 Hz, 6H), 1.19 (d, J = 6.9 Hz, 6H), 1.17 (s, 6H), 1.01 (t, J = 7.5 Hz, 6H). ^{13}C NMR (126 MHz, CD_2Cl_2) δ 165.99, 158.36, 154.41, 149.84, 149.26, 146.84, 146.43, 145.03, 144.85, 141.37, 139.74, 139.28, 136.18, 135.10, 134.62, 134.31, 133.60, 132.79, 131.39, 131.29, 130.99, 130.78, 129.81, 129.58, 128.90, 128.83, 128.74, 127.52, 127.06, 126.86, 124.80, 124.67, 100.60, 73.11, 32.32, 31.11, 29.68, 29.38, 29.26, 26.74, 24.90, 24.51, 24.36, 24.05, 21.18, 17.57, 15.03, 14.33, 12.88, 12.40. ^{19}F NMR (471 MHz, CD_2Cl_2) δ -136.23 – -136.82 (m, 1F), -138.69 – -139.33 (m, 1F), -147.22 – -148.15 (m, 2F).

Synthesis of compound 18·K

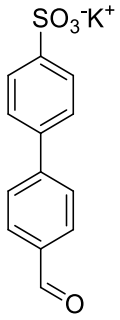

18·K

Biphenyl-4-carboxaldehyde (1.0 g, 5.48 mmol) was added portion wise to the stirred oleum (2.5 mL) at RT. The obtained solution was stirred at 40 °C overnight, cooled to RT and poured into ice. The obtained suspension was warmed to RT and to the obtained solution was added an excess of solid potassium chloride. The obtained white precipitate of the product was collected by filtration, washed with water and with a small amount of methanol. After drying in vacuo for 12 h at 50 °C, the product was obtained as white powder (1.51 g, 92% yield).

^{1}H NMR (500 MHz, DMSO-d_6) δ 10.06 (s, 1H, CHO), 8.00 (d, J = 8.3 Hz, 2H, H_{Ar}), 7.92 (d, J = 8.2 Hz, 2H, H_{Ar}), 7.73 (s, 4H, H_{Ar}). ^{13}C NMR (126 MHz, DMSO-d_6) δ 192.68 (CHO), 148.44, 145.39, 138.66, 135.11, 130.10, 127.36, 126.50, 126.27.

Synthesis of compound 18·NBu$_4$

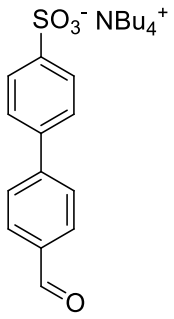

18·NBu$_4$

Potassium salt **18**·K (1.5 g, 5 mmol) was suspended in a mixture of water (20 mL) and dichloromethane (40 mL) and tetra-*n*-butylammonium bromide (1.61 g, 5 mmol) was added. The mixture was intensively shaken until insoluble salt **18**·K completely disappeared. Next, the organic layer was separated, dried over magnesium sulfate and solvent evaporated affording the title compound as colorless oil (2.4 g, 96% yield).

^{1}H NMR (500 MHz, $CDCl_3$) δ 10.00 (s, 1H, CHO), 7.95 (d, J = 8.1 Hz, 2H, H_{Ar}), 7.89 (d, J = 8.2 Hz, 2H, H_{Ar}), 7.68 (d, J = 8.3 Hz, 2H, H_{Ar}), 7.55 (d, J = 8.2 Hz, 2H, H_{Ar}), 3.25–3.17 (m, 8H, NCH_2), 1.60–1.52 (m, 8H, CH_2), 1.39–1.30 (m, 8H, CH_2), 0.91 (t, J = 7.3 Hz, 12H, CH_3). ^{13}C NMR (126 MHz, $CDCl_3$) δ 191.95 (CHO), 147.40, 146.75, 140.14, 135.29, 130.24, 127.69, 126.87, 58.70 (NCH_2), 23.96 (CH_2), 19.68 (CH_2), 13.65 (CH_3). HR-MS (ESI, positive mode): m/z calcd. for $C_{16}H_{36}N^+$ $[M]^+$ 242.2842, found 242.2843. HR-MS (ESI, negative mode): m/z calcd. for $C_{13}H_9O_4S^-$ $[M]^-$ 261.0227, found 261.0231.

Synthesis of BODIPY biphenyl sulfonates 19a·Et*i*Pr$_2$NH and 19b·NBu$_4$

General procedure. Compound **18**·NBu$_4$ (1 eq) and respective pyrrole (2 eq) were dissolved in dichloromethane (100 mL) under a nitrogen atmosphere. Trifluoroacetic acid (4 drops) was added and the mixture stirred overnight at RT in a dark. Next, chloranil (1 eq) was added and the stirring was continued for another 1.5 h. The reaction mixture was cooled to 0 °C and *N*,*N*-diisopropylethylamine (5 eq) was added dropwise. After few minutes boron trifluoride diethyl etherate (7 eq) was added dropwise and the mixture stirred for 1 h at RT. Next, the mixture was washed with water, the organic layer was separated, dried over magnesium

sulfate and the solvent was evaporated under reduced pressure. The residue was purified by silica column chromatography (acetone:dichloromethane, 1:1 to 2:1) affording the pure products.

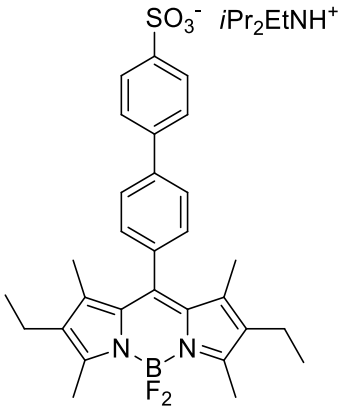

19a·Et*i*Pr$_2$NH

Compound **19a**·Et*i*Pr$_2$NH was obtained as a dark red material (1.37 g, 58% yield) from compound **18**·NBu$_4$ (1.78 g, 3.53 mmol), 3-ethyl-2,4-dimethylpyrrole (953.6 μL, 7.06 mmol), chloranil (868.8 mg, 3.53 mmol), *N*,*N*-diisopropylethylamine (3.13 mL, 18 mmol) and boron trifluoride diethyl etherate (3.1 mL, 25 mmol).

^{1}H NMR (300 MHz, DMSO-d_6) δ 8.19 (s, 1H, *i*Pr$_2$NHEt), 7.90 (d, J = 8.3 Hz, 2H, H$_{Ar}$), 7.78–7.69 (m, 4H, H$_{Ar}$), 7.44 (d, J = 8.2 Hz, 2H, H$_{Ar}$), 3.68–3.55 (m, 2H), 3.19–3.09 (m, 2H), 2.45 (s, 6H, CH$_3$, bodipy), 2.30 (q, J = 7.4 Hz, 4H, *CH*$_2$CH$_3$, bodipy), 1.34 (s, 6H, CH$_3$, bodipy), 1.29–1.21 (m, 15H, CH$_3$, cation), 0.95 (t, J = 7.5 Hz, 6H, CH$_2$*CH*$_3$, bodipy). ^{13}C NMR (75 MHz, DMSO-d_6) δ 153.16, 147.96, 140.19, 140.11, 138.86, 138.09, 133.86, 132.59, 129.95, 128.68, 127.22, 126.24, 125.98, 53.59, 41.82, 18.05, 16.70, 16.37, 14.45, 12.41, 12.21, 11.49. ^{19}F NMR (282 MHz, CDCl$_3$/DMSO-d$_6$) δ -148.45 (1:1:1:1 pattern, J = 32.4 Hz). HR-MS (ESI, positive mode): m/z calcd. for $C_8H_{20}N^+$ $[M]^+$ 130.1590, found 130.1590. HR-MS (ESI, negative mode): m/z calcd. for $C_{29}H_{30}BF_2N_2O_3S^-$ $[M]^-$ 535.2044, found 535.2055.

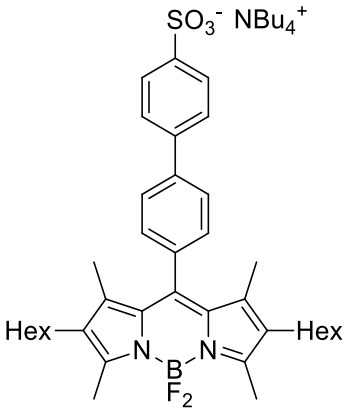

19b·NBu$_4$

Compound **19b**·NBu$_4$ was obtained as a dark red material (0.99 g, 45% yield) from compound **18**·NBu$_4$ (1.24 g, 2.46 mmol), 3-hexyl-2,4-dimethylpyrrole (885 mg, 4.94 mmol), chloranil (610 mg, 2.48 mmol), *N*,*N*-diisopropylethylamine (2.15 mL, 12.34 mmol) and boron trifluoride diethyl etherate (2.13 mL, 17.26 mmol).

^{1}H NMR (500 MHz, CDCl$_3$) δ 8.02 (d, J = 8.1 Hz, 2H), 7.70 (d, J = 8.1 Hz, 2H), 7.63 (d, J = 8.2 Hz, 2H), 7.33 (d, J = 8.1 Hz, 2H), 3.36–3.28 (m, 8H), 2.52 (s, 6H), 2.26 (t, J = 7.4 Hz, 4H), 1.71–1.63 (m, 8H), 1.45 (h, J = 7.3 Hz, 8H), 1.33 (s, 6H), 1.32–1.20 (m, 16H), 1.00 (t, J = 7.3 Hz, 12H), 0.86 (t, J = 6.7 Hz, 6H).

6.2. Quantum yields determination

Quantum yields were determined according to the literature procedure[225] using rhodamine 6G or rhodamine 101 (from Sigma-Aldrich, BioReagent, suitable for fluorescence) as the standards. Absorption and emission spectra for all fluorescent compounds were obtained in 1,2-dichloroethane over a range of concentrations (250 nM to 1.0 μM) where a linear correlation between concentration and absorption was observed and the absorbance was within the range from 0.01 to 0.1. The quantum yield was calculated according to the equation $\Phi_x = \Phi_{st}\left(\frac{Grad_x}{Grad_{st}}\right)\left(\frac{\eta_x}{\eta_{st}}\right)^2$ where the subscripts *st* and *x* denote standard and test respectively, Φ is the fluorescence quantum yield, *Grad* the gradient from the plot of

integrated fluorescence intensity *vs* absorbance, and η the refractive index of the solvent. For rhodamine 6G Φ_{st} = 0.95 in EtOH; for rhodamine 101 Φ_{st} = 1.00 in EtOH.

6.3. Monitoring of the reaction of BODIPY-tagged gold(I) complexes with thiols

General conditions. All experiments were carried out in quartz cuvettes with a path length of 10.00 mm equipped with a stirring bar. The temperature (298 K) was adjusted using a thermostat and controlled with a thermometer over the course of measurements.

General procedure of measurements. The following general procedure was applied in all experiments with thiols. The cuvette was filled with 2 ml of 1 μM solution of the respective gold complex in 1,2-dichloroethane. The measurement was started and the fluorescence intensity at emission maximum was observed. After approximately 1 min 10 μl of 0.02 M solution of *N*,*N*-diisopropylethylamine (Hünig base) in 1,2-dichloroethane (100 eq) was added, followed by the addition of 10 μl of the corresponding *para*-substituted thiophenol solution in 1,2-dichloroethane (0.02 M solution of thiophenol was used to add 100 eq, 0.1 M – to add 500 eq). The dilution, caused by the addition of reagents, was recalculated on the final curves.

6.4. Monitoring of the reaction of BODIPY-tagged phosphine-gold(I) complex with silver salt and acetylenes

Purification of the solvent. 1 L flame-dried Schlenk flask was filled with 500 ml of 1,2-dichloroethane (99+%, for spectroscopy ACS, Acros Organics), followed by addition of *ca.* 50 g of alumina powder (previously preactivated by keeping under vacuum at 200 °C overnight). The obtained suspension was shaken for two days at room temperature. The solvent was distilled under nitrogen into another Schlenk flask and *ca.* 10 g of CaH_2 powder was added. The suspension was stirred for two days at room temperature and the solvent was distilled under nitrogen. Purified 1,2-dichloroethane was kept under an inert atmosphere.

Preparation of stock solution of silver salt. Silver nonaflate (1-1.5 mg) was weighed in a small vial, dissolved in a minimum amount of methanol and transferred into 10 ml flame-dried Schlenk flask. After careful evaporation of methanol, the flask was kept under vacuum at 50 °C overnight. To get 10^{-3} M solution of silver salt the respective amount of 1,2-dichloroethane (2.457 ml for 1 mg of AgONf) was added, the flask was tightly closed and immersed into an ultrasonic bath for 5-10 min, until all silver salt was dissolved. The obtained silver nonaflate solution was used within 12 hours to avoid the formation of triflic acid.

Preparation of stock solution of BODIPY-tagged phosphine-gold(I) complex. [(**12b**)AuCl] (< 1 mg) was weighed in a small vial and transferred with dichloromethane into 25 ml flame-dried Schlenk flask. After evaporation of DCM, the gold complex was dried under vacuum for several hours. The necessary amount of 1,2-dichloroethane was added to obtain a 10^{-4} M solution. The stock solution was kept under an inert atmosphere and was used within 24 h.

Preparation of other stock solutions. Stock solutions (0.3 M) of different phenylacetylenes and *N*,*N*-diisopropylethylamine (Hünig base) were prepared by dissolving the respective amount of the substance in 1,2-dichloroethane. Solutions were kept under an inert atmosphere and used within 24 h.

General procedure of fluorescence time measurements. 1 μM solution of [(**12b**)AuCl] was prepared directly in a cuvette by dilution of 30 μl of 10^{-4} M stock solution in 2.970 ml of 1,2-

dichloroethane. After measurement was started the necessary amount of silver salt stock solution was added (1 eq = 3 μl), followed by addition of 10 μl (1000 eq) of the respective phenylacetylene solution. Prior to the addition of phenylacetylene 50-150 eq of *N*,*N*-diisopropylethylamine were added. This didn't have any significant influence on the fluorescence intensity but enhanced the evolution of fluorescence signal after addition of phenylacetylene and (more importantly) enables reproducible measurements.

6.5. Measurements of FRET efficiency

Different solvents. In a cuvette containing 1.5 ml of 1 μM solution of [(**17**)-O-IPrAu(**16**)] in toluene different amount of solvents (either acetonitrile or 1,2-dichloroethane) were added stepwise. After each addition, the cuvette was shaken and the emission spectrum was measured. The process was continued until the overall amount of added solvent has reached 2 ml. The volumes of aliquots were chosen with intent to obtain the most accurate and complete dependence of FRET efficiency on solvent content and were different for every solvent at each step. To measure the intensity of donor fluorophore in the absence of the acceptor, completely the same experiments were carried out with [IPrAu(**16**)].

Alkyne substrate. 15 ml of 1 μM solution of [(**17**)-O-IPrAu(**16**)] in toluene were loaded into a flame dried glass reactor under a nitrogen atmosphere. The fluorescence emission was monitored by an immersion probe (Hellma Analytics; Serial No. 13316). Approximately one minute after the start of measurements 75 μL of 0.2 M phenyl acetylene solution (1000 eq) in toluene were added. The measurement was continued until no changes in the signal intensity of both donor and acceptor fluorophores were observed.

7. List of Abbreviations

Ac	acetyl
Ar	aryl
BAr^F	tetrakis(3,5-bis(trifluoromethyl)phenyl)borate
BODIPY	4,4-difluoro-4-bora-3*a*,4*a*-diaza-*s*-indacene
Bu	butyl
cod	*cis*,*cis*-1,5-cyclooctadiene
Cy	cyclohexyl
dba	dibenzylideneacetone
DCE	1,2-dichloroethane
DCM	dichloromethane
DDQ	2,3-dichloro-5,6-dicyano-1,4-benzoquinone
DFT	density functional theory
DMAP	4-dimethylaminopyridine
DMSO	dimethyl sulfoxide
EDG	electron-donating group
Et	ethyl
EWG	electron-withdrawing group
FMO	frontier molecular orbital
FRET	fluorescence or Förster resonance energy transfer
Hex	hexyl
hfa	hexafluoroacetylacetonat
HOESY	heteronuclear Overhauser effect spectroscopy
HOMO	highest occupied molecular orbital
IC	internal conversion
*i*Pr	isopropyl
ISC	intersystem crossing
ISIP	inner-sphere ion pair
LUMO	lowest unoccupied molecular orbital
Me	methyl
Mes	mesityl
MLCT	metal-to-ligand charge transfer
NCS	*N*-chlorosuccinimide
Nf	nonafluorobutanesulfonyl
NHC	*N*-heterocyclic carbene
NMR	nuclear magnetic resonance
NOESY	nuclear Overhauser effect spectroscopy
OSIP	outer-sphere ion pair
PDT	photodynamic therapy
PET	photoinduced electron transfer
PGSE	pulsed field gradient spin-echo
Ph	phenyl
phen	phenantroline
pip	piperidine
PM-FTIRRAS	polarization-modulation Fourier transform IR reflection-absorption spectroscopy
PS	photosensitizer
py	pyridine
RET	resonance energy transfer
RNS	reactive nitrogen species
RT, rt	room temperature
SIMes	1,3-bis(2,4,6-trimethylphenyl)imidazolin-2-ylidene

SIPr	1,3-bis(2,6-diisopropylphenyl)imidazolin-2-ylidene
SMFM	single-molecule fluorescence microscopy
SPECT	single-photon emission computed tomography
terpy	terpyridine
Tf	trifluoromethanesulfonyl
TFA	trifluoroacetic acid
THF	tetrahydrofuran
tht	tetrahydrothiophene
TIRF	total internal reflectance fluorescence
Ts	*p*-toluenesulfonyl
TTA	triplet-triplet annihilation
TTET	triplet-triplet energy transfer
UV-Vis	ultraviolet-visible spectroscopy

8. References

[1] W. Rettig, B. Strehmel, S. Schrader, H. Seifert, *Applied Fluorescence in Chemistry, Biology and Medicine*, Springer-Verlag, **1999**.

[2] a) R. Ameloot, M. Roeffaers, M. Baruah, G. De Cremer, B. Sels, D. De Vos, J. Hofkens, *Photochem. Photobiol. Sci.* **2009**, *8*, 453-456; b) A. Rybina, C. Lang, M. Wirtz, K. Grussmayer, A. Kurz, F. Maier, A. Schmitt, O. Trapp, G. Jung, D.-P. Herten, *Angew. Chem. Int. Ed.* **2013**, *52*, 6322-6325.

[3] a) J. H. Sohn, K. H. Kim, H. Y. Lee, Z. S. No, H. Ihee, *J. Am. Chem. Soc.* **2008**, *130*, 16506-16507; b) T. Vorfalt, K. J. Wannowius, V. Thiel, H. Plenio, *Chem. Eur. J.* **2010**, *16*, 12312-12315; c) V. Sashuk, D. Schoeps, H. Plenio, *Chem. Commun.* **2009**, 770-772.

[4] T. Cordes, S. A. Blum, *Nat. Chem.* **2013**, *5*, 993-999.

[5] C. Marín-Hernández, A. Toscani, F. Sancenón, J. D. Wilton-Ely, R. Martínez-Máñez, *Chem. Commun.* **2016**, *52*, 5902-5911.

[6] J. Z. Zhao, S. M. Ji, W. H. Wu, W. T. Wu, H. M. Guo, J. F. Sun, H. Y. Sun, Y. F. Liu, Q. T. Li, L. Huang, *RSC Adv.* **2012**, *2*, 1712-1728.

[7] K. A. Stephenson, S. R. Banerjee, T. Besanger, O. O. Sogbein, M. K. Levadala, N. McFarlane, J. A. Lemon, D. R. Boreham, K. P. Maresca, J. D. Brennan, J. W. Babich, J. Zubieta, J. F. Valliant, *J. Am. Chem. Soc.* **2004**, *126*, 8598-8599.

[8] B. Bertrand, P. E. Doulain, C. Goze, E. Bodio, *Dalton Trans.* **2016**, *45*, 13005-13011.

[9] J. R. Lakowicz, *Principles of Fluorescence Spectroscopy*, Springer-Verlag, New York, **2010**.

[10] B. Valeur, *Molecular Fluorescence: Principles and Applications*, Wiley-VCH, **2001**.

[11] a) A. Loudet, K. Burgess, *Chem. Rev.* **2007**, *107*, 4891-4932; b) R. Ziessel, G. Ulrich, A. Harriman, *New J. Chem.* **2007**, *31*, 496-501; c) A. C. Benniston, G. Copley, *Phys. Chem. Chem. Phys.* **2009**, *11*, 4124-4131.

[12] a) F. J. Monsma, Jr., A. C. Barton, H. C. Kang, D. L. Brassard, R. P. Haugland, D. R. Sibley, *J. Neurochem.* **1989**, *52*, 1641-1644; b) M. C. Yee, S. C. Fas, M. M. Stohlmeyer, T. J. Wandless, K. A. Cimprich, *J. Biol. Chem.* **2005**, *280*, 29053-29059; c) M. S. Gonçalves, *Chem. Rev.* **2009**, *109*, 190-212; d) L. Yuan, W. Lin, K. Zheng, L. He, W. Huang, *Chem. Soc. Rev.* **2013**, *42*, 622-661; e) Y. Ni, J. Wu, *Org. Biomol. Chem.* **2014**, *12*, 3774-3791; f) T. Kowada, H. Maeda, K. Kikuchi, *Chem. Soc. Rev.* **2015**, *44*, 4953-4972.

[13] a) N. Boens, V. Leen, W. Dehaen, *Chem. Soc. Rev.* **2012**, *41*, 1130-1172; b) K. P. Carter, A. M. Young, A. E. Palmer, *Chem. Rev.* **2014**, *114*, 4564-4601.

[14] a) S. G. Awuah, Y. You, *RSC Adv.* **2012**, *2*, 11169-11183; b) A. Kamkaew, S. H. Lim, H. B. Lee, L. V. Kiew, L. Y. Chung, K. Burgess, *Chem. Soc. Rev.* **2013**, *42*, 77-88; c) A. M. Durantini, L. E. Greene, R. Lincoln, S. R. Martínez, G. Cosa, *J. Am. Chem. Soc.* **2016**, *138*, 1215-1225.

[15] a) T. A. Golovkova, D. V. Kozlov, D. C. Neckers, *J. Org. Chem.* **2005**, *70*, 5545-5549; b) C. Trieflinger, K. Rurack, J. Daub, *Angew. Chem. Int. Ed.* **2005**, *44*, 2288-2291.

[16] a) M. Shah, K. Thangaraj, M.-L. Soong, L. T. Wolford, J. H. Boyer, I. R. Politzer, T. G. Pavlopoulos, *Heteroat. Chem* **1990**, *1*, 389-399; b) J. H. Boyer, A. M. Haag, G. Sathyamoorthi, M.-L. Soong, K. Thangaraj, T. G. Pavlopoulos, *Heteroat. Chem* **1993**, *4*, 39-49; c) T. L. Arbeloa, F. L. Arbeloa, I. L. Arbeloa, I. García-Moreno, A. Costela, R. Sastre, F. Amat-Guerri, *Chem. Phys. Lett.* **1999**, *299*, 315-321; d) I. Esnal, I. Valois-Escamilla, C. F. Gómez-Durán, A. Urías-Benavides, M. L. Betancourt-Mendiola, I. López-Arbeloa, J. Bañuelos, I. García-Moreno, A. Costela, E. Peña-Cabrera, *ChemPhysChem* **2013**, *14*, 4134-4142.

[17] S. P. Singh, T. Gayathri, *Eur. J. Org. Chem.* **2014**, 4689-4707.

[18] N. Boens, B. Verbelen, W. Dehaen, *Eur. J. Org. Chem.* **2015**, 6577-6595.

[19] G. Ulrich, R. Ziessel, A. Harriman, *Angew. Chem. Int. Ed.* **2008**, *47*, 1184-1201.
[20] A. Treibs, F.-H. Kreuzer, *Liebigs Ann. Chem.* **1968**, *718*, 208-223.
[21] V. Lakshmi, R. Sharma, M. Ravikanth, *Reports in Organic Chemistry* **2016**, *6*, 1-24.
[22] a) I. J. Arroyo, R. Hu, G. Merino, B. Z. Tang, E. Peña-Cabrera, *J. Org. Chem.* **2009**, *74*, 5719-5722; b) A. Schmitt, B. Hinkeldey, M. Wild, G. Jung, *J Fluoresc* **2009**, *19*, 755-758; c) K. Tram, H. B. Yan, H. A. Jenkins, S. Vassiliev, D. Bruce, *Dyes and Pigments* **2009**, *82*, 392-395; d) B. R. Groves, S. M. Crawford, T. Lundrigan, C. F. Matta, S. Sowlati-Hashjin, A. Thompson, *Chem. Commun.* **2013**, *49*, 816-818.
[23] A. B. Nepomnyashchii, M. Bröring, J. Ahrens, A. J. Bard, *J. Am. Chem. Soc.* **2011**, *133*, 8633-8645.
[24] Z. Li, E. Mintzer, R. Bittman, *J. Org. Chem.* **2006**, *71*, 1718-1721.
[25] V. P. Yakubovskyi, M. P. Shandura, Y. P. Kovtun, *Eur. J. Org. Chem.* **2009**, 3237-3243.
[26] A. Burghart, H. J. Kim, M. B. Welch, L. H. Thoresen, J. Reibenspies, K. Burgess, F. Bergström, L. B.-Å. Johansson, *J. Org. Chem.* **1999**, *64*, 7813-7819.
[27] a) R. W. Wagner, J. S. Lindsey, *Pure Appl. Chem.* **1996**, *68*, 1373-1380; b) L. Li, B. Nguyen, K. Burgess, *Biorg. Med. Chem. Lett.* **2008**, 3112–3116.
[28] a) C.-H. Lee, J. S. Lindsey, *Tetrahedron* **1994**, *50*, 11427-11440; b) B. J. Littler, M. A. Miller, C.-H. Hung, R. W. Wagner, D. F. O'Shea, P. D. Boyle, J. S. Lindsey, *J. Org. Chem.* **1999**, *64*, 1391-1396.
[29] M. Baruah, W. Qin, N. Basarić, W. M. De Borggraeve, N. Boens, *J. Org. Chem.* **2005**, *70*, 4152-4157.
[30] a) K. Yamada, T. Toyota, K. Takakura, M. Ishimaru, T. Sugawara, *New J. Chem.* **2001**, *25*, 667-669; b) S. Y. Moon, N. R. Cha, Y. H. Kim, S.-K. Chang, *J. Org. Chem.* **2004**, *69*, 181-183.
[31] T. V. Goud, A. Tutar, J.-F. Biellmann, *Tetrahedron* **2006**, *62*, 5084-5091.
[32] J.-S. Lee, N.-Y. Kang, Y. K. Kim, A. Samanta, S. Feng, H. K. Kim, M. Vendrell, J. H. Park, Y.-T. Chang, *J. Am. Chem. Soc.* **2009**, *131*, 10077-10082.
[33] N. Boens, V. Leen, W. Dehaen, L. Wang, K. Robeyns, W. Qin, X. Tang, D. Beljonne, C. Tonnelé, J. M. Paredes, M. J. Ruedas-Rama, A. Orte, L. Crovetto, E. M. Talavera, J. M. Alvarez-Pez, *J. Phys. Chem. A* **2012**, *116*, 9621-9631.
[34] a) E. Peña-Cabrera, A. Aguilar-Aguilar, M. González-Domínguez, E. Lager, R. Zamudio-Vázquez, J. Godoy-Vargas, F. Villanueva-García, *Org. Lett.* **2007**, *9*, 3985-3988; b) L. Betancourt-Mendiola, I. Valois-Escamilla, T. Arbeloa, J. Bañuelos, I. L. Arbeloa, J. O. Flores-Rizo, R. Hu, E. Lager, C. F. Gómez-Durán, J. L. Belmonte-Vázquez, M. R. Martínez-González, I. J. Arroyo, C. A. Osorio-Martínez, E. Alvarado-Martínez, A. Urías-Benavides, B. D. Gutiérrez-Ramos, B. Z. Tang, E. Peña-Cabrera, *J. Org. Chem.* **2015**, *80*, 5771-5782.
[35] a) C. F. Gómez-Durán, I. García-Moreno, A. Costela, V. Martin, R. Sastre, J. Bañuelos, F. L. Arbeloa, I. L. Arbeloa, E. Peña-Cabrera, *Chem. Commun.* **2010**, *46*, 5103-5105; b) J. Bañuelos, V. Martín, C. F. Gómez-Durán, I. J. A. Córdoba, E. Peña-Cabrera, I. García-Moreno, Á. Costela, M. E. Pérez-Ojeda, T. Arbeloa, I. L. Arbeloa, *Chem. Eur. J.* **2011**, *17*, 7261-7270; c) C. A. Osorio-Martínez, A. Urías-Benavides, C. F. Gómez-Durán, J. Bañuelos, I. Esnal, I. L. Arbeloa, E. Peña-Cabrera, *J. Org. Chem.* **2012**, *77*, 5434-5438; d) J. O. Flores-Rizo, I. Esnal, C. A. Osorio-Martínez, C. F. Gómez-Durán, J. Bañuelos, I. L. Arbeloa, K. H. Pannell, A. J. Metta-Magaña, E. Peña-Cabrera, *J. Org. Chem.* **2013**, *78*, 5867-5877.
[36] V. Leen, P. Yuan, L. Wang, N. Boens, W. Dehaen, *Org. Lett.* **2012**, *14*, 6150-6153.
[37] H. Wang, M. G. Vicente, F. R. Fronczek, K. M. Smith, *Chem. Eur. J.* **2014**, *20*, 5064-5074.
[38] V. Lakshmi, M. R. Rao, M. Ravikanth, *Org. Biomol. Chem.* **2015**, *13*, 2501-2517.
[39] V. Leen, T. Leemans, N. Boens, W. Dehaen, *Eur. J. Org. Chem.* **2011**, 4386-4396.
[40] T. Rohand, M. Baruah, W. Qin, N. Boens, W. Dehaen, *Chem. Commun.* **2006**, 266-268.

[41] X. Zhou, C. Yu, Z. Feng, Y. Yu, J. Wang, E. Hao, Y. Wei, X. Mu, L. Jiao, *Org. Lett.* **2015**, *17*, 4632-4635.
[42] a) W. W. Qin, T. Rohand, M. Baruah, A. Stefan, M. Van der Auweraer, W. Dehaen, N. Boens, *Chem. Phys. Lett.* **2006**, *420*, 562-568; b) W. Qin, V. Leen, T. Rohand, W. Dehaen, P. Dedecker, M. Van der Auweraer, K. Robeyns, L. Van Meervelt, D. Beljonne, B. Van Averbeke, J. N. Clifford, K. Driesen, K. Binnemans, N. Boens, *J. Phys. Chem. A* **2009**, *113*, 439-447.
[43] a) T. Rohand, W. W. Qin, N. Boens, W. Dehaen, *Eur. J. Org. Chem.* **2006**, 4658-4663; b) G. Duran-Sampedro, E. Palao, A. R. Agarrabeitia, S. de la Moya, N. Boens, M. J. Ortiz, *RSC Adv.* **2014**, *4*, 19210-19213.
[44] V. Leen, V. Z. Gonzalvo, W. M. Deborggraeve, N. Boens, W. Dehaen, *Chem. Commun.* **2010**, *46*, 4908-4910.
[45] V. Leen, M. Van der Auweraer, N. Boens, W. Dehaen, *Org. Lett.* **2011**, *13*, 1470-1473.
[46] B. Verbelen, V. Leen, L. Wang, N. Boens, W. Dehaen, *Chem. Commun.* **2012**, *48*, 9129-9131.
[47] B. Verbelen, S. Boodts, J. Hofkens, N. Boens, W. Dehaen, *Angew. Chem. Int. Ed.* **2015**, *54*, 4612-4616.
[48] a) L. Jiao, W. Pang, J. Zhou, Y. Wei, X. Mu, G. Bai, E. Hao, *J. Org. Chem.* **2011**, *76*, 9988-9996; b) L. Wang, J.-W. Wang, A.-J. Cui, X.-X. Cai, Y. Wan, Q. Chen, M.-Y. He, W. Zhang, *RSC Adv.* **2013**, *3*, 9219-9222.
[49] a) L. Jiao, C. Yu, J. Li, Z. Wang, M. Wu, E. Hao, *J. Org. Chem.* **2009**, *74*, 7525-7528; b) S. L. Zhu, J. H. Bi, G. Vegesna, J. T. Zhang, F.-T. Luo, L. Valenzano, H. Y. Liu, *RSC Adv.* **2013**, *3*, 4793-4800.
[50] a) L. Li, J. Han, B. Nguyen, K. Burgess, *J. Org. Chem.* **2008**, *73*, 1963-1970; b) R. Sauer, A. Turshatov, S. Baluschev, K. Landfester, *Macromolecules* **2012**, *45*, 3787-3796.
[51] a) Z. S. Li, Y. Chen, X. J. Lv, W.-F. Fu, *New J. Chem.* **2013**, *37*, 3755-3761; b) P. Majumdar, X. L. Yuan, S. F. Li, B. Le Guennic, J. Ma, C. S. Zhang, D. Jacquemin, J. Z. Zhao, *J. Mater. Chem. B* **2014**, *2*, 2838-2854.
[52] R. H. Crabtree, *The Organometallic Chemistry of the Transition Metals*, John Wiley & Sons, Inc., **2014**.
[53] S.-G. Lim, S. A. Blum, *Organometallics* **2009**, *28*, 4643-4645.
[54] M. Navarro, S. X. Wang, H. Müller-Bunz, G. Redmond, P. Farràs, M. Albrecht, *Organometallics* **2017**, *36*, 1469-1478.
[55] N. M. Esfandiari, S. A. Blum, *J. Am. Chem. Soc.* **2011**, *133*, 18145-18147.
[56] E. M. Hensle, S. A. Blum, *J. Am. Chem. Soc.* **2013**, *135*, 12324-12328.
[57] C. Feng, D. W. Cunningham, Q. T. Easter, S. A. Blum, *J. Am. Chem. Soc.* **2016**, *138*, 11156-11159.
[58] A. Krasovskiy, V. Malakhov, A. Gavryushin, P. Knochel, *Angew. Chem. Int. Ed.* **2006**, *45*, 6040-6044.
[59] a) E. B. Shera, N. K. Seitzinger, L. M. Davis, R. A. Keller, S. A. Soper, *Chem. Phys. Lett.* **1990**, *174*, 553-557; b) D. C. Nguyen, R. A. Keller, J. H. Jett, J. C. Martin, *Anal. Chem.* **1987**, *59*, 2158-2161.
[60] A. Kiel, J. Kovacs, A. Mokhir, R. Krämer, D.-P. Herten, *Angew. Chem. Int. Ed.* **2007**, *46*, 3363-3366.
[61] a) S. A. Blum, *Phys. Chem. Chem. Phys.* **2014**, *16*, 16333-16339; b) K. Kitagawa, S. A. Blum, *ACS Catal.* **2017**, *7*, 3786-3791.
[62] S. M. Canham, J. Y. Bass, O. Navarro, S.-G. Lim, N. Das, S. A. Blum, *Organometallics* **2008**, *27*, 2172-2175.
[63] a) N. M. Esfandiari, Y. Wang, J. Y. Bass, T. P. Cornell, D. A. Otte, M. H. Cheng, J. C. Hemminger, T. M. McIntire, V. A. Mandelshtam, S. A. Blum, *J. Am. Chem. Soc.* **2010**, *132*, 15167-15169; b) N. M. Esfandiari, Y. Wang, J. Y. Bass, S. A. Blum, *Inorg. Chem.*

2011, *50*, 9201-9203; c) N. M. Esfandiari, Y. Wang, T. M. McIntire, S. A. Blum, *Organometallics* **2011**, *30*, 2901-2907.
[64] J. D. Ng, S. P. Upadhyay, A. N. Marquard, K. M. Lupo, D. A. Hinton, N. A. Padilla, D. M. Bates, R. H. Goldsmith, *J. Am. Chem. Soc.* **2016**, *138*, 3876-3883.
[65] R. Visbal, M. C. Gimeno, *Chem. Soc. Rev.* **2014**, *43*, 3551-3574.
[66] a) C. W. Rogers, M. O. Wolf, *Angew. Chem. Int. Ed.* **2002**, *41*, 1898-1900; b) K. M. Matkovich, L. M. Thorne, M. O. Wolf, T. C. Pace, C. Bohne, B. O. Patrick, *Inorg. Chem.* **2006**, *45*, 4610-4618; c) H.-J. Park, Y. K. Chung, *Inorg. Chim. Acta* **2012**, *391*, 105-113; d) M. E. Moragues, A. Toscani, F. Sancenón, R. Martínez-Máñez, A. J. White, J. D. Wilton-Ely, *J. Am. Chem. Soc.* **2014**, *136*, 11930-11933.
[67] B. W. Michel, A. R. Lippert, C. J. Chang, *J. Am. Chem. Soc.* **2012**, *134*, 15668-15671.
[68] P. Kos, H. Plenio, *Chem. Eur. J.* **2015**, *21*, 1088-1095.
[69] O. Halter, I. Fernández, H. Plenio, *Chem. Eur. J.* **2017**, *23*, 711-719.
[70] P. Kos, H. Plenio, *Angew. Chem. Int. Ed.* **2015**, *54*, 13293-13296.
[71] a) J. C. Irvine, R. H. Ritchie, J. L. Favaloro, K. L. Andrews, R. E. Widdop, B. K. Kemp-Harper, *Trends Pharmacol. Sci.* **2008**, *29*, 601-608; b) J. M. Fukuto, A. S. Dutton, K. N. Houk, *ChemBioChem* **2005**, *6*, 612-619.
[72] J. Rosenthal, S. J. Lippard, *J. Am. Chem. Soc.* **2010**, *132*, 5536-5537.
[73] J. Zhao, W. Wu, J. Sun, S. Guo, *Chem. Soc. Rev.* **2013**, *42*, 5323-5351.
[74] R. Bonnett, *Chemical Aspects of Photodynamic Therapy*, Gordon and Breach Science Publishers, Amsterdam, **2000**.
[75] D. Ravelli, M. Fagnoni, A. Albini, *Chem. Soc. Rev.* **2013**, *42*, 97-113.
[76] a) J. Z. Zhao, S. M. Ji, H. M. Guo, *RSC Adv.* **2011**, *1*, 937-950; b) T. N. Singh-Rachford, F. N. Castellano, *Coord. Chem. Rev.* **2010**, *254*, 2560-2573.
[77] J. Zhao, K. Xu, W. Yang, Z. Wang, F. Zhong, *Chem. Soc. Rev.* **2015**, *44*, 8904-8939.
[78] a) L. Huang, X. Yu, W. Wu, J. Zhao, *Org. Lett.* **2012**, *14*, 2594-2597; b) Y. Cakmak, S. Kolemen, S. Duman, Y. Dede, Y. Dolen, B. Kilic, Z. Kostereli, L. T. Yildirim, A. L. Dogan, D. Guc, E. U. Akkaya, *Angew. Chem. Int. Ed.* **2011**, *50*, 11937-11941.
[79] E. L. Clennan, A. Pace, *Tetrahedron* **2005**, *61*, 6665-6691.
[80] P. R. Ogilby, *Chem. Soc. Rev.* **2010**, *39*, 3181-3209.
[81] C. Ye, L. Zhou, X. Wang, Z. Liang, *Phys. Chem. Chem. Phys.* **2016**, *18*, 10818-10835.
[82] a) M. Galletta, S. Campagna, M. Quesada, G. Ulrich, R. Ziessel, *Chem. Commun.* **2005**, 4222-4224; b) M. Galletta, F. Puntoriero, S. Campagna, C. Chiorboli, M. Quesada, S. Goeb, R. Ziessel, *J. Phys. Chem. A* **2006**, *110*, 4348-4358.
[83] W. H. Wu, J. F. Sun, X. N. Cui, J. Z. Zhao, *J. Mater. Chem. C* **2013**, *1*, 4577-4589.
[84] W. Wu, L. Liu, X. Cui, C. Zhang, J. Zhao, *Dalton Trans.* **2013**, *42*, 14374-14379.
[85] J. Sun, F. Zhong, X. Yi, J. Zhao, *Inorg. Chem.* **2013**, *52*, 6299-6310.
[86] F. Nastasi, F. Puntoriero, S. Campagna, S. Diring, R. Ziessel, *Phys. Chem. Chem. Phys.* **2008**, *10*, 3982-3986.
[87] W. Wu, J. Zhao, H. Guo, J. Sun, S. Ji, Z. Wang, *Chem. Eur. J.* **2012**, *18*, 1961-1968.
[88] W. H. Wu, J. Z. Zhao, J. F. Sun, L. Huang, X. Y. Yi, *J. Mater. Chem. C* **2013**, *1*, 705-716.
[89] H. R. Jia, B. Küçüköz, Y. H. Xing, P. Majumdar, C. S. Zhang, A. Karatay, G. Yaglioglu, A. Elmali, J. Z. Zhao, M. Hayvali, *J. Mater. Chem. C* **2014**, *2*, 9720-9736.
[90] F. Geist, A. Jackel, R. F. Winter, *Inorg. Chem.* **2015**, *54*, 10946-10957.
[91] F. Geist, A. Jackel, P. Irmler, M. Linseis, S. Malzkuhn, M. Kuss-Petermann, O. S. Wenger, R. F. Winter, *Inorg. Chem.* **2017**, *56*, 914-930.
[92] X. Yi, J. Zhao, J. Sun, S. Guo, H. Zhang, *Dalton Trans.* **2013**, *42*, 2062-2074.
[93] J. Agarwal, E. Fujita, H. F. Schaefer, J. T. Muckerman, *J. Am. Chem. Soc.* **2012**, *134*, 5180-5186.
[94] G. A. Andrade, A. J. Pistner, G. P. A. Yap, D. A. Lutterman, J. Rosenthal, *ACS Catal.* **2013**, *3*, 1685-1692.

[95] A. A. Rachford, R. Ziessel, T. Bura, P. Retailleau, F. N. Castellano, *Inorg. Chem.* **2010**, *49*, 3730-3736.
[96] a) J. Zhou, L. Gai, Z. Zhou, W. Yang, J. Mack, K. Xu, J. Zhao, Y. Zhao, H. Qiu, K. S. Chan, Z. Shen, *Chem. Eur. J.* **2016**, *22*, 13201-13209; b) J. F. Zhou, L. Z. Gai, Z. K. Zhou, J. Mack, K. J. Xu, J. Z. Zhao, H. L. Qiu, K. S. Chan, Z. Shen, *RSC Adv.* **2016**, *6*, 72115-72120.
[97] L. Xu, B. Wen, G. Kim, T. Kim, F. Cheng, M. Zhou, L. Xu, T. Tanaka, B. Yin, A. Osuka, D. Kim, J. Song, *Angew. Chem. Int. Ed.* **2017**, *56*, 12322-12326.
[98] M. Üçüncü, E. Karakuş, E. K. Demirci, M. Sayar, S. Dartar, M. Emrullahoğlu, *Org. Lett.* **2017**, *19*, 2522-2525.
[99] F. A. Mettler, M. J. Guiberteau, *Essentials of Nuclear Medicine Imaging*, W. B. Saunders Company, Toronto, **1998**.
[100] X. F. Wang, B. Herman, *Fluorescence Imaging Spectroscopy and Microscopy*, John Wiley and Sons, New York, **1996**.
[101] L. H. Davies, B. Stewart, R. W. Harrington, W. Clegg, L. J. Higham, *Angew. Chem. Int. Ed.* **2012**, *51*, 4921-4924.
[102] B. Stewart, A. Harriman, L. J. Higham, *Organometallics* **2011**, *30*, 5338-5343.
[103] L. H. Davies, J. F. Wallis, M. R. Probert, L. J. Higham, *Synthesis* **2014**, *46*, 2622-2628.
[104] L. H. Davies, J. F. Wallis, R. W. Harrington, P. G. Waddell, L. J. Higham, *J. Coord. Chem.* **2016**, *69*, 2069-2080.
[105] S. S. Jurisson, J. D. Lydon, *Chem. Rev.* **1999**, *99*, 2205-2218.
[106] S. Liu, *Chem. Soc. Rev.* **2004**, *33*, 445-461.
[107] P. S. Donnelly, *Dalton Trans.* **2011**, *40*, 999-1010.
[108] L. H. Davies, B. B. Kasten, P. D. Benny, R. L. Arrowsmith, H. Ge, S. I. Pascu, S. W. Botchway, W. Clegg, R. W. Harrington, L. J. Higham, *Chem. Commun.* **2014**, *50*, 15503-15505.
[109] R. Alberto, R. Schibli, A. Egli, A. P. Schubiger, U. Abram, T. A. Kaden, *J. Am. Chem. Soc.* **1998**, *120*, 7987-7988.
[110] P. J. Blower, J. S. Lewis, J. Zweit, *Nucl. Med. Biol.* **1996**, *23*, 957-980.
[111] a) C. S. Cutler, H. M. Hennkens, N. Sisay, S. Huclier-Markai, S. S. Jurisson, *Chem. Rev.* **2013**, *113*, 858-883; b) W. A. Volkert, W. F. Goeckeler, G. J. Ehrhardt, A. R. Ketring, *J. Nucl. Med.* **1991**, *32*, 174-185.
[112] L. H. Davies, R. W. Harrington, W. Clegg, L. J. Higham, *Dalton Trans.* **2014**, *43*, 13485-13499.
[113] A. M. Leiva, L. Rivera, B. Loeb, *Polyhedron* **1991**, *10*, 347-350.
[114] B. Rosenberg, L. Vancamp, T. Krigas, *Nature* **1965**, *205*, 698-699.
[115] E. Bodio, P. Le Gendre, F. Denat, C. Goze, *Advances in Inorganic Chemistry, Vol 68: Insights from Imaging in Bioinorganic Chemistry* **2016**, *68*, 253-299.
[116] a) L. Eloy, A.-S. Jarrousse, M.-L. Teyssot, A. Gautier, L. Morel, C. Jolivalt, T. Cresteil, S. Roland, *ChemMedChem* **2012**, *7*, 805-814; b) P. D. Harvey, S. Tasan, C. P. Gros, C. H. Devillers, P. Richard, P. Le Gendre, E. Bodio, *Organometallics* **2015**, *34*, 1218-1227.
[117] a) L. Boselli, M. Carraz, S. Mazères, L. Paloque, G. González, F. Benoit-Vical, A. Valentin, C. Hemmert, H. Gornitzka, *Organometallics* **2015**, *34*, 1046-1055; b) M. Frik, J. Jiménez, V. Vasilevski, M. Carreira, A. de Almeida, E. Gascón, F. Benoit, M. Sanaú, A. Casini, M. Contel, *Inorg Chem Front.* **2014**, *1*, 231-241.
[118] L. Adriaenssens, Q. Liu, F. Chaux-Picquet, S. Tasan, M. Picquet, F. Denat, P. Le Gendre, F. Marques, C. Fernandes, F. Mendes, L. Gano, M. P. Campello, E. Bodio, *ChemMedChem* **2014**, *9*, 1567-1573.
[119] M. J. Clarke, *Coord. Chem. Rev.* **2002**, *232*, 69-93.
[120] S. Nobili, E. Mini, I. Landini, C. Gabbiani, A. Casini, L. Messori, *Med. Res. Rev.* **2010**, *30*, 550-580.

[121] S. Tasan, O. Zava, B. Bertrand, C. Bernhard, C. Goze, M. Picquet, P. Le Gendre, P. Harvey, F. Denat, A. Casini, E. Bodio, *Dalton Trans.* **2013**, *42*, 6102-6109.
[122] P.-E. Doulain, R. Decréau, C. Racoeur, V. Goncalves, L. Dubrez, A. Bettaieb, P. Le Gendre, F. Denat, C. Paul, C. Goze, E. Bodio, *Dalton Trans.* **2015**, *44*, 4874-4883.
[123] A. Trommenschlager, F. Chotard, B. Bertrand, S. Amor, L. Dondaine, M. Picquet, P. Richard, A. Bettaïeb, P. Le Gendre, C. Paul, C. Goze, E. Bodio, *Dalton Trans.* **2017**, *46*, 8051-8056.
[124] E. R. Jamieson, S. J. Lippard, *Chem. Rev.* **1999**, *99*, 2467-2498.
[125] T. Sun, X. Guan, M. Zheng, X. Jing, Z. Xie, *ACS Med. Chem. Lett.* **2015**, *6*, 430-433.
[126] J. Yellol, S. A. Pérez, A. Buceta, G. Yellol, A. Donaire, P. Szumlas, P. J. Bednarski, G. Makhloufi, C. Janiak, A. Espinosa, J. Ruiz, *J. Med. Chem.* **2015**, *58*, 7310-7327.
[127] J. M. Zimbron, K. Passador, B. Gatin-Fraudet, C.-M. Bachelet, D. Plażuk, L.-M. Chamoreau, C. Botuha, S. Thorimbert, M. Salmain, *Organometallics* **2017**, *36*, 3435-3442.
[128] I. Chopra, *J. Antimicrob. Chemother.* **2007**, *59*, 587-590.
[129] M. N. Pinto, I. Chakraborty, W. Schultz-Simonton, M. Rojas-Andrade, R. Braslau, P. K. Mascharak, *Chem. Commun.* **2017**, *53*, 1459-1462.
[130] L. R. Sousa, J. M. Larson, *J. Am. Chem. Soc.* **1977**, *99*, 307-310.
[131] a) B. Daly, J. Ling, A. P. de Silva, *Chem. Soc. Rev.* **2015**, *44*, 4203-4211; b) H. N. Kim, W. X. Ren, J. S. Kim, J. Yoon, *Chem. Soc. Rev.* **2012**, *41*, 3210-3244; c) X. Zhou, S. Lee, Z. Xu, J. Yoon, *Chem. Rev.* **2015**, *115*, 7944-8000.
[132] a) X. Li, X. Gao, W. Shi, H. Ma, *Chem. Rev.* **2014**, *114*, 590-659; b) J. C. Carlson, L. G. Meimetis, S. A. Hilderbrand, R. Weissleder, *Angew. Chem. Int. Ed.* **2013**, *52*, 6917-6920.
[133] a) T. Ueno, Y. Urano, K. Setsukinai, H. Takakusa, H. Kojima, K. Kikuchi, K. Ohkubo, S. Fukuzumi, T. Nagano, *J. Am. Chem. Soc.* **2004**, *126*, 14079-14085; b) Y. Urano, M. Kamiya, K. Kanda, T. Ueno, K. Hirose, T. Nagano, *J. Am. Chem. Soc.* **2005**, *127*, 4888-4894; c) Y. Gabe, Y. Urano, K. Kikuchi, H. Kojima, T. Nagano, *J. Am. Chem. Soc.* **2004**, *126*, 3357-3367.
[134] E. J. Choi, E. Kim, Y. Lee, A. Jo, S. B. Park, *Angew. Chem. Int. Ed.* **2014**, *53*, 1346-1350.
[135] E. Kim, Y. Lee, S. Lee, S. B. Park, *Acc. Chem. Res.* **2015**, *48*, 538-547.
[136] a) A. M. Lifschitz, C. M. Shade, A. M. Spokoyny, J. Mendez-Arroyo, C. L. Stern, A. A. Sarjeant, C. A. Mirkin, *Inorg. Chem.* **2013**, *52*, 5484–5492; b) M. R. Rao, K. V. P. Kumar, M. Ravikanth, *J. Organomet. Chem.* **2010**, *695*, 863-869; c) T. K. Khan, R. R. S. Pissurlenkar, M. S. Shaikh, M. Ravikanth, *J. Organomet. Chem.* **2012**, *697*, 65-73; d) B. Dhokale, P. Gautam, S. M. Mobin, R. Misra, *Dalton Trans.* **2013**, *42*, 1512-1518.
[137] G. M. Chu, A. Guerrero-Martínez, I. Fernández, M. Á. Sierra, *Chem. Eur. J.* **2014**, *20*, 1367-1375.
[138] G. M. Chu, A. Guerrero-Martínez, C. R. de Arellano, I. Fernández, M. A. Sierra, *Inorg. Chem.* **2016**, *55*, 2737-2747.
[139] G. M. Chu, I. Fernández, A. Guerrero-Martínez, C. R. de Arellano, M. A. Sierra, *Eur. J. Inorg. Chem.* **2016**, 844-852.
[140] J. C. Lin, R. T. Huang, C. S. Lee, A. Bhattacharyya, W. S. Hwang, I. J. Lin, *Chem. Rev.* **2009**, *109*, 3561-3598.
[141] a) Y. A. Volkova, B. Brizet, P. D. Harvey, A. D. Averin, C. Goze, F. Denat, *Eur. J. Org. Chem.* **2013**, 4270-4279; b) M. Baruah, W. Qin, R. A. Vallée, D. Beljonne, T. Rohand, W. Dehaen, N. Boens, *Org. Lett.* **2005**, *7*, 4377-4380.
[142] C. C. Zhao, Y. F. Zhang, X. Z. Wang, J. Cao, *J. Photochem. Photobiol. A: Chem.* **2013**, *264*, 41-47.
[143] L.-Y. Niu, Q.-Q. Yang, H.-R. Zheng, Y.-Z. Chen, L.-Z. Wu, C.-H. Tung, Q.-Z. Yang, *RSC Adv.* **2015**, *5*, 3959-3964.

[144] C. Hansch, A. Leo, R. W. Taft, *Chem. Rev.* **1991**, *91*, 165-195.
[145] H. M. J. Wang, C. Y. L. Chen, I. J. B. Lin, *Organometallics* **1999**, *18*, 1216-1223.
[146] The crystal structure is not discussed here in detail, due to the modest quality of the X-ray data set.
[147] Because of the similar structures of the complexes **3a** and **3b**, only **3a** was used for the measurements.
[148] Nonetheless, QY were determined for a few selected complexes and good agreement was observed.
[149] In complex **1**, the orthogonality of the three ring systems prevents conjugated electron transfer.
[150] All calculations were carried out at the B3LYP-D3/def2-SVP level.
[151] T. Ueno, Y. Urano, H. Kojima, T. Nagano, *J. Am. Chem. Soc.* **2006**, *128*, 10640-10641.
[152] S. Doose, H. Neuweiler, M. Sauer, *ChemPhysChem* **2009**, *10*, 1389-1398.
[153] D. M. Adams, L. Brus, C. E. D. Chidsey, S. Creager, C. Creutz, C. R. Kagan, P. V. Kamat, M. Lieberman, S. Lindsay, R. A. Marcus, R. M. Metzger, M. E. Michel-Beyerle, J. R. Miller, M. D. Newton, D. R. Rolison, O. Sankey, K. S. Schanze, J. Yardley, X. Y. Zhu, *J. Phys. Chem. B* **2003**, *107*, 6668-6697.
[154] D. Rehm, A. Weller, *Isr. J. Chem.* **1970**, *8*, 259-271.
[155] O. N. Temkin, *Homogeneous Catalysis with metal complexes. Kinetic aspects and mechanism*, Wiley-VCH, Weinheim, **2012**.
[156] *Mechanisms in Homogeneous Catalysis* (Ed.: B. Heaton), Wiley-VCH, Weinheim, **2005**.
[157] D. Brox, A. Kiel, S. J. Wörner, M. Pernpointner, P. Comba, B. Martin, D.-P. Herten, *PLoS One* **2013**, *8*, e58049.
[158] V. Sashuk, L. H. Peeck, H. Plenio, *Chem. Eur. J.* **2010**, *16*, 3983-3993.
[159] Z. Liu, W. He, Z. Guo, *Chem. Soc. Rev.* **2013**, *42*, 1568-1600.
[160] A. Kaloudi-Chantzea, N. Karakostas, C. P. Raptopoulou, V. Psycharis, E. Saridakis, J. Griebel, R. Hermann, G. Pistolis, *J. Am. Chem. Soc.* **2010**, *132*, 16327-16329.
[161] N. Inoue, Y. Suzuki, K. Yokoyama, I. Karube, *Biosci. Biotechnol. Biochem.* **2009**, *73*, 1215-1217.
[162] M. Murata, S. L. Buchwald, *Tetrahedron* **2004**, *60*, 7397-7403.
[163] O. Herd, A. Hessler, M. Hingst, M. Tepper, O. Stelzer, *J. Organomet. Chem.* **1996**, *522*, 69-76.
[164] Z. N. Yu, L.-S. Tan, E. Fossum, *ARKIVOC* **2009**, *14*, 255-265.
[165] a) B.-K. Teo, J. C. Calabrese, *Inorg. Chem.* **1976**, *15*, 2467-2474; b) M. Halim, R. D. Kennedy, M. Suzuki, S. I. Khan, P. L. Diaconescu, Y. Rubin, *J. Am. Chem. Soc.* **2011**, *133*, 6841-6851.
[166] T. E. Müller, S. W.-K. Choi, D. M. P. Mingos, D. Murphy, D. J. Williams, V. W.-W. Yam, *J. Organomet. Chem.* **1994**, *484*, 209-224.
[167] M. Noskowska, E. Śliwińska, W. Duczmal, *Trans. Met. Chem.* **2003**, *28*, 756-759.
[168] ^{10,11}B-^{31}P coupling is not observed in the NMR spectra.
[169] S. Berger, S. Braun, H.-O. Kalinowski, *NMR-Spektroskopie von Nichtmetallen*, Thieme-Verlag, Stuttgart, **1994**.
[170] a) H. Plenio, *Chem. Rev.* **1997**, *97*, 3363-3384; b) O. P. Volos, L. V. Loziuk, E. A. Shablovskaia, *Mikrobiol. Zh.* **1979**, *41*, 390-393.
[171] L.-J. Baker, G. A. Bowmaker, D. Camp, Effendy, P. C. Healy, H. Schmidbaur, O. Steigelmann, A. H. White, *Inorg. Chem.* **1992**, *31*, 3656-3662.
[172] A. O. Borissova, A. A. Korlyukov, M. Y. Antipin, K. A. Lyssenko, *J. Phys. Chem. A* **2008**, *112*, 11519-11522.
[173] G. M. Sheldrick, *Acta Crystallogr. A* **2008**, *64*, 112-122.
[174] H.-C. Su, O. Fadhel, C.-J. Yang, T.-Y. Cho, C. Fave, M. Hissler, C.-C. Wu, R. Réau, *J. Am. Chem. Soc.* **2006**, *128*, 983-995.
[175] *Modern Gold Catalyzed Synthesis* (Eds.: A. S. K. Hashmi, F. D. Toste), Wiley-VCH, Weinheim, **2012**.

[176] The slightly different initial fluorescence intensities of [AuCl(**12b**)] is due to different lamp intensities during the life time of the xenon lamp used as an excitation source in the fluorescence spectrometer.
[177] M. C. Jahnke, T. Pape, F. E. Hahn, *Z. Naturforsch. B* **2013**, *68b*, 467-473.
[178] a) I. Krossing, I. Raabe, *Angew. Chem. Int. Ed.* **2004**, *43*, 2066-2090; b) A. Zhdanko, M. E. Maier, *ACS Catal.* **2014**, *4*, 2770-2775.
[179] a) A. S. Hashmi, *Chem. Rev.* **2007**, *107*, 3180-3211; b) Y.-M. Wang, A. D. Lackner, F. D. Toste, *Acc. Chem. Res.* **2014**, *47*, 889-901.
[180] a) D. Wang, R. Cai, S. Sharma, J. Jirak, S. K. Thummanapelli, N. G. Akhmedov, H. Zhang, X. Liu, J. L. Petersen, X. Shi, *J. Am. Chem. Soc.* **2012**, *134*, 9012-9019; b) D. Malhotra, M. S. Mashuta, G. B. Hammond, B. Xu, *Angew. Chem. Int. Ed.* **2014**, *53*, 4456-4459.
[181] a) N. Mézailles, L. Ricard, F. Gagosz, *Org. Lett.* **2005**, *7*, 4133-4136; b) L. Ricard, F. Gagosz, *Organometallics* **2007**, *26*, 4704-4707.
[182] a) M. Kumar, G. B. Hammond, B. Xu, *Org. Lett.* **2014**, *16*, 3452-3455; b) M. Q. Jia, M. Bandini, *ACS Catal.* **2015**, *5*, 1638-1652.
[183] It was also tested, whether the formation/precipitation of AgCl in the cuvettes in such minute amounts has an effect on the observed fluorescence intensity. No change in the brightness was observed, which confirms that the formation of the cationic gold is responsible for the increase in brightness.
[184] For a control experiment [Au(NTf_2)(**12b**)] was synthesized. The fluorescence intensity of this complex at the same concentration was found to be the same as that of the in situ prepared [Au(ONf)(**12b**)] complex.
[185] C. Reichardt, *Solvents and Solvent Effects in Organic Chemistry*, Wiley-VCH, Weinheim, **2003**.
[186] In the Gutman donor number classification, 1,2-dichloroethane is used as the reference point, with the DN set to zero by definition.
[187] A. Homs, I. Escofet, A. M. Echavarren, *Org. Lett.* **2013**, *15*, 5782-5785.
[188] B. Ranieri, I. Escofet, A. M. Echavarren, *Org. Biomol. Chem.* **2015**, *13*, 7103-7118.
[189] a) R. E. Brooner, R. A. Widenhoefer, *Angew. Chem. Int. Ed.* **2013**, *52*, 11714-11724; b) H. Schmidbaur, A. Schier, *Organometallics* **2010**, *29*, 2-23; c) T. N. Hooper, M. Green, C. A. Russell, *Chem. Commun.* **2010**, *46*, 2313-2315; d) D. Zuccaccia, L. Belpassi, L. Rocchigiani, F. Tarantelli, A. Macchioni, *Inorg. Chem.* **2010**, *49*, 3080-3082.
[190] T. J. Brown, R. A. Widenhoefer, *Organometallics* **2011**, *30*, 6003-6009.
[191] a) A. Grirrane, H. Garcia, A. Corma, E. Álvarez, *Chem. Eur. J.* **2013**, *19*, 12239-12244; b) A. S. Hashmi, *Acc. Chem. Res.* **2014**, *47*, 864-876.
[192] N. Marion, R. S. Ramón, S. P. Nolan, *J. Am. Chem. Soc.* **2009**, *131*, 448-449.
[193] In the presence of a large excess of silver ions, the dinuclear complex might also be a mixed Ag, Au complex.
[194] V. Lavallo, G. D. Frey, S. Kousar, B. Donnadieu, G. Bertrand, *Proc. Nat. Acad. Sci.* **2007**, *104*, 13569-13573.
[195] T. J. Brown, R. A. Widenhoefer, *J. Organomet. Chem.* **2011**, *696*, 1216-1220.
[196] A. Macchioni, *Chem. Rev.* **2005**, *105*, 2039-2073.
[197] E. Y.-X. Chen, T. J. Marks, *Chem. Rev.* **2000**, *100*, 1391-1434.
[198] D. A. Evans, J. A. Murry, P. von Matt, R. D. Norcross, S. J. Miller, *Angew. Chem. Int. Ed.* **1995**, *34*, 798-800.
[199] M. Ludwig, S. Strömberg, M. Svensson, B. Åkermark, *Organometallics* **1999**, *18*, 970-975.
[200] S. P. Smidt, N. Zimmermann, M. Studer, A. Pfaltz, *Chem. Eur. J.* **2004**, *10*, 4685-4693.
[201] G. Kiss, *Chem. Rev.* **2001**, *101*, 3435-3456.
[202] a) A. Bernardi, G. Colombo, C. Scolastico, *Tetrahedron Lett.* **1996**, *37*, 8921-8924; b) T. V. RajanBabu, *Chem. Rev.* **2003**, *103*, 2845-2860; c) A. Fürstner, M. Liebl, C. W. Lehmann, M. Picquet, R. Kunz, C. Bruneau, D. Touchard, P. H. Dixneuf, *Chem. Eur. J.*

2000, *6*, 1847-1857; d) W. Adam, K. J. Roschmann, C. R. Saha-Möller, D. Seebach, *J. Am. Chem. Soc.* **2002**, *124*, 5068-5073.
[203] S. H. Strauss, *Chem. Rev.* **1993**, *93*, 927-942.
[204] a) A. Macchioni, in *Perspectives in Organometallic Chemistry* (Eds.: C. G. Screttas, B. R. Steele), The Royal Society of Chemistry, **2003**, pp. 196-207; b) C. Zuccaccia, N. G. Stahl, A. Macchioni, M.-C. Chen, J. A. Roberts, T. J. Marks, *J. Am. Chem. Soc.* **2004**, *126*, 1448-1464; c) L. Rocchigiani, A. Macchioni, *Dalton Trans.* **2016**, *45*, 2785-2790.
[205] C. Zuccaccia, G. Bellachioma, G. Cardaci, A. Macchioni, *Organometallics* **2000**, *19*, 4663-4665.
[206] A. Macchioni, *Eur. J. Inorg. Chem.* **2003**, 195-205.
[207] G. Bellachioma, G. Cardaci, V. Gramlich, A. Macchioni, M. Valentini, C. Zuccaccia, *Organometallics* **1998**, *17*, 5025-5030.
[208] A. Macchioni, G. Bellachioma, G. Cardaci, G. Cruciani, E. Foresti, P. Sabatino, C. Zuccaccia, *Organometallics* **1998**, *17*, 5549-5556.
[209] G. Bellachioma, G. Cardaci, A. Macchioni, F. Valentini, C. Zuccaccia, E. Foresti, P. Sabatino, *Organometallics* **2000**, *19*, 4320-4326.
[210] A. Macchioni, G. Bellachioma, G. Cardaci, M. Travaglia, C. Zuccaccia, B. Milani, G. Corso, E. Zangrando, G. Mestroni, C. Carfagna, M. Formica, *Organometallics* **1999**, *18*, 3061-3069.
[211] a) A. Macchioni, A. Magistrato, I. Orabona, F. Ruffo, U. Rothlisberger, C. Zuccaccia, *New J. Chem.* **2003**, *27*, 455-458; b) C. Zuccaccia, A. Macchioni, I. Orabona, F. Ruffo, *Organometallics* **1999**, *18*, 4367-4372; c) R. Romeo, N. Nastasi, L. M. Scolaro, M. R. Plutino, A. Albinati, A. Macchioni, *Inorg. Chem.* **1998**, *37*, 5460-5466.
[212] A. Macchioni, C. Zuccaccia, E. Clot, K. Gruet, R. H. Crabtree, *Organometallics* **2001**, *20*, 2367-2373.
[213] C. Zuccaccia, G. Bellachioma, G. Cardaci, A. Macchioni, *J. Am. Chem. Soc.* **2001**, *123*, 11020-11028.
[214] C. Brouwer, C. He, *Angew. Chem. Int. Ed.* **2006**, *45*, 1744-1747.
[215] a) Z. Zhang, R. A. Widenhoefer, *Org. Lett.* **2008**, *10*, 2079-2081; b) R. L. LaLonde, B. D. Sherry, E. J. Kang, F. D. Toste, *J. Am. Chem. Soc.* **2007**, *129*, 2452-2453.
[216] L. Biasiolo, M. Trinchillo, P. Belanzoni, L. Belpassi, V. Busico, G. Ciancaleoni, A. D'Amora, A. Macchioni, F. Tarantelli, D. Zuccaccia, *Chem. Eur. J.* **2014**, *20*, 14594-14598.
[217] G. Ciancaleoni, L. Belpassi, D. Zuccaccia, F. Tarantelli, P. Belanzoni, *ACS Catal.* **2015**, *5*, 803-814.
[218] L. Biasiolo, A. Del Zotto, D. Zuccaccia, *Organometallics* **2015**, *34*, 1759-1765.
[219] A. Arcadi, *Chem. Rev.* **2008**, *108*, 3266-3325.
[220] a) D. Zuccaccia, L. Belpassi, F. Tarantelli, A. Macchioni, *J. Am. Chem. Soc.* **2009**, *131*, 3170-3171; b) N. Salvi, L. Belpassi, D. Zuccaccia, F. Tarantelli, A. Macchioni, *J. Organomet. Chem.* **2010**, *695*, 2679-2686; c) G. Ciancaleoni, L. Belpassi, F. Tarantelli, D. Zuccaccia, A. Macchioni, *Dalton Trans.* **2013**, *42*, 4122-4131; d) G. Ciancaleoni, L. Biasiolo, G. Bistoni, A. Macchioni, F. Tarantelli, D. Zuccaccia, L. Belpassi, *Organometallics* **2013**, *32*, 4444-4447.
[221] D. Zuccaccia, L. Belpassi, A. Macchioni, F. Tarantelli, *Eur. J. Inorg. Chem.* **2013**, 4121-4135.
[222] L. Biasiolo, G. Ciancaleoni, L. Belpassi, G. Bistoni, A. Macchioni, F. Tarantelli, D. Zuccaccia, *Catal. Sci. Technol.* **2015**, *5*, 1558-1567.
[223] L. Stryer, *Annu. Rev. Biochem.* **1978**, *47*, 819-846.
[224] a) V. A. Azov, A. Schlegel, F. Diederich, *Angew. Chem. Int. Ed.* **2005**, *44*, 4635-4638; b) I. Pochorovski, B. Breiten, W. B. Schweizer, F. Diederich, *Chem. Eur. J.* **2010**, *16*, 12590-12602.
[225] U. Resch-Genger, K. Rurack, *Pure Appl. Chem.* **2013**, *85*, 2005-2026.

Abriss des Lebens- und Bildungsganges

Persönliche Daten

Name, Vorname:	Vasiuta, Roman
Adresse:	Klausenburger Str. 128 64295 Darmstadt
Geburtsdatum:	21.08.1990
Geburtsort:	Iwano-Frankiwsk (Ukraine)
Nationalität:	ukrainisch

Promotion

01/2018	**voraussichtlicher Abschluss der Promotion (Dr. rer. nat.)**
11/2017	**Abgabe der Dissertation**
12/2013 – 03/2017	**Praktischer Teil der Dissertation** unter der Leitung von Prof. Dr. H. Plenio, Technische Universität Darmstadt im Fachbereich Anorganische Chemie. Titel der Doktorarbeit: Synthesis of BODIPY-tagged transition-metal complexes

Studium

09/2011 – 06/2013	**Magisterdiplom**, Nationale Taras-Schewtschenko-Universität Kyiv, Institut von Hohe Technologien. Titel der Magisterdiplomarbeit: Synthese von 4-hydroxymethyl-2,4-methanoprolin
09/2007 – 06/2011	**Diplom der Bachelors**, Nationale Taras-Schewtschenko-Universität Kyiv, Fachbereich Chemie, Schwerpunkt organische Chemie.

Schulausbildung

09/2000 – 06/2007	**Ukrainisches Gymnasium Nr. 1**, Iwano-Frankiwsk, Ukraine

Darmstadt, 16.11.2017

Roman Vasiuta

Klausenburger Str. 128

64295 Darmstadt

16.11.2017

Erklärung

Ich erkläre hiermit, daß ich meine Dissertation selbstständig und nur mit den angegebenen Hilfsmitteln angefertigt habe.

Roman Vasiuta

Klausenburger Str. 128

64295 Darmstadt

16.11.2017

Erklärung

Ich erkläre hiermit, noch keinen Promotionsversuch unternommen zu haben.